Breaking Down the Final Steps in 40S Ribosomal Subunit Assembly

by

Bethany Sarah Strunk

A dissertation submitted in partial fulfillment
of the requirements for the degree of
Doctor of Philosophy
(Chemical Biology)
in The University of Michigan
2011

Doctoral Committee:

Associate Professor Bruce A. Palfey, Co-Chair
Associate Professor Katrin Karbstein, Co-Chair, The Scripps Research Institute
Professor Richard R. Neubig
Professor Nils G. Walter
Assistant Professor Patrick O'Brien
Associate Professor Kate S. Carroll, The Scripps Research Institute

Dedication

To my parents….

I learn more and more every day, that even though I feel like you have supported me in every way imaginable, I will only ever be aware of a fraction of the ways in which you have been there for me.
I thank you for all of them.

Acknowledgements

First I need to give credit where it is due: Chapter 2 describes work carried out in collaboration with the laboratories of Yiorgo Skiniotis and Charles Brooks at the University of Michigan. Cherisse Loucks, Min Su, and Justin Schilling from the Skiniotis lab performed all electron microscopy and 3D-reconstructions. Harish Vashisth and Shanshan Cheng performed molecular dynamics flexible fitting of the mature 40S PDB to our premature electron density. Thank you to all of you, it was a blast! Jamie Van Etten performed the limited proteolysis experiments presented in Chapter 3 and Megan Novack is the superstar responsible for most of the figures in Chapter 4. Thank you to all of the Karbstein Lab members, who have put up with my messes and my melodrama. To Crystal Young, Melody Campbell, and Darryl Horn who have made Jupiter quite habitable. To Crystal (again) for trudging through this thesis with me. To all of the w-undergrads I have had the pleasure to work with: Melody (again), Christine Norton, Leena Leon, HeeHo Park, Ariel Joiner, and Megan (again). To the Carroll lab members who set a shining example with their wacky ways. To Jamie, Gabrielle, Eddie, and Kristen; I miss movie nights. To my committee members, thank you for going through this with me. To my brothers and sister and to Jason, you are amazing. And to Katrin, who has always taken me seriously, or at least made me feel as though she has, you have made this an amazing experience.

Table of Contents

List of Figures

List of Tables

List of Abbreviations

AF	ribosome assembly factors
Ap6A	diadenosine hexaphosphate
AMP-PCP	5'-adenylyl (beta,gamma-methylene)diphosphonate
AMP-PNP	5′-adenylyl (beta,gamma-imido)triphosphate
Cryo-EM	cryo-electron microscopy
GO annotations	gene ontology annotations
LC-MS/MS	Liquid chromatography-tandem mass spectrometry
MBP	maltose binding protein
MDFF	molecular dynamics flexible fitting
MTL	mating type locus
Rio	right open reading frame
Rpl	large subunit ribosomal protein
Rps	small subunit ribosomal proteins
SCF	Skp1-Cullin-F-box
snoRNA	small nucleolar RNAs
TAP	tandem affinity purification

Abstract

Eukaryotic ribosome assembly requires almost 200 conserved assembly factors (AFs) that are not part of the mature ribosome. To understand the function of AFs involved in late cytoplasmic steps of 40S maturation, biochemical and structural investigations of the latest steps in 40S maturation were initiated in the model organism *Saccharomyces cerevisiae*. The structure of a late 40S assembly intermediate was determined at 18 Å resolution using cryo-electron microscopy (cryo-EM). The binding sites of the seven AFs bound to this intermediate were identified from cryo-EM structures of particles lacking individual AFs. The positions of AFs as well as the rRNA structure in this pre-40S particle indicate that all seven AFs cooperate to prevent premature translation initiation on multiple levels: by blocking the binding of translation initiation factors, preventing the binding of mRNA, inhibiting joining with the 60S subunit, and preventing formation of the first peptide bond. *In vivo* data suggest that dissociation of most AFs from this intermediate occurs following regulated but translationally-unproductive joining of 60S subunits. The resulting 80S particles, containing pre-40S and mature 60S subunits, are an obligate intermediate on the 40S maturation pathway and accumulate in the absence of the assembly factor Fap7, an ATPase essential for 40S maturation. Data herein and in the literature suggest that these 80S particles are formed without the help of translation factors that bind to free 40S subunits, as these binding sites are blocked by assembly factors. In contrast, the formation of theses 80S particles requires the translation factors eIF5B and Rli1, which regulate subunit joining and promote dissociation of empty 80S

particles, respectively. Furthermore, eIF5A is required for dissociation of the kinase Rio2. To further understand the role of ATP hydrolysis by Fap7 in this process, its ATPase cycle was dissected *in vitro* showing that ATP binding and hydrolysis lead to a cycle of conformational changes, which include dimerization of the protein in an ATP dependent manner and conformational rearrangement of its C-terminus in response to ATP hydrolysis. Finally, it is shown that Fap7 directly interacts with Dim1 *in vitro*, further defining its site of interaction with 40S ribosomes.

Chapter 1

Powering Through Ribosome Assembly

1.1 Introduction

In order to catalyze protein synthesis, ribosomes must be assembled from ribosomal RNA (rRNA) and proteins (Rps). Mature ribosomes are composed of two subunits in all organisms, the large subunit (LSU) and the small subunit (SSU). The LSU comprises three rRNAs in eukaryotes (25S, 5.8S, 5S in *Saccharomyces cerevisiae*) and two in prokaryotes (23S, 5S in *Escherichia coli*), while the SSU has one rRNA in all kingdoms (18S in *S. cerevisiae* and 16S in *E. coli*). All three bacterial rRNAs and three of the four eukaryotic rRNAs are synthesized as a single transcript that must be processed and cleaved at specific sites during the assembly process to produce the mature rRNA species (**Fig. 1.1**; for review, [7, 8]). Although eukaryotic ribosome subunits are in general larger than their prokaryotic counterparts (5500 total nucleotides and 78 Rps in *S. cerevisiae* versus 4567 total nucleotides and 58 Rps in E. coli), the high-resolution crystal structures of prokaryotic ribosomes fit the electron density from cryo-EM of eukaryotic ribosomes [9-11]. This is because ribosomal proteins and rRNA structures unique to eukaryotes are largely restricted to surface ‘‘expansion segments,’’ while the secondary and tertiary structures of the core, including the active site, are well conserved across all domains of life [12-16]. Despite these structural similarities, genetic and proteomic studies paint very

different pictures of the assembly processes in *E. coli* and *S. cerevisiae*. In contrast to the small number of nonessential assembly factors that have been identified in prokaryotes (for review, see [7, 8]), yeast ribosome assembly involves association with 200 mostly essential accessory proteins that are not part of the mature ribosome structure[17]. In the absence of just one of these proteins, ribosome biogenesis is stalled, and cell growth is terminated even under optimal growth conditions. Accessory factors required for eukaryotic ribosome assembly include NTP-dependent enzymes such as GTPases, ATPases, and kinases (**Fig. 1.1**). As such, these enzymes could stabilize or destabilize pre-ribosomal complexes at specific stages in the maturation through energetic manipulations during complex association and/or dissociation. They may also couple unfavorable maturation events to their favorable enzymatic activities. In the first part of this review, we provide an overview of the function of nucleotide-hydrolyzing enzymes in ribosome assembly. Next, we expand the commonly discussed classes of energy-releasing factors, to include RNA and protein modifying enzymes, which also have the ability to perturb free-energy landscapes. Finally, we discuss possible commonalities to explore why so much energy is released during ribosome assembly.

1.2 Classes of NTP Hydrolyzing Enzymes

Enzymes can change the free energy of a pre-ribosomal intermediate either by using chemical energy to perform mechanical work and remodel the RNA–protein complex (RNP), or by covalent modification of the intermediates. Of the ~200 ribosome assembly factors in *S. cerevisiae*, ~20% have gene ontology (GO) annotations [18] that identify

them as nucleoside triphosphate dependent enzymes such as GTPases, ATPases, and kinases, either through direct biochemical evidence or sequence homology with enzymes of known function. In addition, there are enzymes that utilize energy from non-nucleotide sources, at least in their direct interaction with the pre-ribosome. For example, endo- and exonucleases release energy stored in the phosphodiester bonds of the rRNA backbone. Additionally, methylases release the energy stored in S-adenosyl methionine (SAM) through methylation of rRNA. Finally, ubiquitin-conjugating enzymes and pseudouridylases likewise use high-energy bonds to modify components of pre-ribosomal complexes. Thus, the number of accessory factors with the potential to change the free-energy landscape of ribosome is higher than GO annotations imply. The following subsections review the classes of energy-releasing factors playing essential roles in eukaryotic ribosome assembly.

GTPases

GTPases have been studied extensively as their activity is central to cellular signaling, transport, cytoskeleton organization, and translation (for reviews, see [19, 20]. GTPases, like the other NTP-dependent enzymes discussed below, are P-loop NTPases. As such they contain a conserved nucleotide-binding domain, defined by the Walker A motif, responsible for binding of the α- and β-phosphates, and the Walker B motif, responsible for coordination of a Mg2+ ion that binds to the β- and γ-phosphates and participates in GTP hydrolysis. The GTP- and GDP-bound forms of these proteins differ in two exposed loops (the switch I and II regions) located on the surface of the molecule. These loops form part of the interface with effector molecules rendering their binding sensitive to the

nucleotide state. Because effectors bind more strongly in the GTP-bound state than the GDP-bound state, the GTP-bound form is considered the "active" state. Therefore, GTP hydrolysis "deactivates" the GTPase. GTP hydrolysis is stimulated by interaction with a GTPase activating protein (GAP). Unlike prototypical GTPases, the characterized GTPases in ribosome assembly bind nucleotides weakly and are thus not expected to be dependent on guanine nucleotide exchange factors to exchange GDP for GTP [21].

Yeast ribosome assembly requires the action of six GTPases: Bms1 for assembly of the 40S subunit; Nog1, Nog2, Nug1, Lsg1, and Ria1 for assembly of the 60S subunit (**Fig. 1.1**, shown in green; [22-31]. Interestingly, GTPases form the largest class of essential assembly factors in bacteria suggesting that their role is conserved. It is not known, however, if the essential functions of these proteins are in ribosome assembly or other cellular processes. Roles of GTPases in ribosome assembly have been recently reviewed in depth [21] and will not be further discussed here.

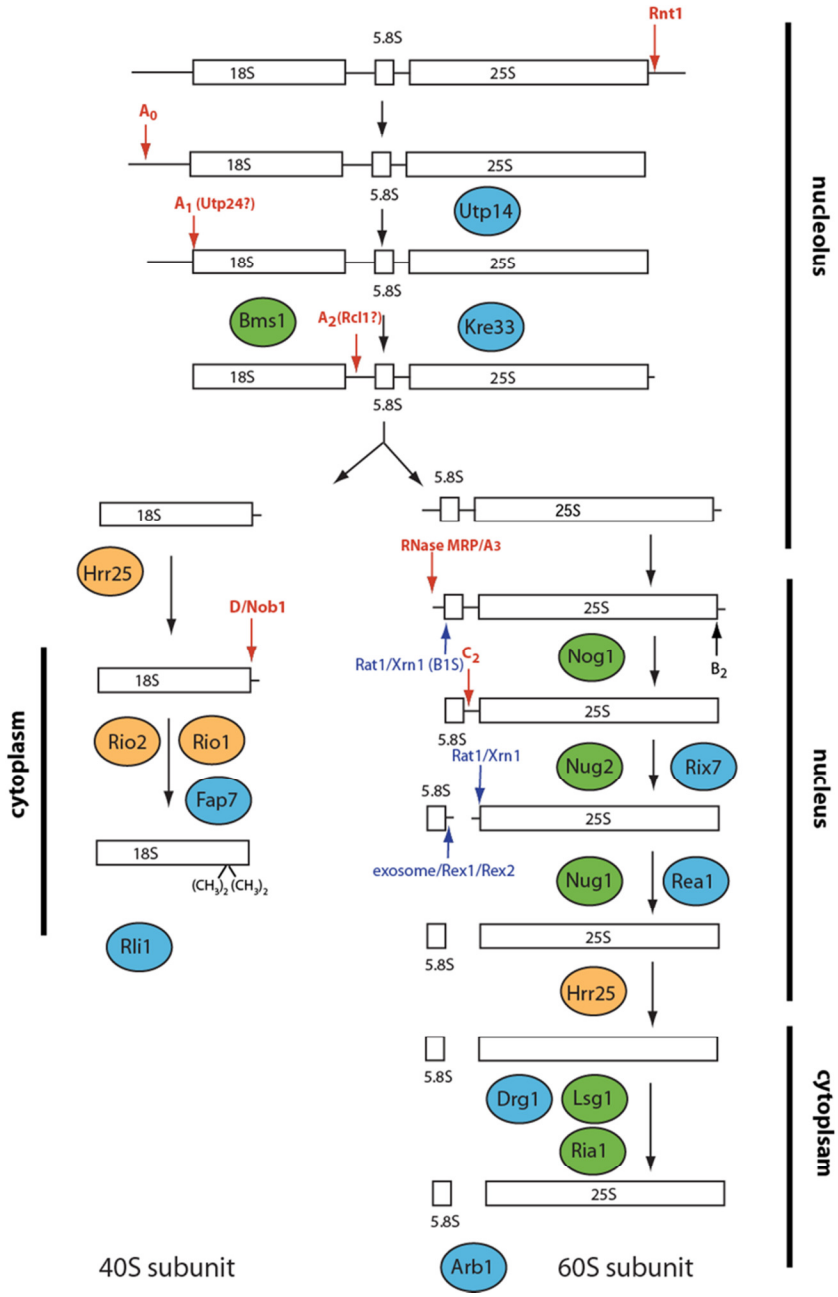

Figure 1-1 rRNA cleavage involves many steps and energy-consuming factors. Endo- and exonucleolytic steps are indicated by red or blue arrows, respectively. The steps are labeled with the name of the nuclease if known or suggested, or the name of the cleavage site. Cleavage at site A2 requires prior cleavage at site A1 [3], cleavage at site D requires prior cleavage at site A2 [6], and processing to site B1S requires prior cleavage at site A3 [6]. For simplicity only the major 60S processing pathway is shown. Putative ATPases are shown in cyan (for simplicity DEAD box proteins are omitted), GTPases are shown in green and kinases are shown in orange.

AAA^{+}-ATPases

ATPases associated with diverse cellular activities (AAA+-ATPases) perform a wide range of functions including protein unfolding, dissociation of protein–protein interactions, and unidirectional translocation along a track. These proteins are characterized by their nucleotide-dependent oligomerization into (usually hexameric) ring structures and the extensive conformational change they undergo during the ATPase cycle [32]. It appears that these conformational changes are transduced within the protein and to its substrate via the function of two sensor elements (which correspond to the switch I and II in GTPases and are also found in ABC transporters and some helicases), although the exact mechanism of mechano-chemical coupling is still debated. Rix7, Rea1, and Drg1 are AAA+-ATPases essential for assembly of the large ribosomal subunit in yeast (**Fig. 1.1**, shown in cyan; [33-35].

Depletion of Rix7 inhibits cleavage at the 3′-end of 5.8S rRNA, transport of pre-60S particles to the nucleus, and destabilizes 27SB pre-rRNA [33]. A synthetic lethal screen with the temperature-sensitive (ts) Rix7-31 identified a point mutation in Nsa1 (**Fig. 1.2**; [36]). These two proteins also interact in a yeast two-hybrid screen, although direct *in vitro* interactions could not be detected. Furthermore, while the majority of Rix7 is free in the nucleus, a small portion can be found associated (substoichiometrically) with Nsa1-containing pre-ribosomes, but not with other pre-ribosomal particles, indicating that this interaction is transient. Whereas in wild-type strains Nsa1 dissociates from pre-ribosomal particles in the nucleus, in cells containing a ts N-terminal truncation (Rix7Δ14N), Nsa1

is retained on cytoplasmic ribosomes and is even detected in polysomes, suggesting that removal of Nsa1 from pre-ribosomes is disrupted at the nonpermissive temperature [36]. Additionally, pre-ribosomal particles purified via TAP-tagging of assembly factors that act after Nsa1 are missing proteins when purified from the Rix7Δ14N background relative to wild-type strains, while pre-ribosomal particles purified via factors that act prior to Nsa1 accumulate additional proteins compared to the same particles from wild-type cells. Thus, recycling of Nsa1 coincides with a shift in the composition of nuclear pre-60S particles. Together, these data indicate that Rix7 interacts with a nuclear pre-60S particle via Nsa1 to facilitate recycling of Nsa1 and remodeling of the pre-ribosomal particle (**Fig. 1.2**; [36]). It remains to be seen whether the shift in pre-ribosome composition is the cause or a consequence of Nsa1 removal.

Rea1 is also required for 3′-maturation of 5.8S rRNA, but is a component of a later nuclear pre-60S particle that precedes association of the nuclear export adaptor Nmd3 [34, 37]. Addition of ATP, but not AMP-PNP, ADP, or GTP, to pre-ribosomes results in dissociation of Rea1p and Nog2p from this particle and may reflect an essential pre-export remodeling step coupled to ATP hydrolysis by Rea1p [34].

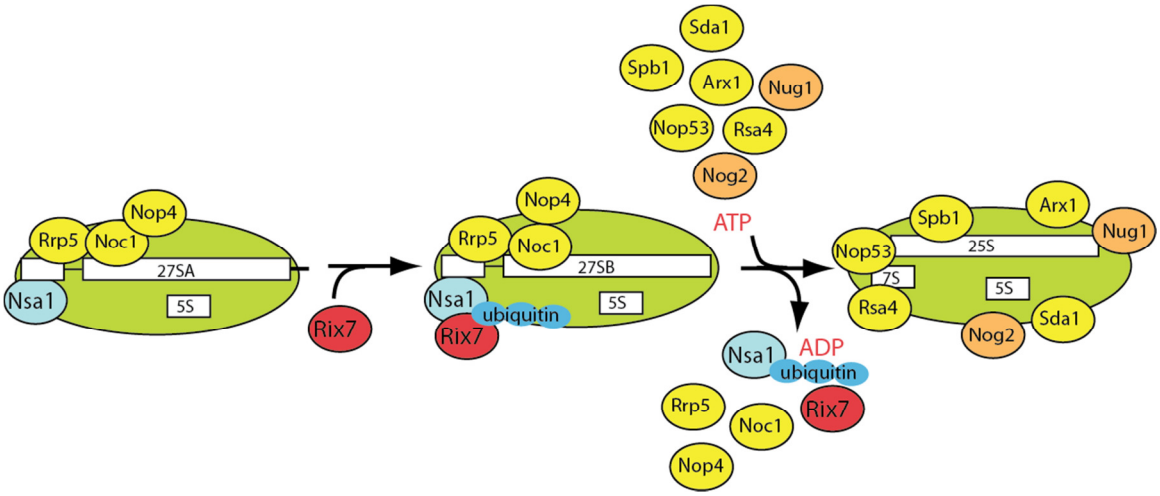

Figure 1-2 Model for Rix7 catalyzed remodeling of pre-60S subunits. Nsa1 binds to pre-60S subunits containing 27SA rRNA, other early 60S assembly factors including Rrp5, Noc1 and Nop4 are also bound to this intermediate. Rix7 interacts with Nsa1, potentially only in the ubiquitinated/sumoylated form, to remove it from pre-ribosomes (directly or indirectly). Nsa1 removal coincides with loss of the early 60S assembly factors Rrp5, Noc1 and Nop4, and allows binding of the later 60S assembly factors Rsa4, Nop53, Spb1, Nog2, Sda1, Arx1 and Nug1. Energy consuming assembly factors are shown in orange while other assembly factors are shown in yellow. Nsa1 and Rix7 are highlighted in blue and red, respectively.

Drg1 associates with 60S pre-ribosomes in the cytoplasm [35]. Inactivation of Drg1 leads to accumulation of Rlp24, Nog1, and Tif6 in the cytoplasm, and depletion from the nucleus [35]. Accordingly, the rRNA processing defects of these cells resemble Nog1, Rlp24, or Tif6 depleted cells.

A common theme for all three AAA+-ATPases is their proposed role in shifting the composition of pre-ribosomal assembly intermediates. It is tempting to speculate that these proteins are involved in breaking a number of very strong protein–protein or RNA–protein interactions (as in protein unfolding or SNARE dissociation), which could require hydrolysis of multiple ATP molecules.

DExH/D proteins

DExH/D ATPases are named for a conserved amino acid sequence in the Walker B motif and are further subclassified into DEAD, DEAH, and DExH branches. These families demonstrate different nucleotide specificities and different levels of basal ATPase activity and are thus believed to have distinct modes of action [38]. Because the ATPase activity of many DExH/D proteins is enhanced in the presence of RNA, they are also referred to as RNA-dependent ATPases. Several DExH/D proteins unwind RNA duplexes or disrupt RNA–protein interactions. In some cases, they facilitate duplex annealing and even disruption of protein–protein interactions, and some are simply ATP-dependent RNA-binding proteins (for review, see [39] [38]). All DExH/D proteins share a common fold created by two RecA-like helicase domains joined by a flexible linker [39, 40]. Functional specificity is conferred by variable extensions flanking the helicase domains [38, 40].

Although they share sequence similarity with helicases that couple ATP hydrolysis to unwinding of long duplexes, DExH/D proteins are not processive, consistent with the observation that RNA duplexes are typically short [41]. Furthermore, DEAD-box proteins do not translocate through a substrate duplex. Rather, they use single-stranded regions as binding platforms from which they can separate a nearby duplex by binding anywhere within that duplex, destabilizing it locally [41, 42]. This leads to unwinding of no more than two helical turns of a duplex in a single binding event. The lack of processivity is also consistent with a new view of the mechanism by which DEAD-box

helicases unwind duplexes. For at least a subset of DEAD-box proteins, ATP hydrolysis is neither coupled to nor required for duplex unwinding [42, 43]. Instead, duplex separation is induced by ATP-dependent binding to single-stranded RNA. ATP hydrolysis is required only for dissociation of the DEAD-box protein after unwinding. While the universality of this mechanism is still under investigation (especially for DExH proteins), it reconciles the finding that some DEAD-box proteins are merely ATP-dependent RNA-binding proteins [44]. In this new model, all DEAD-box proteins are ATP-dependent RNA-binding proteins, some hydrolyzing ATP to release single-stranded RNA. This new mechanistic insight also is consistent with the observation that nucleotide hydrolysis itself is not irreversible for these and other NTP-hydrolyzing enzymes, as that step is barely energetically favorable [45]. Instead, it appears that dissociation of one (or more) of the products is what renders these processes irreversible [46, 47].

Nineteen out of 37 DExH/D proteins encoded in the *S. cerevisiae* genome are involved in ribosome biogenesis, and 17 of these are essential (see Table 1; for review, see [48]). Seven (Dhr1, Dhr2, Dbp8, Rok1, Fal1, Rrp3, Dbp4) are required for SSU biogenesis [49-55], while eight (Dbp2, Dbp6, Dbp9, Mak5, Drs1, Dbp10, Spb4, Mtr4) are required for LSU biogenesis [56-63]. Prp43 and Has1 associate with, and are required for, both SSU and LSU biogenesis at stages after these subunits have entered separate processing pathways, suggesting that these proteins may have more general functions in the ribosome assembly process [63-68]. Interestingly, DEAD-box proteins are also among the identified bacterial assembly factors, pointing to conserved roles. Potential substrates

in ribosome assembly include “misfolded” rRNA–rRNA duplexes (see “Quality Control by Alternative RNA Structures,” below), duplexes between rRNA and small nucleolar RNAs (snoRNAs), as well as the more than 50 RNA-binding proteins associated with pre-ribosomal particles during assembly. The size, complexity, and dynamic nature of maturing pre-ribosomal particles, the host of potential cofactors, as well as the possibility that these proteins may act at stages that differ from where maturation stalls in their absence, all pose a tremendous challenge to investigators seeking to understand the role(s) of these proteins in ribosome biogenesis. In addition, a subset of these proteins may cooperate to some extent as they demonstrate synthetic lethal interactions and are associated in coimmunoprecipitation experiments [54, 63, 69].

Work in the Baserga laboratory has probed the function of DExH/D proteins involved in both SSU and LSU biogenesis using systematic mutagenesis of conserved residues in motifs responsible for ATP hydrolysis in each helicase [55, 63]. Unique rRNA processing defects were observed for these mutants, and most mutants were unable to support growth [55, 63]. This work has provided a wealth of information that will be of tremendous help to future researchers, however, definite roles for any of the investigated helicases have yet to be determined.

Seventy-five small nucleolar RNA (snoRNAs) of two different classes, box C/D and box H/ACA, are involved in yeast ribosome assembly. The three essential snoRNAs—U3, U14, and snR30—are required for early rRNA cleavage events [70-73], while the other

72 are nonessential and specify rRNA residues for methylation or pseudouridylation [74]. Because the duplexes formed between snoRNAs and rRNAs are extensive and, based on nearest neighbor rules, are expected to be stable for years, it is anticipated that *in vivo* duplex dissociation is accelerated by RNA helicases. Thus, much effort has concentrated on identifying DExH/D/snoRNA pairs. An *in vivo* screen by Tollervey and colleagues examined accumulation of snoRNAs in pre-ribosomal particles when DExH/D proteins required for maturation of the SSU were individually depleted [75]. While none of the 72 nonessential snoRNAs accumulated significantly in high-molecular-weight fractions in this screen, U3 and U14 accumulated in the absence of multiple DExH/D proteins. This finding could indicate that multiple helicases cooperate to dissociate these essential snoRNAs, or it could indicate that indirect effects can complicate such screens, for example, if dissociation of an upstream inhibitory structure is required for downstream dissociation of a snoRNA. One of the helicases required for proper distribution of U14, Dbp4, has been previously implicated in modulating U14's essential function through a genetic interaction with the U14 snoRNA [51], bolstering the argument that Dbp4 is required for U14 dissociation from pre-ribosomes [76]. Nevertheless, this example points to the importance of additional experiments to test and verify models suggested from such screens.

One such set of experiments includes the purification of native complexes associated with individual DExH/D proteins to narrow the field of potential substrates and cofactors of these proteins. This approach has been successfully used in the splicing field to assign

substrates to RNA helicases. Interestingly, Prp43p, which was not included in the screen for snoRNA accumulation, coprecipitates many box-C/D snoRNAs and a few box-H/ACA snoRNAs. The efficiency of the co-IP is increased in a cold sensitive (cs) mutant at low temperature [65-67]. At least one rRNA residue targeted by Prp43-bound snoRNAs is also undermethylated when the cs strain is grown at low temperature [67]. These results suggest that Prp43 may play a general role in modulating snoRNP dissociation, perhaps specifically box-C/D snoRNA dissociation, from ribosome precursors. Interestingly, Prp43 [65], as well as the snoRNA components Nop1, Cbf5, Gar1, Nhp2, and Nop56/58, interact with many Pol I transcription factors [77-82], indicating that snoRNA-directed rRNA modification (and snoRNA removal) could occur cotranscriptionally at some sites, akin to cleavage at site A2 [83].

A final class of experiments to delineate helicase/substrate pairs utilizes *in vitro* studies that evaluate ATPase and helicase stimulation upon binding to specific RNA substrates. These experiments are based on the assumption that the RNA substrate will bind more strongly to the helicase and/or better stimulate its ATPase activity. They are inspired by early experiments from the Fuller-Pace laboratory, which demonstrated that the ATPase activity of the bacterial DEAD-box protein DbpA is highly stimulated by a very specific hairpin structure in the 23S rRNA [84]. The advantage of such experiments lies in the rigor by which unwanted secondary effects can be excluded in a controlled system. However, the length of yeast pre-rRNA (~7000 nucleotides), its potential for alternative interactions, and the abundance of snoRNAs suggest that identifying the "right" substrate

might be akin to looking for a needle in a haystack. Consistent with this suggestion, a recent tour-de-force manuscript from the Uhlenbeck lab indicates that a specific RNA substrate was not found for any of the four tested helicases, despite screening of a large number of RNAs under a wide variety of conditions [85]. This finding shows that prior information will be required to fine-tune biochemical experiments in reconstituted systems. Interestingly, protein cofactors can increase the rate of ATP hydrolysis. For example, Ntr1 and Esf2 moderately stimulate the ATPase rates of Prp43 and Dbp8, respectively [86, 87]. These proteins may impart specificity, and knowledge of their binding sites may help in identifying helicase function.

While much progress has been made in developing tools to understand the roles that DExH/D proteins play in ribosome biogenesis, definitive assignments of substrates for these RNA-dependent ATPases will require combined approaches: Further *in vivo* investigations will be required to identify substrates and effectors for individual DExH/D proteins, which can then be included in biochemical experiments to extend and verify potential models.

ABC-ATPases

ATP-binding cassette (ABC)-ATPases are characterized by ATP-dependent dimerization of two nucleotide-binding sites harbored within one or two polypeptides, such that two ATP molecules are sandwiched between the two domains (for review, see [88, 89]. Each ATP is coordinated by residues from each opposing nucleotide-binding domain, and the two nucleotides make up approximately half of the area of the dimer interface [88].

Conformational rearrangements induced by ATP-dependent dimerization are transmitted to an effector domain. Classic examples of ABC-ATPases are membrane-associated transporters. However, there are soluble ABC-ATPases, two of which, Arb1 and Rli1, are essential for ribosome assembly (**Fig. 1.2**, shown in cyan; [90-92]. Mutation of conserved residues predicted to be involved in ATP binding and hydrolysis is lethal for both Rli1 and Arb1, suggesting that ATPase activity is central to the essential roles of both proteins [90, 93]. Rli1 was initially identified as a factor involved in translation initiation and co-purifies with the multi-subunit initiation factor eIF3 via direct interaction with the Hcr1 subunit [90-92, 94]. Not incidentally, the phenotype from deletion of Hcr1 resembles that from deletion of Rli1 [90, 95].

In a highly unusual manner, Arb1 and Rli1 are required for LSU and SSU rRNA processing and maturation; they are both shuttling proteins that mainly reside in the cytoplasm and are both required for export of nascent subunits [91-93] Furthermore, while Arb1 binds to pre-60S ribosomes, its depletion reduces the amount of 40S subunits relative to 60S. Similarly, Rli1 binds to pre-40S subunits, but its deletion reduces the amount of 60S subunits, indicating that these proteins may be involved in fine-tuning the relative levels of ribosomal subunits. Furthermore, the parallels in the observed phenotypes might reflect the similar functions of these factors.

While Arb1 is an essential protein, its depletion only leads to moderate defects in SSU and LSU rRNA processing [93], suggesting either that it acts after rRNA processing is

complete, or that its essential role is in a different cellular process (or both). Consistent with both of these possibilities, Arb1 interacts with the very-late cytoplasmic 60S assembly factors Tif6 (see **Fig. 1.5**, below) and Lsg1, as well as with several translation initiation factors, including the eIF3 complex, eIF2A and eIF4A, as well as Zuo1 and Ded1, both of which are typically involved in translation [93]. Rli1 depletion also has very moderate effects on pre-rRNA processing [92]. In contrast, the effects on translation initiation are much stronger and even observed in extracts [90]. Furthermore, it has been shown that deletion of Rli1 abolishes cell growth after only 4 h (less than two cell divisions), much faster than typically observed for ribosome assembly proteins. Because ribosomes are stable and effects on cell growth are only observed once existing pools of ribosomes are diluted via cell division, effects on cell growth are slow to emerge after depletion of ribosome assembly factors. The rapid manifestation of Rli1's growth defect further indicates that the essential function from Rli1 may be in translation initiation and not ribosome assembly.

Because both factors have such unusual pleiotropic effects on multiple steps in ribosome assembly and because they are both mainly cytoplasmic proteins that interact with very late cytoplasmic pre-ribosomes, we speculate that both proteins function in an as-yet-undiscovered “handoff” between the ribosome assembly machinery and the translation initiation machinery, perhaps removing a final set of “blocking” assembly factors to allow binding of initiation factors (see **Fig. 1.5**, below). This model would suggest the presence of a final check before ribosomal subunits are released into the pool of

translating ribosomes. The modest effects on ribosome assembly could then be indirect and due to reduced translation of mRNAs, 30% of which encode ribosomal proteins [96].

Protein Kinases

Protein kinases transfer a phosphate from ATP to a serine, threonine, or tyrosine (or, in rare cases, histidine) within a protein. This modification can affect a protein's activity, ability to interact with other proteins, and cellular localization. Controlled protein phosphorylation by vast networks of kinases is central to the regulation and coordination of cellular processes including metabolism, growth, differentiation, and response to stress [97, 98]. Although many proteins involved in ribosome assembly are phosphorylated *in vitro* [99] and *in vivo* [100, 101], the significance of these modifications and the kinases responsible for them remain largely unknown. Three essential kinases (shown in orange in **Fig. 1.1**) are involved in ribosome assembly in *S. cerevisiae*: Rio1, Rio2, and Hrr25. Rio1 and Rio2 facilitate SSU assembly, and Hrr25 is required for maturation of both subunits.

The right open (Rio) reading frame kinases are conserved from archaea to humans (for review, see [102]. Crystal structures of the archaeal Rio proteins indicate that these proteins possess a kinase-like fold, consistent with the conservation of amino acids required in all eukaryotic protein kinases (ePKs) [103, 104]. However, there are several differences between Rio kinases and ePKs: The Rio kinase domain is exceptionally short, lacking loops and helices highly conserved in most ePKs. Among the missing features is

the “activation loop,” which is regarded as essential for substrate binding and specificity in ePKs. Consistent with this finding, the structures of Rio kinases in the presence of nucleotide indicate that these proteins bind ATP in a more extended conformation than typical ePKs. Despite this divergence, it has been shown that Rio kinases can autophosphorylate [102, 103], although the rates for these phosphorylation events relative to conventional ePKs have not been determined. The Rio1 and Rio2 subfamilies are distinguished by conserved amino acids in their kinase motifs, indicating perhaps a different mode of activity, as well as a conserved N-terminal winged helix domain, a nucleic-acid-binding motif, found only in the Rio2 subfamily [104].

Rio1 and Rio2 are required for processing of the 20S rRNA. Rio2 is a stable component of pre-ribosomal particles containing the 20S rRNA precursor [69, 81, 105]. Rio1, in contrast, interacts only transiently with pre-ribosomes, as would be expected if Rio1 phosphorylates a pre-ribosomal component and then dissociates. Consistent with such a role, mutations in the Rio1 kinase domain abolish *in vitro* kinase activity and growth *in vivo*[106]. However, these data were obtained prior to knowledge of Rio1's essential role in ribosome assembly, and the specific effects of these mutations on ribosome assembly was not determined. As Rio1 is required for cell cycle progression [106], it cannot be ruled out that inactivation of Rio1's kinase activity disrupts an essential process other than ribosome assembly. A Rio2 mutant in which *in vitro* kinase activity is largely abolished can support growth, at least when the mutant protein is overexpressed [107]. A requirement for Rio2 but not its kinase activity could be consistent with an

inhibitory/regulatory role for this activity rather than an essential role. Persistent binding of Rio2 to the pre-40S complex may allow maintenance of inhibitory phosphorylation of some component of this complex, even in the presence of competing phosphatase activities. Removal of Rio2 or inhibition of its kinase activity might then be required for assembly progression. Alternatively, Rio2 may simply be an ATP-dependent RNA-binding protein, perhaps modulated by its own phosphorylation.

Hrr25 is one of four yeast homologs of mammalian casein kinase I and has documented roles in the DNA damage response, vesicle budding, meiosis, and cell survival during stress [108-111]. Hrr25 binds to 90S and 40S, as well as to 66S pre-ribosomes, and its depletion leads to 18S and 25S processing defects [112, 113]. Recent data from the Maitra and Tschocher laboratories suggest that cycles of phosphorylation and dephosphorylation, mediated by Hrr25, are required for export of both ribosomal subunits [112-114]. Hrr25 phosphorylates Tif6 at serine 174 *in vitro* and *in vivo* [113, 114]. Mutation of this residue to alanine prevents phosphorylation, traps Tif6 in the nucleus, and leads to defective 60S assembly [114]. The S174D mutation, mimicking a constitutively phosphorylated protein, is also inviable, indicating that dephosphorylation of Tif6 is also required for ribosome assembly [113, 114]. Similarly, phosphorylation and subsequent dephosphorylation of Enp1 and Rps3 are required for stable incorporation of Rps3 into the small subunit [112]. This phosphorylation is abolished in Hrr25 knockout cells, indicating that Hrr25 is either directly or indirectly responsible. Because Rps3 is linked to a stabilization of the beak, which protrudes from the SSU, its stable

incorporation could impede passage of this particle through the nuclear pore. Phosphorylation prior to and dephosphorylation following nuclear export might promote a conformational rearrangement that renders nuclear export irreversible [112]. Together, these data indicate that Hrr25 regulates (and perhaps synchronizes) the export of both subunits (**Fig. 1.5**, below).

Other ATPases

Fap7, Utp14, and Kre33 (**Fig. 1.1**, shown in cyan) have sequence homology with P-loop-type ATPases but do not fall into one of the classes described above. Utp14 and Kre33 are associated with early nucleolar pre-ribosomes and are required for assembly of the 40S subunit. Utp14 is required for the early nucleolar rRNA processing steps A0, A1, and A2, and its depletion leads to accumulation of the dead-end 23S rRNA, as found for most Utps [115]. A mutant form of Kre33 is defective in pre-40S export to the cytoplasm [116].

Fap7 is conserved from archea to humans and bears weak sequence homology with adenylate kinases and AAA+-ATPases. This protein is required for cytoplasmic cleavage at site D to produce the mature 3′-end of the 18S rRNA (**Figs. 1.1, 1.5**, below; [117]). Fap7 is believed to act through direct interaction with the small ribosomal protein Rps14, as these two proteins interact *in vivo* [69] and *in vitro* [117]. Rio2, an essential kinase discussed above, accumulates in pre-40S complexes in Fap7-depleted cells [117]. Fap7 may be involved in removing Rio2 from the pre-40S particle.

1.3 Enzymes Using Non-nucleotide Energy Sources

The enzymes discussed above promote ribosome assembly by binding and hydrolyzing or transferring the terminal phosphate of nucleoside triphosphates. However, modification of any component in a pre-ribosomal complex alters the free energy of that complex. Furthermore, principles of metabolism demonstrate that thermodynamically unfavorable reactions can be driven by coupling them to thermodynamically favorable, irreversible reactions, as long as the net process is favorable. Likewise, unfavorable manipulations of the pre-ribosome could be coupled to favorable or irreversible modifications. Any such modification, therefore, has the potential to destabilize or stabilize the formation of specific structures in the pre-ribosome, enforcing directionality of the maturation process. Outlined below are examples of such modifications in ribosome biogenesis.

Cleavage of polycistronic rRNA precursors

Synthesis of three rRNAs in a single transcript may be a strategy that evolved to coordinate synthesis of these molecules, reflecting the need for tight co-regulation of ribosomal components. In addition, however, phosphodiester cleavages during rRNA processing release energy stored in these bonds and are thus irreversible modifications (especially if one of the released pieces is degraded via the exosome or Rat1/Xrn1 nucleases). If rRNA cleavage steps are coupled to unfavorable steps in the assembly process, they could provide directionality to the maturation process. Perhaps this is why rRNA cleavage is performed in a stepwise fashion (**Fig. 1.1**), as it allows the energy to be harnessed at multiple points. Incidentally, these cleavage steps should then be regarded as potential regulatory points, as shown for the favorable steps in metabolic pathways.

Consistent with the idea of cleavage steps as energy-releasing control points, it has been shown that Rcl1, the candidate for the enzyme that catalyzes cleavage at site A2, requires the GTPase Bms1 for delivery to pre-ribosomes [30]. Furthermore, two Rio kinases and the ATPase Fap7 regulate cytoplasmic cleavage at site D [107, 117, 118]. We speculate that the strict ordering of cleavage in polycistronic rRNA precursors is imposed to take advantage of the irreversible nature of these steps at specific stages in the ribosome assembly process. Additionally, or alternatively, it has been suggested that ordering could help "proofread" the assembly of ribosomes [6]. Finally, in the even more complex mammalian system, there are more cleavage steps, perhaps to allow more irreversible steps that could provide for control points.

rRNA modifications

Modifications of specific rRNA residues, including pseudouridylation, 2′-O methylation, and base modifications (usually methylation), occur in all domains of life (for review, see [74]). Many of these modifications are clustered around conserved positions in the active site of the mature ribosome, and without them ribosome assembly and function are compromised [119-121]. Modest amounts of energy are released during each of these essentially irreversible modifications: methylation exchanges the high-energy bond in the SAM cofactor (generated in an ATP-consuming process) for a more stable bond to a rRNA base or ribose; pseudouridylation is an isomerization that converts uridine bases to pseudouridine. Pseudouridylation requires no energy input or cofactor but releases energy through the exchange of the N-glycosidic bond between the uracil and ribose for a lower-energy carbon–carbon glycoside bond [122]. Both modifications locally increase the

structural stability of the rRNA through enhanced intramolecular interactions such as hydrogen-bonding potential and base-stacking [122, 123]. Thus, strategically placed modifications may help shift the energetic landscape of the nascent ribosome to help enforce directionality, thereby favoring maturation. Although no single rRNA modification has been identified as essential, global disruption of rRNA methylation by point mutations in the modifying enzymes results in defects in ribosome assembly and function [124]. Furthermore, it has recently been shown that loss of the hypermodification of ψ1191 delays the conversion of 20S to 18S rRNA [125].

Further supporting the potentially important regulatory role of methylating enzymes are recent results obtained with Dim1/KsgA and Emg1/Nep1. Dim1 is responsible for the almost universally conserved dimethylation of two adenines near the 3′-end of the mature 18S rRNA [126, 127]. Although this methylation event is not strictly required, Dim1's association with the complex is essential [126, 127], and recent work with the bacterial homolog KsgA indicates that its binding prevents premature translation initiation [128], pointing to an important regulatory role. Interestingly, methylase activity is required to release KsgA [129]. The role of the putative methylase Emg1/Nep1 is more nebulous. A lethal mutation in Nep1 can be rescued by deletion of the snoRNA snR57, or by overexpression of the ribosomal protein Rps19 [130]. snR57 and Rps19 are predicted to bind near each other in the 3′ domain of 18S rRNA, which also contains an RNA sequence identified in a three-hybrid screen with Nep1 (**Fig. 1.3**; [130]). Together, these results suggest a model in which Nep1 competes with snR57, to facilitate the

incorporation of Rps19, possibly by effecting a conformational switch in the rRNA structure. In this model, snR57 negatively regulates this conformational switch, while Nep1 is a positive regulator. Rps19 is mutated in 25% of cases of the human blood disorder Diamond Blackfan Anemia [131], and mutations in Nep1 cause Bowan Conradi Syndrome, a disease with similar phenotypes [132], further supporting the importance of this step.

i. Post-translational modifications of ribosomal proteins and accessory factors

The principles that might allow rRNA modifications to assist in driving ribosome assembly also apply to post-translational modifications of proteins. Protein modifications in many cases trigger or abolish interactions with complex signaling networks. A number of ribosomal proteins and ribosome assembly factors are post-translationally modified. These modifications include phosphorylation, methylation, acetylation, ubiquitination, and sumoylation. Of these, phosphorylation (discussed above), ubiquitination, and sumoylation are perhaps the most intriguing because of potential relationships with well-characterized pathways in which these modifications play regulatory roles. Ubiquitin is an essential protein of 76 amino acids that can be covalently conjugated to substrate proteins [133, 134]. Ubiquitin conjugation begins with ATP-dependent activation of the ubiquitin polypeptide and culminates in ligation of ubiquitin's C-terminal carboxylate to a lysine in the target protein. As there are lysines within ubiquitin, polyubiquitin chains can be generated. In a similar process, sumoylation is the conjugation of a small ubiquitin-related modifier (SUMO) to lysines. Both of these modifications can be reversed enzymatically by deconjugating enzymes [133, 135]. Polyubiquitination is frequently a

signal directing proteasome-mediated degradation of the modified protein, but sumoylation, monoubiquitination, and polyubiquitination can also modulate protein function by altering conformation and/or ability to interact with other factors [136-138].

Ribosomal proteins and assembly factors have been identified in proteome-wide screens for ubiquitinated or sumoylated proteins [139-141]. Accordingly, rRNA transcription, early and late processing steps, and nuclear export of both subunits are influenced by the ubiquitin–proteasome system [141, 142]. Below we explore examples of how ubiquitination or sumoylation affect ribosome assembly.

Three of the four genes for ubiquitin in yeast are fusion proteins with ribosomal proteins [143]. Deleting the ubiquitin moiety from the Rps31–ubiquitin fusion leads to slow growth and accumulation of the 20S precursor to 18S rRNA, which is also incorporated into polysomes. Together, these results indicate that ubiquitination of Rps31 is important to ensure that only mature 40S subunits enter the pool of translating ribosomes [144].

Nsa1 exists in both ubiquitinated and sumoylated forms [36, 141]. Interestingly, the AAA+-ATPase Rix7, which directly or indirectly removes Nsa1 from the pre-60S particle (**Fig. 1.2**; [36]), is closely related to Cdc48, which powers the dissociation of ubiquitinated substrates from unmodified binding partners [145, 146]. It is speculated that ubiquitination and/or sumoylation of Nsa1 regulates its removal from the pre-ribosome by Rix7 [36].

Sumoylation of the 60S assembly factor Ebp2 weakens its association with the ribosome assembly factors Loc1 and Nop12, leading to preferential binding of factors involved in nonribosomal processes, including a mating type switch [147]. This finding suggests that sumoylation regulates Ebp2 binding to pre-60S ribosomes to allow cellular resources to be directed to other pathways under certain conditions.

F-box proteins provide target specificity for the Skp1-Cullin-F-box (SCF)-complex-mediated ubiquitination of proteins that are destined for degradation by the proteasome. The nucleolar F-box protein Dia2 interacts physically or genetically with 15 ribosome assembly factors [148-150], and its partners Cdc53 and Hrt1 bind three additional ones [148, 151]. In addition, Dia2 interacts with the cullin Rtt101 and Mms1. Both Rtt101 and Mms1 have been implicated in the destruction of nonfunctional ribosomes [152]. We speculate that SCF complexes containing Dia2 and Rtt101/Mms1 or Cdc53/Hrt1 target pre-ribosomes for destruction, either as part of a passive, constant degradation pathway [6], or as part of an active, targeted mechanism [153]. Together, these examples suggest that pre-ribosomes are polyubiquitinated and thereby targeted for degradation as part of quality-control pathways. In addition, ubiquitination and sumoylation are also used as reversible regulatory modifications, akin to phosphorylation

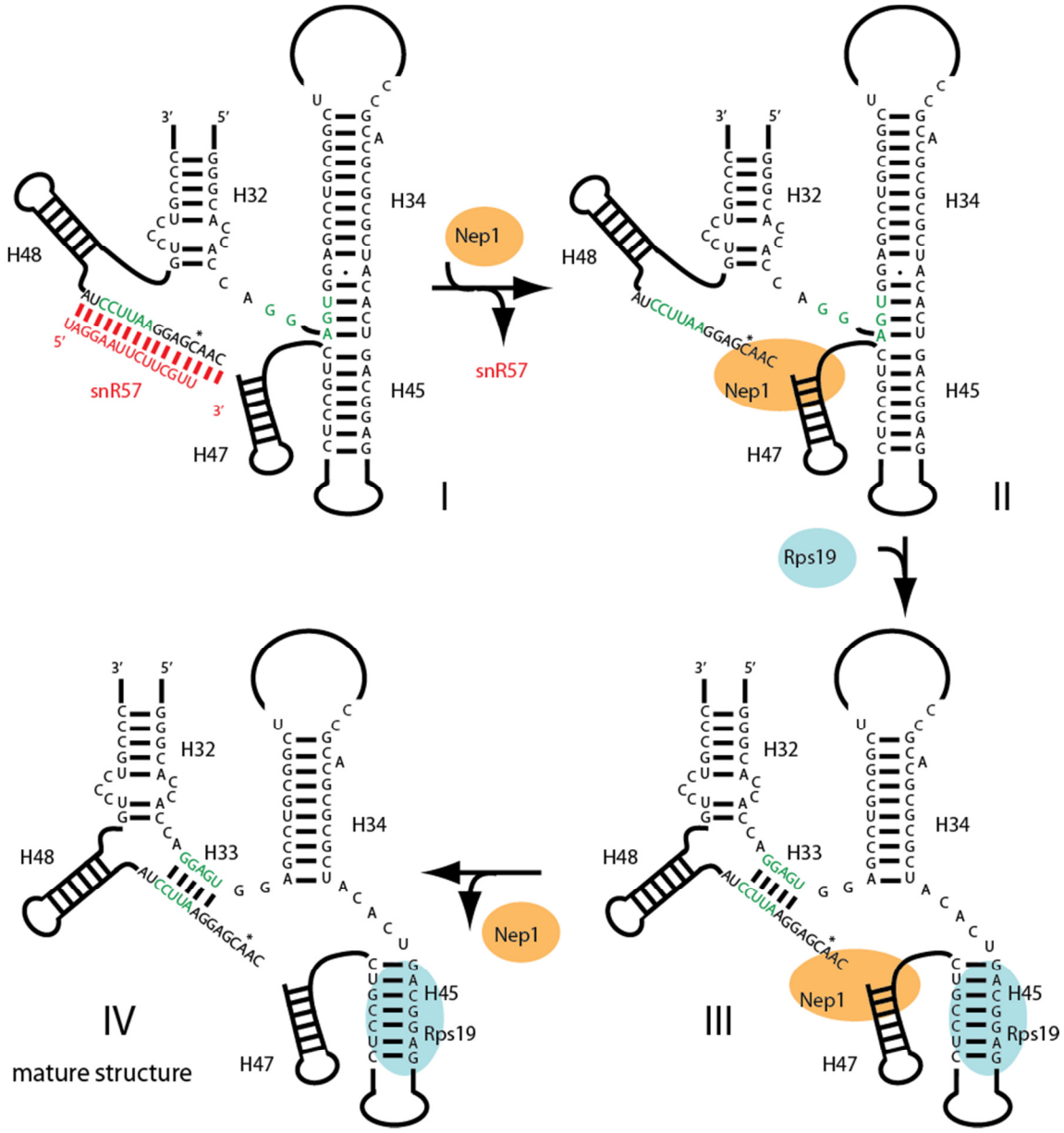

Figure 1-3 Model for a conformational change in the 3'-major domain of 18S rRNA induced by the methylase Nep1. snR57 (shown in red) binds to pre-18S rRNA (complex I) to methylate G1572, marked by an asterisk. This interaction prevents the formation of H33 in mature 18S ribosomes (shown in green in complex IV). Nep1 binds to the GCAACUU sequence highlighted in bold and could function to displace snR57, consistent with suppression of the Nep1 deletion by deletion of snR57. The ensuing formation of H33 (shown in green) allows binding of Rps19 (shown in blue) to its suggested site in H45, prior to dissociation of Nep1.

Protein folding: Protein-prolyl-isomerases (PPIs)

PPIs catalyze the cis–trans-isomerization of X-Pro peptide bonds, the rate-limiting step in folding of many proteins [154, 155]. As enzymes, PPIs do not change the free energy of a system. However, because they accelerate the rate of interconversion and may thus render assembly processes irreversible via kinetic means (by speeding by a branch point and avoiding misfolding), we will consider them here. Interestingly, the nucleolar yeast PPI Fpr3 and the nuclear Fpr4 together interact with 10 different ribosome assembly factors in large-scale studies [24, 65, 81, 82, 148, 156-158]. This suggests that they could play a substantial role in facilitating ribosome assembly. Furthermore, knockdown of the human PPI parvulin affects assembly of both ribosomal subunits [159], indicating that peptide bond isomerization could be important for ribosome assembly kinetics.

1.4 Why use so much energy?

In prokaryotes, *in vitro* reconstitution of functional ribosomal subunits from purified or *in vitro* transcribed rRNAs and recombinant or purified Rps has been demonstrated for both subunits with variable efficiency, and assembly maps for both subunits have been constructed [160-167]. In these systems an energy barrier can be overcome by heating or raising salt concentrations [160]. Thus, assembly of the prokaryotic ribosome (at least to the RI assembly intermediate) is determined and driven by the intrinsic properties of its component rRNAs and proteins. Consistent with this finding, only few assembly factors (other than rRNA-modifying enzymes and the nucleases required for cleavage of the polycistronic rRNA transcript) have been identified in prokaryotes [21, 168, 169]. These assembly factors include DEAD-box ATPases and GTPases.

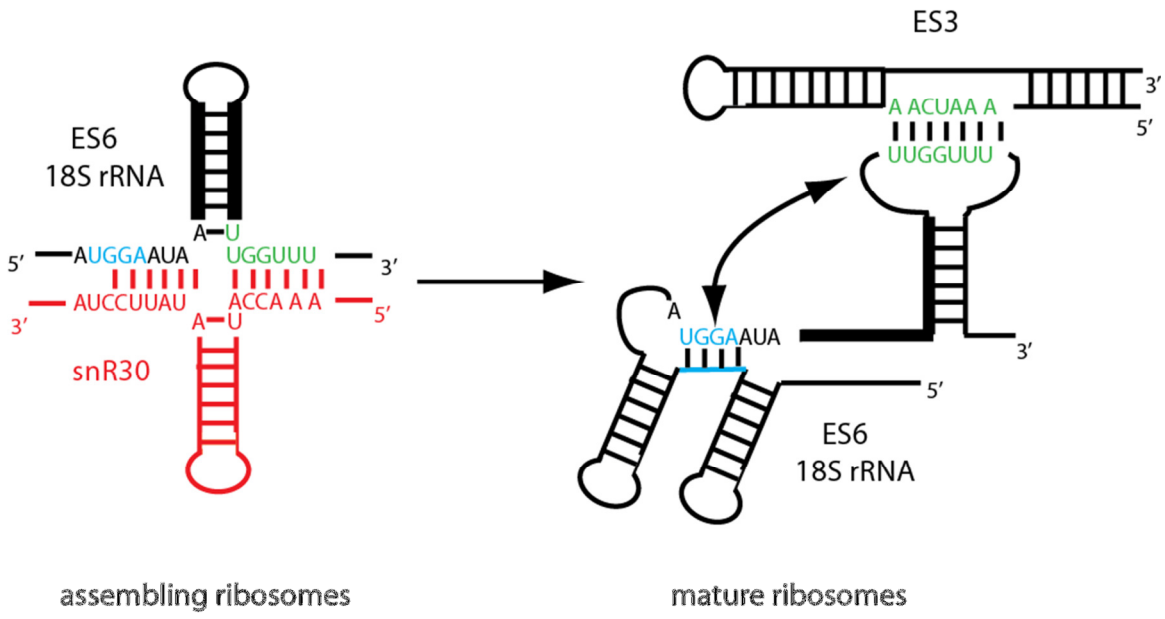

Figure 1-4 Dissociation of snR30 leads to a conformational switch in pre-ribosomes. Interaction of snR30 (in red) with expansion segment 6 (ES6) in 18S rRNA (Fayet-Lebaron et al. 2009) prevents the proposed interaction between ES6 and ES3 (green), as well as a suggested pseudoknot in ES6 (blue) (Alkemar and Nygard 2003; Alkemar and Nygard 2006).

While these cofactors enhance ribosome assembly *in vivo*, they are nonessential under normal growth conditions, which is perhaps surprising given the requirement for energy input into the *in vitro* system. Either these factors are redundant, or aspects of the *in vivo* assembly process eliminate the need for energy input. For instance, cotranscriptional assembly could simplify the assembly process by limiting potential interactions of the growing oligonucleotide: Correct rRNA structures can form before additional sequences that lead to off-pathway interactions are transcribed [170-172]. Additionally, each cleavage step of the polycistronic rRNA transcript *in vivo* produces irreversible steps as discussed above. Stages of structural maturation may be coupled to these cleavage events

imposing directionality on this process. Finally, subcellular compartmentalization, for example, tethering of the nascent pre-ribosomal complex to the rDNA from which it is being transcribed, may allow early maturation steps to be completed before components localized elsewhere are encountered, again minimizing the potential for off-pathway conformations [7, 17].

If prokaryotic and eukaryotic ribosomes do not differ extensively in complexity and prokaryotic ribosomes can largely self-assemble, why are so many energy-releasing enzymes required in eukaryotic ribosome assembly? The large number of essential assembly factors in eukaryotes may explain the need for energy input during the assembly process. By definition, ribosome assembly factors are temporarily bound to pre-ribosomes and not found in mature ribosomes. Numerous studies indicate that individual proteins associate with and dissociate from pre-ribosomal complexes at specific stages throughout assembly, often as part of smaller subcomplexes (for review, see [173]). If ribosome binding by an assembly factor is thermodynamically stable at one point but unfavorable at another, the relative free energies of the bound and dissociated states must be altered in the meantime. Energy-releasing assembly factors could accomplish this. But then we are left with the question: Why do eukaryotes power an essentially spontaneous process? Here we consider three (not mutually exclusive) answers: (1) intracellular export, (2) quality control, and (3) integration with other cellular processes. It should be noted that some of these have been outlined previously by Tollervey and coworkers [7].

Intracellular transport

Eukaryotes bear the added burden of exporting maturing ribosomal subunits from the nucleus to the cytoplasm. While this certainly accounts for some of the additional energy input as exemplified by Hrr25, it does not explain all of it. In fact, the separation of early and late stages of ribosome assembly by the nuclear envelope should simplify the assembly process by preventing encounter of the nascent rRNA with late-binding, cytoplasmic, ribosomal proteins [6, 7], and by conferring directionality to the process.

Quality control

One explanation for the great expansion of ribosome assembly factors in eukaryotes is that the greater complexity of eukaryotic cellular processes and tighter regulation of gene expression demand greater fidelity of translation. Mistakes in translation may have far more catastrophic implications for a multicellular organism than for a bacterium. In addition, 80% of mRNAs in yeast are present in less than two copies/cell [174], suggesting that sequestering of a transcript could have profound consequences on the proteome of a cell [6]. Eukaryotic accessory factors may facilitate more stringent quality control in ribosome biogenesis or, minimally, provide alternative mechanisms for this control [7]. Outlined below are potential quality-control mechanisms that require energy input into ribosome assembly.

Alternative RNA structures

rRNA sequences may have evolved to prevent aberrant or premature rRNA duplex formation through sequestering of key rRNA segments in alternative duplexes either

within the nascent rRNA or with specific snoRNAs. Such a role has been proposed for the essential snoRNA U3, whose binding prevents the formation of the central pseudoknot, an essential tertiary structure motif in the SSU [175]. Recent data suggest such a similar role for another essential snoRNA, snR30 (**Fig. 1.4**). Kiss and coworkers recently showed that snR30 binds two elements in ES6, an expansion segment present in eukaryotic rRNA [176]. Intriguingly, one of the two snR30 base-pairing sites in ES6 has previously been suggested to form a long-range tertiary interaction with ES3, which would tie together the central and 5′-domains via an interaction on the "foot" of the small ribosomal subunit [177-179]. Binding of snR30 would prevent this interaction, and the timing of its release is likely to coincide with a major folding event, perhaps even the release of U3 snoRNA, as formation of the central pseudoknot is also expected to position the subdomains of 18S rRNA with respect to each other. The activity of specialized helicases would be required to disrupt these duplexes and might explain the function of at least a subset of the 17 DExH/D proteins in ribosome assembly. Analogously, during spliceosome assembly, the helicase Brr2 disrupts the stable U4/U6 duplex to allow for formation of the alternative U2/U6 duplex, which forms the active site [180]. Interestingly, the Brr2 helicase is controlled in multiple layers via Prp8 [181], a long-enigmatic protein at the heart of the spliceosome, as well as by ubiquitination [182]. Analogous regulatory switches may exist in ribosome assembly. Each helicase may require "specificity" factors, thus explaining the existence of a further subset of the nearly 200 eukaryotic accessory factors.

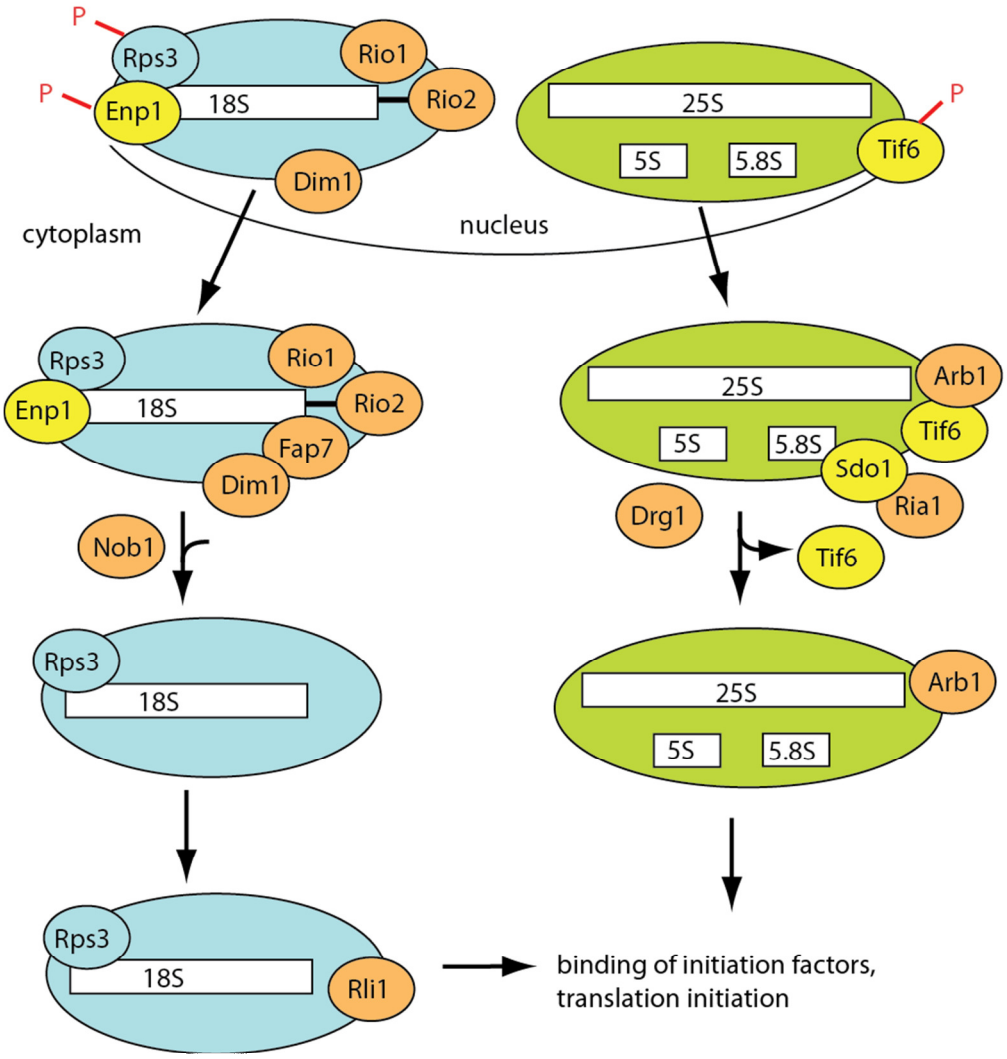

Figure 1-5. Late cytoplasmic assembly intermediates are regulated in multiple layers. 40S subunits are shown in blue and 60S subunits and shown in green. Energy-consuming assembly factors are shown in orange, select other assembly factors in yellow. Phosphorylation of Enp1, Rps3 and Tif6, catalyzed by Hrr25, and subsequent dephosphorylation, are required for maturation and export of the 40S and 60S subunits, respectively. Nob1-dependent cleavage at the 3'-end of 18S rRNA is regulated by the kinases Rio1 and Rio2, and the ATPase Fap7. The binding site for the bacterial homolog of Dim1, KsgA overlaps with the binding site for IF3, indicating that Dim1-containing ribosomes cannot initiate translation. Rli1 binds to both pre-ribosomes and eIF3, indicating a link between assembling and initiating ribosomes. Release of Tif6 requires binding of the Shwachman-Diamond protein Sdo1, perhaps to recruit the GTPase Ria1, which can remove Tif6 from ribosoms in vitro. In addition, Drg1 is required to release Tif6 from pre-ribosomes. Arb1 binds to pre-ribosomes containing Tif6, but also interacts with initiation factors, linking the ribosome assembly and translation machineries.

Checkpoints

Binding of accessory factors may also prevent downstream events by physically blocking the binding of ribosomal proteins or other assembly factors. This could be used as a quality-control mechanism if correct completion of a certain assembly step is required for removal of the roadblock. Such a mechanism could account for the presence of assembly factors as well as energy-releasing enzymes to remove them. As described above, the binding sites for RNA methylase KsgA/Dim1 and translation initiation factor IF3 overlap, suggesting that KsgA/Dim1 binding prevents translation initiation by immature ribosomes. This roadblock has a built-in switch, as methylation is required for KsgA release [129]. It is tempting to speculate that similar roles are played by Rlp7, Rlp24, and Mrt4, ribosome assembly factors with high sequence similarity to the ribosomal proteins Rpl7, Rpl24, and P0, respectively. In this model, removal of assembly factors is required for incorporation of essential ribosomal proteins and could thus provide a checkpoint for correct assembly.

Cooperativity in binding of assembly factors

Literature data suggest that the ribosome assembly machinery is organized in a highly cooperative manner. While the enzymatic function of several proteins is dispensable at least for a short time, deletion of these proteins leads to severe assembly defects [126, 127, 183-189]. For example, it has been shown that inactivating Dim1 has no effects on ribosome assembly, while deletion is lethal [126, 127]. Furthermore, electron microscopy has shown in several cases that the SSU processosome at the 5′-end of nascent transcripts is disrupted when just one protein is missing [83, 190-193]. This suggests that there is

substantial cross talk between factors. This observation could account for the many "glue" proteins, which have no function detectable by bioinformatics other than to bind to other proteins. One possible reason for this remarkable cooperativity is the heightened potential for quality control, as all aspects of the nascent ribosome can be checked simultaneously and forward progress can be stalled if mistakes were made. A less cooperative machinery might allow assembly to progress even if one factor is missing. Interestingly, this observation could also indicate that removal of just one protein would destabilize the entire complex, explaining, perhaps, why the use of the powerful hexameric AAA+-ATPases is restricted to later 60S assembly intermediates, which may be assembled less cooperatively.

Degradation of misassembled ribosomes

A passive kinetic quality control system has been proposed, wherein each step of ribosome assembly competes with degradation [6]. In that model, the longer a ribosomal intermediate takes to transition from one stage to another, the more likely it is to be degraded. This mechanism would lead to quality control, as assembly mistakes or missing factors slow down conversion steps, sending a larger fraction of assembly intermediates to the decay pathway. Consistent with such a view, literature data show 10 physical interactions between energy-consuming regulatory ribosome assembly factors and the TRAMP complex or the exosome, including three with the small subunit assembly factors Kre33, Dhr1, and Rli1 [80-82, 151, 194]. A passive quality-control system may be enhanced by energy input according to the classic principle of kinetic

proofreading [195]. Binding of specialized "assembly" factors to undesired structures may also trigger active degradation [153, 196, 197].

Multilayered control mechanisms for late cytoplasmic assembly intermediates

The cytoplasmic assembly steps of both ribosomal subunits are especially highly regulated (**Fig. 1.5**). Cytoplasmic maturation of 40S subunits involves the action of two ATPases, Fap7 and Rli1, and all three kinases required for ribosome assembly, Rio1, Rio2, and Hrr25. Similarly, the cytoplasmic portion of 60S subunit maturation requires the activity of two GTPases (Ria1 and Lsg1), two ATPases (Drg1 and Arb1), and the kinase Hrr25. The necessity for the intricate regulation of these late steps may arise because by the time they reach the cytoplasm, pre-ribosomes are largely assembled and may have some mature functionalities. Furthermore, they can encounter mature subunits to join for translation, if not properly safeguarded. In this context, the number of regulatory interactions with Tif6 is especially intriguing, because Tif6 binding to 60S ribosomes prevents the binding of 40S subunits [198] Thus, removal of Tif6 should only occur if ribosomes are fully matured. Tif6 removal is likely catalyzed directly by the GTPase Ria1 [25]; however, the ATPase Drg1 appears to be upstream of this process as mutations also lead to Tif6 accumulation in cytoplasmic pre-ribosomes [35]. Tif6 is also the direct target of the export-regulating kinase Hrr25 [113, 114]. Finally, the severe growth defect caused by deletion of Sdo1 can be rescued by mutations in Tif6p that weaken its association with the pre-60S particle [199]. Sdo1 interacts with Ria1 [80], suggesting that it may help recruit Ria1 to pre-ribosomes. Mutations in human homolog of Sdo1 cause Shwachman–Diamond Syndrome [200], a rare blood disease that

predisposes to cancer and is caused by bone marrow failure, providing further evidence for the importance of regulation in Tif6 removal.

Integration with other cellular processes

Another reason for the expanded repertoire of eukaryotic ribosome assembly factors may be the increased need to coordinate ribosome assembly with other cellular processes such as stress response, growth state, cell cycle progression, etc. These points of cross talk are most likely to occur at the energy-releasing steps, which impart the ability to temporarily stall this process at specific stages under adverse conditions. Some examples of such cross talk have even been documented in bacteria, where GTPases involved in ribosome assembly also regulate cell cycle progression and sporulation [21]. In principle, such cross talk could occur via two means. First, components shared between ribosome assembly and other cellular processes could provide for direct cross talk between such processes. Second, signaling networks could affect ribosome assembly and other processes. Such signaling networks may involve kinases or other post-transcriptional modifications such as ubiquitination. Data in the literature indicate that both mechanisms occur, as outlined below.

Cross talk of ribosome biogenesis through shared components

Examples of cross talk between ribosome assembly and other cellular processes mediated through shared components include replication, rRNA transcription, tRNA export, cell cycle control, and stress response (e.g., [106, 201-207], and this cross talk is more

evolved in higher organisms. Because the connection to the cell cycle has been recently and expertly reviewed [208, 209], it will not be covered here.

Fap7, Yar1, and Ltv1 have been implicated in late 40S assembly and the response to oxidative and osmotic stress [112, 117, 210]. Deletion of the nonessential Yar1 and Ltv1 render yeast hypersensitive to oxidative stress, while mutations in Fap7 were identified in a screen for mutants defective in activation of the Skn7 transcription factor, which regulates both the osmotic and oxidative stress response [211]. Furthermore, oxidative stress also leads to nuclear accumulation of Dim2 [193]. These results suggest that oxidative stress inhibits 40S assembly, perhaps not unexpected, given the observation that oxidative stress downregulates transcription of Rps and ribosome assembly factors [212].

Co-regulation of pathways

Co-regulation of biochemical pathways can also occur via simultaneous phosphorylation of components of multiple pathways via the same kinase. While there is good evidence that ribosome assembly is regulated by phosphorylation, the exact kinase cascades and, indeed, the targets of that phosphorylation have not been determined in most cases.

Nutrient availability affects transcription rates of rRNA and r-protein mRNAs [212, 213]. Furthermore, splicing of ribosomal proteins is also sensitive to nutrient availability [214]. The production of ribosomal components and the assembly of these components are

directly regulated by the Tor-pathway [215], although the exact mechanisms of this regulation remain obscure. Localization of the RNA-binding proteins Dim2, Rrp12, and the GTPase Nog1 are affected by inhibition of this pathway [193, 216]. However, it is not clear that either protein is a target of the Tor kinase (or downstream effectors), and the observed effects might be due to phosphorylation and inactivation of other ribosome assembly factors. Nevertheless, these data provide strong evidence that assembly of both ribosomal subunits is directly responsive to nitrogen deprivation and inhibition of the Tor pathway.

Intriguingly, another Tor-target, Atg1, which is a regulator of the starvation induced autophagy pathway, phosphorylates 11 ribosome assembly factors *in vitro* (although eight of them are nuclear proteins and Atg1 is thought to be a cytosolic protein) (Table 2; [99]. Furthermore, Gcn2, a kinase activated by amino acid deprivation, and its cofactors Gcn1 and Gcn20 interact genetically as well as physically with more than 20 ribosome assembly factors, including four nucleotide-utilizing enzymes, indicating that these proteins may regulate ribosome assembly (Table 2; [24, 69, 80, 81, 157, 194]. We speculate that nutrient stress may result in phosphorylation and inactivation of ribosome assembly proteins.

Perhaps most suggestive is the potential co-regulation of ribosome assembly and invasive growth, a response to nutrient stress, during which yeast cells fail to separate after division, creating long multicellular chains that invade their growth medium. Recent

work has shown that the nonessential kinase Ksp1 is required for the invasive growth pathway [217]. Ksp1 translocates to the nucleus during invasive growth, and nuclear localization is required for invasive growth, suggesting that at least a subset of its substrates are nuclear proteins [217]. Ksp1 phosphorylates eight 40S and four 60S assembly factors *in vitro* [99] and interacts with the 60S assembly factors Sdo1 and Dbp7 *in vivo* (Table 2; [80, 148]. Furthermore, reduction of Rps26 and deletion of the 40S component Asc1 both abolish the invasive growth pathway [218, 219]. Finally, a large-scale mutagenesis approach has identified genes required for invasive growth. While ribosome assembly factors are underscreened (because they are essential), mutations in Utp5, Utp7, Utp10, Brix1, and Nog2, as well as in 10 r-proteins with two orthologs (including Rps26), abolish invasive growth, indicating that ribosome assembly is essential for invasive growth [220]. This is perhaps surprising given that invasive growth is a response to nitrogen limitation. We speculate that invasive growth and ribosome assembly are somehow co-regulated via the action of Ksp1. Alternatively, it is possible that Ksp1 up-regulates ribosome assembly under conditions that induce invasive growth, and that the reduction in ribosomal subunits is responsible for the observed invasive growth deficiency in Ksp1 mutant strains.

Table 2 also illustrates interactions between growth-promoting pathways and ribosome assembly, including the protein kinase C (PKC) and casein kinase 2 (CK2) pathways. PKC binds or phosphorylates six energy-consuming ribosome assembly factors (Table 2), and PKC phosphorylates 16 additional assembly factors *in vitro* [99]. In addition, the

RNase III Rnt1 interacts with the PKC regulatory subunit Bcy1 [82]. While most of these interactions are not validated, they are consistent with the known influence of the PKC signaling pathway on transcription of ribosomal components.

Data in the literature document physical interactions between CK2 and eight energy-consuming assembly factors (Table 2), and 17 other assembly factors. Interactions with Utp18 and Utp22 are found with each one of CK2's four subunits, and Nop7 and Nop12 show genetic or direct physical interactions with three subunits. The interaction between Utp22, Rrp7, CK2, and the r-protein transcription factor Ifh1 has been validated, and it has been suggested to provide an interface for co-regulation of rP transcription and ribosome assembly [205]. Furthermore, interactions between Rio1 and CK2 depend on Rio1's C-terminal tail, and CK2 phosphorylates six serines in that tail *in vivo* and *in vitro* [221]. Serine-to-alanine mutation produces a slow-growth phenotype and leads to cell cycle phenotypes similar to those seen in the Rio1 deletion [221]. Finally, phosphorylation activates Rio1's kinase activity, indicating that the CK2 pathway could activate 40S assembly by modulating Rio1's activity in response to optimal growth conditions.

1.5 Perspective

Work over the last decade has re-created the ribosome assembly field, demonstrating that in eukaryotes, ribosome assembly is much more complex than indicated by the facile reconstitution of ribosomal subunits from bacteria. Almost 200 protein and many RNA cofactors for ribosome assembly have been identified, most of which are essential *in vivo*,

and it is likely that most ribosome assembly factors have already been identified. In addition, for many assembly factors, it is known whether they are required for assembly of the small or large ribosomal subunit and roughly at which step in the respective assembly pathway they act. More recently, work has started to identify subcomplexes, functional and physical units within assembling ribosomes. This work is the first step in attacking the next frontier: establishing the function for these assembly factors. Much work to date has focused on the NTP-dependent factors discussed herein, simply because of their potential importance as regulatory enzymes, and much progress has been made. Nevertheless, the molecular details of the function of many proteins and how their interplay is managed remains elusive and will be exciting to follow in the future. A second frontier is to understand how ribosome assembly is regulated in living cells. This will be a prerequisite for targeting this pathway with drugs, a potentially fruitful area, due to the importance of ribosome assembly for cell growth. Furthermore, the link between defects in ribosome assembly and cancer marks this pathway as a new target for anti-cancer drugs. As described above, the literature points to several pathways as potential regulators. It will be exciting to learn which assembly factors are targeted, if multiple targets exist, and what the composition of these signaling networks is.

Table 1.1: DExH/D Helicases Involved in *S. cerevisiae* Ribosome Assembly

Protein	Classification	Null Phenotype	Target Ribosomal Subunit	ribosome biogenesis/rRNA processing defect	Suggested Function	References
Dbp8p	DEAD Box	Inviable	SSU	A0, A1, A2 inhibited[b]		[54]
Dbp4p	DEAD Box	Inviable	SSU	A0, A1, A2 inhibited[*]	U14 removal	[51, 76]
Dhr1p	DEAH	Inviable	SSU	A1, A2 inhibited[b]		[53]
Dhr2p	DEAH	Inviable	SSU	A0, A1, A2 inhibited[b]		[53]
Rrp3p	DEAD Box	Inviable	SSU	A0, A1, A2 inhibited[b]		[50]
Rok1p	DEAD Box	Inviable	SSU	A0, A1, A2 inhibited[*]	snR30 removal	[49, 52, 75]
Fal1p	DEAD Box	Inviable	SSU	A0, A1, A2 inhibited[b]		[222]
Prp43p	DEAH	Inviable	SSU and LSU	A0, A1, A2 inhibited, reduced 20S and 7S[†]	snoRNA removal	[65-67]
Has1p	DEAD Box	Inviable	SSU and LSU	A0, A1, A2 inhibited, 27SA3 and 27SB accumulation[*]		[64]
Dbp3p	DEAD Box	Viable; synthetic slow growth with Dbp7p	LSU	A3 inhibited or delayed, 27SA2 accumulation[*]		[223]
Dbp6p	DEAD Box	Inviable	LSU	decreased 27SA2, 27SB, 7S[*]		[224]
Dbp7p	DEAD Box	slow growth, synthetic enhancement with Dbp3p	LSU	decreased 27SA2, 27SB, 7S[*]		[225]
Dbp9p	DEAD Box	Inviable	LSU	decreased 27SA2, 27SB, 7S[*]		[54]
Mak5p	DEAD Box	Inviable	LSU	60S subunit deficit[†]		[226]
Drs1p	DEAD Box	Inviable	LSU	60S subunit deficit[†]		[57]
Dbp2p	DEAD Box	Inviable	LSU	60S subunit deficit, suspected A3 cleavage defect[†]		[62]
Spb4p	DEAD Box	Inviable	LSU	27SB accumulation[†]		[56, 58]
Dbp10p	DEAD Box	Inviable	LSU	27SB accumulation, C1 and C2 cleavage defect[b]		[61]
Mtr4p	DExH	Inviable	LSU	7S accumulation, required for exosome-mediated 3'-end processing of 5.8S rRNA	part of the TRAMP complex	[59]

**Deletion phenotype*
[†]Point mutation or conditional mutant phenotype
[a]Dominant phenotype from point mutations after 48 hours

Table 1.2: Interactions between Energy Consuming Assembly Factors and Protein Kinases

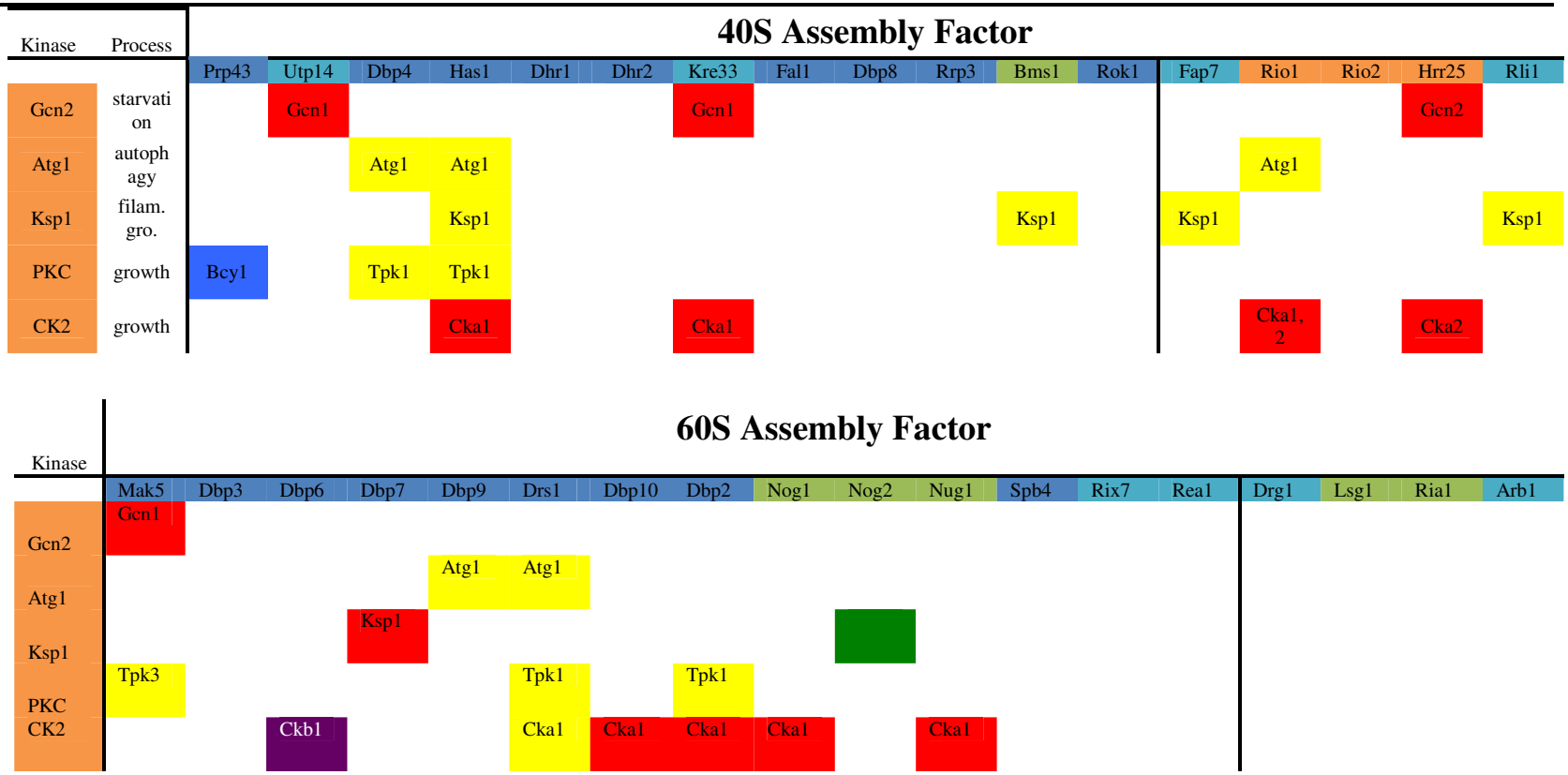

Physical Interactions are shown in red, *in vitro* phosphorylation is shown in yellow, genetic interactions are shown in purple, and interactions in protein complementation assay are shown in blue. NTP-utilizing assembly factors are color-coded dark blue for DExH/D ATPases, light blue for other ATPases, green for GTPases and orange for kinases.

Chapter 2

Ribosome Assembly Factors Prevent Premature Translation Initiation by 40S Assembly Intermediates

2.1 Introduction

In eukaryotes, the assembly of the ribosomal subunits from the four rRNAs (18S, 5.8S, 25S and 5S) and 78 ribosomal proteins is facilitated by a conserved macromolecular machinery comprising ~200 assembly factors (AFs). These proteins, mostly essential, catalyze the modification, cleavage from precursor transcripts and folding of the rRNA, and facilitate the binding of ribosomal proteins [227]. While the components of this assembly line have been identified, their functions remain largely unknown. Pioneering cryo-EM studies [10, 228-232] followed by the crystal structures of prokaryotic [233-236] and very recently of eukaryotic mature ribosomes [237, 238] have provided functional insight to the complex architecture. However, little is known about the structure of assembly intermediates, or the binding sites for AFs.

While most ribosome assembly steps take place in the nucleolus, where rRNA is transcribed, the final maturation steps of both subunits occur in the cytoplasm. There, assembling ribosomal subunits encounter large pools of mature subunits, mRNA, and translation factors, representing a unique challenge: the prevention of premature translation initiation on immature subunits. This is of particular concern for assembling 40S subunits, as translation initiation factors, mRNAs and the 60S subunit all bind to 40S

subunits to initiate translation, and furthermore, because premature 40S ribosomes, when incorporated into 80S ribosomes, are rapidly degraded [239]. These considerations suggest the existence of mechanisms to prevent 80S formation before 40S maturation is complete. Here we report the structure of a late, cytoplasmic pre-40S assembly intermediate. Our results show that bound AFs are positioned to cooperatively prevent each step in the course of translation initiation: the binding of initiation factors, the opening of the mRNA channel, the joining of 60S subunits, and finally the formation of the decoding site.

2.2 Results

Using cryo-electron microscopy (cryo-EM), we have determined, at 18 Å resolution, the structure of a late pre-40S ribosome assembly intermediate, purified from *S. cerevisiae* via Tandem affinity purification (TAP) of the complex associated with TAP-tagged Rio2, an essential kinase required for 18S rRNA production (**Fig. 2.1, Appendix - Figure S1**). As expected [112], this particle includes seven stably bound AFs: the methylase Dim1, the endonuclease Nob1, which produces the mature 3'-end, its regulator Pno1 (also referred to as Dim2), as well as the kinase Rio2, the GTPase-like protein Tsr1, the export adaptor Ltv1, and Enp1, a protein of unknown function (**Fig. 2.1A**). Furthermore, all small subunit ribosomal proteins (Rps), except Rps10 and Rps26 are present (**Appendix - Table S1**). The 3D cryo-EM reconstruction, as well as 2D class averages of negative stained particles (**Appendix - Fig. S2**) clearly show all features of the mature small subunit (SSU): the head, beak, platform, left and right foot [240].

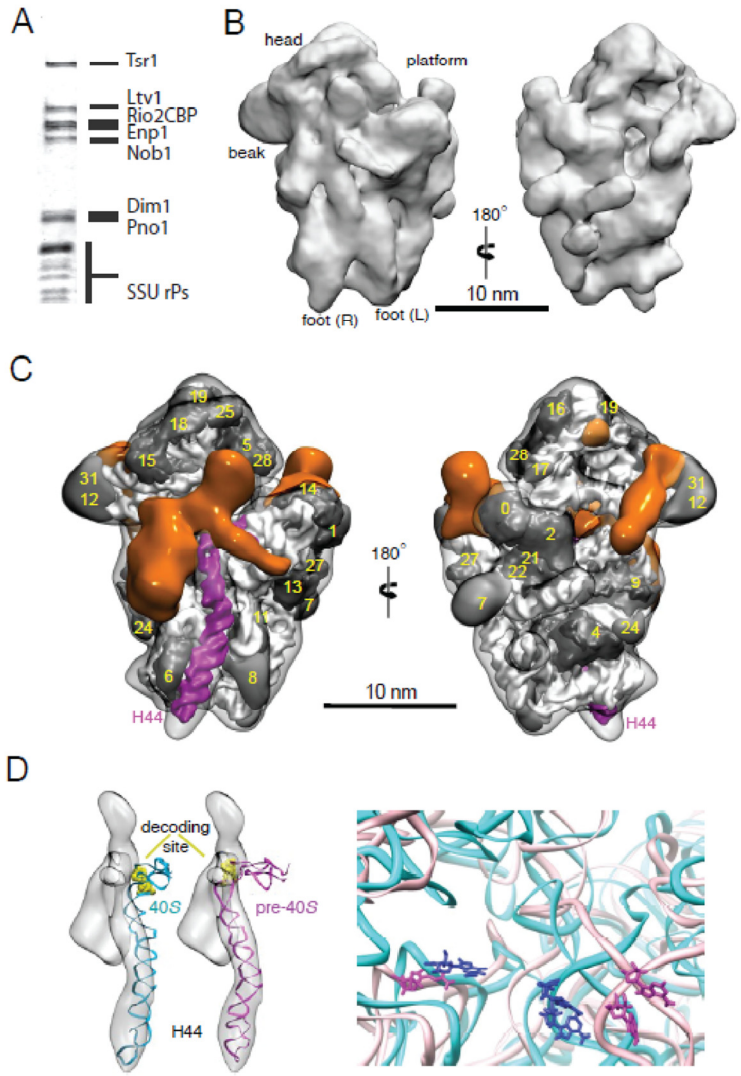

Figure 2-1 Molecular architecture of late pre-40S ribosomes. (A) SDS-PAGE analysis of pre-40S particles purified via Rio2-TAP. (B) 18Å cryo-EM reconstruction of pre-40S particles purified via Rio2-TAP. (C) Densities of AFs (in orange) revealed after explicit-solvent molecular dynamics flexible fitting (MDFF) of the structure of mature 40S ribosomes into the cryo-EM map. rRNA is shown in white, Rps are shown in graphite and are annotated as in (13). H44 and H45 are highlighted in magenta. Subunit (left) and solvent (right) interface views are shown. (D) H44 is distorted in pre-40S particles. Rigid-body docking of the mature H44 structure (cyan) does not fit the corresponding density in the cryo-EM map (gray). MDFF allows for improved fit of H44 (magenta), accompanied by a change in the positioning of the decoding site residues (yellow). Close-up view reveals that the distance between G577 and A1755 is increased from 3 to ~4.5 nm in the pre-40S (magenta) or mature 40S (cyan) ribosomes.

For a better interpretation of the EM densities, we applied explicit-solvent molecular dynamics flexible fitting (MDFF) [241-244] to fit an atomic model of the mature 40S ribosome into the cryo-EM map (**Appendix - Fig. S3&4**, see Materials and Methods).

Subtraction of the resulting model from our reconstruction clearly revealed the densities corresponding to AFs, which are located in three major regions (orange in **Fig. 2.1C**): on the subunit interface, at the back of the beak, as well as on the back of the platform. All of these regions are important for translation initiation as discussed below. In addition, MDFF allowed us to characterize a major difference in conformation between mature and pre-40S particles at the upper part of H44, which affects the decoding site region, as discussed below (**Fig. 2.1D**).

To assign the extra densities to individual AFs, we individually depleted (or deleted) the assembly factors Nob1, Rio2, Tsr1 and Ltv1, and determined the cryo-EM structures of the resulting particles to resolutions of 20 Å, 22 Å, 26 Å and 20 Å, respectively (**Fig. 2.2A,B, S5-10**). Comparisons, including *t*-test difference mapping, of the wild type cryo-EM map with maps of partial particles lacking individual AFs allows for localization of factors. *E.g.* in the Nob1 depletion, Nob1 was the only missing protein, allowing us to unambiguously assign its density at the platform. In contrast, in the Rio2 depletion, Nob1 and Dim1 were also missing. In that case, additional information from previous footprinting data was used to assign the two possible densities to Dim1 and Rio2. This assignment was also aided by the available crystal structures for Dim1 and Rio2, which fit the assigned densities well with cross correlation values of 0.854 and 0.904, respectively (**Fig. 2.2C and Appendix - Fig. S8**).

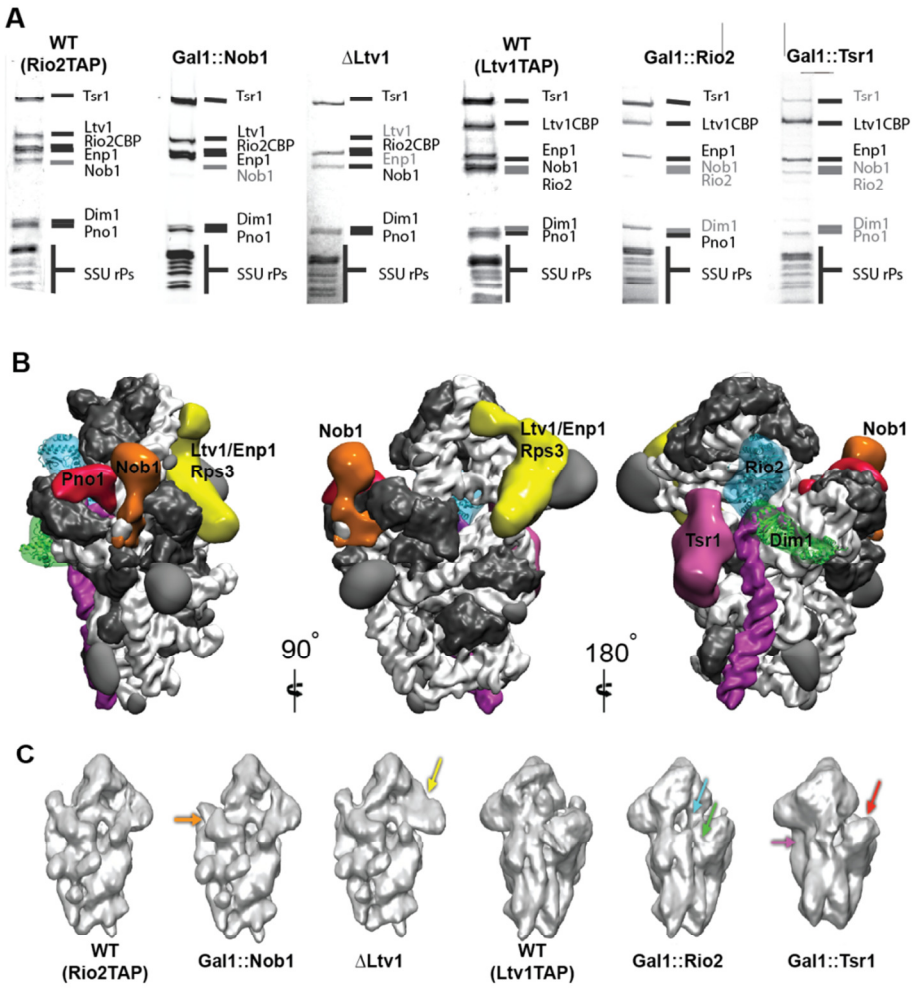

Figure 2-2 Assigning assembly factors to premature densities (A) SDS-PAGE analysis of wild-type Rio2TAP, Gal1::Nob1, Δ-Ltv1, wild-type Ltv1TAP, Gal1::Rio2 and Gal1::Tsr1 used in the cryo-EM shows depleted and co-depleted proteins. (B) cryo-EM maps for the wild type, Gal1::Nob1, Δ-Ltv1 (solvent view) and wild type, Gal1::Rio2, Gal1::Tsr1 (subunit view) pre-40S particles identify densities belonging to individual assembly factors (See also **Appendix - Fig. S5-S14**). Colored arrows point to the missing densities with color-coding as in (C). (C) Positioning of AFs on pre-40S particles. The structures of archeal Rio2 (blue) and human Dim1 (green) are docked within the corresponding cryo-EM densities.

In addition, we obtained a 30 Å 3D reconstruction of negative stained recombinant Tsr1 (**Appendix - Fig. S11-12**), and employed antibody labeling against Ltv1 and Enp1 (**Fig. S13&14**) to substantiate our assignments for Tsr1, Ltv1 and Enp1 (see Supplementary Materials for a detailed discussion on AF assignment). These results are summarized in **Figure 2.2C**. Importantly, these placements are largely consistent with previous cross-

linking data, as well as a systematic analysis of protein-protein interactions [[245-248], **Fig. S15&16**, see supplemental discussion].

The cryo-EM maps show that the AFs on the subunit interface, Rio2, Tsr1 and Dim1 overlap the binding sites of translation initiation factors eIF1, and eIF1A (**Fig. 2.3A**), as previously shown for the bacterial homologs of Dim1 and eIF1 [128]. Furthermore, the binding sites for the nuclease Nob1 and its regulator Pno1 overlap the binding site for eIF3 at the platform (**Fig. 2.3B**). Thus, recruitment of initiation factors that directly bind to the 40S subunit is prevented by the joint activity of Nob1, Pno1, Tsr1, Dim1 and Rio2.

During translation initiation, recruitment of the mRNA to the 40S subunit is facilitated by the activity of eIF1 and eIF1A [5]. Their joint binding promotes a conformational switch in the 40S subunits, whereby the mRNA channel opens up, breaking the latch between helix 18 and helix 34 (**Fig. 2.3C**). This opening is stabilized on the solvent side by a hinge formed between the beak and shoulder region [5] (**Fig. 2.3D**). The Enp1/Ltv1/Rps3 complex at the back of the beak overlaps the bridge formed upon mRNA channel opening (**Fig. 2.3D**). Furthermore, the latch on the front site is closed in pre-40S particles (**Fig. 2.3C**). Thus, the structure suggests that opening of the mRNA channel is inhibited by the Enp1/Ltv1/Rps3 complex.

Despite the abundance of mRNAs and 60S subunits, 80S ribosomes are rarely (<10% of particles) observed in pre-40S purifications. Depletion of Tsr1 from the pre-40S particle leads to a >7-fold increase in peptides of ribosomal proteins from the 60S subunit (Rpl)

that co-purify with pre-40S subunits, such that the number of Rpl peptides is similar to that of Rps peptides, and co-purifying Rpl4, Rpl5 and P0 are identified by SDS-PAGE (**Fig. 2.2A, 2.4A**). Furthermore, the amount of 25S rRNA is increased 20-fold (**Fig.2.4C**), and 80S particles are frequently observed in cryo EM images upon Tsr1 depletion (**Fig. 2.4B**). To confirm that depletion of Tsr1 leads to formation of 80S ribosomes containing pre-40S-bound Ltv1 *in vivo*, we carried out sucrose gradient analysis to separate free proteins from 40S, 80S and polysome fractions, and used the TAP-tag on Ltv1 to probe for its localization. As expected, depletion of Tsr1, but not Rio2, shifts Ltv1 from being exclusively bound to a 40S-like particle to an 80S particle, indicative of 60S subunit binding (**Fig. 2.4D**). Northern analysis confirms that this 80S particle contains 20S and 25S rRNAs, indicating that it is not a 90S pre-ribosome, which would contain 35S rRNA, but not 25S or 20S rRNAs (**Fig. 2.4E**). This is also confirmed by Northern analysis of the TAP purification, which shows no 35S pre-rRNA in any strain (data not shown). Tsr1 and Pno1 are both depleted in the Tsr1 depletion but present in all other purifications, and therefore could both contribute to this effect. Alternatively, the loss of all interface-binding AFs together could also be responsible for this effect. Pno1, but not Tsr1, can be found in polysome fractions (data not shown, [117, 249]), indicating that the presence of Pno1 does not antagonize 80S formation. Furthermore, depletion of human Tsr1 leads to increased turnover of cytoplasmic 40S pre-ribosomes, as expected when pre-40S ribosomes form inactive 80S ribosomes, which are degraded by the no-go pathway [250]. These data indicate that Tsr1 inhibits the premature association of 60S subunits with pre-40S subunits in the cytoplasm. This anti-subunit-association activity of Tsr1 can be readily explained by the large surface it occupies on the subunit interface, and is

analogous to that performed by eIF6 and Nmd3 for late cytoplasmic 60S precursors [198, 251, 252]. We also note however that Tsr1 does not provide a complete block to 60S joining, as low amounts of 60S subunits can be found co-purifying with wild type Rio2TAP pre-40S subunits, consistent with the previous observation that low amounts of Nob1 and 20S rRNA can be found in polysomes [239].

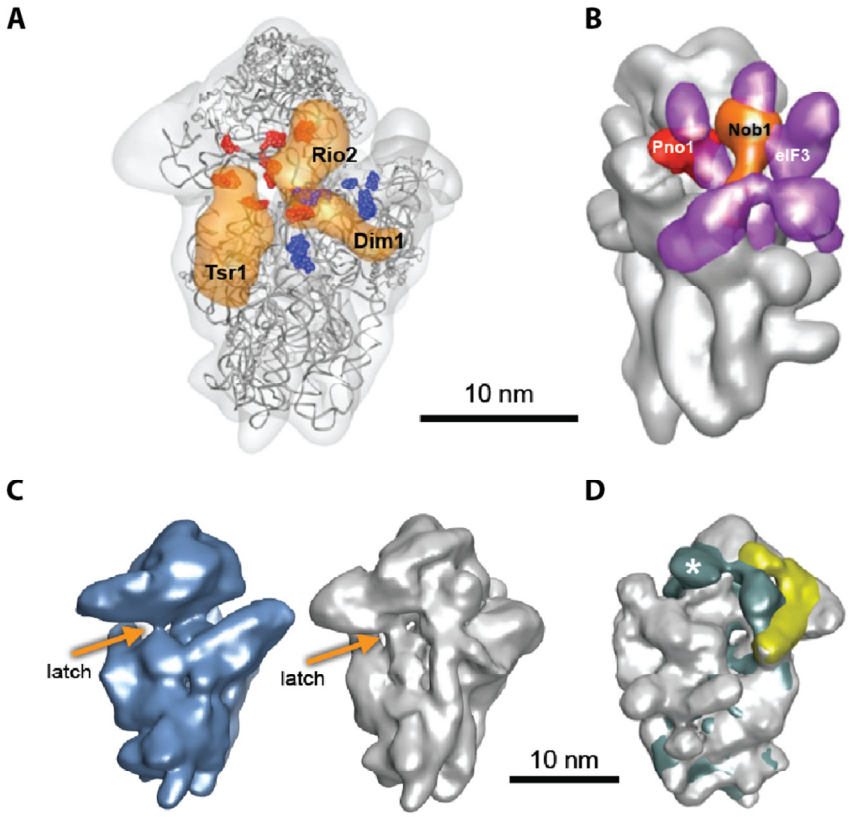

Figure 2-3 Assembly factors obstruct translation initiation factor binding sites, and prevent mRNA binding. (A) Tsr1, Rio2 and Dim1 block binding of eIF1 and eIF1A. Sites of RNA footprints from Fe-labeled eIF1 and eIFA are shown in red and blue, respectively [1, 2]. (B) Nob1 and Pno1 block binding of eIF3. Nob1 and Pno1 densities are shown in orange and red, respectively. The density for eIF3 [4] is shown in purple. (C) The latch between H18 and H34 closes the mRNA channel in mature [5, 6] (blue) and pre-40S ribosomes (grey). The Tsr1 density was removed here to allow for better visualization of the latch. (D) Overlay of the structure of mature 40S ribosomes with eIF1 and eIF1A bound [5] (in aqua) and pre-40S particles (grey) shows that the hinge on the back of the beak (aqua) and the density for the Enp1/Ltv1/Rps3 complex (yellow) partially overlap. RACK1 is present only in mature 40S and its density is indicated with an asterisk.

During decoding, A1755/A1756 flip out of H44 and G577 rotates around the glycosidic bond to interrogate the mRNA/tRNA base pair by hydrogen-bonding with the minor groove [253]. The cryo-EM map of the pre-40S particle shows that H44 is kinked in the lower part, which drives the upper portion outwards and to the left (from the perspective of the 60S subunit). As a result, the nucleotides that make up the decoding site are displaced from their location in mature 40S subunits as indicated by the cryo-EM density (**Fig. 2.1D**). Importantly, A1755/A1756 and G577 move into opposite directions (**Fig. 2.1D**) so that their distance increases, thereby precluding interactions of all three nucleotides with the mRNA/tRNA duplex. Thus, the shift in H44 disrupts the decoding site and prevents the subsequent steps leading to peptide bond formation.

2.3 Discussion

Collectively these data indicate that in a highly redundant and multi-pronged approach all seven late-binding cytoplasmic ribosome AFs contribute to chaperoning pre-40S subunits to prevent them from prematurely engaging the translational apparatus. In this model, binding of translation factors eIF1, eIF1A, and eIF3 is precluded by binding of Dim1, Tsr1, Rio2, Pno1 and Nob1, while opening of the mRNA channel is prevented by binding of Enp1 and Ltv1 (**Fig. 2.3**). Tsr1 blocks the premature binding of 60S subunits (**Fig. 2.4**), and the decoding site is disrupted as a result of a prominent kink in H44 (**Fig. 2.1**). Bacteria lack all of these factors, with the exception of Dim1, which blocks binding of IF3, the homolog of eIF1 [128]. However, during 30S assembly in bacteria the GTPase Era binds to the anti-Shine-Dalgarno sequence [254]. Since bacterial mRNA recruitment occurs via base pairing between Shine-Dalgarno and anti-Shine Dalgarno sequences,

binding of Era might prevent mRNA recruitment [254] analogous to Enp1 and Ltv1, although by entirely different mechanisms. Overlapping the function of Era is RbfA, whose binding to the bacterial SSU leads to a deformation in H44 similar to the one observed here. Interestingly, the binding site for RbfA is similar to the Pno1 binding site [255]. Thus, it seems possible that the function of AFs is conserved between kingdoms, but different proteins have evolved to maintain these functions, reflecting the differences in the translation initiation pathways. The lack of redundancy in prokaryotes might reflect the fact that SSU assembly intermediates in polysomes are not as efficiently degraded in bacteria [256], as they are in eukaryotes [239].

Rps10 and Rps26 are the only ribosomal proteins that are not yet bound to the late pre-40S particles examined here (**Appendix - Table S1**), consistent with the observation that their depletion does not stall processing of the 18S precursor, 20S rRNA [188]. Furthermore, binding of Rps26 to 20S rRNA is negligible and does not increase when 20S rRNA is accumulated, indicating that Rps26 binds after formation of 18S rRNA [257]. Rps26 binds on the platform [238], where it overlaps the binding sites of Pno1 in the pre-40S particle (**Fig. S17A**), indicating that Rps26 cannot bind before Pno1 dissociates. Similarly, Rps10 binds to the beak, overlapping the binding sites for Ltv1/Enp1 (**Fig. S17B**). Incorporation of these Rps might be a final regulated step in 40S assembly.

Furthermore, although Rps3 is present in pre-40S particles (**Appendix - Table S1**), the cryo-EM map shows that it is not occupying its final position (**Fig. S17C**). This finding is

consistent with previous data suggesting that in this pre-40S particle, but not mature 40S ribosomes, Rps3 is salt labile [112]. Additionally, Rps14 is repositioned on the platform, consistent with previous findings that the interactions of its C-terminal extension with rRNA form late during ribosome assembly [187]. The late assembly of both the platform region, where Rps26 and Rps14 bind, as well as the head/beak region, where Rps10 and Rps3 bind, is paralleled in the *in vitro* assembly of the bacterial SSU, where the head and platform region are the last to form, and intermediates lack the homologs for Rps14, Rps26, and Rps3 [258].

Nob1, the nuclease for cleavage at the 3'-end of 18S rRNA, is present in the late pre-40S particle purified here, yet, the particle only contains the 20S rRNA (**Fig. 2.4B**), and Nob1 does not cleave even after addition of Mn^{2+}, a known cofactor (unpublished results). These findings suggest that either an external signal is required to activate Nob1, or that Nob1 is mispositioned in the presence of these assembly factors and thereby inactive. Previous *in vivo* and *in vitro* footprinting show that Nob1 protects the active site [259], and the EM-map shows that Nob1 is positioned in proximity to the cleavage site (**Fig. 2.2**), suggesting that any rearrangement, if it occurs, is limited. The C-terminal extensions of Rps14 and Rps5 are important for D-site cleavage and engage rRNA immediately prior to that step [187, 260].

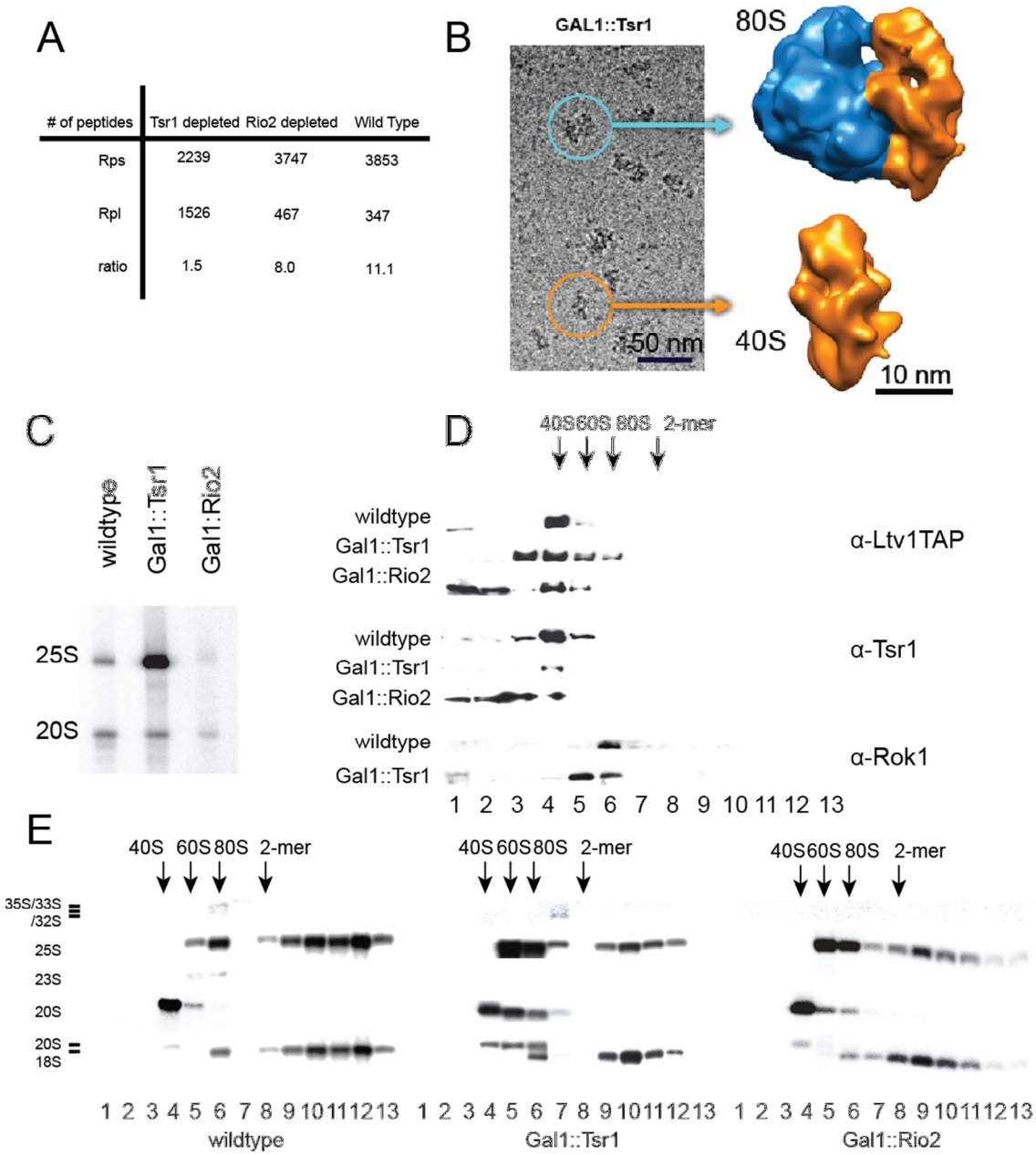

Figure 2-4 Tsr1 blocks 60S subunit joining. (A) Peptides from ribosomal proteins belonging to the large subunit (Rpl; identified by mass spectrometry) co-purify heavily with pre-40S particles purified from Gal1::Tsr1 strains, but not from the wild type control, or the Gal1::Rio2 strain. (B) 3D cryo-EM reconstructions confirm that larger particles in Ltv1TAP purifications from Gal1::Tsr1 cells are 80S particles. (C) Northern blotting shows that 25S rRNA from the large subunit co-purifies with pre-40S particles in Gal1::Tsr1 cells relative to wild type or Gal1::Rio2 cells. (D) Western blot of fractions from 10-50% sucrose gradients demonstrates that Ltv1TAP shifts from being bound only to 40S-preribosomes to 80S fractions when Tsr1 is depleted, but not when Rio2 is depleted. (E) Northern probing on gradient fractions demonstrates that 80S fractions in the Tsr1 depleted strain contain 20S and 25S rRNA, but not 35S or 23S pre-rRNA. The position of 40S, 60S and 80S fractions determined by absorbance is indicated. Fig. S19 shows the absorbance profiles from these gradients.

The data presented here provide important clues about triggers for rearrangements that could reposition Nob1 and its essential effector Pno1, as well as Rps5 and/or Rps14. Previous work has shown that the bacterial homolog for Dim1 is inhibited by ribosomal protein S21. Although bacterial S21 has no eukaryotic sequence homolog, its binding site is almost identical to that of Rps26, suggesting that Rps26 is a functional homolog of S21 [238]. We show that Pno1 occupies the Rps26 binding site in pre-40S particles (**Fig. S17A**). Because Pno1 binds directly to Nob1, and affects its interaction with rRNA [248], reverse communication from the Dim1 site could reposition Pno1, thereby regulating Nob1.

Interestingly Dim1 itself is positioned to receive signals regarding assembly of the head/beak region, which is shown here to be incomplete, as Rps10 is absent and Rps3 is not fully incorporated: Binding of the bacterial homologs for Rps3, and its direct binding partners Rps20 and Rps29, to the head of the SSU stabilizes an RNA conformation that inhibits the activity of Dim1's bacterial homolog at the subunit interface [261]. Thus, completion of head assembly could trigger changes at the Dim1 site, which could be relayed to reposition Pno1 and Nob1 for final pre-rRNA cleavage.

Chapter 3

Biochemical Characterization of Fap7's Nucleotide Binding and ATPase Activity

3.1 Introduction

More than 30 NTP utilizing enzymes are required during assembly of the large and small ribosomal subunits [227]. Their exact roles and the nature in which the energy released by each of these proteins is utilized are in many cases still not known. At least three ATP utilizing enzymes are required in the transition from the stable, late cytoplasmic 40S assembly intermediate to mature ribosomes. One of these, Fap7, has sequence homology to AAA-type ATPases and adenylate kinases, although its sequence is distinct from both classes of proteins [262, 263]. Depletion of this protein or mutation of conserved amino acid motifs within Fap7's putative Walker A and Walker B motifs, which are required for nucleotide binding and hydrolysis respectively, leads to 20S accumulation [117]. The Walker B mutant, D82AH84A, displays an rRNA processing phenotype indistinguishable from Fap7 depletion. Thus, ATP binding and/or hydrolysis are predicted to be essential for Fap7's role in ribosome assembly.

The Fap7 homologs in the infectious yeast *Candida albicans* and humans have been the focus of recent studies [262-265]. To date, neither has been implicated in ribosome assembly; to our knowledge, however, experiments to test this possibility have yet to be performed. Both, however, have been shown to bind ATP. The Fap7 homolog in *C.*

albicans, Hbr1, was shown to mediate suppression of white-opaque phenotypic switching in response to hemoglobin by regulating expression of the mating-type-like (MTL) locus [266]. Hbr1 was shown to bind ATP, and residues required for wildtype ATP binding affinity were also implicated in regulation of the MTL genes [262]. ATP hydrolysis by Hbr1 was dismissed as negligible but conformational changes upon ATP binding were detected and predicted to behave as a functional switch [262].

The human homolog of Fap7, hCinap, was identified through its interaction with coilin, a protein localized to nuclear cajal bodies which house the assembly and maturation of some nuclear RNA-protein complexes take place [263]. hCinap influences cajal body number and organization, but it has diffuse nuclear localization and differentially segregates from coilin under certain conditions; functions hCinap beyond cajal bodies are therefore predicted [262, 263, 265]. This human Fap7 homolog was shown to have ATPase as well as adenylate kinase activity with an unusually broad NMP substrate specificity [264].

In vitro ATP binding, hydrolysis, and adenylate kinase activity of yeast Fap7 have yet to be demonstrated. What is known about Fap7 has thus far been determined through *in vivo* studies. It is estimated that there are approximately 8,350 molecules of Fap7 per yeast cell [267]. If Fap7 were distributed homogeneously throughout an average sized yeast cell [268], this number would translate to a concentration of approximately 1.4 μM. Fap7 has both nuclear and cytoplasmic distribution [211], and depletion of Fap7 leads to a large accumulation of methylated 20S rRNA in the cytoplasm [117]. Fap7 is not stably associated with pre-40S particles, but small amounts co-fractionate with 40S and 80S particles in sucrose gradients [117]. In addition, Fap7 binds directly to Rps14 and Dim1,

and crosslinks to ribosomal proteins from both subunits, reflecting an interaction with 80S particles containing pre-40S subunits as described in chapter 4. Depletion of Fap7 leads to retention of Tsr1 on assembling 40S subunits.

In order to understand how ATP hydrolysis by Fap7 is harnessed in the late stages of small subunit maturation, we initiated a biochemical and kinetic investigation of nucleotide binding and ATP hydrolysis by Fap7. The data show that Fap7 has distinct conformations in the apo, ATP, and ADP bound forms. Fap7 therefore undergoes conformational changes upon ATP binding and hydrolysis; the nucleotide bound state of Fap7 may therefore determine its interactions with targets on the pre-40S particle. Furthermore, the conformational change Fap7 undergoes upon ATP hydrolysis could provide mechanical energy for manipulation of proteins and rRNA to advance the assembly process in an irreversible manner.

3.2 Materials and Methods

Cloning and protein purification. Full-length Fap7 was PCR-amplified from yeast genomic DNA and cloned between the Nde1 and HindIII sites of pET23a (Novagen). This construct was transformed into BL21 cells and grown at 37 °C in LB Lennox medium to an OD_{600} of 0.4 before induction for 4 h with 1 mM IPTG at 30 °C. Cell pellets were resuspended in QBA (50 mM Tris, pH 8.0, 100 mM KCl, 2 mM EDTA) with 1 mM PMSF and 1 mM benzamidine, and sonicated. The soluble fraction was applied to a 5 ml Hi-TRAP Q column (GE Healthcare) and eluted in a linear gradient of 150-1000 mM KCl over 20 column volumes. Fractions containing Fap7 were pooled and QBB (50 mM Tris, pH 8.0, 1 M KCl, 2 mM EDTA) was added to a final concentration of 390 mM

KCl. A solution of 3.9 M $(NH_4)_2SO_4$ in water was slowly added to a final concentration of 50% while continuously stirring on ice; precipitated contaminants were removed by centrifugation at 50,000 x g. Fap7 was precipitated from the supernatant by adding 3.9 M $(NH_4)_2SO_4$ to a final concentration of 70% and centrifuged at 50,000 x g. The protein pellet containing Fap7 was redissolved in dialysis buffer (50 mM Tris, pH 8.0, 250 mM KCl, 2 mM EDTA) and dialyzed >4 h to remove residual $(NH_4)_2SO_4$. Dialyzed protein was purified over a 1 ml Mono Q column (GE Healthcare) with a gradient of 230-1000 mM KCl over 15 column volumes. Fractions containing Fap7 were pooled, concentrated and then applied to a Superdex 75 gel filtration column (GE Healthcare) with gel filtration buffer (200 mM KCl, 50 mM HEPES, pH 7.5, 1 mM DTT, 1 mM TCEP). At this point, Fap7 was more than 95% pure and free of visible contaminants. Glycerol was added to 15% and Fap7 was stored at -80 °C. Protein concentration was determined in 8M Guanidium-HCl by absorption at 280 nm using a calculated extinction coefficient of 29,910 $M^{-1}cm^{-1}$ [269].

ATPase assays. Prior to initiating reactions, Fap7 was incubated in gel filtration buffer plus 15% glycerol and 2 mM DTT for 2 hours at 30°C to ensure reduction of disulfide bonds. Assays and separation of ATP from free phosphate were performed as in [270]. Hydrolysis of γ-^{32}P-ATP by Fap7 was measured in 10 µl reactions at 30°C. Time points were taken by quenching 1 µl of the reactions with 1 µl of 0.75 M KH_2PO_4 (pH 3.3). 1 µl of the quenched reaction was spotted onto a PEI-F cellulose TLC plate (J.T. Baker). The TLC plate was developed in 1 M formic acid and 0.5 M LiCl and quantitated by phosphorimager analysis.

For single-turnover experiments, trace (< 1 nM) γ-^{32}P-ATP was used to initiate reactions with varying concentrations of Fap7 in a final reaction buffer of 75 mM HEPES, pH 7.6, 200 mM KCl, 10 mM MgCl2, 10% glycerol and 2 mM DTT. These data were fit with Equation 1 to obtain rate constants, k_{obs}, for ATP hydrolysis:

$$fraction_{reacted} = fractionmax_{reacted} - fractionmax_{reacted} \cdot exp(-k_{obs} \cdot t) \quad (1)$$

For calculating dissociation and inhibition constants for AMP-PNP in single turnover assays, the plot of k_{obs} versus AMP-PNP concentration was fit to equation 2, where k_{obs} in the first term of the equation is the single turnover rate constant of Fap7 in the absence of AMP-PNP. $\Delta_{max,1}$ is the maximum increase in the observed rate constant due to binding of AMP-PNP to a Fap7 dimer bound by one molecule of γ-^{32}P-ATP. The second term of the equation is the inhibition of ATPase activity resulting from the competition of AMP-PNP for γ-^{32}P-ATP in the second ATP binding site.

$$k_{obs} = k_0 + \Delta_{max,1} * \frac{[AMP-PNP]}{[AMP-PNP]+K_{d,app,1}} + (k_0 + \Delta_{max,1}) + * \frac{1}{\left(1+\frac{[AMP-PNP]}{K_{d,app,2}}\right)} \quad (2)$$

For multiple turnover experiments, trace γ-^{32}P-ATP was mixed with the desired concentrations of unlabeled ATP and equimolar $MgCl_2$ to keep the free $MgCl_2$ concentration uniformly at 10 mM. This mix was used to initiate reactions in a final buffer composition of 75 mM HEPES, pH 7.6, 200 mM KCl, 10% glycerol, 2 mM DTT and 0.2, 1, 5, or 10 mM $MgCl_2$ with 2, 5, or 10 μM Fap7.

Total ATP hydrolyzed was calculated by multiplying fraction ATP hydrolyzed by the total ATP present in each reaction. Kinetics parameters were determined by fitting the burst equation (3) to the pre-steady-state time course [271],

$$\frac{moles\ ATP\ hydrolyzed}{mole\ protein} = A[1 - exp(-k_{burst} \cdot t)] + k_{SS} \cdot t \quad (3)$$

where A is the burst amplitude and k_{burst} and k_{SS} are the observed rate constants for the burst and the linear phases, respectively. Data-fitting was performed using KaleidaGraph software (Synergy Software).

Fluorescence Assays. Fap7 was incubated in gel filtration buffer plus 15% glycerol and 2 mM DTT for 1.5 hours at 30°C to ensure reduction of disulfide bonds. Because Fap7 fluorescence is sensitive to pipetting/mixing alone (perhaps due to loss of protein on the tips), fluorescence at each nucleotide concentration was measured in an independent mix. Reduced Fap7, buffer alone, or free tryptophan as a control were distributed to individual tubes for each data point and ADP or AMP-PNP were added for the final nucleotide concentration in 75 mM HEPES pH 7.6, 200 mM KCl, 10 mM $MgCl_2$, 10% glycerol and 2 mM DTT in a volume of 100 µl. Protein-nucleotide mixes were equilibrated an additional 30 minutes; tryptophan fluorescence was then measured by excitation at 295 nm and emission at 321 nm (Varian Cary Eclipse Fluorescence Reader, Palo Alto, CA). Absolute fluorescence was determined by subtracting the buffer control at each nucleotide concentration. The relative change in fluorescence (ΔF_{rel}) was determined by subtracting the absolute fluorescence at each nucleotide concentration ($F_{Fap7+nuc}$) from the fluorescence in the absence of nucleotide (F_{Fap7}) and dividing by fluorescence in the absence of nucleotide ($\Delta F_{rel} = \frac{(F_{Fap7+nuc} - F_{Fap7})}{F_{Fap7}}$).

Data for ADP binding were fit with equation 4 based on a single binding site model to determine nucleotide dissociation constants:

$$\Delta_{fluorescence,rel} = \Delta_{max} * \frac{[nucleotide]}{[nucleotide] + K_{d,app,1}} \quad (4)$$

Data for AMP-PNP were fit to equation 5 based on a two binding site model.

$$\Delta_{fluorescence} = \Delta_{max,1} * \frac{[nucleotide]}{[nucleotide] + K_{d,app,1}} + \Delta_{max,2} * \frac{[nucleotide]}{[nucleotide] + K_{d,app,2}} \quad (5)$$

Data fitting was performed using KaleidaGraph software (Synergy Software).

Limited proteolysis

In 50 µl reactions, 25 µM recombinant Fap7 was incubated with 10 µl of 20 mg/ml trypsin or 10 µl of 20 mg/ml chymotrypsin for 0 seconds, 15 seconds, or 2 minutes. The reaction was stopped by diluting 1:1 in SDS-PAGE loading dye and boiling for 5 minutes. Samples were loaded on 12% SDS-PAGE gels and stained with Coomassie blue.

3.3 Results

To investigate the function of Fap7 on a molecular level, recombinant *S. cerevisiae* Fap7 (22.7 kDa, 197 amino acids) was purified from *E. coli*. After two anion exchange columns, an ammonium sulfate precipitation and gel filtration, no contaminants were observed by SDS-PAGE (**Fig. 3.1A**), and the protein's identity was confirmed by mass spectrometry. In size exclusion chromatography, Fap7 purifies primarily as a monomer with an apparent molecular weight of 30 kDa at concentrations as high as 100 µM. A small percentage (<5%) partitions to higher molecular weight fractions that correspond to dimers as well as tetramers. Protein from fractions corresponding to monomeric Fap7 was pooled for further analysis.

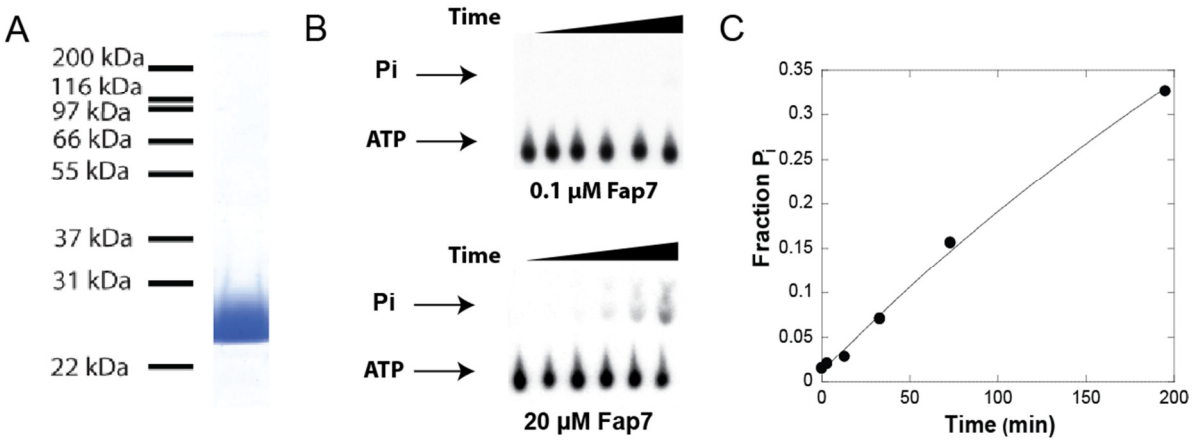

Figure 3-1 Fap7 is an ATPase. (A) 12% SDS-PAGE gel of recombinantly purified Fap7 stained with coomassie blue. (B) γ-^{32}P-ATP and free phosphate generated by incubation with 0.1 and 20 µM Fap7, separated by TLC. (C) Fraction free phosphate quantified with a phosphorimager and plotted versus incubation time with 20 µM Fap7. Fitting of the curve with a single exponential returns an observed rate constant (k_{obs}) of 2.5 x 10^{-3} min^{-1} .The progress curves of reactions that did not approach completion within the experiment (> 90% of ATP hydrolyzed) were fit to lines to estimate initial rates and gave the same rates.

Fap7 dimerizes upon ATP binding

The homology of Fap7 with adenosine-dependent P-loop kinases led us to investigate the ability of recombinant protein to hydrolyze ATP. Radiolabeled γ-^{32}P-ATP was incubated for varying amounts of time with Fap7, and remaining ATP was separated from the $^{32}P_i$ product via thin layer chromatography (TLC, **Fig. 3.1B**). The fraction of free phosphate quantified and the reaction progress curve was fit to a single exponential to determine the observed rate constant for ATP hydrolysis (**Fig. 3.1C**). These experiments show that at a concentration of ~20 µM, Fap7 hydrolyzed ATP at a rate four orders of magnitude above that of the uncatalyzed reaction. The increase in ATPase activity as Fap7 concentration is increased demonstrates that this reaction depends on Fap7 concentration; ATPase assays during protein purification also confirm that the ATPase activity co-purifies with Fap7. Mutation of the active site in the Walker B mutant D82AH84A does not reduce the single turnover rates of ATP hydrolysis (**Fig 3.2A**); but does reduce the steady-state rate by 80% (**Fig 3.2B),** demonstrating that ATPase activity arises from Fap7.

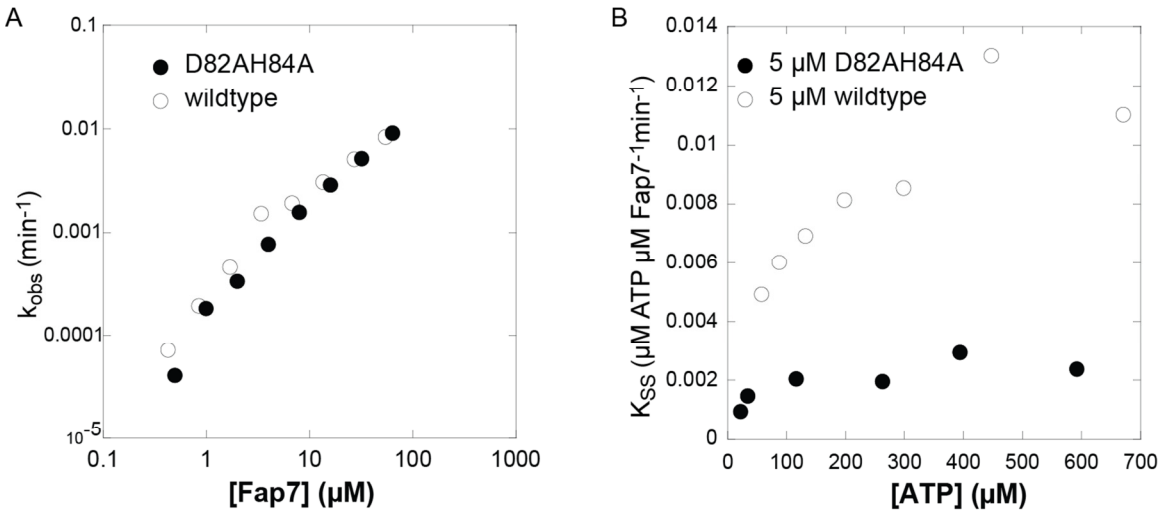

Figure 3-2 The Fap7 D82AH84A Walker B mutant has decreased steady state rates of ATP hydrolysis. (A) Fap7 concentration dependence of single turnover rates of ATP hydrolysis of the Fap7 D82AH84A mutant and wildtype plotted on a log-log scale. (B) Steady state rates of ATP hydrolysis of 5 µM wildtype Fap7 and 5 µM Fap7 D82AH84A.

ATP hydrolysis leads to conformational changes involving the C-terminal helix

To further investigate the behavior of Fap7 upon nucleotide binding, we monitored changes in Fap7's intrinsic tryptophan fluorescence as previously described for other proteins [272]. Fap7 has one tryptophan (W83) in the Walker B ATP binding motif [273] and two near its C-terminus (W167 and W171) (**Fig. 3.6G**). Because W83 is located in the ATP binding site, a fluorescence signal change upon nucleotide binding that is not entirely obscured by the two C-terminal tryptophans was expected. The intrinsic fluorescence of Fap7 was monitored by excitation at 295 nm and emission at 321 nm in the presence of 0 to 400 µM AMP-PNP or ADP. To rule out possible fluorescence artifacts, control experiments were carried out using free tryptophan and increasing concentrations of nucleotide (**Fig 3.6B and E**).

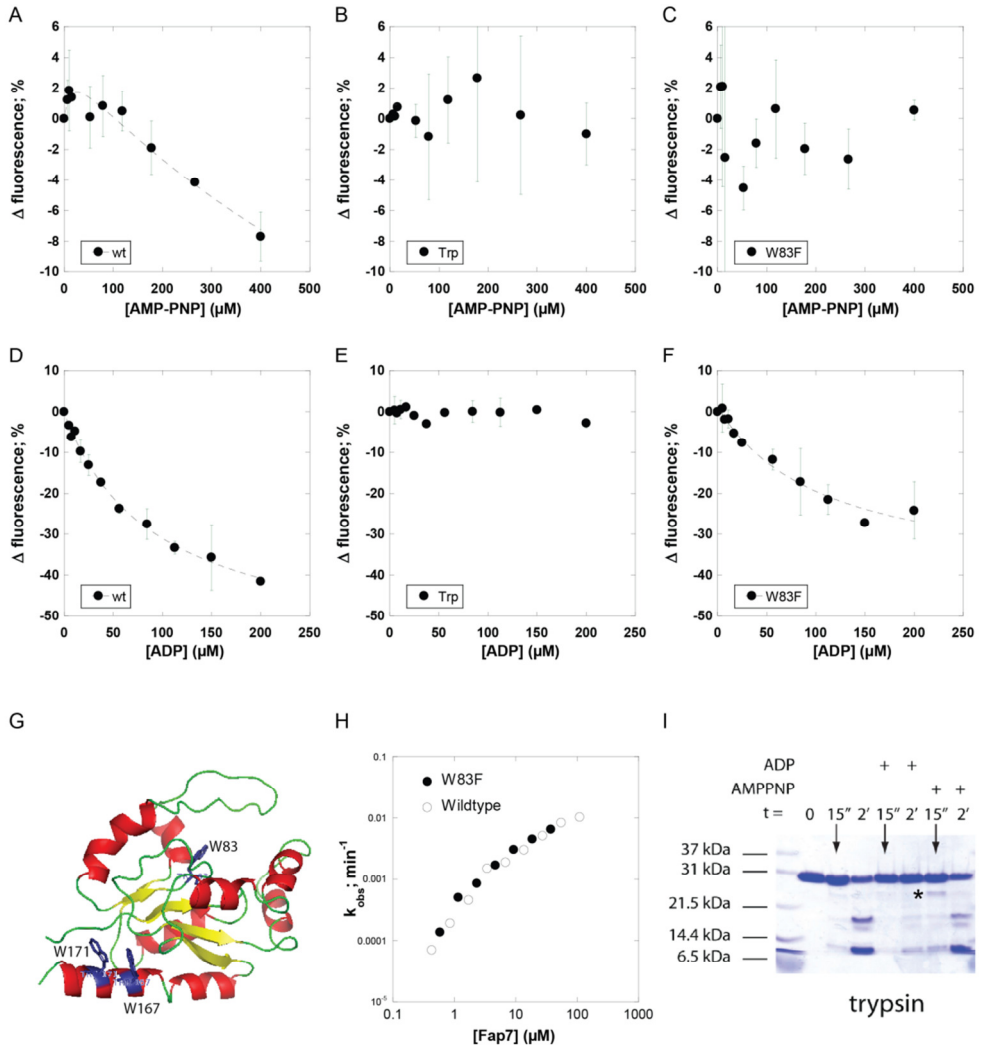

Figure *3-3 Fap7 undergoes a conformational change upon ATP hydrolysis.* Tryptophan fluorescence of (A) wildtype Fap7, (B) free tryptophan, and (C) W83F mutant Fap7 at increasing concentrations of AMP-PNP. The wildtype curve fits to a biphasic binding function (the sum of two square hyperbolas) with apparent nucleotide binding affinities of 10 μM in the first phase and 100-300 μM in the second phase. Tryptophan fluorescence of (D) wildtype Fap7, (E) free tryptophan, and (F) W83F mutant Fap7 at increasing concentrations of ADP. Both wildtype and mutant curves fit to a single binding function with an apparent affinity of ~90 μM. (G) Model of Fap7 generated through alignment with human Fap7 (hCinap) and fit to the crystal structure available for the human protein with Swiss Model. Tryptophans are labeled and modeled as blue sticks. (H) Comparison of single-turnover concentration dependence of Fap7 W83F and wildtype Fap7. (I) Limited proteolysis of Fap7 with trypsin in the presence and absence of the ATP analog AMP-PNP and ADP for time (t) = 0, 15 s, or 2 min demonstrates that binding of these nucleotide alters accesibility of Fap7 to proteolytic cleavage by trypsin and that accessibility in the presence of ATP is different from that in the presence of ADP. Proteolysis fragment specific to Fap7 bound to AMP-PNP is marked with an asterisk.

Fap7 fluorescence shows a biphasic dependence on AMP-PNP concentration (**Fig. 3.6A**); this is similar to the observation in single turnover experiments with AMP-PNP and consistent with two ATP binding sites. Below 50 μM AMP-PNP, a small but

reproducible increase in fluorescence was observed, which was followed by a decrease at higher AMP-PNP concentrations. This decrease in fluorescence at higher AMP-PNP concentrations could be fit to a simple binding equation with a $K_{1/2}$ of ~100 μM, although this number has some uncertainty due to the variability of the amplitude of the first phase; this also precludes reliable extraction of the $K_{1/2}$ value for the first phase.

Mutation of the active site tryptophan (W83F) abolished both the increase and the decrease in fluorescence observed in the presence of AMP-PNP (**Fig. 3.6C**). The W83F mutation has no effect on growth in yeast (data not shown), ADP affinity, or the concentration dependence of the ATPase activity (**Fig. 3.6H**), indicating that the mutation does not affect nucleotide binding. The loss in fluorescence signal upon mutation of W83, therefore, indicates that a change in the chemical environment of W83 alone is responsible for fluorescence changes. The initial increase and subsequent decrease in fluorescence of W83 indicates that binding of the first and second AMP-PNP affects this nucleotide differentially. Perhaps the dimerization associated with ATP binding leads to the initial fluorescence increase, which counteracts the decrease normally observed upon ATP binding. Alternatively, or additionally, it is possible that the two AMP-PNP molecules bound to the two Fap7 molecules in the dimer are bound in different conformations. This would be consistent with the order of magnitude difference in the affinities of the tight binding and weak binding ATP (~20 and ~100 μM - 250 μM from fluorescence and kinetics experiments, respectively).

Similar fluorescence titrations performed with ADP show fluorescence quenching, with an ADP concentration dependence that fits to a single binding site model with a dissociation constant of approximately 90 μM (**Fig. 3.6D**). The maximal fluorescence

quench upon ADP binding is higher than that observed upon binding of AMP-PNP (40% versus 10%), suggesting that either more tryptophans are changing their chemical environment, or that quenching of a single tryptophan is more substantial. Mutation of the active site tryptophan (W83F) reduces the overall fluorescence and magnitude of the quench, but does not affect the shape of the curve (**Fig. 3.6F**). Together, these data suggest that while W83 contributes to the quench, tryptophans W167 and W171 are also involved. Because W167 and W176 are distant from the active site in the predicted structure for Fap7 (**Fig. 3.6G**), this result indicates that ADP binding leads to a conformational change in Fap7 that alters the environment of the C-terminal tryptophans. A single binding site model fits well to the quench observed in both the wild-type and mutants. The simplest interpretation of these data is that in the presence of ADP Fap7 is monomeric; however, the data are also consistent with either a symmetric Fap7 dimer (containing two ADP binding sites of equal affinity), or an asymmetric dimer in which one ADP either binds so tightly that it is essentially saturated at the lowest concentration (but gives no change in fluorescence) or it binds so weakly that it does not bind under the conditions tested.

The contribution of W167 and W171 to fluorescence quenching upon addition of ADP but not AMP-PNP indicates that binding of these nucleotides leads to distinct conformational changes. Thus, hydrolysis of ATP to ADP is accompanied by a change in the environment of the C-terminal helix containing W167 and W171. Conformational changes linked to ATP hydrolysis are further supported by limited proteolysis of Fap7 by trypsin and chymotrypsin both in the presence and absence of ADP or AMP-PNP (**Fig 3.6I**). These experiments demonstrate that susceptibility of Fap7 to proteolytic digestion

is altered by the presence of nucleotide, and that protections and enhancements are different in the ATP and ADP bound forms as previously shown for the homolog of Fap7 in *C. albicans* [262].

The Fap7 dimer turns over ATP sequentially

Single-turnover ATPase and fluorescence experiments thus far indicate that ATP binding leads to dimerization of Fap7, which is required for efficient ATPase activity. Under single-turnover conditions, where the ATP concentration is only around 1 nM, the second nucleotide binding site will not be significantly populated by ATP at any Fap7 concentration. To investigate the ATPase behavior of Fap7 under conditions where both sites can be saturated, we carried out multiple turnover ATPase experiments.

Kinetic analysis shows that between 50 and 1000 μM ATP (and 2 or 5 μM Fap7), the ATPase activity displays a burst followed by a slower steady-state rate. This finding indicates that there is a rate-limiting step after ATP hydrolysis. Interestingly, the maximum magnitude of the burst corresponds to ~50% of the Fap7 concentration even at very high concentrations of ATP (**Fig. 3.7A and B**). This finding provides additional evidence for the existence of two ATPase sites, which turn over their bound ATP sequentially, with a rate-limiting step occurring after the hydrolysis of the first ATP. The steady-state rate of ATP hydrolysis is ~0.01 min^{-1}, while the burst rate approaches 1 min^{-1} μM (**Fig. 3.7C and 3.6D**), suggesting that ATPase activity is highest when both Fap7 sites are bound to ATP.

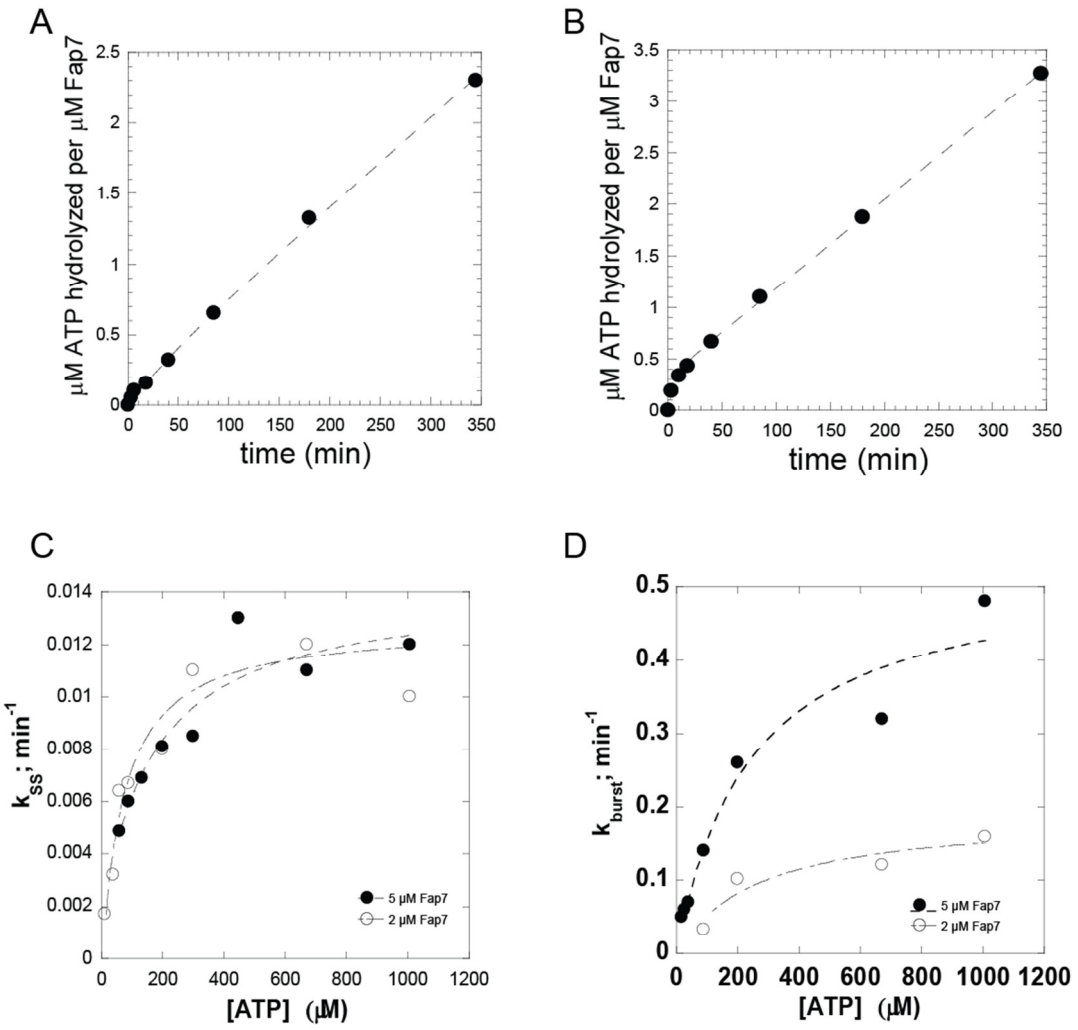

Figure 3-4 ATP is hydrolyzed sequentially from the Fap7 dimer. Multiple turnover example plots with (A) 2 µM Fap7 and 60 µM ATP and (B) 2 µM Fap7 and 200 µM ATP. The curve is fit to burst equation (see Materials and Methods). (C) Summary plot of steady-state rates for 2 µM and 5 µM Fap7 at increasing ATP concentrations. Fitting the curve to the Michaelis Menton equation results in a K_m of 80 µM for 2 µM Fap7 and 120 µM for 5 µM Fap7. (D) Summary plot of burst rate estimations for 2 µM and 5 µM Fap7 at increasing ATP concentrations indicates apparent dissociation constants of ~250 µM.

Comparison to kinetic simulations

The data described above provide strong evidence for a model in which ATP binding to Fap7 leads to dimerization. In addition, the data also indicate that a second ATP can be bound to the dimer with an ~10-fold weaker affinity. Binding of this second ATP increases the rate of ATP hydrolysis. Furthermore, multiple-turnover experiments

indicate that both ATP molecules are turned over sequentially with a rate-limiting step occurring after the hydrolysis of the first ATP.

To further test and confirm this model, we carried out kinetic simulations using Berkeley Madonna. The simplified model is schematically shown in **Figure 3.8** and the values for rate constants are listed in **Table 3.1**. Simulation results predict a Fap7 concentration dependence similar to that observed under single-turnover conditions, with a transition from a slope of 2 to a slope of 1 at around 3 μM Fap7 (**Fig. 3.9A**).

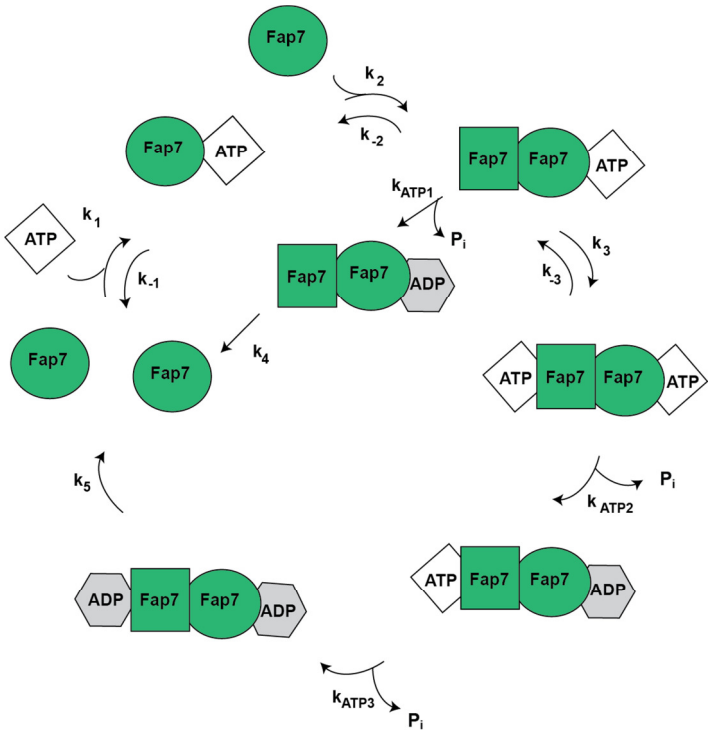

Figure 3-5 Model for sequential turnover of ATP from Fap7 dimer. Rate constants are listed in Table 3.1.

In this model, the apparent second order rate constant for ATP binding is below that expected for diffusion controlled processes and ATP binding becomes rate-limiting at higher Fap7 concentrations. This observation suggests that ATP binding involves more

than a simple association. A slow conformational change that is required for stable ATP binding and also stabilizes dimerization could explain this low apparent binding rate. If ATP hydrolysis from the $Fap7_2ATP_2$ complex is ~100-fold higher than that from the $Fap7_2ATP_1$ complex, and turnover from the second Fap7 protomer is rate-limiting and occurs prior to dissociation of the first ADP, burst and steady state rate constants from multiple turnover simulations are also within 2 fold of the experimental results (**Fig. 3.9B-D**).

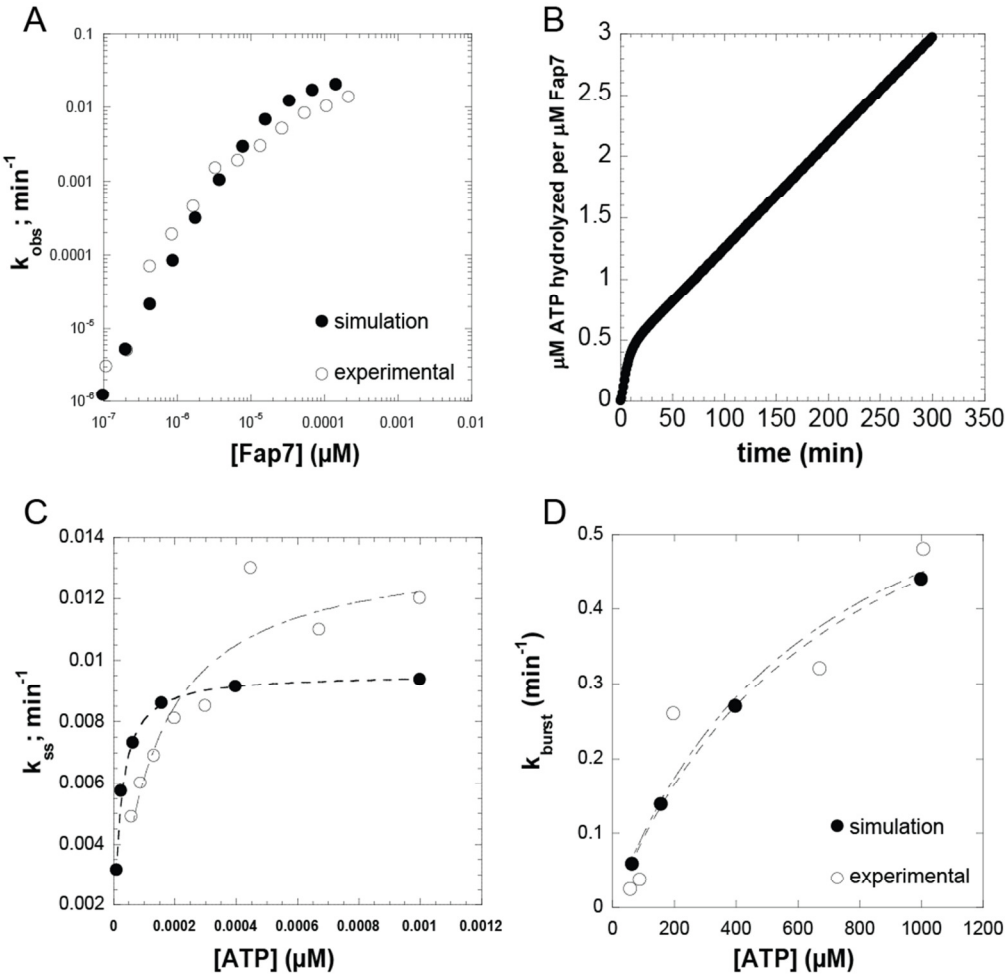

Figure 3-6 Comparison of experimental data to model based simulations. (A) Single-turnover simulation plotted with simulated single-turnover data. Concentration of ATP in both cases is ~1 nM. (B) Example of a multiple-turnover simulation with 158 μM ATP and 5 μM Fap7. (C) Steady-state rate determined from experimental data plotted with steady-state rate generated in simulations with 5 μM Fap7. (D) Burst rate determined from experimental data plotted with steady-state rate generated in simulations with 5 μM Fap7. Model and rates used are illustrated in Figure 3.7 and listed in Table 3.1.

3.4 Discussion

Fap7 is an ATPase that undergoes a conformational change upon ATP hydrolysis

Single and multiple turnover ATPase assays, fluorescence experiments, and limited proteolysis all provide evidence for the following model (**Fig. 3.8**): ATP binding to Fap7 leads to dimerization and the formation of the $Fap7_2ATP$ complex that has an ATP hydrolysis rate constant of 0.01-0.02 min^{-1} . Once another ATP is bound, ATP is turned over rapidly and sequentially, leading to a burst in multiple-turnover experiments that approaches 1 min^{-1}; this is followed by a 10-100 fold slower steady-state rate reflecting turnover from the $Fap7_2ATP{\cdot}ADP$ complex. The steady state rate of ATP hydrolysis of 0.01 μM ATP hydrolyzed per μM Fap7 determined in this study is similar to steady state rate of 0.06 0.01 μM ATP hydrolyzed per μM protein observed for the human Fap7 homolog, hCinap.

The observation that changes in fluorescence involve only the active site tryptophan W83 upon ATP binding yet involve both W83 and the C-terminal tryptophans W167 and W171 when ADP is bound indicates that the ATP-bound form of Fap7 is conformationally different from the ADP-bound form. Different accessibility of Fap7 to proteolysis in the presence of AMP-PNP versus ADP also indicates that the ATP- and ADP-bound forms are different. In other words, Fap7 undergoes a conformational change upon binding ATP and hydrolysis of ATP. The conformational change that takes place upon ATP hydrolysis may expose the C-terminus of Fap7 to solvent, thereby resulting in quenching of fluorescence of W167 and W171.

Together, these data indicate that an active Fap7 dimer assembles in an ATP-dependent manner; the associated change in its structure may reveal binding sites for additional co-factors. ATP hydrolysis results in a further conformational change. This coordinated cycle of ATP hydrolysis and coupled conformational changes could allow the protein to transduce the energy of ATP hydrolysis to mechanical energy on the pre-ribosome.

Implications for understanding Fap7's role in ribosome assembly

ATP hydrolysis is predicted to be required for ribosome assembly because point mutations in both the Walker A and Walker B motifs are essential [117]. The Walker B mutant D82AH84A demonstrates 18S rRNA processing defects as severe as Fap7 depletion and also shows an 80% decrease in the steady-state rate of ATP hydrolysis. Assuming that the primary defect of the D82AH84A mutant is its ability to hydrolyze ATP, this finding suggests that turnover of both ATP molecules in the Fap7 dimer is essential for assembly of the 40S ribosomal subunit. Alternatively, interaction of Fap7 with other cellular factors may modulate its ATPase activity during ribosome assembly. The failure of the Walker B mutant D82AH84A to support assembly may reflect the failure of these factors to enhance its ATPase activity. It cannot yet be ruled out, however, that this mutant has an ATPase independent defect that impairs its ability to support ribosome assembly. Investigation of Fap7's ATPase activity in the presence of interacting factors may help resolve these uncertainties. Alternative explanations for the trends we have observed are included in Chapter 5.

The nucleotide binding and ATPase hydrolyzing characteristics of Fap7 profiled in this work can now be used as a framework for investigating how these behaviors are utilized to facilitate cleavage of the 20S rRNA *in vivo*. Fap7 binds directly to Rps14 as well as

Dim1 and crosslinks efficiently to the translation initiation and ribosome assembly factor eIF5A ([117], Chapter 4). These interactions localize the target of Fap7 action at the intersection of the body and platform of the pre-40S particle on the subunit interface, where these proteins are known to bind **(Fig. 4.10)**. Future experiments will interrogate how the dissociation constants and rate constants observed here are altered in the presence of these factors.

Table 3.1: Equations and Rate Constants for Fap7 ATPase Model

Step	Rate constants
$Fap7 + ATP \overset{k_1}{\underset{k_{-1}}{\leftrightarrow}} Fap7 \cdot ATP$	k_1 = 1000 $M^{-1}min^{-1}$; k_{-1} = 0.125 min^{-1}
$Fap7 \cdot ATP + Fap7 \overset{k_2}{\underset{k_{-2}}{\leftrightarrow}} Fap7_2 \cdot ATP$	k_2 =3x10^7 $M^{-1}min^{-1}$; k_{-2} = 45 min^{-1}
$Fap7_2 \cdot ATP + ATP \overset{k_3}{\underset{k_{-3}}{\leftrightarrow}} Fap7_2 \cdot ATP_2$	k_3 = 1x10^6 $M^{-1}min^{-1}$; k_{-3} = 250 min^{-1}
$Fap7_2 \cdot ATP \xrightarrow{k_{ATP1}} Fap7_2 \cdot ADP + P_i$	k_{ATP1} = 0.025 min^{-1}
$Fap7_2 \cdot ADP \xrightarrow{k_4} 2Fap7 + ADP$	k_4 = 0.01 min^{-1}
$Fap7_2 \cdot ATP_2 \xrightarrow{k_{ATP2}} Fap7_2 \cdot ADP \cdot ATP$	k_{ATP2} = 1 min^{-1}
$Fap7_2 \cdot ADP \cdot ATP \xrightarrow{k_{ATP3}} 2Fap7 + ADP + P_i$	k_{ATP3} = 0.01 min^{-1}
$Fap7_2 \cdot ADP_2 \xrightarrow{k_7} 2Fap7 + 2ADP$	k_7 = 0.01 min^{-1}

The effects from Fap7 depletion or mutation are indistinguishable from those observed upon mutation of R134 in the C-terminal tail of Rps14, and include retention of Tsr1 on pre-40S particles ([117, 187], Chapter 4). Because Fap7 does not appear to directly bind Tsr1 (Chapter 4), and because the binding sites for Dim1, Rps14 and eIF5A with which Fap7 interacts are too far away from Tsr1, Fap7 is unlikely to directly remove Tsr1 from

pre-40S ribosomes. However, Dim1 and Tsr1 are both directly bound to H44, and rearrangements of Dim1 on helix 44 (the decoding site helix located on the subunit interface) could affect binding of Tsr1. Furthermore, Rps14's C-terminal tail interacts directly with nucleotides in H23 [274], which are also bound by Dim1. It is possible that by binding directly to Dim1 and Rps14, Fap7 aligns these residues with respect to each other in order to produce the mature tertiary structure of the platform region.

Chapter 4

An obligate 80S intermediate in the yeast small subunit ribosome biogenesis pathway

4.1 Introduction

The final maturation of the ribosomal small subunit occurs following export of the 20S rRNA precursor of the 18S rRNA to the cytoplasm (**Fig. 4.1**). The last assembly steps include the only universally conserved rRNA modification (dimethylation of two adenosines near the 3' end of the 18S rRNA by Dim1), incorporation of two ribosomal proteins: Rps10 and Rps26 [275], and cleavage at site D within the 20S precursor by the Nob1 endonuclease to produce the mature 3' end of 18S rRNA. The stable cytoplasmic pre-40S intermediate contains methylated 20S rRNA, lacks Rps10 and Rps26, and has seven stably bound assembly factors, including Dim1 and Nob1. These assembly factors are not part of the mature ribosome and prevent the pre-40S particle from engaging in translation on multiple levels [275]; therefore, cytoplasmic maturation must also involve dissociation of these factors. Depletion of Fap7 and Rio1, two cytoplasmic assembly factors not stably associated with this particle, results in accumulation of methylated 20S rRNA [117, 276]. Fap7 and Rio1 are therefore believed to be involved in these final maturation steps through transient association with cytoplasmic precursors (**Fig. 4.1**).

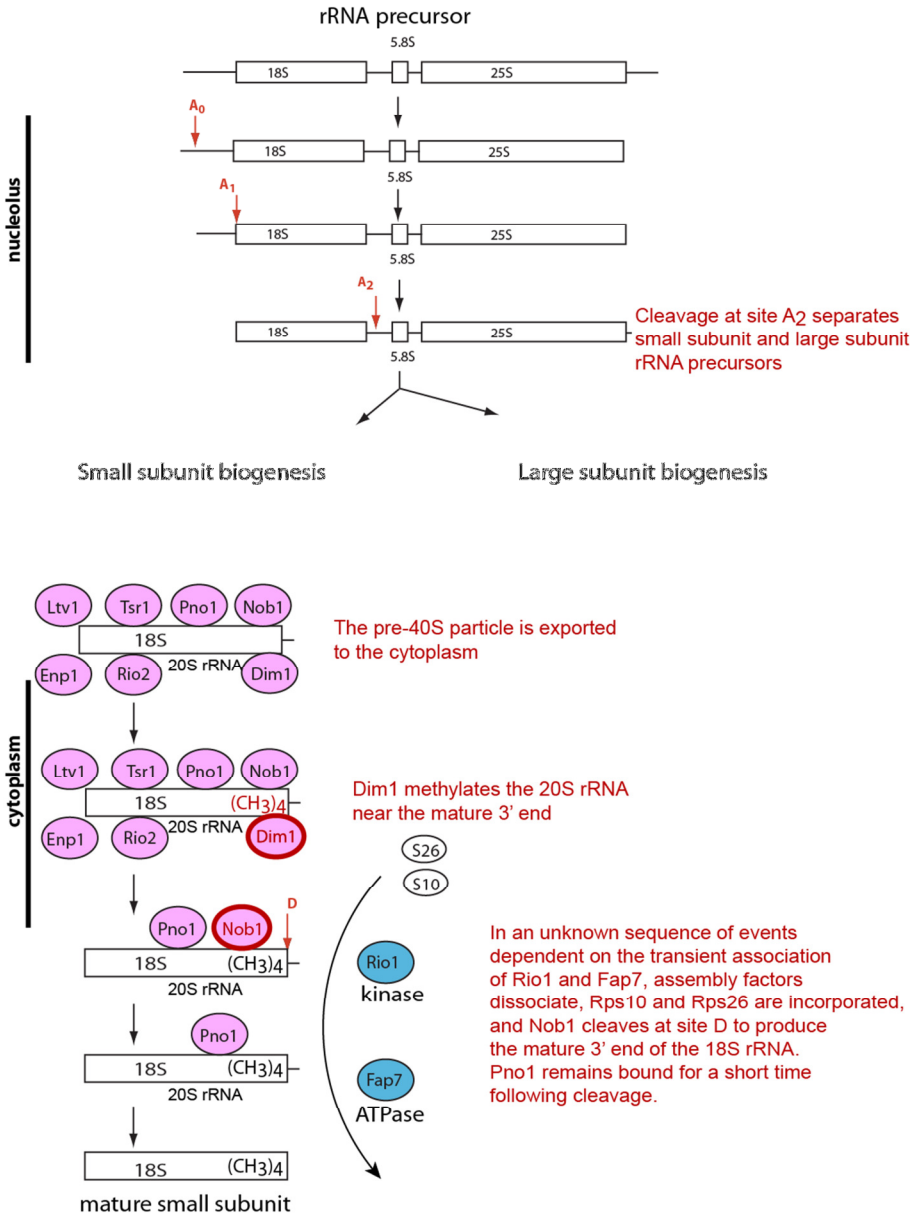

Figure 4-1 Late events in small subunit maturation. The 18S rRNA is transcribed as part of a polycistronic 35S rRNA precursor in the nucleolus. Four cleavage events (red arrows: A_0, A_1, A_2, and D) are required to produce the mature 18S rRNA. The last of these, cleavage at site D, takes place following export to the cytoplasm as the 20S rRNA undergoes methylation near the mature 3' end. Seven assembly factors (pink ovals), which are stably bound to a well characterized cytoplasmic intermediate, include the rRNA methylase, Dim1, and the endonuclease responsible for cleavage at site D, Nob1. This pre-40S intermediate lacks 2 of the 32 ribosomal proteins associated with the mature small subunit: Rps10 and Rps26 (white ovals). The final maturation events include incorporation of these ribosomal proteins and cleavage at site D. Two transiently associated assembly factors, Rio1 and Fap7 (blue ovals), are required for D site cleavage.

20S rRNA precursors enter 80S particles as well as polysomes, and their abundance in these complexes increases upon depletion of factors that specifically disrupt 20S

processing [117, 187, 227, 239]. During translation initiation, joining of the mature 40S and 60S subunits involves the binding of initiator tRNA and mRNA to the small subunit and requires more than twelve core initiation factors, which work together to facilitate recognition of the start codon in the P-site for formation of the first peptide bond [277, 278] (**Fig. 4.11**). Binding of the initiator tRNA is mediated by eIF1A, eIF1, eIF2, and members of the eIF3 complex. Following tRNA binding, these factors mediate binding of the 5' capped mRNA and scanning for the start codon through interactions with subunits of the eIF4F complex and Pab1, which bind the 5'cap and poly A tail, respectively. Links between translation initiation factors and ribosome biogenesis have been recognized for several years [92, 95, 279], hinting at a potential requirement for translation initiation in the final steps of ribosome maturation. However, even though data indicate that 20S cleavage can take place within 20S particles, Soudet and colleagues showed that 20S processing was not impaired by deletion of eIF1A and essential subunits of the eIF3 complex [239]. Canonical translation initiation is therefore not a requirement for ribosome biogenesis.

Here we demonstrate that subunit joining mediated by eIF5B, but independent of translation factors that bind to 40S subunits, is an obligate step in 40S ribosome maturation. In our model, the resulting 80S particle does not bind mRNA and must be dissociated in an Rli1/Dom34 dependent manner. Assembly factors dissociate in a partially ordered way from 80S subunits, aided by the activity of the ATPase Fap7 and the translation initiation factor eIF5A, thereby facilitating progression to a 40S subunit that can engage in canonical translation initiation.

4.2 Materials and Methods

Yeast strains

Galactose-inducible strains were created by PCR-based recombination [280] into the Rio2TAP strain from Open Biosystems. The Rio2 deletion strain was generously provided by J.P. Gélugne [118]. The Rps14 R134A mutant strain was generously provided by J.L. Woolford [187]. The eIF5A degron strain was generously provided by A. Henderson [277, 281, 282]. Yeast strains used here are listed in Table 1.

Sucrose density gradients and analysis

Sucrose gradient centrifugation was performed as described [283] with some modifications. Strains were grown to mid-log phase in YP galactose, then shifted to 200 ml YP dextrose (12 hours for wildtype and Gal1::Nob1, 16 hours for Gal1::Fap7, 10 hours for Gal1::Rio1) or YP dextrose with 30 µg/ml doxycycline (12 hours for Tet07::Rio1) and grown to an OD_{600} of 0.5. Wildtype Rps14 was depleted from JWY615 (ΔRps14A/Gal1::Rps14B) cells expressing Rps14B R134A from a plasmid [187] from mid-log phase in galactose to glucose for 6 hours to OD_{600} 0.5. eIF5A was depleted as described [277] by shifting from galactose to glucose for 6 hours. Cycloheximide was added at 0.1 mg/ml just prior to harvesting by centrifugation. Cells were washed once in ice cold gradient buffer (20 mM Hepes, pH 7.4, 5 mM $MgCl_2$, 100 mM $MgCl_2$, 0.1 mg/ml cycloheximide, 3 mM DTT) then resuspended in 1.5 ml/g dry weight of ice cold gradient buffer with 1 mM PMSF, 1 mM benzamidine, Complete EDTA-free Protease Inhibitor Cocktail (Roche), 1 ng/µl pepstatin, 1 ng/µl leupeptin, 1 ng/µl aprotinin, and 1 U/µl RNAsin (Promega). Resuspended cells were frozen as pellets in liquid nitrogen and ground to a powder under liquid nitrogen with a mortar and pestle. Lysate from thawed

cells was cleared by centrifuging at 10,000 x g for 10 minutes. Six OD_{260} units (~50 µl) of lysate were applied to 11 ml 10-50% sucrose gradients or 60 OD_{260} units (~500 µl) were applied to 36 ml 5-40% sucrose gradients in gradient buffer and centrifuged for 2 hours at 40,000 RPM in an SW41 rotor or 6 hours at 32,000 RPM in an SW31 rotor, respectively. Gradients were scanned and fractionated with a UV detector and fraction collector from Brandel, Inc. Protein was precipitated from 100 µl or 500 µl of each reaction by acetone precipitation (diluted 5-fold with PBS and incubated with 3 volumes ice cold acetone overnight at -20°C followed by centrifugation at 15,000 g and resuspension in sample buffer (1% SDS, 8 M Urea, 10 mM Tris, pH 6.8, 10 mM EDTA, 0.01% bromophenol blue) and analyzed by Western blot and mass spectrometry. RNA for Northern analysis was isolated from 100 µl of each gradient fraction by 2-fold dilution in water followed by phenol-chloroform extraction and ethanol precipitation.

In vivo formaldehyde cross-linking and purification of Fap7TAP associated complexes

Cells expressing TAP-tagged Fap7 from a galactose promoter were grown to mid-log phase in 3l of YP media supplemented with 0.2% galactose and 2% raffinose or 2% galactose. *In vivo* cross-linking was performed according to [284]. The culture was transferred to centrifuge tubes on ice and ¼ volume crushed ice was added. 37% formaldehyde was added to a final concentration of 1% of the original culture volume. Cultures were incubated on ice to cross-link for one hour. The cross-linking reaction was stopped by addition of 2.5 M glycine to a final concentration of 0.1 M and incubation on ice for 15 minutes. Affinity-purification of TAP-tagged Fap7 was performed essentially as described [112, 285, 286]. Cells were washed with water, resuspended in 0.5 ml of freezing buffer/g dry weight cells (buffer: 100 mM NaCl, 50 mM Tris/HCl, pH 7.5, 10

mM $MgCl_2$, 0.075% NP-40, 5 mM RVC (New England Biolabs), 1 mM PMSF, 1 mM benzamidine, Complete EDTA-free Protease Inhibitor Cocktail (Roche), 1 ng/µl pepstatin, 1 ng/µl leupeptin, and 1 ng/µl aprotinin), then frozen in liquid nitrogen and milled in a Retsch PM-200 cryomill. Frozen, milled cells were vortexed to homogeneity in 1.5 ml lysis buffer (freezing buffer supplemented with 50 units/ml RNasin Ribonuclease Inhibitor (Promega) with 5 mm zirconia/silica disruption beads (0.5 ml beads/g dry weight cells) and thawed by rocking at 4°C for 30 minutes. Lysate was cleared for 10 min at 10,000 x g and rocked with 200 µl IgG beads (GE Healthcare) for 2 hours at 4°C. Beads were washed 3 times with 10 ml IgG bind buffer (100 mM NaCl, 50 mM Tris/HCl, pH 7.5, 10 mM $MgCl_2$, 0.075 % NP-40) and 5 ml TEV cleavage buffer. Particles bound to IgG beads were rocked in 1.2 ml TEV cleavage buffer with 12 µl AcTEV protease (Invitrogen) for 2 hours at 16°C. Flow through from TEV cleavage step was mixed with 3 µl 1M $CaCl_2$ to titrate EDTA and 3 ml calmodulin binding buffer (100 mM NaCl, 50 mM Tris/HCl, pH 7.5 10 mM $MgCl_2$, 1 mM imidazole, 2 mM $CaCl_2$, 10 mM β-mercaptoethanol) and rocked with 200 µl calmodulin beads (Stratagene) for 1 hour at 4°C. Particles bound to calmodulin beads were washed twice with 2 ml calmodulin binding buffer and eluted with calmodulin elution buffer (100 mM NaCl, 50 mM Tris/HCl, pH 7.5, 10 mM $MgCl_2$, 1 mM imidazole, 2 mM EGTA, 10 mM β-mercaptoethanol) in 2 fractions: E1 200 µl, E2 250 µl. RNA from 50 µl of E2 was extracted with phenol:chloroform and ethanol precipitated for Northern analysis. Proteins from the remaining 200 µl of E2 were precipitated with 3.6 volumes of ice-cold acetone and incubated at -20°C overnight followed by centrifugation at 15,000 g and resuspension in sample buffer (1% SDS, 8 M Urea, 10 mM Tris, pH 6.8, 10 mM EDTA,

0.01% bromophenol blue). Protein samples were analyzed by Western blot and mass spectrometry.

Western Analysis

Protein samples were run on 12% SDS-PAGE gels and transferred to membranes (Whatman – Protran BA 85). Rio2TAP was detected with polyclonal Anti-TAP antibody (Open Biosystems). Native Tsr1, Ltv1, Enp1, Pno1, and Dim1 were detected with polyclonal antibodies generated against full length recombinant protein in rabbits at Josman, LLC. Native Nob1 was detected with polyclonal anti-Nob1 (Bioacademia). Native Rio2 was detected with polyclonal anti-Rio2 (Santa Cruz).

Northern Analysis

For RNAs larger than 1000 nucleotides, RNA samples were loaded onto a 1.25% agarose gel containing 6.7% formaldehyde and ran for 12 h with circulating MESA buffer (MOPS-EDTA-sodium acetate) at 95V. The RNA was transferred overnight onto a Hybond-N membrane by passive transfer. RNAs smaller than 500 nucleotides were run on an 8% 0.5X TBE-7M urea denaturing polyacrylamide gel at 25W for 1h and transferred onto a Hybond-N membrane in 0.5X TBE at 8V for 1h with a Trans-Blot SD Semi-Dry Electrophoretic Transfer Cell (BioRad). After blocking, RNA was probed for ITS1 between cleavage sites D and A_2 (probe B-gctctcatgctcttgcc), 18S rRNA (gcccgttcccttggctgtg), 25S rRNA (probeY-catggcttaatctttgagac), or initiator $tRNA_i$-^{Met} (tcggtttcgatccgaggacatcagggttatga).

Mass Spectrometry

Samples were run on 12% SDS-PAGE gels and the area of interest was excised from the gel. Gel samples were subjected to proteolytic digestion with trypsin and analyzed using

LC/MS/MS. Product ion data were searched against the SwissProt database using the Mascot search engine. Mascot output files were parsed into the Scaffold program for filtering to assess false discovery rates and allow correct protein identifications. Mass spectrometry analysis was performed by the Proteomics Core at Scripps Florida.

In vitro protein binding experiments.

Proteins were recombinantly expressed and purified as described [245]. 3 µM MBP-tagged bait protein was combined with 10 µM untagged prey in 100 µl binding reactions with final binding buffer concentrations of 50 mM HEPES, pH 7.6, 100 mM KCl and 10 mM $MgCl_2$ and 1 mM DTT in the presence or absence of 1 mM ATP. The protein mix was incubated at 4°C with 25 µl of amylose resin (New England Biolabs) equilibrated with binding buffer and incubated at 4°C on an orbital shaker for 30 minutes. The slurry was loaded onto a Bio-Spin disposable chromatography column, washed three times with 100 µl binding buffer (supplemented with 1 mM ATP for binding in the presence of ATP) and amylose bound protein was eluted with 25 µl of 50 mM HEPES, pH 7.5, 100 mM NaCl, 10 mM $MgCl_2$, and 20 mM maltose. Input, flow-through, final wash, and elution samples were run on 12% SDS-PAGE gels and stained with Coomassie Blue (BioRad).

Table 4.1: Yeast Strains Used in this Study.

Strain	Description	Genotype	Reference
YKK87	Rio2TAP	BY4741 Rio2TAP::His	Open Biosystems
YKK132	Gal1::Fap7TAP	BY4741 Gal1::Fap7TAP::Clonat/His	This work
YKK216	Gal1::Fap7/Rio2TAP	BY4741 Gal1::Fap7::Clonat Rio2TAP::His	This work
YKK217	Gal1::Nob1/Rio2TAP	BY4741 Gal1::Nob1::KAN/pRS416 pTEF::Nob1 D92N Rio2TAP::His	This work
YKK358	Tet07::Rio1	*MAT**a** URA3::CMV-tTA MATa his3Δ1 leu2Δ0 met15Δ0 kanMX3::TetO7-RIO1*	Open Biosystems, [239]
YKK356	Gal1::Rio2	*MAT**a** His3Δ leu2Δ met15Δlys2Δura3Δ Rio2::KAN*/pEV80 (pGAL1::Rio2-PROTA URA3) /pRS415 +pCyc1::Rio2 D229A	[118]
UBHY-R	Gal1::Ubiquitin-Argenine-LacI-Hyp2	*W303-1A MAT**a** leu2-3, 112 his3-11, 15 ade2-1 ura3-1 trpl-1 canl-100* +YCpUB-RHyp2	[281]
HYY13	Parent strain for UBHY-R	*MAT**a** leu2-3, 112 his3-11, 15 ade2-1 ura3-1 trpl-1 canl-100 Hyp2::LEU2 Anb1::HZS3* +pHSTC-Hyp2	[282]
JWY615	ΔRps14A/Gal1::Rps14B/rps14b R134A	*Mat**α** his3Δ200 trp1Δ101 leu2Δ2 ura3-167 rps14a::TRP1 rps14b::LEU2 +pGAL-RPS14A* + pRS313-rps14b R134A	[187]

4.3 Results

Depletion of Fap7 leads to accumulation of 80S ribosomes containing pre-40S subunits

Depletion of Fap7 leads to a large accumulation of 20S rRNA, the precursor to 18S rRNA, in the cytosol. To better understand the role Fap7 plays in late 40S assembly, and to delineate where it acts in the 40S assembly pathway, we investigated the composition of pre-40S particles that accumulate upon Fap7 inactivation. Genomic Fap7 was placed under the control of a galactose-inducible promoter and expression of Fap7 was shut-off by shifting cells from galactose to glucose-containing media for 16 hours. To trap translating ribosomes on mRNA in polysomes, cyclohexamide was added prior to cell harvesting and lysis. Lysates prepared from wildtype and Fap7 depleted cells were fractionated in 10-50% sucrose gradients and rRNA sedimenting in these gradients was detected by UV absorbance (**Fig. 4.2A**). As expected for cells in which 40S assembly has been disrupted and 40S subunit content is reduced, Fap7 depleted cells showed a reduction in free 40S subunits, a reduction in translating ribosomes in polysomes, and an increase in free 60S subunits [105] relative to wildtype. Unexpectedly, Fap7 depletion also resulted in a large increase in 80S subunits, which corresponds to joined 60S and 40S subunits. This increase is not observed upon depletion of Rio1, Rio2, or Nob1, all of which also inhibit 20S processing in the cytoplasm (**Fig. 4.3**). The same accumulation is observed when the Fap7 mutant D82AH84A, driven by its native promoter, is provided on a plasmid (**Fig. 4.2D**), while wildtype Fap7 restores the wildtype phenotype (**Fig. 4.2E**).

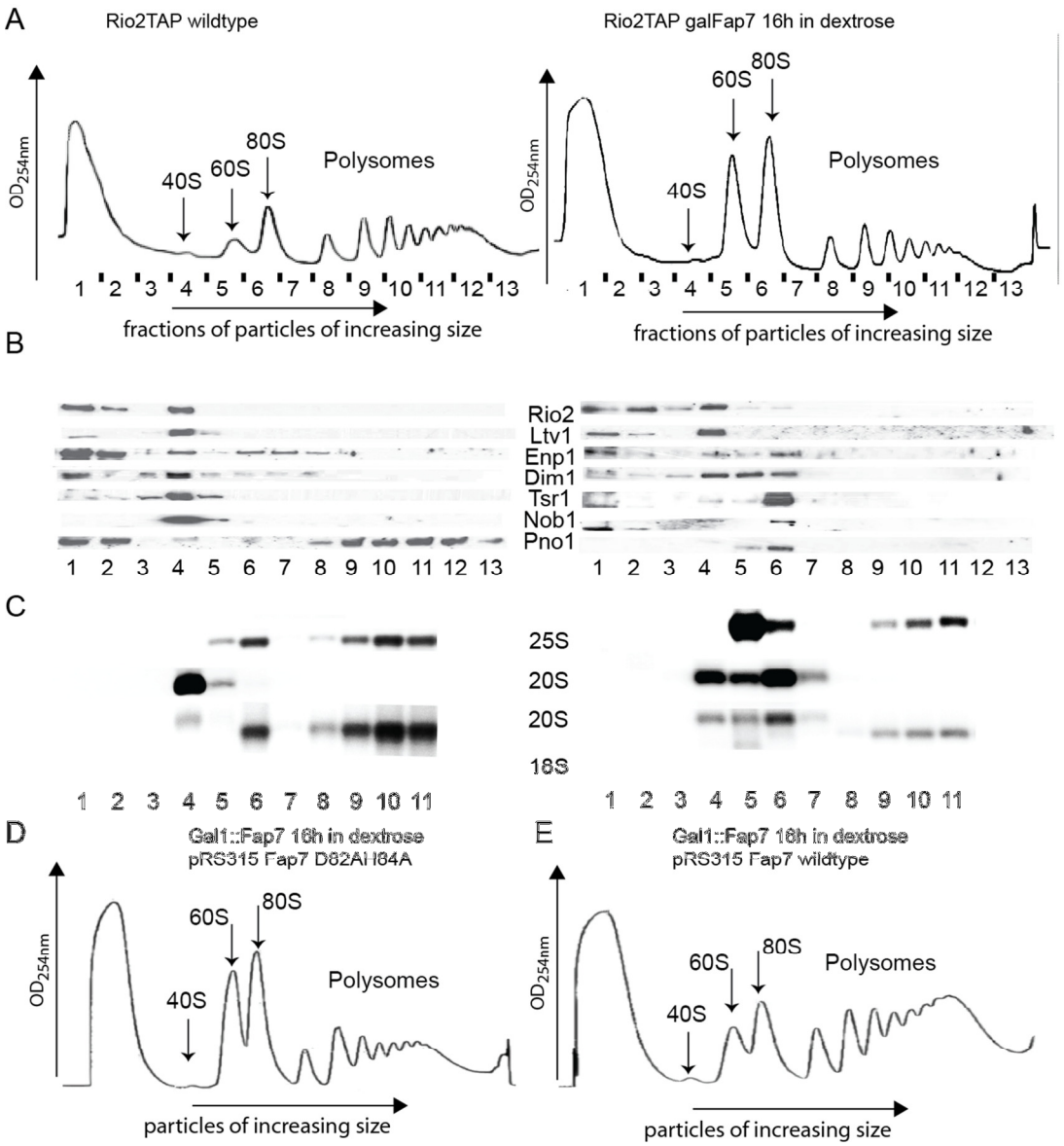

Figure 4-2 An 80S intermediate accumulates upon Fap7 inactivation (A) Polysome profiles of yeast lysates sedimented by sucrose gradient centrifugation indicate that upon Fap7 depletion, free 60S subunits increase and the monosome to polysome ratio of 80S ribosomes increases. (B) Western blots probed for assembly factors in sucrose gradient centrifugation fractions. (C) Northern blots of RNA in sucrose gradient fractions probing for indicated rRNA species. (D) Polysome profile of Gal1::Fap7 strain with Fap7 mutant D82AH84A provided on a plasmid under the control of its native promoter. (E) Polysome profile of Gal1::Fap7 strain with wildtype Fap7 provided on a plasmid under the control of its native promoter.

To better understand the nature of 80S particles that accumulate in the absence of Fap7, we prepared large amounts of 80S particles and analyzed them for RNA and protein

content using Northern analysis, SDS-PAGE and mass spectrometry.

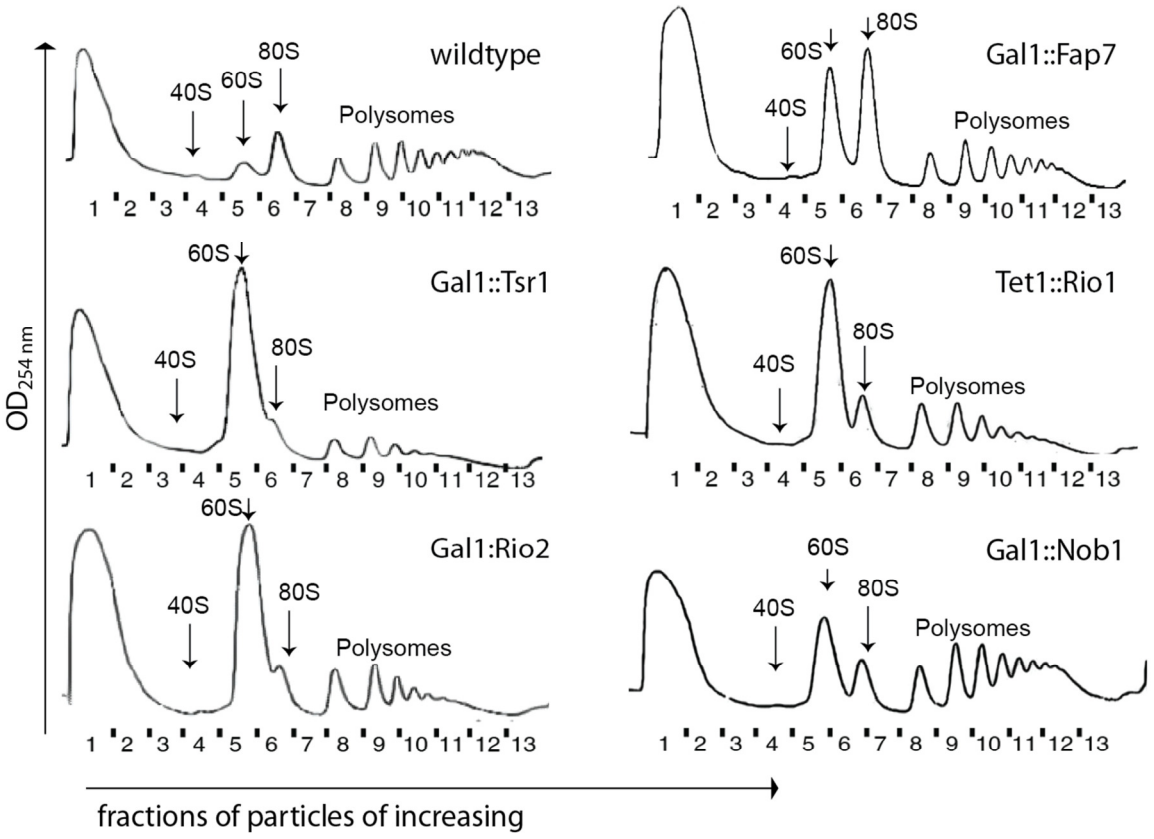

Figure 4-3 80S accumulation upon stalling of 20S processing is unique to Fap7 inactivation. Polysome profiles from wiltype cells and Fap7 depleted cells compared to cells in which cleavage at site D in the 20S rRNA (which produces the mature 3' end of the 18S rRNA) is stalled through inactivation or depletion of other assembly factors required for this step in 40S maturation.

80S ribosomes contain 20S pre-rRNA

RNA was extracted from gradient fractions and rRNAs were separated by formaldehyde-agarose gel electrophoresis. Northern analysis of the rRNA from the Fap7 depleted cells revealed that 20S rRNA is detectable in the 40S and 80S fractions, with the highest signal falling in the 80S fraction, and that most of the small subunit rRNA of the 80S peak is 20S rRNA and not mature 18S rRNA (**Fig. 4.2C**). Quantification of the relative 18S to 20S signal in the 80S fractions in the Fap7 mutant indicates that the mature 18S rRNA makes up only 20-40% of the small subunit rRNA species present (**Fig. 4.2C**). As

expected, the 80S fraction also contains large subunit (25S) rRNA (**Fig. 4.2C**). In contrast, the mature 18S rRNA was the only 40S rRNA detectable in polysomes. Thus, disruption of 20S processing by depletion of Fap7 leads to stable association of pre-40S particles with 60S subunits, but these 80S particles do not enter polysomes; in other words, it is unlikely that they are binding mRNA. Substantial association of the 20S rRNA with 60S subunits in 80S fractions has also been observed in a carboxy-terminal point mutant of Rps14 [187] and to a lesser extent upon depletion of Rio1 [239]. The 20S rRNA is often found to a small extent in the 80S peak as well as polysomes, even in wildtype cells [239], raising the possibility that an 80S particle harboring the 20S rRNA could be a normal and perhaps obligatory assembly intermediate.

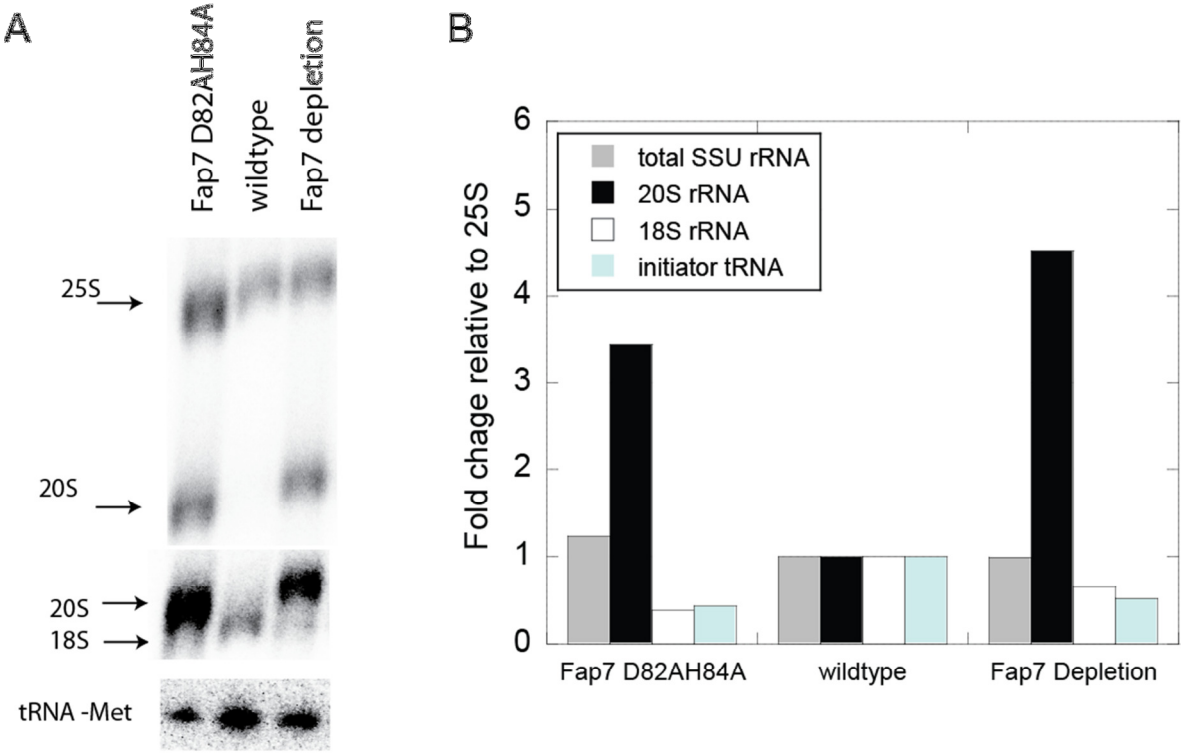

Figure 4-4 tRNA levels are consistent with the binding of mature 18S rRNA only. (A) Northern analysis of 20S, 18S, and 25S rRNAs and initiatior tRNA-Met from 80S fractions from wildtype strains and Gal1::Fap7 strains with either no plasmid or Fap7 D82AH84A expressed from plasmid pRS315 under its native promoter. (B) Quantification of indicated RNA species from northern blot relative to wildtype, normalized to the 25S rRNA.

tRNA levels in 80S ribosomes correlate with binding to mature 18S rRNA

In canonical translation initiation, 40S and 60S subunit joining is preceded by both binding of initiator tRNA to the P-site of the 40S subunit and mRNA recruitment. Initiating 80S ribosomes are therefore expected to contain both tRNA and mRNA. If pre-40S ribosomes bound mRNA, this mRNA would likely associate with already translating mature ribosomes, and should sediment in polysomes. The observation that pre-40S ribosomes accumulate in 80S fractions and are not observed in polysome fractions strongly suggests that these 80S ribosomes do not have mRNA bound. To test if the 80S ribosomes contained initiator tRNA, which is typically required for 60S joining, we used Northern blotting after PAGE to analyze small RNAs from the 80S fraction (**Fig. 4.4A**). Initiator tRNA was detectable in 80S fractions from the wildtype and Fap7 mutant cells. However, normalization to 25S levels indicates that only 40% of the 80S particles have tRNA bound (**Fig. 4.4B**). This is also the percentage of 80S particles containing mature 18S rRNA in the Fap7 mutant cells (**Fig. 4.4B**), strongly suggesting that the tRNAs observed in 80S particles in Fap7 depleted cells are all associated with mature 40S particles only, and that 80S particles containing pre-40S subunits do not have tRNA bound.

Pre-40S subunits in 80S particles are associated with assembly factors

The accumulation of 20S rRNA in 80S complexes upon inactivation of Fap7 indicates that it is joining with 60S particles. However, the exclusion of these 80S complexes from polysomes and their relative (and likely complete) lack of tRNA indicate that the pre-40S subunit and the 60S subunit have not joined through the canonical translation initiation pathway and are not pre-initiation complexes. To further investigate the nature of the pre-

40S particles in these unusual 80S complexes, we began an investigation of the protein composition of these particles using western blot analysis of the gradient fractions from Fap7 depleted cells; we probed for the presence of the seven assembly factors (AFs) stably bound to the cytoplasmic pre-40S particle modeled in chapter 2 and compared the results to those of wildtype cells. The AFs we examined were Nob1, the endonuclease responsible for the cleavage event producing the mature 3' end of the 20S rRNA, the Nob1 regulator Pno1, the methylase Dim1, the kinase Rio2, as well as Tsr1, Ltv1, and Enp1. In wildtype cells, all AFs show peaks in 40S fractions, as expected from their association with pre-40S ribosomes (**Fig. 4.2B**). In addition, Pno1 shows association with polysomes, demonstrating that this factor can be bound to pre-40S ribosomes that bind to mRNA. As expected, based on their early association with pre-40S particles [173], Dim1, Enp1 and Pno1 are also found in early 90S pre-ribosomes (**Fig. 4.2B**).. Upon Fap7 depletion, Tsr1, Nob1, Pno1, Dim1 and Enp1 all localize to 80S fractions, with all but Dim1 showing the largest association with 80S particles upon depletion of Fap7. In contrast, Ltv1 and Rio2 remain primarily in free and in 40S fractions in the Fap7 mutant. Dissociation of Rio2 and Ltv1 from the pre-40S complex therefore occurs independently of Fap7 activity in these cells (**Fig. 4.2B**).

The peptide composition of 80S complexes from wildtype and Fap7 depleted cells are similar but distinct

Although western blots indicated the 80S complexes that accumulated upon inactivation of Fap7 were associated with five of the seven AFs known to be stably associated with cytoplasmic pre-40S particles, Coomassie stained SDS-PAGE gels of the proteins present in these particles indicated that these AFs were not stoichiometrically represented in these

80S complexes (**Fig. 4.5**). In fact, the peptide composition, as visualized by Coomassie

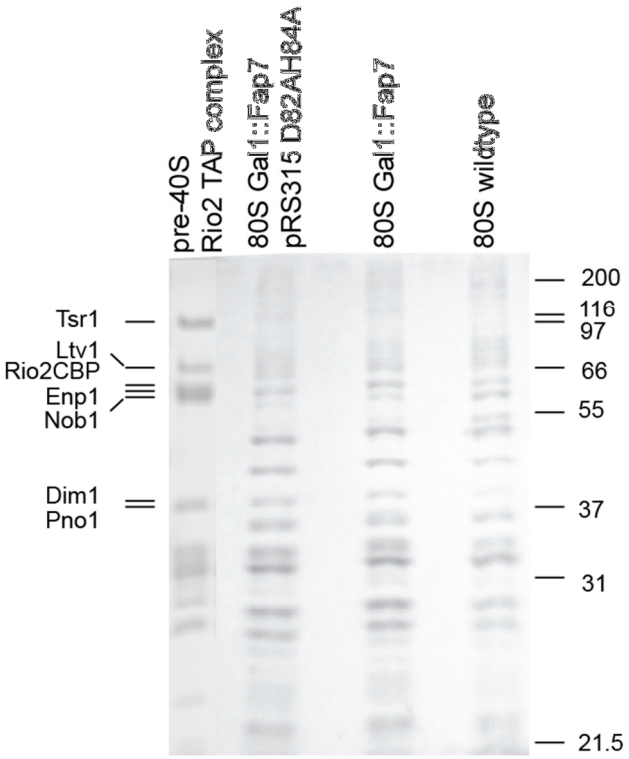

Figure 4-5 Protein composition of 80S fraction that accumulates upon disruption of Fap7 resembles 80S fraction in wildtype cells. Coomassie stained SDS-PAGE gel of proteins in the 80S fraction of sucrose gradients of both wildtype strains and Gal1::Fap7 strains with either no plasmid or Fap7 D82AH84A expressed from plasmid pRS315 under its native promoter. The pre-40S complex purified through a TAP-tag on Rio2 TAP is included for reference; assembly factors in this complex are labeled.

staining, is not starkly different from that observed in the 80S complexes present in wildtype cells. In addition to the expected large subunit ribosomal proteins (Rpl) and small subunit ribosomal proteins (Rps), there are several bands present in the 80S complexes from both wildtype and Fap7 depleted cells that do not correspond in size to the seven assembly factors probed for by western blot. For identification, all bands were excised from the Coomassie stained SDS-PAGE gel and analyzed by mass spectrometry. The results are summarized in **Tables 4.2** and **4.3**.

Rps10 and Asc1/Rack1 are fully represented in premature 80S ribosomes

As expected, analysis of the levels of ribosomal proteins from large subunits (Rpl) indicates that all Rpl are fully bound in the 80S complex that accumulates upon Fap7 depletion. This analysis also indicated that the Fap7 mutant sample is more abundant as, on average. 1.8-fold more peptides were observed. Importantly, not a single Rpl showed more peptides in the wildtype 80S fractions than analyzed proteins present in the 80S fractions from wildtype and Fap7 mutant cells. Using this analysis of the peptide content from 60S proteins as a base line, we next turned to analyze the protein content from the assembling 40S subunits. Rps10 and Rps26 are both absent in stable pre-40S particles because their binding sites are blocked by the Ltv1/Enp1 complex and Pno1, respectively [275]. In contrast, the levels of Rps10 in 80S ribosomes from Fap7 depleted cells are at the level of those observed in wildtype cells, indicating that Rps10 is bound prior to Fap7 activity. This is consistent with the observation that Ltv1 dissociates before Fap7 activity as described above. In contrast, Rps26, the other ribosomal protein absent from Ltv1 and Rio2 associated pre-40S complexes, is underrepresented in the mutant 80S ribosome and reflects the levels of mature 40S rRNA in the samples, indicating that Rps26 is not fully bound to pre-40S subunits prior to Fap7 activity. As Pno1 is not stoichiometrically represented in these 80S complexes, this finding suggests that Rps26 incorporation requires D-site cleavage and not simply dissociation of Pno1. Asc1/yRack1, a core component of mature small ribosomal subunits [287], is fully represented in both mature and premature 80S fractions, establishing the association of this protein as upstream or independent from Fap7 in the maturation pathway. Furthermore, this finding also suggests that Asc1 can bind ribosomes in the absence of protein synthesis.

Table 4.2: Translation factors in 80S ribosomes from wildtype and Fap7 D82AH84A cells.

	#Assigned spectra						
	D82AH84A	**Wildtype**	**D82AH84A:wt ratio**	**MW/kDa**	**Function**	**Phenotype**	**Reference**
Pab1	17	24	**0.7***	64	Translation initiation	-	-
eIF4G1	9	0	**D82AH84A only**	107	Translation initiation	60S deficiency 20S accumulation	[279]
EF1a	8	10	**0.8***	50	Translation elongation	-	-
eIF5b	3	9	**0.3***	112	Translation initiation	20S accumulation	[279]
eIF5A	1	5	**0.2***	17	Translation initiation	20S accumulation	This work
EF-2	0	4	**wt only**	93	Translation elongation	-	-
Clu1	0	4	**wt only**	145	Bound to eIF3	-	-
Rli1	0	3	**wt only**	68	80S dissociation	40S deficiency	[91]
eIF4E	0	3	**wt only**	24	Translation initiation	-	-

*80S fractions from wildtype and mutant cells were separated by SDS-PAGE and the entire lane was analyzed by mass spectrometry after in gel trypsin digestion. Representation of mutant proteins is likely overestimated, as the total number of peptides corresponding to ribosomal proteins was nearly two-fold higher in the Fap7 D84AH84A relative to wildtype (D82AH84A to wildtype ratio: 1.8 for large subunit proteins, 1.5 for small subunit proteins).

Table 4.3: Small subunit ribosomal proteins in 80S ribosomes from wildtype and Fap7 D82AH84A cells.

		# assigned spectra	
Ribosomal protein	**MW/kDa**	**D82AH84A**	**wildtype**
Asc1	35 kDa	43	31
Rps0	28 kDa	28	23
Rps1	29 kDa	27	44
Rps2	27 kDa	24	13
Rps3	27 kDa	61	33
Rps4	29 kDa	66	36
Rps5	25 kDa	72	22
Rps6	27 kDa	29	25
Rps7	22 kDa	73	35
Rps8	22 kDa	31	16
Rps9	22 kDa	48	47
Rps10	13 kDa	11	7
Rps11	18 kDa	29	13
Rps12	15 kDa	18	12
Rps13	17 kDa	29	20
Rps14	15 kDa	12	11
Rps15	16 kDa	23	11
Rps16	16 kDa	47	20
Rps17	16 kDa	32	18
Rps18	17 kDa	33	19
Rps19	16 kDa	36	14
Rps20	14 kDa	25	19
Rps21	10 kDa	18	9
Rps22	15 kDa	20	15
Rps23	16 kDa	32	17
Rps24	15 kDa	40	26
Rps25	12 kDa	18	11
Rps26	14 kDa	9	12
Rps27	9 kDa	9	5
Rps28	8 kDa	7	5
Rps29	7 kDa	13	9
Rps30	7 kDa	13	6
Rps31	9 kDa	12	5

*80S fractions from wildtype and mutant cells were separated by SDS-PAGE and the entire lane was analyzed by mass spectrometry after in gel trypsin digestion. Representation of mutant proteins is likely overestimated as the total number of peptides corresponding to ribosomal proteins was nearly two-fold higher in the Fap7 D84H84 relative to wildtype (D82H84 to wildtype ratio: 1.8 for large subunit proteins, 1.5 for small subunit proteins).

80S from Fap7 depleted cells is associated with a unique subset of translation factors

eEF1α, Pab1 and Stm1 are the only translation factors approaching equal representation in both samples[1]. eEF1α is the eukaryotic homolog of the bacterial elongation factor EF-Tu and is involved in the delivery of amino-acyl tRNA to the A site during translation elongation [288]. Pab1 binds the polyA tail and also interacts with eIF4G. EF-2, eIF5A, eIF5B, Rli1, and eIF4E were all found in both the mutant and wildtype samples, but were overrepresented in the wildtype 80S fraction relative to Rpl. EF-2 is a GTPase that catalyzes translocation during elongation [289]. eIF4E is a component of the eIF4F mRNA cap binding complex that, like Pab1, interacts directly with eF4G. eIF5A is required for formation of the first peptide bond but not for subsequent elongation cycles [277]. eIF5B is a GTPase that catalyzes 60S subunit joining [288]; Rli1 has subunit dissociation activity [290]. The potential significance of the overrepresentation of Rli1 and eIF5B in the wildtype 80S fraction is punctuated by the previous implication of both of these proteins in small subunit biogenesis: Rli1 depletion leads to large and small subunit deficiencies [92] and eIF5B deletion specifically impairs 20S processing [279]. The only translation factor found in the mutant 80S fraction but not the wildtype was eIF4G1, and no peptides corresponding to eIF4G2 were observed[2]. Interestingly, eIF4G1, but not eIF4G2, was previously implicated in assembly of both ribosomal subunits [279]. eIF4G interacts with Asc1 [157, 219] and this interaction may serve to dock eIF4G1 in pre-mature 80S ribosomes.

[1] While the Fap7 depleted sample was 1.8-fold more abundant (as determined by the levels of Rpl), for proteins that were less abundant, that ratio does not always hold. Because all translation factors are relatively low abundant, an exact determination of their levels was not possible.

[2] eIF4G1 is about 2-3 fold more abundant than eIF4G2; however, this relative abundance predicts that if both eIF4G1 and eIF4G2 bind, peptides specific to both proteins should be identified.

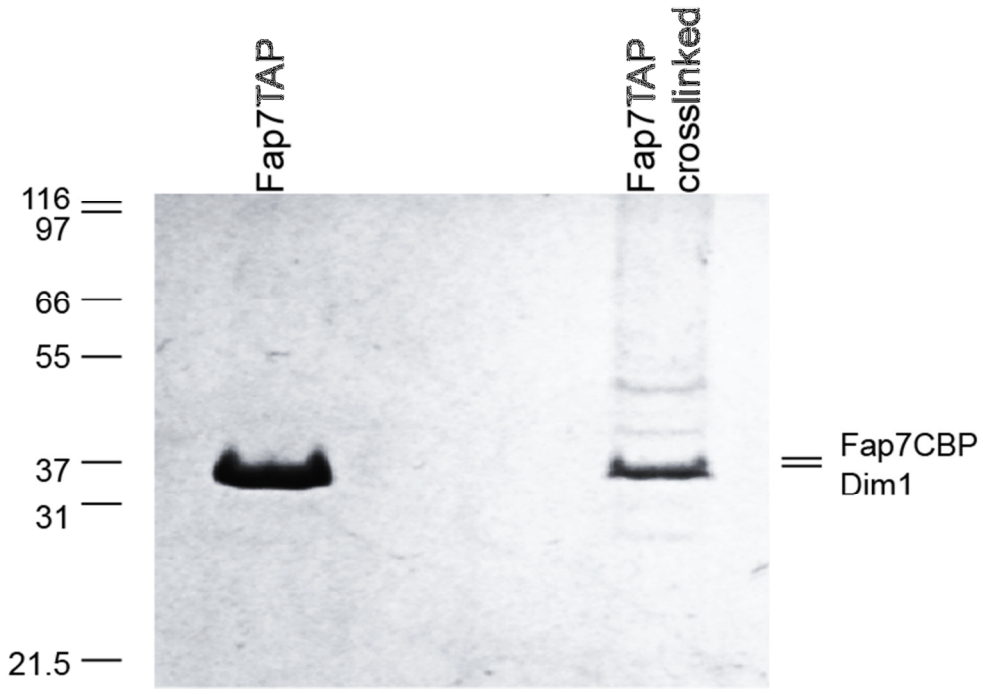

Figure 4-6 *in vivo* formaldehyde cross-linking of Fap7TAP allows co-purification of transiently associated peptides. Coomassie stained 12% SDS-PAGE gel of peptides purified through a tap tag on FAP7 following cross-linking with 1% formaldehyde (Fap7TAP cross-linked) or without cross-linking (Fap7TAP).

Wildtype Fap7 cross-links 80S complexes in vivo

The accumulation of an 80S particle with 20S rRNA upon inactivation of Fap7 suggests that Fap7 acts in the context of an 80S particle. Consistent with this, a small amount of Fap7 co-fractionates with pre-40S ribosomes as well as 80S-like particles in sucrose gradients [117]. The majority of Fap7, however, is not ribosome bound [117], implying that interactions between this intermediate and Fap7 must be transient. To identify novel Fap7 interactions *in vivo*, yeast cells expressing TAP-tagged Fap7 from a galactose inducible promoter were grown to mid-log phase in 0.2% galactose and 2% raffinose. Cells were then treated with 1% formaldehyde to covalently cross-link Fap7 to transiently associated proteins or RNA (**Fig. 4.6**), and proteins purified through cross-links to complexes associated with wildtype Fap7TAP were analyzed by mass spectrometry

(**Table 4.4**). As expected, Fap7's binding partner Rps14 is among the proteins pulled down with Fap7, but several additional ribosomal proteins were also identified (**Table 4.4**). Several large subunit ribosomal proteins were also identified (**Table 4.4**). This finding suggests that the 80S particle does not simply accumulate upon depletion or inactivation of Fap7, but is a *bona fide* substrate for wildtype Fap7. The most abundant proteins co-purifying with Fap7 are eEF1α, Dim1, and eIF5A. When overexpressed, Fap7 also interacts with EF-2 and EF-3 (a guanine nucleotide exchange factor for eIF1α). eEF1α, Dim1, and eIF5A are cross-linked to Fap7 associated complexes under both conditions.

Fap7 directly interacts with Dim1 in vitro

The data above demonstrate that Fap7 acts in the context of an 80S particle from which Ltv1 and Rio2 have already dissociated, while the other assembly factors (Tsr1, Enp1, Nob1, Pno1 and Dim1) remain bound. Furthermore, Dim1 is the only assembly factor co-purified with Fap7TAP. To test if Fap7 interacts directly with Dim1 or any other assembly factor, *in vitro* binding assays were performed between untagged Fap7 and maltose-binding-protein (MBP)-tagged Tsr1, Ltv1, Nob1, Rio2, Pno1, or Dim1 or (MBP)-Fap7 and untagged Dim1, Enp1, Tsr1 and eIF5A in the presence or absence of 1 mM AMP-PCP. These data demonstrate a direct interaction between MBP-tagged Fap7 and Dim1 (**Fig. 4.7**). This interaction is sensitive to the location of the MBP-tag, as it was substantially less efficient with MBP-tagged Dim1 than with MBP-tagged Fap7, as previously observed for certain interactions between AFs [244]. Together, *in vivo* cross-linking and *in vitro* binding data suggest that Fap7 may facilitate 20S processing through a direct interaction with Dim1 and Rps14 [117].

Table 4.4: Proteins cross-linked to Fap7TAP *in vivo*

	# assigned spectra	MW/kDa	cellular function	assembly phenotype	reference
eEF1α	36	50 kDa	Translation elongation	-	-
Tsa1	14	22 kDa	Ribosome-associated thioredoxin peroxidase	-	-
Bmh2	11	31 kDa	14-3-3 protein	-	-
eIF5A	9	17 kDa	Translation initiation	20S accumulation	this work
Dim1	7	36 kDa	18S rRNA dimethylase	33S accumulation	[127]
eIF4A	2	45 kDa	Translation initiation	-	-
eEF1β	2	23 kDa	Translation initiation	-	-
Asc1	3	35 kDa	ortholog of RACK1; core 40S component	-	-
Rps0	9	28 kDa	40S ribosomal protein	-	-
Rps14	3	15 kDa	40S ribosomal protein	-	-
Rps16	6	16 kDa	40S ribosomal protein	-	-
Rps18	2	17 kDa	40S ribosomal protein	-	-
Rps19	4	16 kDa	40S ribosomal protein	-	-
Rps22	2	15 kDa	40S ribosomal protein	-	-
Rps24	2	15 kDa	40S ribosomal protein	-	-
Rpl7	2	22 kDa	60S ribosomal protein	-	-
Rpp0	7	34 kDa	60S ribosomal protein	-	-
Rpl11	2	20 kDa	60S ribosomal protein	-	-
Rpl12	6	18 kDa	60S ribosomal protein	-	-
Rpl23	2	14 kDa	60S ribosomal protein	-	-
Rpl26	3	14 kDa	60S ribosomal protein	-	-
Rpl5	3	34 kDa	60S ribosomal protein	-	-
Rpl6	3	20 kDa	60S ribosomal protein	-	-

Cells were formaldehyde cross-linked, Fap7-associated particles purified by TAP purification, and proteins separated by SDS-PAGE. The entire lane was analyzed by mass spectrometry after in gel digestion. Top scoring proteins are identified.

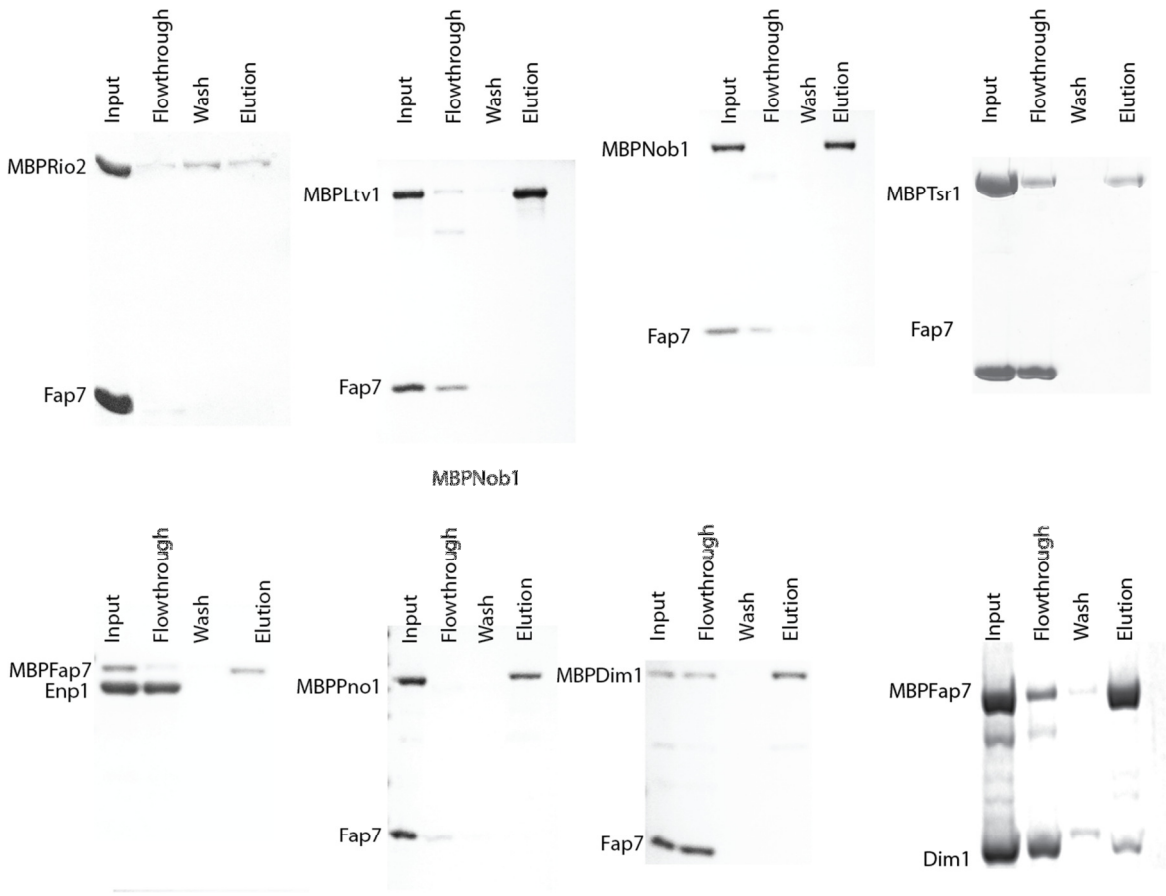

Figure 4-7 Dim1 interacts directly with Fap7 *in vitro*. Coomasssie stained SDS-PAGE gels of pulldowns to test for protein-protein interactions between recombinantly purified Fap7 and late assembly factors. 3 µM MBP-tagged bait proteins were incubated with 10 µM untagged prey and bound to amylose resin. 10% of input, 5% of flowthrough, 5% of last of 3 washes with binding buffer and 20% of elution were loaded on gel.

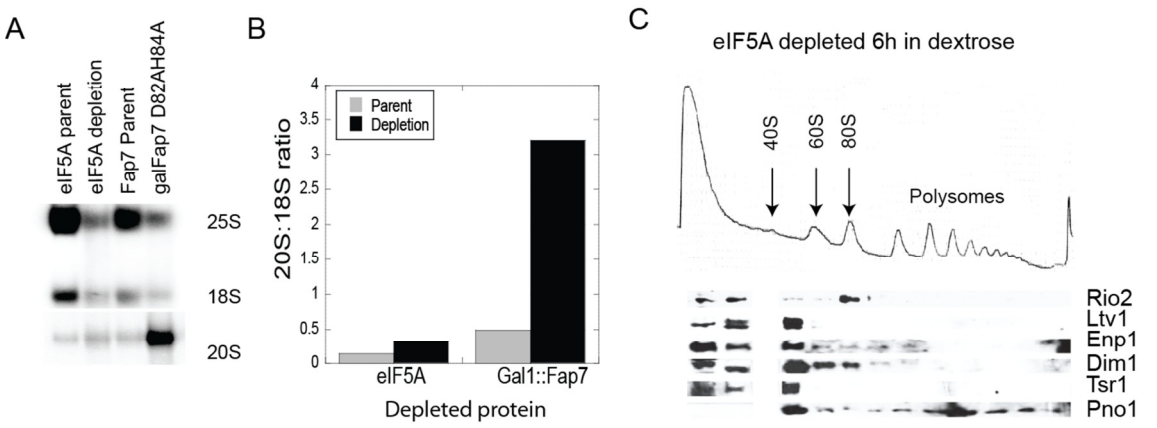

Figure 4-8. eIF5A facilitates 20S processing and dissociation of Rio2 from pre-40S particles. (A) Polysome profile from sucrose gradient analyis of strain depleted for eIF5A. (B) Western blots of gradient fractions probing for cytoplasmic assembly factors (labeled).

eIF5A/Hyp2 is a small subunit assembly factor required for 20S processing

The 80S particles that accumulate with 20S rRNA upon mutation of Fap7 suggest that Fap7 acts in the context of an 80S particle, and 80S components that interact with Fap7 could, in turn, play a role in small subunit maturation. One such factor is eIF5A (Hyp2), which was cross-linked to Fap7 and is underrepresented in 80S ribosomes from the Fap7 mutant, suggesting that it could function in ribosome assembly, analogous to eIF5B and Rli1 [91, 279]. To test this hypothesis, we analyzed 18S rRNA maturation upon depletion of eIF5A [277, 281, 282]. Northern analysis of ribosomal rRNAs following depletion indicates that 20S rRNA accumulates 3.6-fold in this sample relative to 18S rRNA levels, implicating eIF5A as a factor involved in 20S processing (**Fig. 4.8A**). Furthermore, polysome analysis of eIF5A depleted cells indicates that both free 60S levels and 80S levels increase, as observed in the Fap7 mutant strain (**Fig. 4.8B**). Western analysis for cytoplasmic small subunit assembly factors across the gradient indicated that Dim1, Rio2, and Pno1 are associated with an 80S particle upon depletion of eIF5A. Association of Nob1 with this particle has not yet been tested. Therefore, as observed upon depletion of Fap7, a subset of assembly factors are bound to an 80S particle consistent with

accumulation of pre-40S subunits associating with 60S subunits. While depletion of Fap7 does not significantly alter the distribution of Rio2 in free and 40S fractions, depletion of eIF5A results in a shift of Rio2 from 40S to 80S particles. This finding suggests a requirement for eIF5A to effect Rio2 dissociation. The absence of Ltv1 in the 80S fractions was also observed upon depletion of Fap7, indicating that Ltv1 leaves upstream or independently from the action of both eIF5A and Fap7. The presence of Tsr1 in 80S fractions in Fap7 depleted cells but not eIF5A depleted cells indicates that dissociation of Tsr1 is specifically dependent on Fap7.

Similar 80S particles accumulate in the Fap7 D82AH84A and Rps14 R134A mutants

A point mutation in the C-terminal tail of the small subunit ribosomal protein, Rps14 R134A, has been shown previously to display very similar assembly phenotypes to those observed upon depletion of Fap7. Both demonstrate unusually large accumulation of 20S rRNA, and both result in a shift of 20S rRNA to 80S ribosomes [117, 187]. Furthermore, Fap7 and Rps14 interact directly *in vitro* [117].

To further investigate the relationship between these two mutations, we analyzed the distribution of cytoplasmic assembly factors in sucrose density gradients in cells expressing Rps14 R134A (see materials and methods and [187]). As observed upon depletion of Fap7, mutation of R134 in Rps14 leads to accumulation of Tsr1, Enp1, Dim1, Nob1, and Pno1 in 80S particles, while Rio2 and Ltv1 sediment with pre-40S ribosomes only (**Fig. 4.9**). These data indicate that mutation of Rps14 R134 and depletion of Fap7 are closely linked.

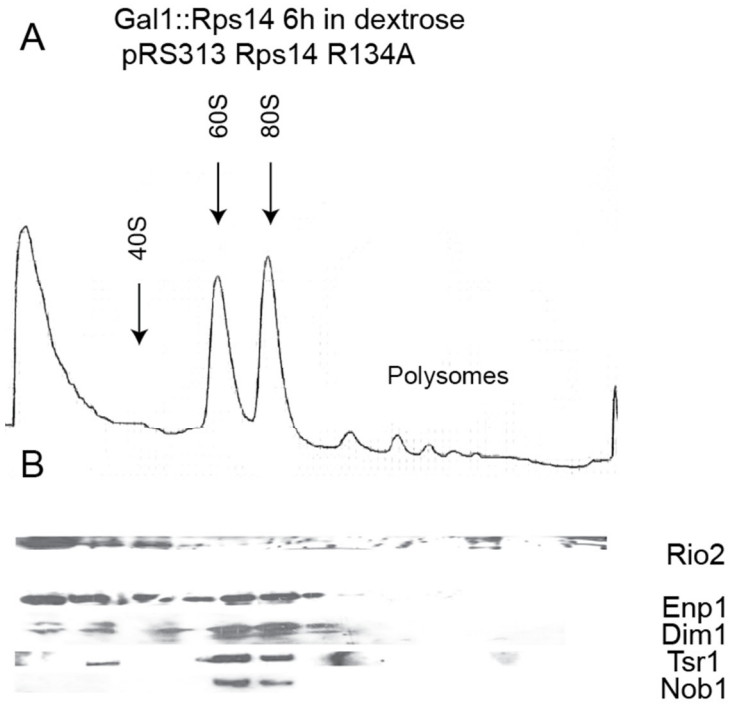

Figure 4-9 Assembly factors accumulate in 80S fraction in Rps14 C-terminal point mutant R134A. (A) Polysome profile from sucrose gradient analysis of Rps14 R134A mutant strain. (B) Western blots of gradient fractions probing for cytoplasmic assembly factors (labeled).

4.4 Discussion

An 80S particle is a small ribosomal subunit assembly intermediate

Fap7 is required for cytoplasmic cleavage of the 20S rRNA by the Nob1 endonuclease to produce the mature 3' end of the 18S rRNA [117]. Granneman and colleagues [117] demonstrated that depletion or mutation of Fap7 leads to a large accumulation of the 20S precursor to the 18S rRNA in the cytoplasm. Here we demonstrate that the 20S rRNA that accumulates upon depletion of Fap7 is found in an 80S particle, i.e. pre-40S subunits joined with 60S subunits. Wildtype Fap7 co-purifies with ribosomal proteins from both the large and small subunit as well as 80S associated translation factors, suggesting that the 80S particle is the *bona fide* target of Fap7 and not just a result of Fap7 depletion. One of the factors co-purifying with Fap7 is eIF5A, an 80S associated protein [278]

required for the formation of the first peptide bond [277, 278]. For the first time, we demonstrate that depletion of eIF5A also leads to accumulation of 20S pre-rRNA in 80S particles and is therefore a ribosome assembly factor. Consistent with an 80S target for eIF5A in ribosome assembly, TAP-tagged eIF5A co-purifies with 80S associated factors and both large and small subunit proteins, but not with factors known to bind free 40S subunits [291]. Furthermore, mutation of an essential residue in the C-terminal extension of Rps14 leads to accumulation of 20S rRNA in 80S particles [187]. The requirement to pass through an 80S intermediate also explains the 20S rRNA processing defect observed upon deletion of eIF5B, a protein required for joining of 40S and 60S subunits [288]. Taken together, these data indicate that an 80S particle is an obligate intermediate in the small subunit biogenesis pathway that forms prior to cleavage at site D.

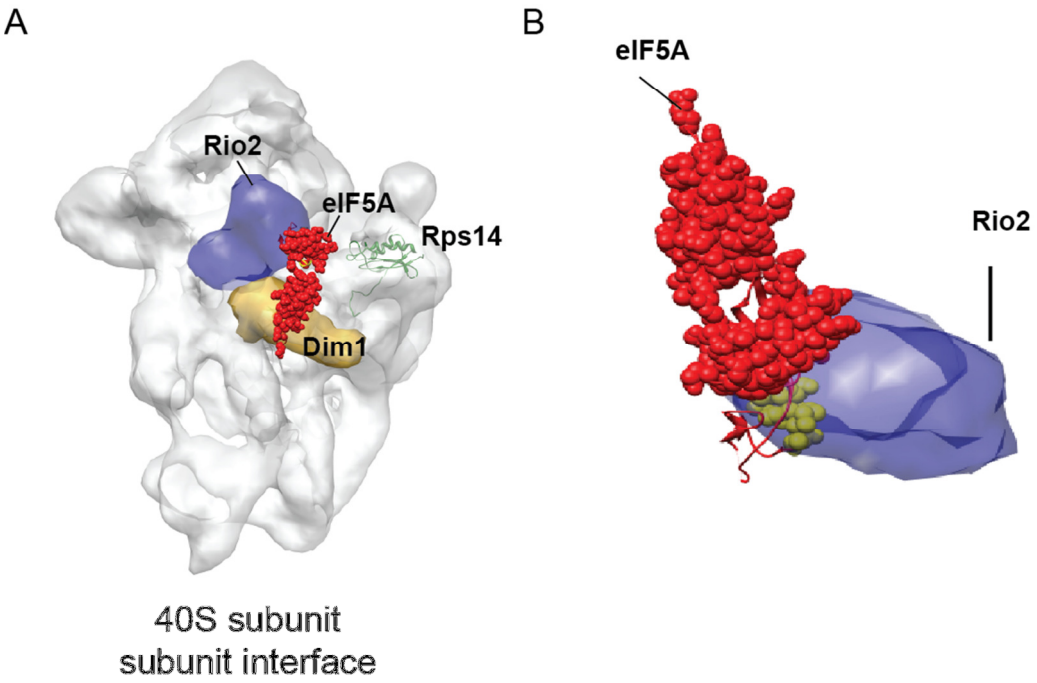

Figure 4-10 Fap7 and eIF5A target the subunit interface near the platform containing Rps14, Dim1, and Rio2. (A) Subunit interface view of electron density of cytoplasmic pre-40S particle [275] with *T. thermophilus* EF-P (eIF5A) crystal structure overlaid through fitting of associated 30S structure [278] in pre-40S volume. Rio2 is shaded in blue, Dim1 in orange, Rps14 as green ribbon, and EF-P domains I and II as red spheres. (B) Zoomed top-down view of EF-P and Rio2 from (A). Domains I and II of EF-P are modeled as red spheres and domain III not present in eIF5A is modeled as red ribbon. Additional C-terminal residues present in eIF5A are modeled as yellow spheres.

Fap7 targets an 80S intermediate near the P and E site through a direct interaction with Dim1 and Rps14 in proximity to eIF5A

Fap7 interacts directly with the small subunit ribosomal protein Rps14 [117], suggesting that it mediates cytoplasmic cleavage of the 20S rRNA through a direct interaction with small ribosomal subunits. Here, we demonstrate that Fap7 cross-links to Rps14 and Dim1 *in vivo*, and also show an interaction with Dim1 and Fap7 *in vitro*. Dim1 co-sediments with 80S particles in both wildtype and Fap7 mutant cells, consistent with Fap7 targeting an 80S intermediate. The binding sites for Dim1 and Rps14 are located in close proximity to each other on the subunit interface adjacent to the platform (**Fig 4.10A**). Interestingly, this is also the location of the binding site for eIF5A, which also cross-links to Fap7. These interactions therefore indicate that the Fap7 binding site is located on the subunit interface, adjacent to the platform region.

The similarity in phenotypes between the Fap7 mutant and the Rps14 C-terminal point mutant, R134A (this work, [117, 187]), suggests a common defect for these two mutants in the assembly pathway. The R134A mutation does not prevent binding of Rps14 to the rRNA nor does it disrupt the direct interaction between Rps14 and Fap7 [117]. Therefore, failure to recruit Fap7 does not explain the shared phenotypes of these two mutants. Rps14 assembles onto pre-rRNA early in the nucleolus; however, the R134 mutation does not produce an assembly phenotype until the late cytoplasmic 40S maturation steps. Along with other residues in the RpS14 C-terminus, R134 interacts with rRNA in mature 40S subunits [232, 237, 292], but the specific disruption of 20S processing in this mutant suggests that engagement of the C-terminal tail does not take place until this stage. Alternatively, it is possible that the interaction is made but irrelevant prior to 20S

processing. Regardless, the close linkage between the phenotype upon depletion or mutation of Fap7 and mutation of Rps14 indicates that either tail engagement requires Fap7 activity or Fap7 activity requires tail engagement.

The function of Fap7 in ribosome assembly

Fap7's ability to hydrolyze ATP, the conformational change it undergoes during the hydrolysis cycle (Chapter 3), and the essential nature of residues in both its Walker A and Walker B motifs [117, 211] suggest that it could provide mechanical energy to facilitate an otherwise unfavorable process to facilitate 18S maturation. This could involve direct removal of proteins from the pre-40S intermediate or conformational rearrangements in rRNA or proteins that in turn facilitate subsequent events in the assembly process. This and previous work [117] suggest that Fap7 mediates an event(s) required for Nob1 cleavage at site D through a direct interaction with Rps14 and Dim1 in the context of an 80S intermediate. Rps14 and Dim1 are both required for early cleavage events and export of pre-40S particles from the nucleus to the cytoplasm [173]. Depletion of either Rps14 or Dim1 obscures specific requirements for these proteins in D-site cleavage because the assembly pathway is stalled upstream of 20S rRNA production in their absence [126, 293]. Point mutations in the C-terminal tail of Rps14 uncovered a specific requirement for this protein in 20S cleavage, but no such mutants have been discovered for Dim1. The direct interaction between Fap7 and Dim1 and the *in vivo* cross-linking of both of these proteins together with ribosomal proteins from both the large and small subunit strongly suggests that Dim1 is required for Fap7 mediated cleavage at site D. It is possible that Fap7 binds Dim1 in order to induce dissociation of Tsr1, which binds to the other side of H44.

Does Fap7 regulate ribosome assembly in response to oxidative stress?

Fap7 was originally identified in a screen for genes required for activation of transcription by Pos9/Skn7, a transcription factor central to activating cellular defenses in response to peroxide induced stress [212]. How Fap7 mediates this response is not yet understood, but its localization to both the nucleus and the cytoplasm suggests thatdirect roles in both transcription and cytoplasmic ribosome assembly are possible.

Here, we observe cross-linking of Fap7 to Tsa1. Upregulation of transcription of Tsa1 in response to peroxide induced stress requires Fap7 [211]. Furthermore, Tsa1 is associated with translating ribosomes and is believed to act as a peroxidase, protecting the translational machinery against oxidative damage [294]. Under conditions of peroxide induced stress, Tsa1 shifts away from the ribosome, forming higher order complexes that serve to chaperone proteins against stress induced denaturation in a manner independent of its peroxidase activity [294]. It is unclear whether the physical interaction between Fap7 and Tsa1 identified here is direct or whether it occurs in the context of pre-ribosomal particles or as free proteins. Either way, the association of these two proteins may hint at a non-transcriptional role for Fap7 and Tsa1 in mediating the cellular response to oxidative stress. Yeast reduce protein synthesis under peroxide induced stress [212, 295]; perhaps they also stall ribosome assembly under the same conditions.

eIF5A removes Rio2 via steric exclusion

We have shown that eIF5A is required for 40S maturation; its depletion leads to the retention of Rio2 on pre-40S particles that are associated with 60S subunits. The bacterial homolog of eIF5A, EF-P, binds between the P and the E site in the 70S ribosome. Interestingly, when the structure of EF-P is superimposed on the pre-40S particle (**Fig.**

4.10B), the two domains that eIF5A shares with EF-P [296] fit almost perfectly against Rio2 bound in the P-site. Domain III of EF-P would have steric overlap with Rio2. In eIF5A, however, this domain is replaced with a smaller C-terminal extension. We suggest that binding of eIF5A displaces Rio2 due to steric overlap between the C-terminal extension and Rio2. The finding that eIF5A associates with maturation-associated 80S particles also explains why eukaryotic eIF5A is smaller than its bacterial counterpart, as its initial binding must occur in the presence of Rio2.

The 80S intermediate accumulating in the Fap7 mutant is not a pre-initiation complex

The events preceding 60S subunit joining during canonical initiation of translation in yeast require at least 12 initiation factors [288]. Translation initiation begins with binding of eIF1, eIF1A, the eIF3 complex, and eIF5 to 40S subunits. eIF3 prevents the premature joining of 60S subunits and, together with eIF1 and eIF1A, promotes binding and positioning of the initiator tRNA in the P-site as a ternary complex with GTP-bound eIF2 [297]. Following association of the ternary complex, eIF3 helps recruit 5'-capped mRNA through interaction with members of the eIF4 complex and Pab1 (poly(A) binding protein) bound to the 5' UTR and the poly(A) tail of the RNA message ([288], **Fig. 4.11**). eIF1A and eIF1, together with components of the eIF4 complex, facilitate scanning along the mRNA to locate the start codon. eIF5 and eIF1 regulate GTP hydrolysis and P_i release from eIF2 upon recognition of the start codon, triggering dissociation of eIF1, eIF5, eIF3 and eIF2·GDP [288, 297]. eIF1A remains bound to the 40S subunit with the initiator tRNA and the mRNA start codon positioned in the P-site and stimulates eIF5B-mediated joining of the 60S subunit [288]. eIF5A is believed to stabilize the initiator tRNA in the P-site for formation of the first peptide bond [277, 278].

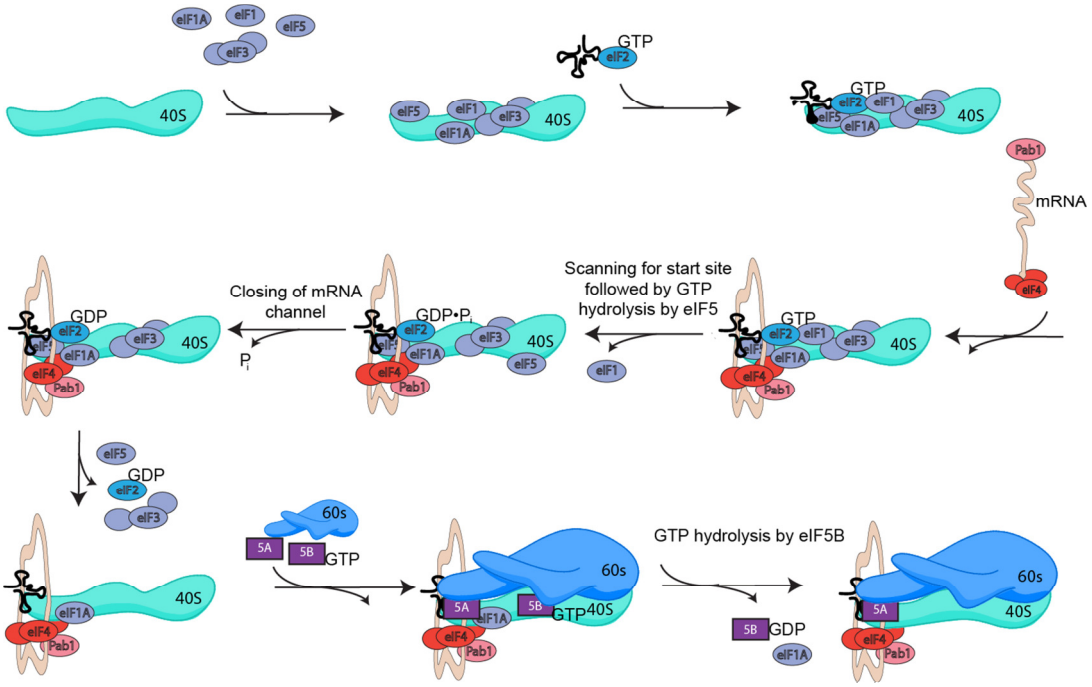

Figure 4-11 Subunit joining in canonical translation initiation pathway.

Our data, as well as data in the literature [239, 279], indicate that the formation of the 80S complex required for 40S maturation requires only a subset of the canonical translation initiation factors. Although initiator $tRNA_i^{Met}$ is present in the 80S peak from both mutant and wildtype cells, the tRNA levels correlate with that of the mature 18S rRNA present, suggesting that 80S complexes containing pre-40S particles do not have tRNA bound. The exclusion of the 20S rRNA from polysomes in the absence of Fap7 suggests that mRNA is also not bound[3]. eIF1, eIF1A, and eIF3 are not required for 20S cleavage; we have previously shown that AF binding sites overlap the binding sites for translation initiation factors eIF1, eIF1A and eIF3 [275]. Furthermore, mRNA recruitment is indirectly blocked by stabilization of the mRNA binding channel in the closed position; delivery of initiator tRNA to these particles (by either eIF2 or eIF1α) is blocked by Rio2

[3] A special class of mRNAs restricted to monosomes and bound to pre-40S containing 80S ribosomes could also explain this observation. However, mRNAs known to exist in monosomes are not abundant enough to account for the large 80S peak observed upon mutation of Fap7 298. Arava, Y., et al., *Genome-wide analysis of mRNA translation profiles in Saccharomyces cerevisiae.* Proc Natl Acad Sci U S A, 2003. **100**(7): p. 3889-94..

positioned in the P-site and Tsr1 positioned in the eIF1α binding site. It follows that formation of 80S complexes during 40S maturation occurs independently of translation initiation factors that commonly bind 40S subunits (see **Fig 5.1**). This is consistent with data from Soudet and colleagues [239], demonstrating that 40S maturation does not require eIF1, eIF1A or essential subunits of eIF3, which all bind free 40S subunits. In contrast, eIF5B, which mediates subunit joining in canonical translation initiation, is required for efficient 40S maturation [279], suggesting that it likely catalyzes subunit joining in the 40S maturation pathway as well. Furthermore, our data also indicate that eIF5A is required to remove Rio2. 80S formation in the absence of initiation factors and initiator tRNA is precedented in translation initiation from the cricket paralysis virus (CrPV) intergenic region *i*nternal *r*ibosome *e*ntry *s*ite (IRES), which binds to the P and E site of the 40S ribosome [299], and requires only eIF5A. Similarly, many other IRES require only a subset of translation initiation factors.

Mass spectrometry of 80S particles that form in wildtype and Fap7 depleted cells indicates that the translation initiation factor eIF4G1 (but not eIF4G2) is specifically associated with 80S particles in Fap7 depleted cells, and not found in wildtype cells. This is consistent with recent observations indicating that depletion of eIF4G1 (but not eIF4G2) leads to 20S accumulation [279]. The presence of eIF4G1 exclusively on the 80S particle that accumulates in the absence of Fap7 suggests an early role for this protein, either prior to or following 60S subunit joining in the steps leading from the Rio2 and Ltv1 associated particles to the mature 40S subunit, although it is still unclear what its function might be. Interestingly, picorna virus protease cleaves eIF4G1, and the C-terminal cleavage product binds 40S subunits, blocks cap-dependent translation and

enhances cap-independent translation [300]. Perhaps eIF4G1 plays a similar role during 40S maturation by promoting initiation factor independent 60S subunit joining, while antagonizing canonical translation initiation. This model would require a similar modification to eIF4G1's canonical function, perhaps through a posttranslational modification. Both wildtype and maturation associated 80S particles contain eEF1α as well as Pab1 (the latter potentially being recruited via eIF4G1 in Fap7 depleted cells [219]). The absence of eEF2 in 80S maturation intermediates is consistent with these 80S particles not being translation competent.

Why does 40S maturation require 60S joining and then subsequent disruption of the resulting 80S particle?

The requirement for joining and subsequent dissociation of 60S subunits in the pre-40S maturation pathway may appear to be an unreasonable complication in an already very complicated pathway. However, an obvious advantage of 60S subunit joining is a quality control check to verify proper assembly of pre-40S subunits prior to their entry into the translating pool of ribosomes. Tests included in this pathway include eIF5B-dependent joining of 60S subunits, binding of eIF4G (the master translation initiation factor), as well as binding of eIF5A. Furthermore, the controlled and regulated joining of 60S subunits may protect the pre-40S particle from unwanted interactions. For instance, the localization of Ltv1, Enp1 and Rps3 on cytoplasmic 40S subunits indicates that their binding should prevent opening of the mRNA channel, but this work indicates that Ltv1 is the first factor to dissociate. Subsequent regulated binding of 60S subunits could be a mechanism to prevent binding of mRNA and subsequent translation initiation. All other assembly factors could then dissociate without compromising the mechanism we

previously discovered for chaperoning 40S subunits [275]. The previously mysterious requirements for the subunit joining factor eIF5B and the subunit dissociation factor Rli1 in ribosome assembly are neatly explained by this model. Future experiments will test for specific requirements for these proteins in joining and dissociation of the 80S intermediate identified here, as well as the mechanisms by which other 80S-associated translation factors mediate 40S maturation.

Chapter 5

Perspectives and future directions

5.1 Summary

Classic *in vitro* work in bacteria has led to a detailed understanding of the biophysical, thermodynamic, and structural basis for the ordered and correct assembly of ribosomal proteins on ribosomal RNA. Furthermore, it has enabled reconstitution of active subunits from ribosomal RNA and proteins *in vitro*. Ribosome assembly in eukaryotes, however, requires approximately 200 essential assembly factors (AFs) and occurs via ordered events that initiate in the nucleolus and culminate in the cytoplasm. Some of these assembly factors are believed to perform roles such as facilitating proper folding of ribosomal RNA and incorporation of ribosomal proteins as well as processing and cleavage of rRNA precursors [7, 17, 173, 227]. Some of these factors are also believed to regulate and integrate the maturation process with other cellular pathways, including the cell cycle and responses to environmental stress [204, 208, 210]. In many cases, the roles of these assembly factors are not yet understood. This work investigates the roles of a subset of these assembly factors in late cytoplasmic steps of maturation of the yeast 40S subunit.

In Chapter 2 [275], the cryo-electron microscopy (cryo-EM) structure of a late cytoplasmic 40S ribosome assembly intermediate from *Saccharomyces cerevisiae* is presented. The positions of bound AFs were defined using cryo-EM reconstructions of

pre-ribosomal complexes lacking individual components. The positions of these factors and the conformation of the rRNA they are bound to indicate that one role of eukaryotic initiation factors is to chaperone pre-40S subunits to prevent premature initiation of translation with these particles in the cytoplasm. The seven AFs prevent each step in the translation initiation pathway by obstructing the binding sites for initiation factors, preventing the opening of the mRNA channel, blocking 60S subunit joining, or disrupting the decoding site. We suggest that these highly redundant mechanisms ensure that pre-40S particles do not enter the translation pathway, which would result in their rapid degradation

The pre-40S particle modeled in Chapter 2 [275] is stable for days at 4°C and at least hours at room temperature, yet 40S maturation *in vivo* is completed in minutes. This particle is therefore not competent for Nob1 mediated 20S rRNA cleavage, despite the fact that Nob1 is bound at or near its target. Furthermore, no significant loss of assembly factors is observed in this timescale, although both Dim1 and Ltv1 appear to be substoichiometric in purifications. These considerations suggest that *in vivo* dissociation of assembly factors and 40S maturation is promoted by external factors.

One of these factors, Fap7, has sequence homology to ATP-dependent NTPases and is required for 18S rRNA maturation. Mutations in conserved residues in Fap7's predicted Walker A and Walker B motifs disrupt rRNA maturation. ATP binding and hydrolysis by Fap7 are therefore believed to be essential for Fap7's function in ribosome assembly. Chapter 3 of this work investigated ATP binding and hydrolysis by recombinant Fap7. We demonstrate that the coordinated cycle of ATP binding and hydrolysis by Fap7 is associated with a conformational change that may provide mechanical energy to facilitate

the final stages of rRNA processing in the pre-40S particle. In Chapter 4, we demonstrate that Fap7 targets the maturing 40S subunit through direct interactions with Rps14 [187] and Dim1 and may facilitate 40S maturation through facilitation of the C-terminal tail of Rps14 and/or the removal of Tsr1. We also show that the Fap7 pre-40S target is joined with 60S subunits in a previously unrecognized 80S intermediate. The 40S and 60S subunits in this intermediate are not bound to initiator tRNA or mRNA and therefore have not joined through canonical translation initiation.

It was known that late steps in 40S ribosome assembly, including cleavage of the mature 3'-end of 18S rRNA, can take place in pre-40S subunits that have engaged in translation initiation and bound mRNA, but that translation initiation is not required for 40S maturation. Our discovery of an 80S intermediate explains the requirement for a subset of 80S associated translation in the 40S maturation process. We demonstrate that eIF5B-dependent joining of 60S subunits is a prerequisite for maturation of 40S subunits. Based on previous data and findings here, we suggest that Rli1/Dom34 disrupt these 80S complexes to free pre-40S subunits containing only the nuclease Nob1, its regulator Pno1, and the methylase Dim1. These subunits can then enter the canonical translation initiation pathway or complete maturation prior to translation initiation. We have used the data acquired in this work to outline the following model for the events that lead from the stable assembly intermediate modeled in Chapter 2 [275] to the mature translation competent 40S subunit:

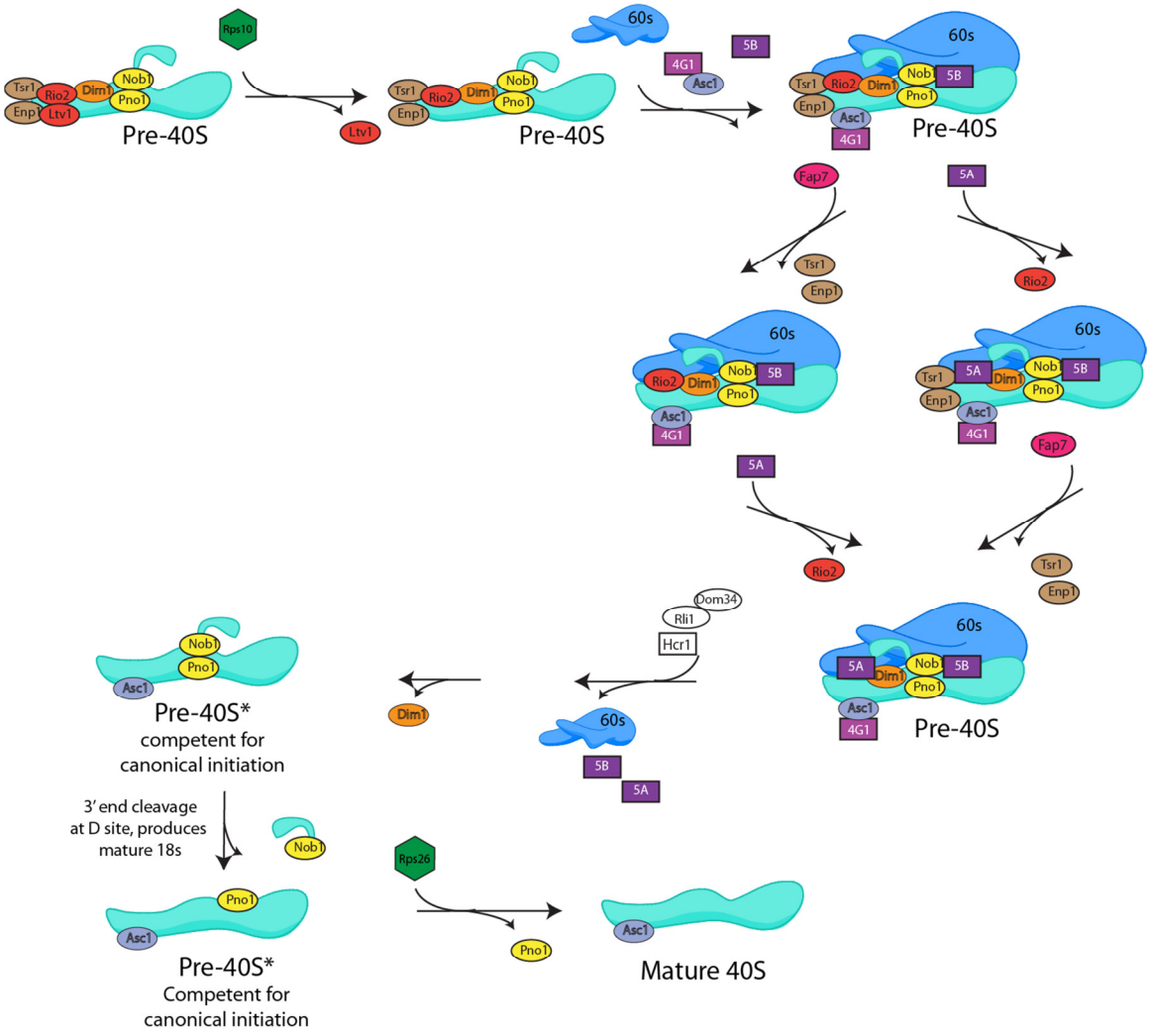

Figure 5-1 Model for ordering of late steps in small subunit biogenesis.

5.2 Ordering late steps in 40S assembly

Our data indicate that the seven assembly factors associated with these purified complexes dissociate sequentially as 40S maturation progresses (**Fig. 5.1**). Ltv1 is the first factor to leave and is lost upon depletion of eIF5A and Fap7. The binding site for Ltv1/Enp1 and Rps3 overlaps the binding site for Rps10, which is missing in stable pre-40S subunits containing all seven assembly factors [275]. Consistent with this overlap and the loss of Ltv1, mass spectrometry indicates that Rps10 is bound to pre-40S subunits

that accumulate in Fap7 depleted cells. Rio2 and Tsr1 are the next factors to dissociate, and our data indicate that they dissociate in parallel pathways, as Rio2 is lost but Tsr1 is not in 80S fractions from Fap7 depleted cells; 80S fractions from eIF5A depleted cells have lost Tsr1 yet retain Rio2. These results also indicate that Fap7 (directly or indirectly) leads to Tsr1 dissociation, while eIF5A leads to Rio2 dissociation (as described above).

The retention of Enp1, Nob1, Tsr1, Pno1, and Dim1 on the 80S particle that accumulates in the Fap7 mutant shows that, in wildtype cells, these factors remain bound until after subunit joining. The levels of 20S rRNA in the Fap7 depleted strain exceed the levels of these assembly factors, and as a result, assembly factors are substoichiometrically represented in 80S particles (**Fig. 4.3**, Table 2). This finding suggests that they can eventually dissociate in an unproductive manner without leading to 20S cleavage. Consistent with this finding, in the 80S particle from eIF5A depleted cells, only small amounts of Enp1 and Pno1 are found in 80S particles, suggesting that these factors can dissociate after Tsr1 is removed.

Finally, an essential subunit dissociation step in the biogenesis pathway prior to translation initiation is implicit to this model. Rli1 and Dom34 break apart empty 80S subunits after translation has been completed [290]. Interestingly, Dom34 has synthetic lethal interactions with almost every Rps, in addition to the late 40S assembly factors Tsr2 and Yar1 [301]; its deletion also leads to accumulation of 80S ribosomes. Furthermore, Rli1 binds 20S rRNA and is required for 40S maturation [91]. Rli1 also directly binds Hcr1, a loosely associated member of the eIF3 subcomplex, which is also required for 20S maturation. We therefore suggest that after dissociation of Tsr1, the

Rli1/Dom34 complex binds in the GTPase site, which is partially occupied by Tsr1, to promote 80S dissociation. Its recruitment to 80S ribosomes might be facilitated by Hcr1, which is bound in the A-site. This model also explains the unusually large accumulation of 20S in Fap7 mutants: the 80S particle stalled upon depletion of eIF5A, but not Fap7, is subject to Dom34/Hbs1 mediated no-go decay.

It is not yet known whether Dim1 remains bound during this late Rli1-dependent step. We do note that very small amounts of Dim1 can be found in polysomes, both in wildtype cells as well as in the eIF5A depleted cells, suggesting that at least a fraction of Dim1 remains bound after Rli1 dissociation to enter the canonical translation initiation pathways. Dim1 overlaps the binding site for eIF1, suggesting that mRNA recruitment and binding of eIF2 can occur in the absence of eIF1, perhaps aided by a suggested interaction between Pno1 and eIF2 [302].

According to this model, Pno1 and Nob1 are the last assembly factors to remain bound. This is consistent with the previous finding that their interaction is required for Nob1-dependent cleavage of 20S rRNA [248]. Furthermore, Pno1 is always observed in polysomes, consistent with binding late in the assembly pathway, when 40S subunits are already able to initiate translation in the canonical pathway. We do not observe Nob1 in polysomes, as has been previously observed. It is possible that this is a limitation of the Nob1 antibody, which has poor affinity (previous observations have used TAP-tagged Nob1 and an antibody against the TAP-tag). It is also possible that the differences are directly attributable to the TAP-tag. Lastly, Rps26 shares a binding site with Pno1 and its association may therefore be one of the last steps in small subunit assembly. Consistent with this finding, we observe only partial occupancy of Rps26 in the Fap7 depleted cells.

5.3 Future directions

Through this work, we have identified general chaperoning functions of assembly factors in late stages of 40S maturation as well as a novel 80S intermediate in this pathway. However, we initially set out to learn how Nob1 cleavage at site D was regulated and mediated, especially with regard to the essential role of Fap7 in this process. Future experiments will dissect the minimal requirements for this cleavage event. Now that we understand that an 80S intermediate exists in this pathway, we will investigate the existence and nature of stalled 40S and 80S intermediates that accumulate upon depletion of 80S associated translation factors identified in this and previous work. These investigations will include analysis of assembly factors and translation factors with these intermediates, allowing us to test and refine our model for the sequence of events leading to 20S cleavage.

The identification of an interaction between Fap7 and Tsa1 also opens a new avenue for investigation of regulation of ribosome assembly in response to oxidative stress. An important first question to answer will be whether or not Tsa1 itself is required for ribosome maturation. Additional experiments will test whether or not 20S processing is altered under conditions of oxidative stress and whether the levels or functional states of Tsa1 and or Fap7 influence this effect

Future experiments will also include further interrogation of the ATP binding and hydrolyzing behaviors of Fap7. We believe that the simplest interpretation of our *in vitro* data is that Fap7 binds ATP and dimerizes in an ATP-dependent manner; that ATP hydrolysis from the $Fap7_2ATP_2$ species is approximately 100-fold faster than that from the $Fap7_2ATP_1$ species; and that turnover is sequential. We have not, however, been able

to detect ATP-dependent dimerization of Fap7 *in vitro*. Evidence for Fap7 dimerization i*n vivo* was obtained through the association of untagged Fap7 with Fap7TAP and their co-purification from cells expressing both Fap7 protein constructs. Analytical ultracentrifugation of Fap7 in the presence of the poorly hydrolyzeable ATP analog AMP-PNP may allow detection of a Fap7 dimer *in vitro*.

We still cannot rule out the possibility that the squared dependence of Fap7 ATPase activity at low Fap7 concentrations is an artifact due to perhaps loss of protein to pipette tips or the side of microfuge tubes at these low concentrations. If this is the case, then one explanation for the two site behaviors we have unmistakably observed in fluorescence experiments and with the influence of AMP-PNP on single turnover rate constants may be that each Fap7 monomer can bind two ATPs. Fap7's sequence homology to adenylate kinases, which have two nucleotide binding sites, gives credence to this possibility. Adenylate kinases catalyze phosphate transfer from one adenylate nucleotide to another by binding either one ATP and one AMP, or two ADP molecules. They are not expected to bind two ATPs simultaneously. However, their activity is inhibited by diadenosine hexaphosphate (Ap6A) [303], i.e. two nucleoside bases and six associated phosphates, mimicking to some extent the binding of two ATP molecules. This implies that an adenylate kinase binding two ATP molecules simultaneously is not outside the realm of possibility. Stoichiometry experiments to determine the number of ATP molecules bound to each Fap7 molecule under saturating conditions may answer this question. In any case, the Fap7 homolog in humans exhibits mononucleoside kinase activity, demonstrating the ability to transfer phosphates from ATP to mononucleoside phosphates including ATP [264]; we will test for this activity in yeast Fap7 as well.

We expect that factors that interact directly with Fap7 during ribosome assembly will modulate its essential activity in this process, whether it be nucleotide binding, ATP hydrolysis, or adenylate kinase activity. Our data show that the steady-state rate of ATP hydrolysis by Fap7, but not its single turnover rate, is reduced by 80% in the D82AH84A Walker B mutant. It may be that turnover of both ATPs from the $Fap7_2ATP_2$ species, which would affect the steady-state rate but not the single-turnover rate according to our model, is required for 40S maturation. Alternatively, it may be that adenylate kinase activity of Fap7, if it exists, is its essential activity in 40S maturation and this mutant may specifically impair adenylate kinase activity. Future experiments will also explore how each of these Fap7 activities is influenced by factors with which it interacts, including Rps14 and Dim1. We will test for the ability of the D82AH84A mutant to interact with these proteins and for its ATPase and putative adenylate kinase activities to be modulated by these factors. It may be that failure to interact with and/or to be activated by Rps14, Dim1 or other factors in the cell could explain the failure of this mutant to support ribosome assembly.

Appendix

Supplementary text and figures to Chapter 2

Supplementary Results

1. Assignment of densities for individual AFs

The endonuclease Nob1 binds at the back of the platform

Nob1 produces the mature 18S rRNA by endonucleolytic cleavage of 20S rRNA at site D [247], [304]. To understand how Nob1 is positioned within this late 40S precursor particle we purified pre-40S complexes from a Rio2-TAP strain with Nob1 expression under control of a galactose-inducible promoter (*GAL1::Nob1*). SDS-PAGE analysis indicates that Nob1 is the only depleted AF (**Fig. 2A**). We obtained a 3D cryo-EM reconstruction from Nob1-depleted pre-40S particles (Nob1-depl) to a resolution of 20Å (**Figs. 2B, S5, S6**). Difference mapping reveals that the density attributed to Nob1 is located on the back of the platform (**Figs. 2C, S7A**). This places Nob1 in proximity to Rps5 and Rps14, consistent with direct protein-protein interactions between Nob1 and these proteins [259]. Visualization of the WT map at lower threshold, but still below substantial noise levels, reveals an extra density that emanates from Nob1 and extends behind the platform (**Fig. S7B**). It is likely that this density represents a portion of ITS1 bound to Nob1 prior to cleavage, as expected from previous footprinting data [259]. Consistent with this hypothesis, this density is not present at any threshold cut-off of the Nob1-depl 3D map (data not shown).

Rio2 and Dim1 reside on the subunit interface

Rio2, a serine/threonine kinase with unidentified substrate and capable of autophosphorylation [305], is essential for 18S rRNA production [107, 118]. To localize Rio2 in the pre-40S subunit we employed a TAP-tag on Ltv1 to isolate particles from a yeast strain with Rio2 expression under control of a galactose inducible promoter (*GAL1::Rio2*). Particles purified via TAP-tags on Ltv1 and Rio2 are virtually identical [112] (**Fig. 2A).** SDS-PAGE analysis of the pre-40S complex depleted for Rio2 (referred to as Rio2-depl) also indicates heavily decreased occupancy for Nob1 and Dim1 **(Fig. 2A)**, a universally conserved methylase acting on two adenosine residues in the loop of helix 45 [306]. The loss of Nob1 and Dim1 upon depletion of Rio2 is consistent with direct protein-protein interactions between Rio2 and Dim1, as well as Nob1 [245]. We generated a 3D reconstruction of the Rio2-depl complex at a resolution of 22Å **(Figs. 2B, S5, S6, S8A)** and compared it to the WT map. This map lacks density at the previously identified position of Nob1, as well as at two interconnected regions at the subunit interface (**Figs. 2B, S8A)**.

rRNA footprinting has shown that KsgA, the conserved bacterial ortholog of Dim1 [129, 307], interacts with conserved regions of H44 and H27 in 30S ribosomal subunits [128]. These biochemical constraints are satisfied by docking the crystal structure of hDim1 (PDB ID: 1ZQ9) (Dong et al. *2005,* unpublished data) within the longitudinal lower density missing in Rio2-depl (green in **Figs. 2C, S8B**). The docking results in a very good fit with a cross-correlation (CC) value of 0.854. In this position, the active site of hDim1 is adjacent to its substrate, the tandem adenosine nucleotides near the 3' end of rRNA (labeled in yellow in **Fig. S8B**) [306].

Rio2 interacts directly with Dim1, as well as with Rps15, located in the head region, and Rps5 and Rps14 [245], which line the mRNA exit channel at the platform. Attributing the third missing density of Rio2-depl particles to Rio2 satisfies all of these interactions. Accordingly, this position was used to dock the crystal structure of archeal Rio2 [104] (PDB ID: 1ZAO), which contains ~80% of the yeast Rio2 residues, into the WT pre-40S 3D map. Docking of this structure into the density fits well with a CC value of 0.904 (blue in **Figs. 2C, S8B**). In this orientation the N-terminus of Rio2 is buried behind H44 and the C-terminus is surface-exposed, consistent with our ability to isolate of pre-40S particles via C-terminally TAP-tagged Rio2.

Localization of Tsr1 and Pno1

Tsr1, a GTPase-like protein, is essential for yeast viability and required for 18S rRNA production [23]. We isolated pre-40S particles from a yeast strain with Tsr1 expression under control of a galactose inducible promoter via TAP-tagged Ltv1 (*GAL1::Tsr1*). SDS-PAGE and mass-spectrometry of the pre-40S complexes purified from the *GAL1::Tsr1* strain revealed that Tsr1 depletion resulted in a strong reduction in the levels of Rio2, Dim1, Pno1 and Nob1 (**Fig. 2A**). To localize Tsr1 and Pno1 we obtained a 3D cryo-EM map of Tsr1-depleted pre-40S particles (Tsr1-depl) calculated at a resolution of ~26Å (**Figs. 2B, S5, S6, S9A,C**). Surprisingly, in this reconstruction but in none of the other 3D maps produced in this study, H44 does not display the pronounced kink. In addition to the densities previously assigned to Rio2, Dim1, and Nob1, the 3D reconstruction of Tsr1-depl particles reveals two new missing densities compared to the WT 3D map. One is a fairly large density located to the left of H44 on the 60S binding

interface (**Figs. 2B, Fig. S9A**). The second is a smaller density located on the platform (**Figs. 2B, S9C**).

To determine which density represents Tsr1, we purified recombinant *S. cerevisiae* Tsr1 from *E. coli* (rTsr1) as described in Campbell and Karbstein [245] and examined it by single particle negative stain EM. 2D projection averages of this 91 kDa protein revealed a preferred orientation of an elongated particle with a hook-like appearance, displaying a handle that is formed by a globular domain (**Fig. S11**). Additionally, examination of 2D averages of rTsr1 with an N-terminal maltose binding protein (MBP)-tag shows that the protruding globular domain forms the N-terminus (**Fig. S11**). Using the random conical tilt method [308], we calculated a 3D reconstruction of rTsr1 embedded in negative stain to a resolution of ~30Å (FSC=0.5) (**Fig. S12**). The reconstruction reveals a density that is very similar to the one on the subunit interface contacting H44 from the left (**Figs. 2B, S9, S12A**), and which fits well within the identified pre-40S density. This analysis also suggests that the N-terminal portion of Tsr1 interacts with the N-terminal portion of Rio2, consistent with direct binding interactions between these two proteins that are sensitive to N-terminal tagging of Rio2 [245].

The second unidentified density in the Tsr1-depl 3D map is located on the back of the platform, between Nob1 and Rps14 (**Figs. 2B, S9A,C**). This position is close to the 3'-end of 18S rRNA. The highly conserved C-terminal KH domain of Pno1's archeal homolog, aDim2, binds directly the universally conserved GGAUC sequence at the 3' end of the 16S rRNA, and forms a trimeric complex with eIF2α, which has been crystallized [302]. Furthermore, the central KH-like domain of Pno1 binds and regulates Nob1 [248]. Docking of the *Pyrococcus horikoshii* aDim2 crystal structure (PDB ID:

2E3U), containing the two C-terminal KH-domains, in the density next to Nob1 satisfies the interaction with Nob1 and is in the proximity to the 18S rRNA 3'-end (**Figs. 2C, S9D**).

Ltv1 and Enp1 bind on the head and beak

To localize Ltv1, a non-essential nuclear export adaptor [309], we deleted Ltv1 in the Rio2-TAP strain. SDS-PAGE and mass spectrometry show that upon deletion of Ltv1, Rps3 is also lost, while Enp1 is heavily reduced in these particles (called ΔLtv1 hereafter) compared to the WT preparation (**Fig. 2A, Table S1**). Rps20, and Rps29 are also absent, consistent with direct interactions of these proteins with Rps3, however, they also appear to be underrepresented in WT particles. This finding is consistent with previous data showing that Ltv1 and Enp1 form a complex with Rps3 that dissociates from pre-40S ribosomes upon high-salt treatment [112]. Furthermore, Enp1 and Ltv1 also associate directly according to protein-protein interaction studies [245]. The 3D cryo-EM reconstruction of ΔLtv1 was determined at 20Å resolution **(Figs. 2B, S5, S6, S10A)** and shows a reorientation of the beak structure to a position similar to the one in mature 40S particles (**Fig. S10A)**. Comparison of the WT and ΔLtv1 EM maps reveal that the beak repositioning in the ΔLtv1 particle is due to the absence of a density connecting the beak to H16 (**Fig. S10A**). In addition, the ΔLtv1 map has decreased density on top of the head region and at the top portion of the beak (**Figs. 2B, S10)**.

Because deletion of Ltv1 results in loss of Rps3 and heavy reduction in Enp1 levels, the structural differences observed in the ΔLtv1 map are attributed to all three factors. However, as Enp1 is not entirely lost **(Fig. 2A)**, a subpopulation of the ΔLtv1 projections must include particles with bound Enp1. To examine these particles we

employed multiple reference-supervised alignment [310, 311] on our original ΔLtv1 cryo-EM dataset using the WT and ΔLtv1 maps as initial volume references. After multiple iterations ~80% of particles were stably assigned (based on CC values) to the ΔLtv1 reference, and their 3D reconstruction shows the same features as the initially calculated ΔLtv1 map **(Fig. S18)**. The remaining ~20% of the ΔLtv1 particles were stably assigned to the WT pre-40S reference and their 3D reconstruction shows a retracted beak structure **(Fig. S18)**. The beak in these particles is also connected with H16, albeit with a smaller density compared to WT. This analysis suggests that that the bridge connecting H16 with the beak is formed partially by Enp1, and its presence suffices to keep the beak in a retracted position. In contrast, density differences on the top of the head and the remaining density at the beak should be attributed to Ltv1 and Rps3, respectively (**Figs. 2B,C, S10A,B**). To provide additional evidence for this conclusion we examined pre-40S particles labeled with antibodies against Enp1 by negative stain EM. 2D class averages of Enp1-antibody labeled pre-40S particles reveal additional density directly at the beak structure (**Fig. S13**), providing strong evidence that Enp1 localizes on the beak. In contrast, 2D averages of Ltv1-antibody-labeled pre-40S show antibody binding at the top of the head (**Fig. S14**), indicating that the missing density in the ΔLtv1 map (compared to WT) on the head should be assigned to Ltv1. Together, these data indicate that Ltv1 binds at the top of the head, while Enp1 and Rps3 make up the connection between the beak and H16.

2. Explicit-Solvent Molecular Dynamics Flexible Fitting (MDFF) of mature rRNA into the cryo-EM maps

In order to compare the structures of pre-40S particles with mature 40S subunits, and to better define the boundaries of additional densities that could be attributed to the bound AFs, we docked the 4.15 Å crystal structure of mature *S. cerevisiae* 40S subunit [237] (PDB ID: 3O2Z) within our WT pre-40S 3D map. Rps with low or no occupancy in our sample were omitted, and we retained only the Rps present in both recent crystal structures [237, 238] (PDB ID: 3O2Z & 2XZM) **(Table S4)**. Rigid body docking gave an overall good fit of rRNA and Rps, but showed areas where the mature rRNA structure does not represent the pre-40S cryo-EM density well **(Fig. S3)**. The two most distinct differences were found in the beak structure and the decoding site. In the premature 40S, the beak is more extended and tilted away from the 60S subunit binding interface, while the decoding site helix, H44, is characterized by a leftward kink that drives its upper portion out towards the 60S subunit (**Figs. 1D, S3)**.

To better isolate extra densities arising from AFs, we applied explicit-solvent molecular dynamics flexible fitting (MDFF), as previously applied to other ribosome cryo-EM structures [243]. After MDFF, CC values were increased from 0.673 to 0.805 **(Table S5)**. As expected based on the initial overall good fit of the 40S model into the electron density, most regions of rRNA undergo at most modest changes **(Fig. S3)**. In contrast, the two regions that did not initially fit well into the EM map (beak, H44), are now fully enveloped by the density **(Figs. 1D, S3)**. MDFF also revealed that the movement of H44 away from the platform is accompanied by "unwinding" of the top portion of H44, so that from ~nt 1752 to the 3'-end, the helical structure is disrupted. The resulting single stranded RNA is able to span a greater distance, thereby allowing for the

outward and leftward movement of H44 **(Fig. 1D).** Detailed procedures and controls for the MDFF are described in the Materials and Methods section.

Supplementary Discussion

Locations of assembly factors are consistent with a large body of previous data

Using RNA-protein cross-linking Tollervey and colleagues identified potential sites of protein-rRNA contact for all AFs present in our model, except Pno1 [246] **(Fig. S15)**. Data for the proteins that gave distinctly localized cross-linking hits, Dim1, Rio2 and Enp1, are highly consistent with our map **(Fig. S15B-D)**. In contrast, cross-links for Nob1, Tsr1, and Ltv1 are dispersed (**Fig. S15E-G**). This is possibly due to the fact that cross-linking experiments were done in lysates, and thus report on a mixed population of 40S precursors. Despite this limitation, a subset of cross-links for Tsr1 and Ltv1 is consistent with their placement in our cryo-EM map **(Fig. 15F,G)**. For Nob1, the cross-links could be consistent with an earlier intermediate [247]. Most of the Nob1 volume in this structure protrudes from the complex, which explains the lack of cross-links consistent with this structure **(Fig. 15E)**. Previous *in vivo* and *in vitro* RNA footprinting data are consistent with the Nob1 placement observed in this work but not the cross-linking data [259].

Comparison to other previous data

In contrast to previous statements [112] the pre-40S beak is visible by cryo-EM and negative-staining EM (**Figs. 1B, S2)**. However, in negative stain the density for the beak is diffuse, likely due to its orientation on the carbon support of the grid that prevents complete stain embedding. Accordingly, the beak is clearly resolved in the cryo-EM map **(Fig. 1B)**. Inspection of the previously published negative stain EM data [112] shows a

similar diffuse beak structure, indicating that the beak is present in these particles, as in ours.

Rio2TAP and Ltv1TAP-associated pre-40S ribosomes were previously purified using the same methodology [112]. As expected in both cases the same assembly factors are co-purified. However, in our purifications Hrr25, a kinase implicated in phosphorylating the Ltv1/Enp1/Rps3 complex [112], is a very minor contaminant, whose occupancy varies somewhat from prep to prep while always remaining low. Similarly, Hrr25 co-purification by Schafer et al. is variable and low, albeit somewhat increased [112]. We do observe that co-purification of Hrr25 increases upon depletion of Nob1, Rio2 and especially Tsr1, all of which accumulate 20S pre-rRNA, indicating that perhaps Hrr25 is associated with only a small subfraction of pre-ribosomes, as expected from a kinase which acts transiently. The abundance of this subfraction of pre-ribosomes is dictated by the relative rates of its formation and decay, the flux through the pathway. It is known that different strain backgrounds present a different flux through the pathway, and we note that our strain background is different from the one used by Schafer et al. (BY4741 vs. MGD353-13). Furthermore, the relative levels of 23S and 25S rRNA, which are indicative of the flux are different in these strains, and finally, we observe an upshift in 20S rRNA levels upon shift to glucose, which is not observed in MGD353-13 cells (Schafer et al., 2006).

Materials and Methods

Purification of pre 40S particles

Yeast cells expressing TAP-tagged proteins were grown at 30° C in YP media with 3% dextrose to an OD_{600} of 1.5 in a 10L fermenter, or with 2% dextrose to an OD_{600} of 0.6-

0.8 in flasks. Depletion/deletion strains were grown in YP galactose to mid log phase, and then grown in glucose for 12h (or 20h for Tsr1 depletion). Affinity-purifications of TAP-tagged bait proteins were performed essentially as described [112, 285] using 20-40 g of cells as starting material. Two elutions of 200-300 µl and 250-400 µl, respectively, were collected and the second elution was concentrated to 20-40 µl using a *Millipore Biomax-100K NMWL* filter device for analysis by EM, SDS-PAGE or mass spectrometry.

Mass Spectrometry

Samples were run on SDS-PAGE gels and the area of interest was excised from the gel. Gel samples were subjected to proteolytic digestion with trypsin and analyzed using LC/MS/MS. Product ion data were searched against the SwissProt database using the Mascot search engine. Mascot output files were parsed into the Scaffold program for filtering to assess false discovery rates and allow for correct protein identifications.

Yeast strains

Galactose-inducible strains were created by PCR-based recombination [280] into the Rio2TAP or Ltv1TAP strain from Open Biosystems. Similarly, the entire TAP-tagged Ltv1 open reading frame and ~ 450 nt flanking sequence was amplified by PCR from genomic DNA of the Ltv1TAP strain from the Open Biosystems and genomically integrated into a Rio2 deletion strain generously provided by J.P. Gélugne [118]. Yeast strains used here are listed in **Table S3**.

Antibody labeling of pre 40S particles

For EM imaging of antibody-labeled specimen, pre-40S particles including Ltv1-CBP or Enp1-HA were incubated with the corresponding primary antibody (1°-CBP or 1°-HA

(Covance)) for 15-30 min at a molar ratio of ~1:1. The mix was diluted and applied to a glow-discharged continuous carbon grid for negative stain embedding.

Specimen preparation and EM imaging of negative-stained samples

Pre-40S complexes and recombinant Tsr1 were prepared for electron microscopy using the conventional negative staining protocol [312], and imaged at room temperature with a Tecnai T12 electron microscope operated at 120 kV using low-dose procedures. Images were recorded at a magnification of 71,138x and a defocus value of ~1.5µm on a Gatan US4000 CCD camera. All images were binned (2 x 2 pixels) to obtain a pixel size of 4.16 Å on the specimen level. A total of 3417 WT Rio2-TAP pre-40S particle images were manually excised using Boxer [part of the EMAN 1.9 software suite [313]]. The selected particles were subjected to reference-free alignment and classification into 50 classes using SPIDER [314] **(Fig. S2B).** For antibody labeled pre-40S complexes, 503 Ltv1-CBP/1º-CBP and 250 Enp1-HA/1º-HA particle images were manually excised and subjected to classification into 10-30 classes **(Figs. S13-S14).** For the 2D analysis of MBP-Tsr1, 759 particle projections were subjected to classification into 30 classes **(Fig. S11).** For 2D analysis and 3D reconstructions of Tsr1 we interactively selected 4927 particle pairs from 106 60º/0º image pairs. The untilted specimen images were subjected to classification into 25 classes (**Fig S11**). Based on this classification, seven independent 3D reconstructions were derived from particles belonging to seven classes (marked with red circles in **Fig. S11**). The random conical tilt technique [308] was used to calculate a first back projection map using the images of the tilted specimen. After angular refinement, the corresponding particles from the images of the untilted specimens were added, and the images were subjected to another cycle of refinement. Using the resulting

maps as reference models, we calculated final 3D reconstructions with the program FREALIGN [315]. FREALIGN was also used for further refinement of the orientation parameters, as well as for correction of the contrast transfer function (CTF). As all reconstructions revealed volumes with similar features, we merged 3450 60º/0º projections from all seven classes and used FREALIGN to calculate a final density map **(Fig. S12A).** The resolution of the final 3D reconstruction was ~30 Å according to Fourier shell correlation (FSC) using the FSC = 0.5 criterion **(Fig. S12B,C).**

Cryo-EM sample preparation and imaging

2 µl of 40S pre-ribosomal samples at an OD_{260} of 10-20 were adsorbed on glow-discharged Quantifoil R2/2 200 mesh grids, and vitrified using a Vitrobot (FEI Mark IV). Specimens were imaged on a Tecnai F20 transmission electron microscope (FEI) equipped with a field emission electron source operated at 200kV. Images were recorded at a magnification of 66,964x on a Gatan US4000 CCD camera and defocus values ranging from -1.5 to -4.0 µm. The pixel size under these conditions is 2.24 Å on the specimen level.

Single-particle reconstruction

Particles from cryo-EM images were excised using Boxer. The CTF parameters were determined for each micrograph using *ctfit* and CTF correction was applied accordingly using *Applyctf* [313] (part of EMAN 1.9 package). An *ab initio* model was generated by randomly selecting 100 WT Pre-40S particles from the total dataset, and randomly assigning an orientation value for each individual particle resulting in a noisy, sphere-like initial reference to minimize model bias (data not shown). 3D reconstructions were performed using model-based projection matching in EMAN. 11,604 WT Rio2-TAP

projections were selected to obtain a 3D reconstruction at 18 Å resolution (FSC=0.5) **(Figs. 1B, S1).** 9132 Nob1-depletion projections were refined to generate a 3D reconstruction at 20 Å resolution (FSC=0.5) **(Figs. 2B, S5, S7)**. 7069 Rio2-depletion projections were used to obtain a 3D reconstruction at 22 Å resolution (FSC=0.5) (**Fig. 2B, S5, S8).** For Tsr1-depl refinement we initially applied multiple reference-supervised alignment [310, 311] to separate any 80S-like particles from the total 9484 projections. In this process, we used our WT pre-40S 3D map and the published 80S 8.9 Å 3D map from *Thermomyces lanuginosus* [316] (EMD 1345) as initial references to separate the projections into two subsets. Accordingly, 759 projections were stably assigned to the 80S reference subset and produced a low-resolution 3D map as further proof of the existence of 80S-like particles **(Fig. 4B).** The final reconstruction for Tsr1-depl was calculated from the best 5127 projections at a resolution of 26 Å (FSC=0.5) **(Figs. 2B, S5, S9).** 10,235 ΔLtv1 pre-40S projections were refined to calculate a 3D reconstruction at 20 Å resolution (FSC=0.5) **(Figs. 2B, S5, S10).** To examine the presence of Enp1 particle subpopulation, we employed supervised alignment [310, 311] using the WT and the ΔLtv1 maps as initial volume references. After several cycles of refinement, 1324 projections were assigned to the WT pre-40S subset, and 7068 projections were assigned to the ΔLtv1 pre-40S subset **(Fig. S18).**

For determination of the statistical significance of differences observed between the 3D maps at different conditions we applied a Student's *t*-test. To this end, variance in each dataset was determined by the bootstrap technique described by Penczek et al. [317]. The subset particles were randomly selected to calculate a 3D map for each trial, and a total of 50 maps were generated to calculate average and variance maps, which were

subsequently compared by a Student's *t*-test [318]. Differences were visualized with a cut-off density corresponding to a significance level of 95% (P=0.05).

MDFF: overview and controls

We have used MDFF simulations to improve the fit of mature 40S initial models into different target cryo-EM maps of the pre-40S subunit. Due to the limited resolution of the cryo-EM maps, MDFF simulations were applied under very stringent conditions and several control experiments were performed to ensure that the results accurately reflect the data.

During MDFF a force field is applied to steer the RNA structure into the EM density map, while opposing restrains are used to ensure that no gross structural distortions are observed. In addition, the presence of explicit-solvent plays a significant role in maintaining structural rigidity during application of steering forces, especially in highly charged heterogeneous systems such as the ribosome. The MDFF experiments in this work were carried out using explicit solvent *and* restraining forces twice as high as originally recommended in the *absence* of solvent (Trabuco et al., 2008; Trabuco et al., 2009). This was despite the fact that it has been suggested that restraining forces could be lowered or even omitted in the presence of explicit solvent (Trabuco et al., 2009). Moreover, the ribosomal proteins were also restrained during these runs, preserving their interaction with RNA. Thus, the MDFF experiments in this work were carried out extremely conservatively.

To test the validity of MDFF in this work, we have carried out each simulation experiment in triplicate. Furthermore, we have used three independent and microscopically different maps (wild type, Nob1-depl and Ltv1Δ), as well as two

different starting structures encoding rRNA from different organisms (PDB codes: 3JYV and 3O2Z). In all cases MDFF yields essentially the same structure (**Figures S20-23)**, demonstrating the robustness of the protocol and the validity of the results. Finally, rRNA never redistributes into densities arising from r-proteins, even though in the originally used pbd file (3JYV), the identities of several r-proteins was unknown and thus not included in the atomic model. These densities remain essentially "empty". This is indicated in Fig. S4, where the subtraction of the 18S rRNA MDFF model from the pre-40S Rio2-TAP 3D volume reveals the densities attributed to proteins (AFs and Rps). The Rps present in our model are shown as black ribbons within the volume density. The remaining densities are attributed to AFs and Rps not included in our initial model.

MDFF: initial structure preparation

Our initial model was the recently published crystal structure of the eukaryotic yeast ribosome from Yusupov and colleagues [237] (PDB ID: 3O2Z). This crystal structure contains 18S rRNA residues 1 to 1800 (with the exception of 668 to 678), and several ribosomal proteins. We included the following proteins from these coordinates in our model: S0, S2, S4, S5, S9, S11, S13, S14, S15, S16, S18, S19, S22, S23, S24, S25, S27, and S28. S5, S18, and S19 were obtained from the recently published model using a 5.5 Å cryo-EM structure of the eukaryotic ribosome from Beckmann and colleagues [292], (PDB ID: 31ZB); S1 and S14 were used from the crystallographic coordinates from Ban's group eukaryotic mature 40S structure [238] (PDB ID: 2XZM). Our basis for using the coordinates from these structures, as opposed to those from 3O2Z, is that S1, S5, S14, S18, and S19 contain more complete amino acid sequences than those solved in

the crystal structure by the Yusupov group **(Table S4),** while maintaining similar secondary-structure elements and three-dimensional folds. We also added the missing rRNA nucleotides from 668 to 678, as well as all hydrogen and other missing atoms. Explicit TIP3P water was added to solvate the 18S rRNA and proteins in a periodic simulation box of size 300 Å x 306 Å x 265 Å. The system was initially neutralized by placing 1416 Mg^{2+} and 1232 Cl^- ions into the minima of electrostatic potential using *meadionize* plugin for VMD [319]. Finally, we also added 348 Na^+ and 348 Cl^- ions to the bulk water to maintain ionic concentration. The final system contains ~2.3 million atoms including solvent, ions, proteins and 18S rRNA.

Prior to the recent publication of the crystal structure from Ben-Shem et al. *(21)*, the only available structure for the eukaryotic ribosome 40S subunit had been modeled according to the 8.9 Å resolution cryo-EM reconstruction of the 80S ribosome from *Thermomyces lanuginosus* by Frank and colleagues [232, 316], with the ribosome sequence being over 85% identical to that of yeast [320]. All the initial validations of the MDFF protocol were carried out with these 40S coordinates (PDB ID: 3JYV). We have subsequently compared the results from MDFF using both 3JYV and 3O2Z as starting models and show that there are no differences (see following sections and **Figs. S19-S23).**

The 3JYV coordinate file deposited by Taylor et al. (2009) contains the 40S ribosome bound to P/E-tRNA. The ribosomal proteins present are: S0, S2, S3, S5, S9, S11, S13, S14, S15, S16, S18, S19, S20, S22, S23 and S29, as well as RACK1. In our modeling, we excluded S3, S9 (residues 6-21), S20, S29, RACK1, and P/E-tRNA from

the original structure. We obtained the complete *S. cerevisiae* 18S rRNA sequence containing 1800 residues from Gen Bank (Z75578.1) and aligned it with the sequence of 18S rRNA present in the mature 40S structure using Clustal W [321]. Upon alignment, the following changes were made to the original sequence (PDB ID: 3JYV, chain A): (a) the nucleotides previously at positions 898, 1041, 1042, 1182, 1287, and 1444, are now 899, 1042, 1043, 1183, 1286, and 1443, respectively (we note that the shift in position of these residues is concurrent with remaining nucleotides), and (b) the sequence GUGUC (884, 1001, 1003, 1284 and 1285) was substituted to AAACU. We adjusted the Cartesian coordinates accordingly, and in case of substitutions corrected the nucleotide type. We solvated and ionized this system employing the same protocol used for the initial model described above. The final periodic simulation box of dimensions 270 Å x 320 Å x 200 Å contained ~1.6 million atoms. We note that the simulation boxes in both cases were large enough to engulf the complete target cryo-EM maps used, which is currently a requirement for the explicit-solvent MDFF protocol used here (see below).

MDFF: initial equilibration phase

The initial equilibration phase for both structures of the 40S subunit (PDB ID 3O2Z and 3JYV) included an energy-minimization of the final systems for 5,000-10,000 cycles of conjugate-gradient optimization followed by a short 200 ps molecular dynamics (MD) simulation in the NVT ensemble. The temperature was held at 310K using the Langevin thermostat with a damping coefficient of 5 ps^{-1}. A 2-fs time-step with rigid bonds was used in this initial run. Non-bonded interactions were cut-off beyond 12 Å with smooth switching taking effect at 10 Å. Long-range electrostatic interactions were

handled using the particle mesh Ewald (PME) method [322]. We generated all MD trajectories with NAMDv2.7 [323] and the CHARMM force field [324]. We used VMDv1.8.7 for system creation and visualization [319], and VMDv1.8.8.a17 for generating input files used in MDFF simulations (see below).

MDFF: simulation details

The protocol of Trabuco et al. was followed for MDFF simulations [241, 243, 244]. The results show that MDFF improves the fit of the model **(Figs. S3, S19-23),** and multiple repeats of the same simulation give the same result **(Fig. S20, S22 C,D)**, showing that MDFF is consistent and our procedure is robust. To further validate the MDFF results, a four-step procedure (described below) was repeated with different initial structures (PDB ID: 3O2Z and 3JYV) fit into the WT 3D map **(Figs. S19-20);** as well as one initial structure (PDB ID: 3JYV) fit into three independent maps (WT, Nob1-depl and ΔLtv1) **(Fig. S22-23, Table S5).** The rRNA assumed very similar final structures in all runs **(Fig. S21, S23)**. The final validation of our MDFF approach is the observation that the rRNA does not occupy assembly factor density when fit into the WT and depletion 3D maps**.**

The four steps of the MDFF protocol are as follows:

1. In the first step, each initial atomic-model is rigid-body docked into the target map using SITUS software [325]. The docking of 3O2Z in the WT map is shown in **Fig. S3.**

2. In the next step, RNA is flexibly fit using a scaling factor of 0.5 kcal/mol (a value of 0.3 kcal/mol results in forces on the order of 10-15 pN per atom for a carbon atom as suggested by Trabuco et al. *(23)*). This value is tolerated because MDFF was carried out

in explicit solvent. The angles or distances in the RNA secondary structure were restrained with force constant values of 400 kcal mol^{-1} rad^{-2} or 400 kcal mol^{-1} $Å^{-2}$. In this step, the proteins were restrained with a force constant of 400 kcal mol^{-1} rad^{-2} (secondary-structure elements) and 200 kcal mol^{-1} rad^{-2} (non-secondary-structure elements). These values for restraints preserve the secondary structure of RNA and proteins during fitting into the map. We carried out this step for ~3 ns repeatedly until the RMSD converges **(Figs. S19, S20, S22, and S23)**. We repeated this step three times for the WT map and the Nob1-depleted map using 3JYV as an initial atomic model **(Fig. S20 and S22)**, and once for the WT map using 3O2Z as an initial atomic model **(Fig. S19).**

3. In the third step, a 3D map corresponding only to the density from protein components of the complex was generated. To this end, a simulated map of the fitted RNA structure was filtered to 18 Å and was subsequently subtracted from the WT pre-40S 3D map **(Fig. S4)**. In this step, we positionally restrain the rRNA with a large force constant of 10 kcal $mol^{-1}Å^{-2}$, and proteins are restrained in the same manner as earlier step.

4. In the final step, we refine the structure of proteins present in our model by reducing the restraints on the secondary structure with a force constant of 200 kcal mol^{-1} rad^{-2}. The cross correlation values at each step of MDFF for the different maps are presented in **Table S5**. Results of the fitting protocol are shown in **Figs. S3-S4 and S19-S23**.

Crystal structures of Dim1, Rio2, and Pno1 (or structures of homologous proteins, as described above and in the main text) were fit into the WT pre-40S density as rigid bodies and no flexible fitting was carried out. It should also be noted that no crystal

structures for AFs were present in any of the initial atomic models used for MDFF of rRNA and Rps in our pre-40S 3D map.

Supplementary Figures

Fig. S1

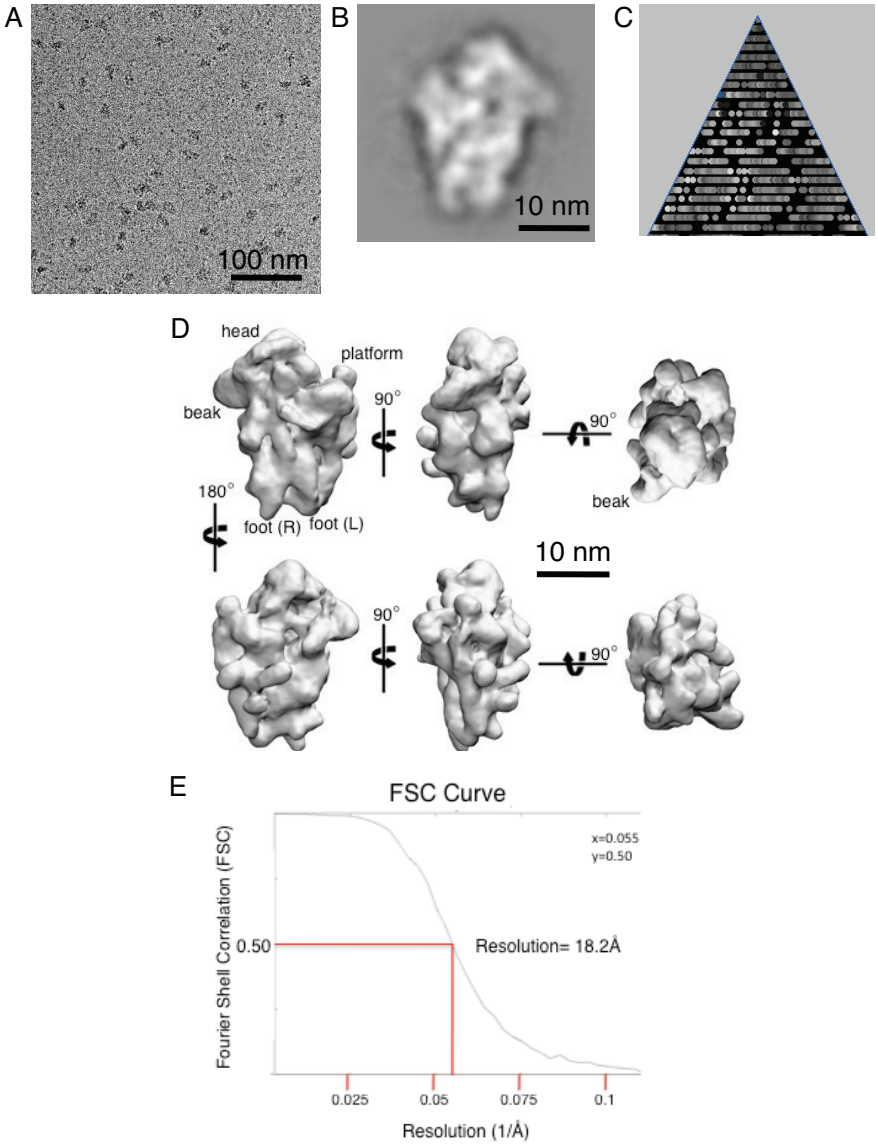

Fig. S1. Cryo-EM 3D reconstruction of Rio2-TAP pre-40S particles

A. Raw cryo-EM image of pre-40S particles.
B. Cross-section of cryo-EM 3D reconstruction for WT Rio2-TAP pre-40S.
C. Angular distribution profile for Rio2-TAP pre-40S refinement.
D. Different views of cryo-EM 3D reconstruction of WT Rio2-TAP pre-40S.
E. Fourier Shell Correlation (FSC) curve for the Rio2-TAP pre-40S, indicating a final resolution of 18.2Å (FSC=0.5).

Fig. S2 (page 1)

A

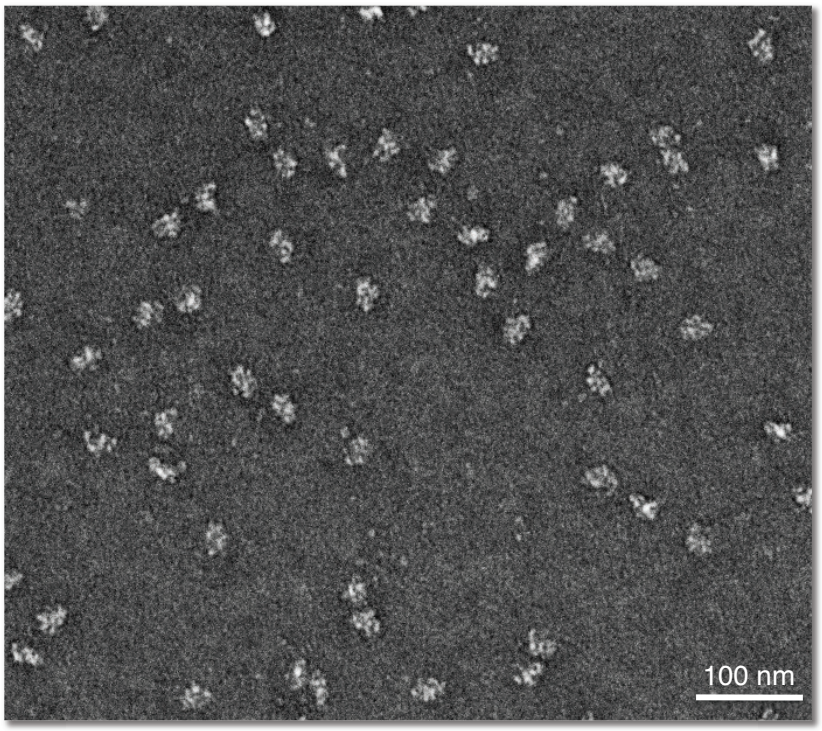

Fig. S2. 2D EM analysis of pre-40S Rio2-TAP particles embedded in negative stain.

A. Raw EM image of wild-type Rio2-TAP pre-40S particles embedded in negative stain.

Fig. S2 (page 2)

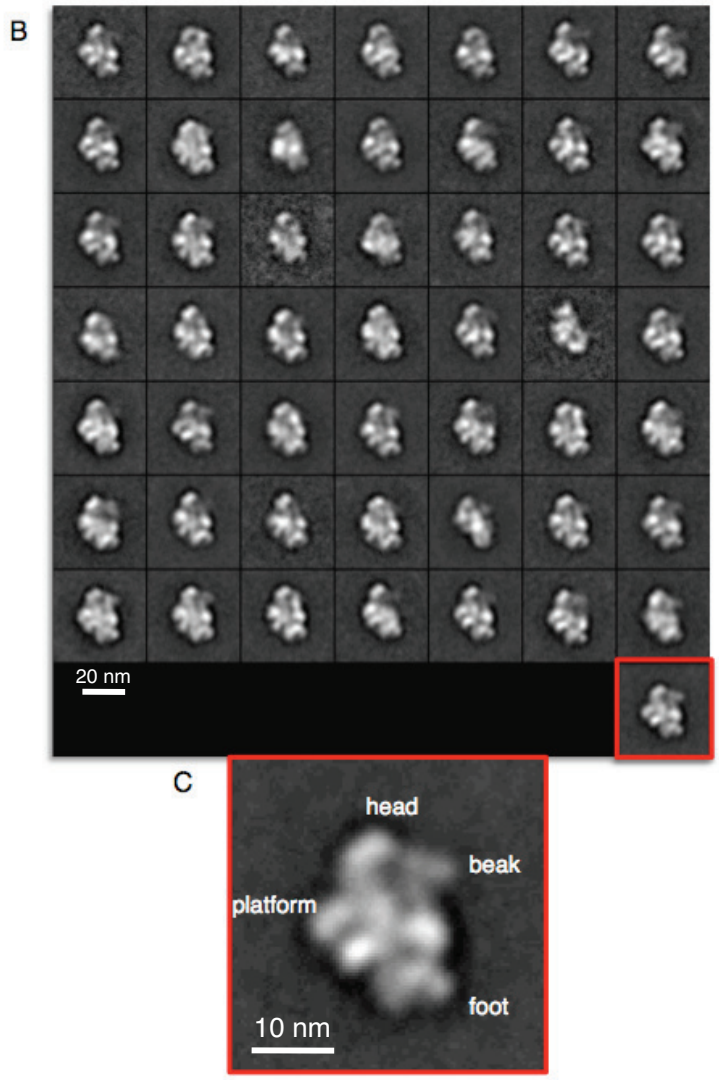

B. Classification and averaging of negative stained wild-type Rio2-TAP pre-40S particles into 50 classes.

C. Enlarged view of one class average showing the characteristic 40S subunit features: the head, beak, platform and foot.

Fig. S3

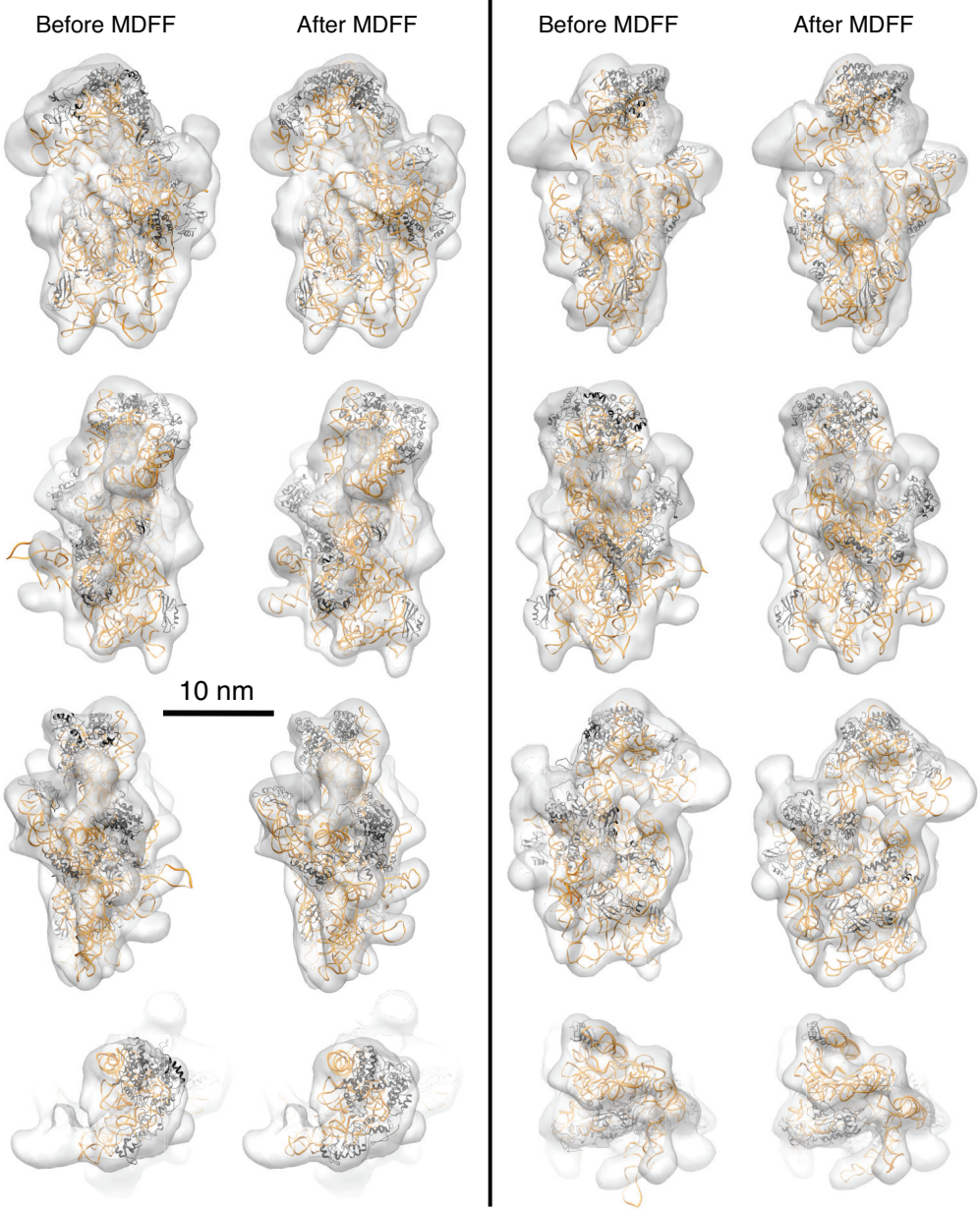

Fig. S3. **MDFF of rRNA and Rps into the pre-40S 3D map.**
Fit of the 18S rRNA (orange) and Rps (black) into the 3D volume of WT pre-40S before and after MDFF.

Fig. S4

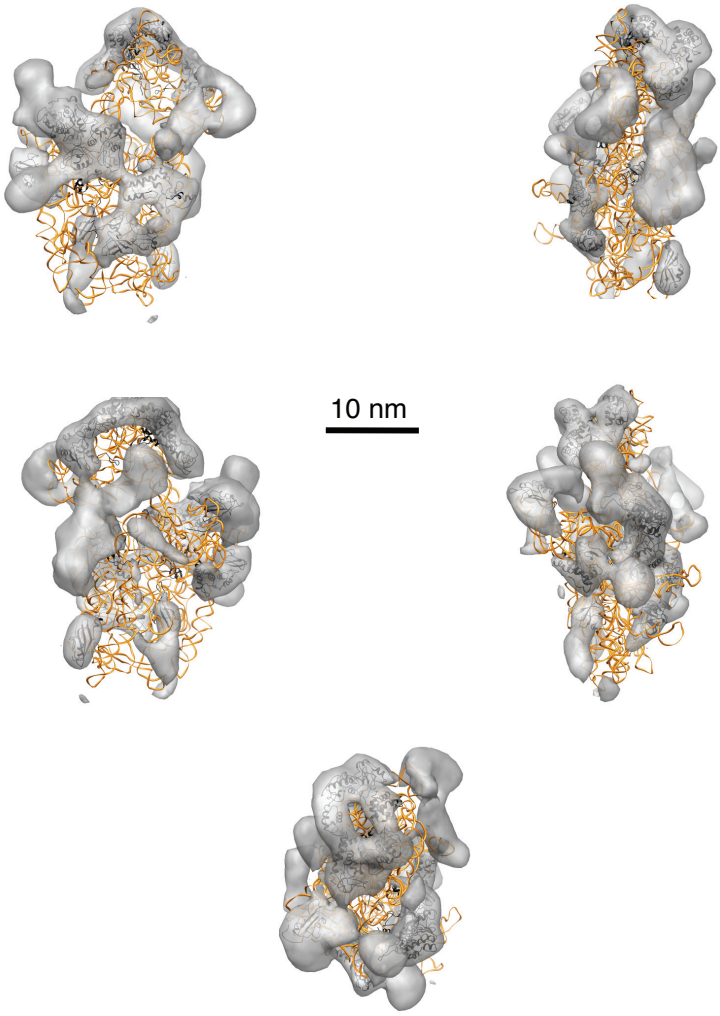

Fig. S4.

Subtraction of the 18S rRNA MDFF model from the pre-40S Rio2-TAP 3D volume reveals the densities attributed to proteins (AFs and Rps). The Rps present in our model are shown as black ribbons within the volume density. The remaining densities are attributed to AFs and Rps not included in our initial model.

Fig. S5

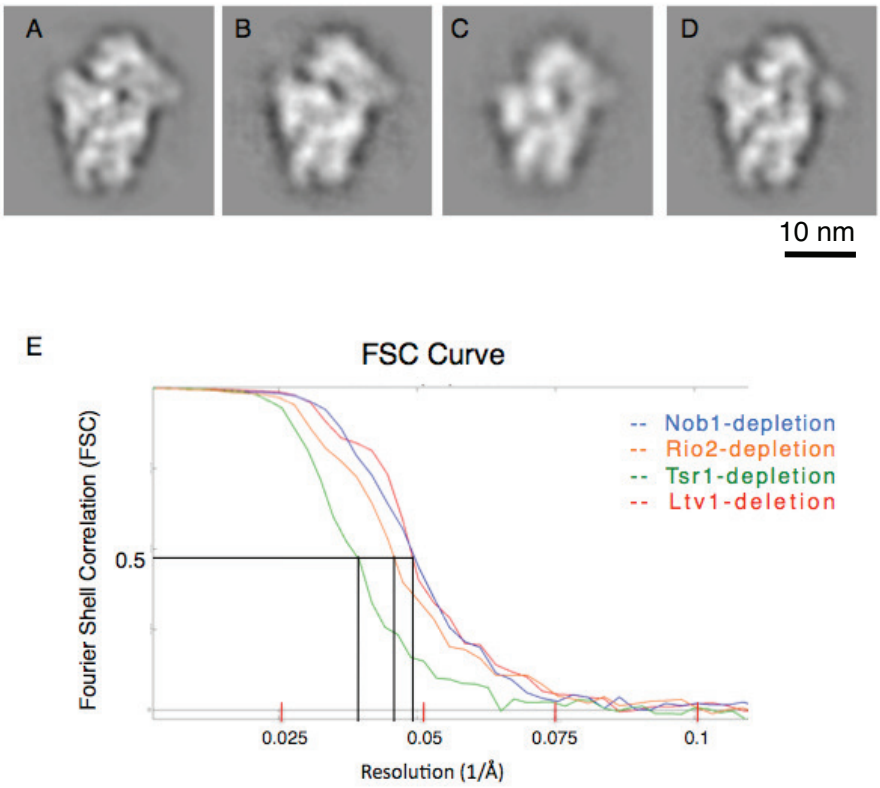

Fig. S5. Cryo-EM 3D reconstructions of pre-40S particles with assembly factors deleted or depleted.

A-D. Cross-sections of 3D reconstructions for (A) Nob1-depletion, (B) Rio2-depletion, (C) Tsr1-depletion, and (E) ΔLtv1 pre-40S particles.

E. FSC curves for the pre-40S 3D map indicate a resolution of ~20Å for Nob1-depletion (blue), ~22Å for Rio2-depletion (orange), ~26Å for Tsr1-depletion (green), and ~20Å for Ltv1-deletion (red) (FSC=0.5).

Fig. S6

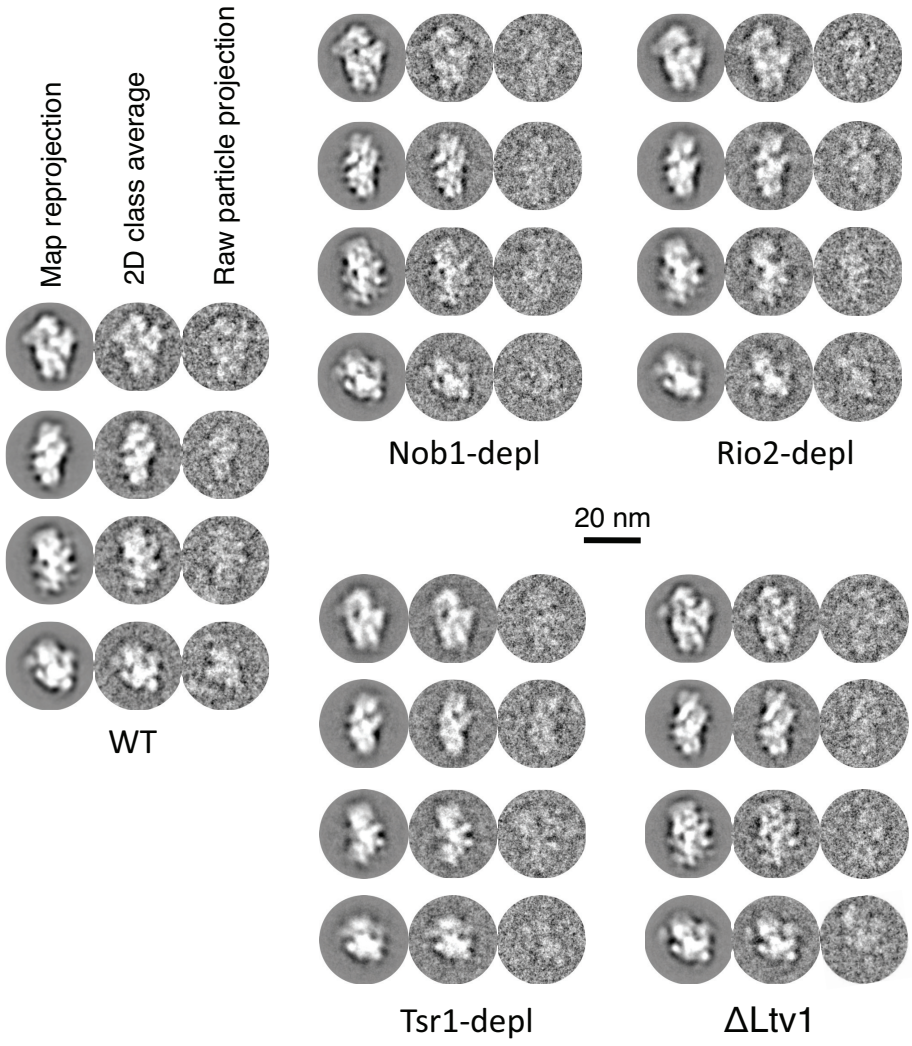

Fig. S6.

Comparison of 3D map re-projections, 2D class averages and raw particle images for WT, Nob1-depletion, Rio2-depletion, Tsr1-depletion, and ΔLtv1 pre-40S particles.

Fig. S7

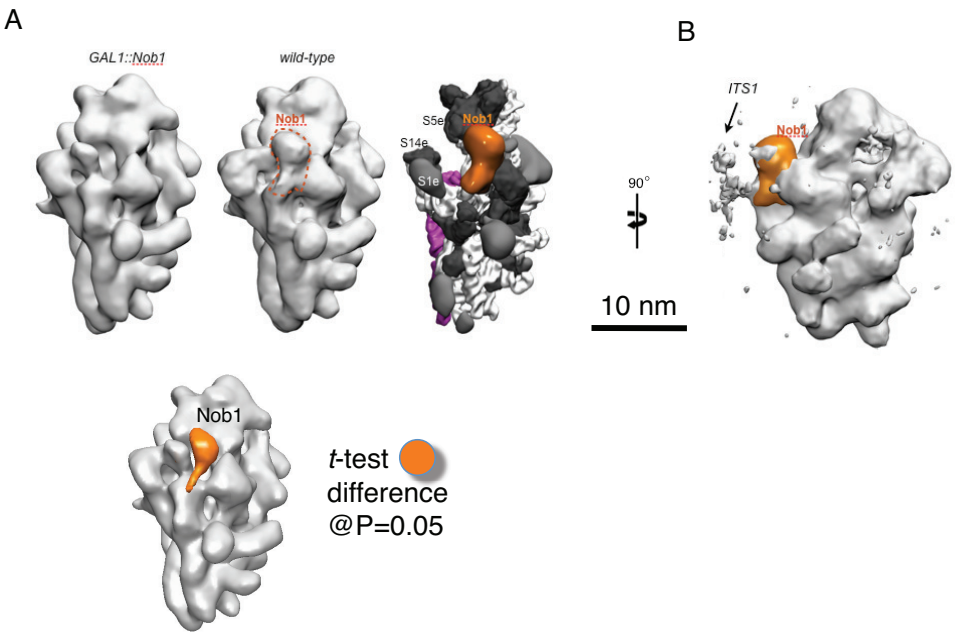

Fig. S7. Nob1 is located on the back of the platform.

A. 20Å cryo-EM structure of the Nob1-depleted sample. The WT cryo-EM map and MDFF model are shown for comparison, with the density corresponding to Nob1 in orange. Student's *t*-test difference mapping between the WT and Nob-depleted particles also reveal the expected density difference (shown in orange, with a density cut-off at P=0.05).

B. Visualization of the WT particle 3D map at lower threshold indicates ITS1 bound to Nob1.

Fig. S8

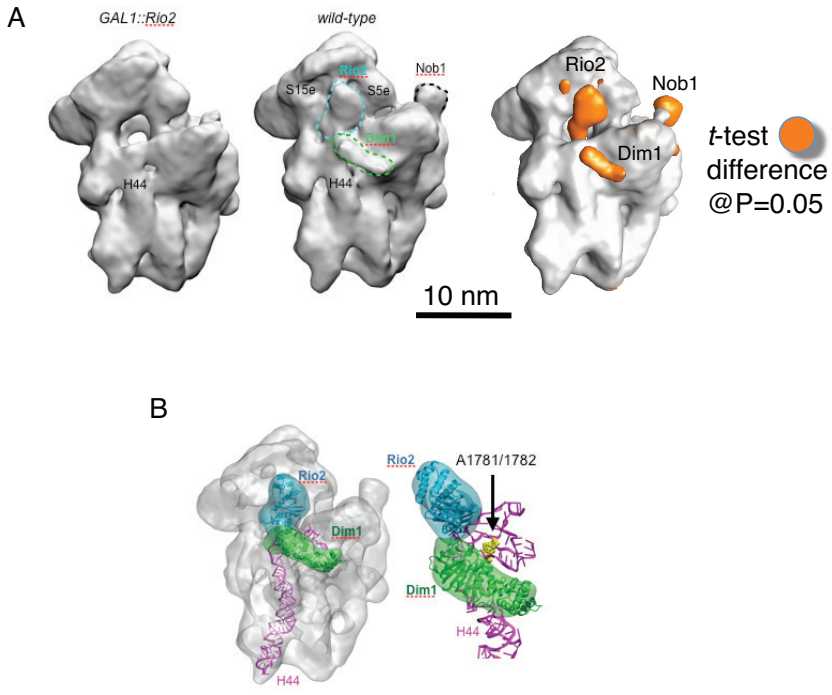

Fig. S8. Rio2 and Dim1 chaperone the decoding site.

A. 22Å cryo-EM map of the Rio2-depleted sample. The WT map is shown for comparison, and the densities corresponding to Rio2 and Dim1 in the WT map are shown in blue and green, respectively. Student's *t*-test difference mapping between the WT and Rio2-depleted particles also reveal the expected density differences (shown in orange, with a density cut-off at P=0.05).

B. Crystal structures for archeal Rio2 (1ZAO) and human Dim1 (1ZQ9) are docked into their respective densities. Dim1 methylation sites at A1781/1782 are labeled with yellow space fill.

Fig. S9

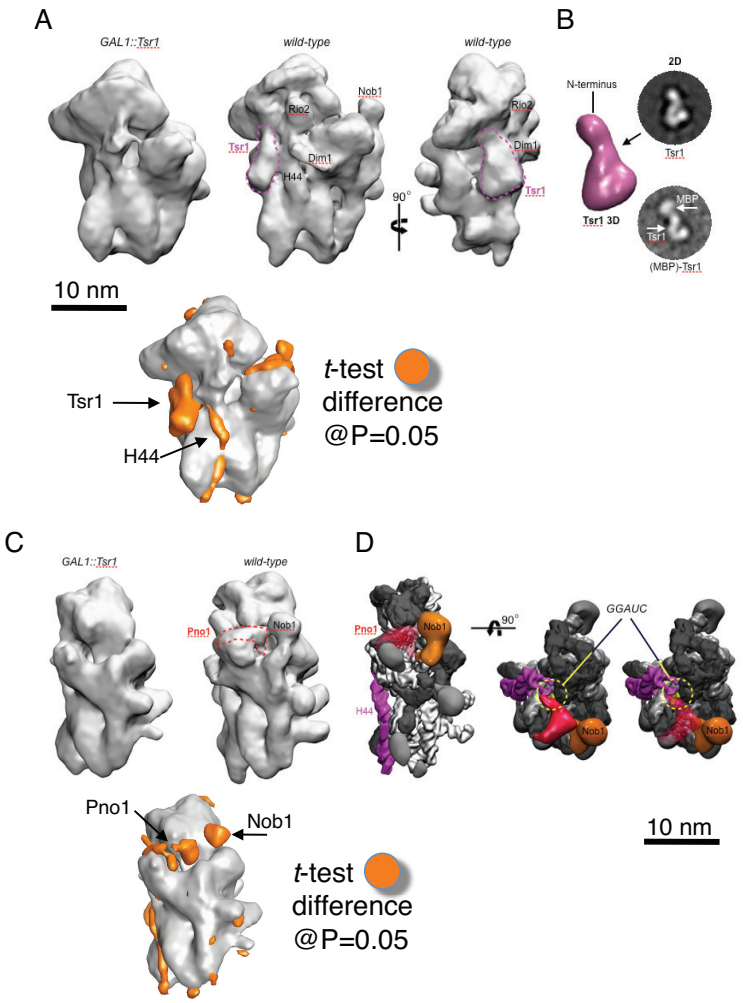

Fig. S9. Tsr1 binds Helix 44; Pno1 is located near the 18S rRNA 3'-end.

A,C Cryo-EM map of the Tsr1-depleted pre-40S particles. The WT map is shown for comparison, and the densities corresponding to Tsr1 and Pno1 are shown in magenta (A) and red (C), respectively. Student's *t*-test difference mapping between the WT and Tsr1-depleted particles also reveal the expected density differences (shown in orange, with a density cut-off at P=0.05).

B. Representative 2D projection averages of recombinant Tsr1 and (MBP-)Tsr1, and 3D EM reconstruction of Tsr1.

D. The positioning of Pno1 (red density) enables its interaction with the 3'-end of rRNA (yellow) and Nob1 (orange).

Fig. S10

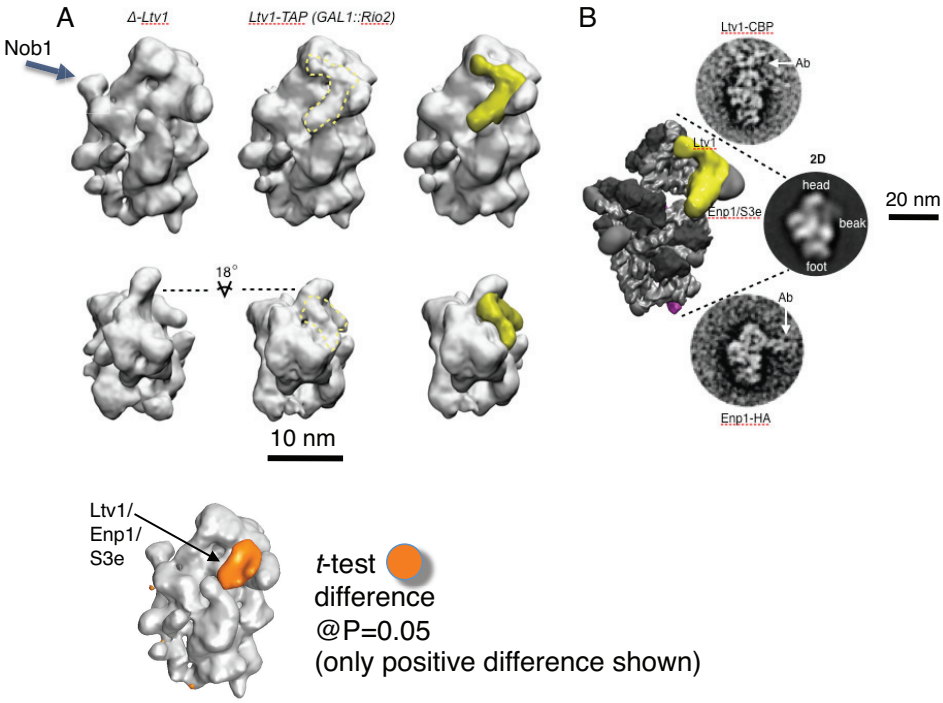

Fig. S10. Ltv1 and Enp1 bridge the beak and shoulder in pre-40S subunits.

A. 20Å cryo-EM map of the ΔLtv1 particles. The Ltv1-TAP (Gal::Rio2) map is shown for comparison, and the densitiy corresponding to Ltv1, Enp1 and Rps3 is shown in yellow; (lower panel) The beak is rotated 18° away from the subunit interface, as compared with Ltv1-TAP (Gal::Rio2). Student's *t*-test difference mapping between the Ltv1-TAP (Gal::Rio2) and ΔLtv1 particles also reveal the expected density difference (shown in orange, with a density cut-off at P=0.05).

B. 2D projection averages of samples labeled with antibody against the CBP-tag in Ltv1 (top) or the HA-tag in Enp1 (bottom). A 2D average of unlabeled pre-40S in negative stain is shown for comparison (middle). (10 nm scale bar corresponds to cryo-EM 3D maps, 20 nm scale bar corresponds to negative stain EM).

Fig. S11

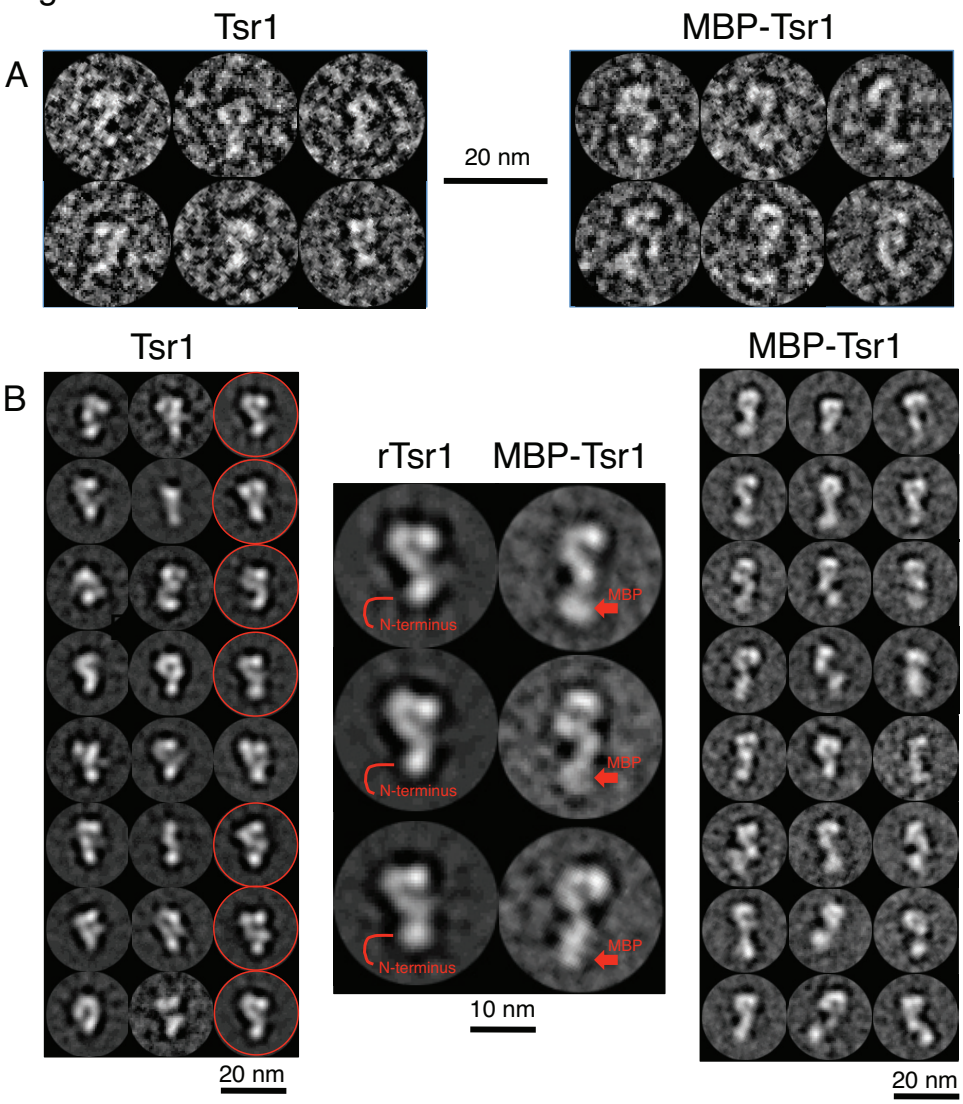

Fig. S11. Negative stain EM analysis of purified recombinant Tsr1.

A. Raw EM images of rTsr1 and MBP-Tsr1 embedded in negative stain.
B. Class averages of rTsr1 and MBP-Tsr1. Enlarged views of class averages are shown side-by-side for comparison. Particles belonging to the class averages boxed in red were used for the 3D reconstruction of rTsr1 (see Fig. S12).

Fig. S12

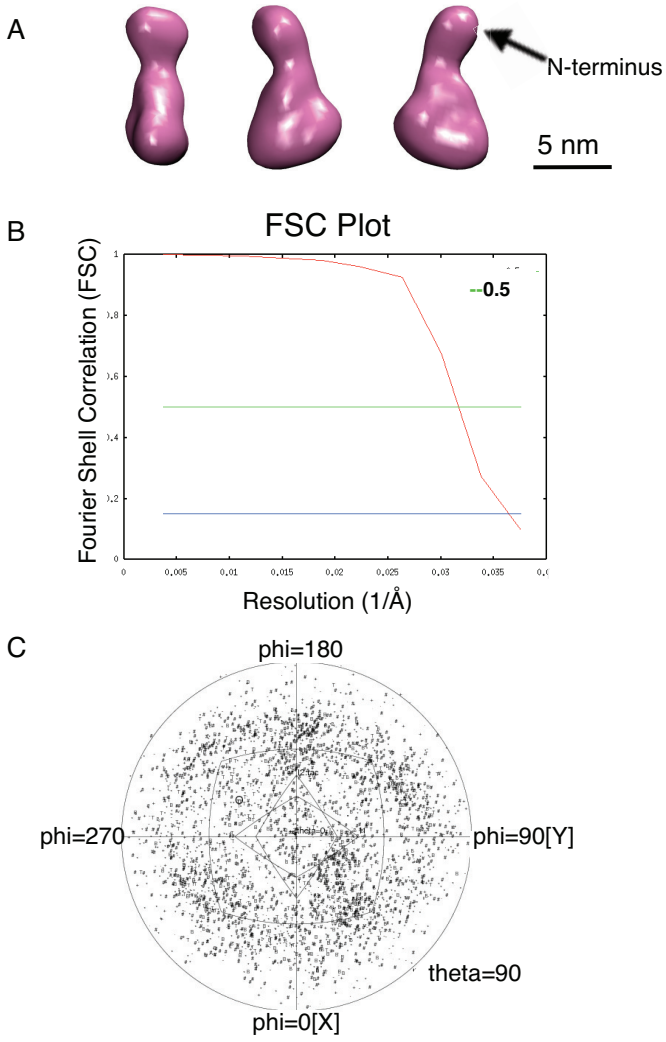

Fig. S12. 3D reconstruction of rTsr1 using the Random Conical Tilt Method.

A. 3D volume of rTsr1 (3 views).
B. Fourier Shell Correlation (FSC) curve of rTsr1 3D reconstruction (resolution= ~30Å @FSC=0.5).
C. Angular distribution of projections used for final 3D reconstruction of Tsr1.

Fig. S13

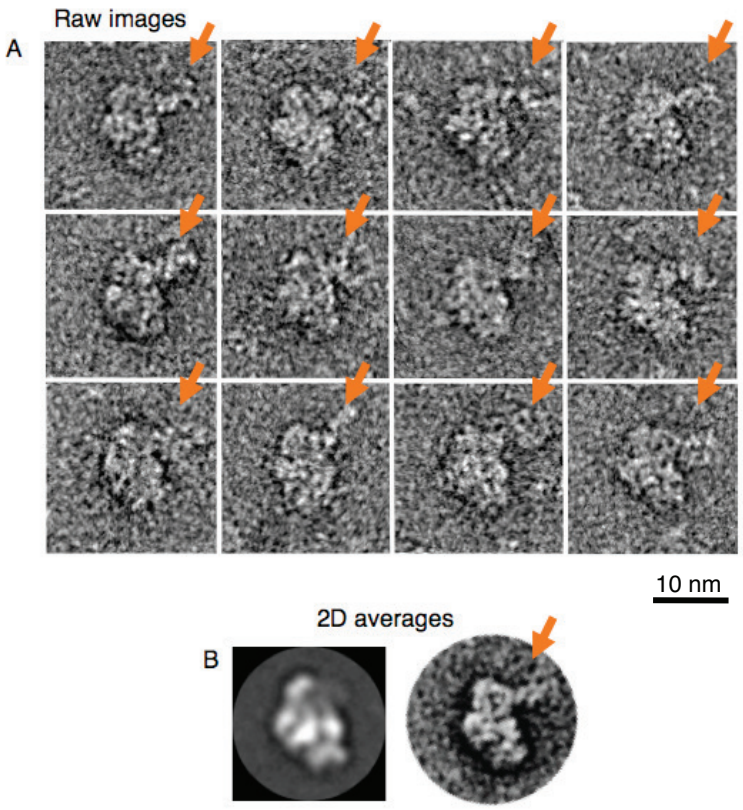

Fig. S13. Antibody-labeling of Enp1 on pre-40S complexes.

A. Raw EM images of negative stained pre-40S complexes with HA 1^{o}-antibody bound to Enp1-HA. The orange arrows indicate the extra density attributed to the antibody.

B. Comparison of the class average of Rio2-TAP pre-40S particles (left) and Enp1-HA pre-40S with HA 1^{o}-antibody (right) showing increased density on the beak.
(Raw images and class averages show the particle in roughly the same orientation).

Fig. S14

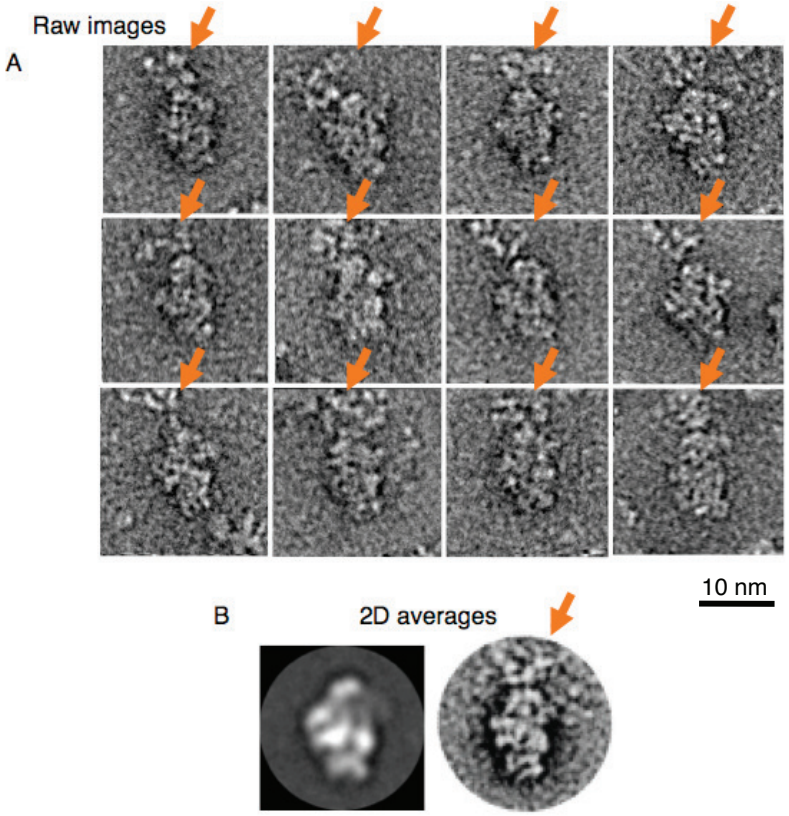

Fig. S14. Antibody-labeling of Ltv1 on pre-40S complexes.

A. Raw EM images of negative stained pre-40S complexes with CBP 1°-antibody bound to Ltv1-CBP. The arrows indicate the extra density attributed to the antibody.

B. Comparison of the class average of Rio2-TAP pre-40S particles (left) and Ltv1-CBP pre-40S with CBP 1°-antibody to Ltv1 (right) showing increased density on the head region.
(Raw images and class averages show the particle in roughly the same orientation).

Fig. S15

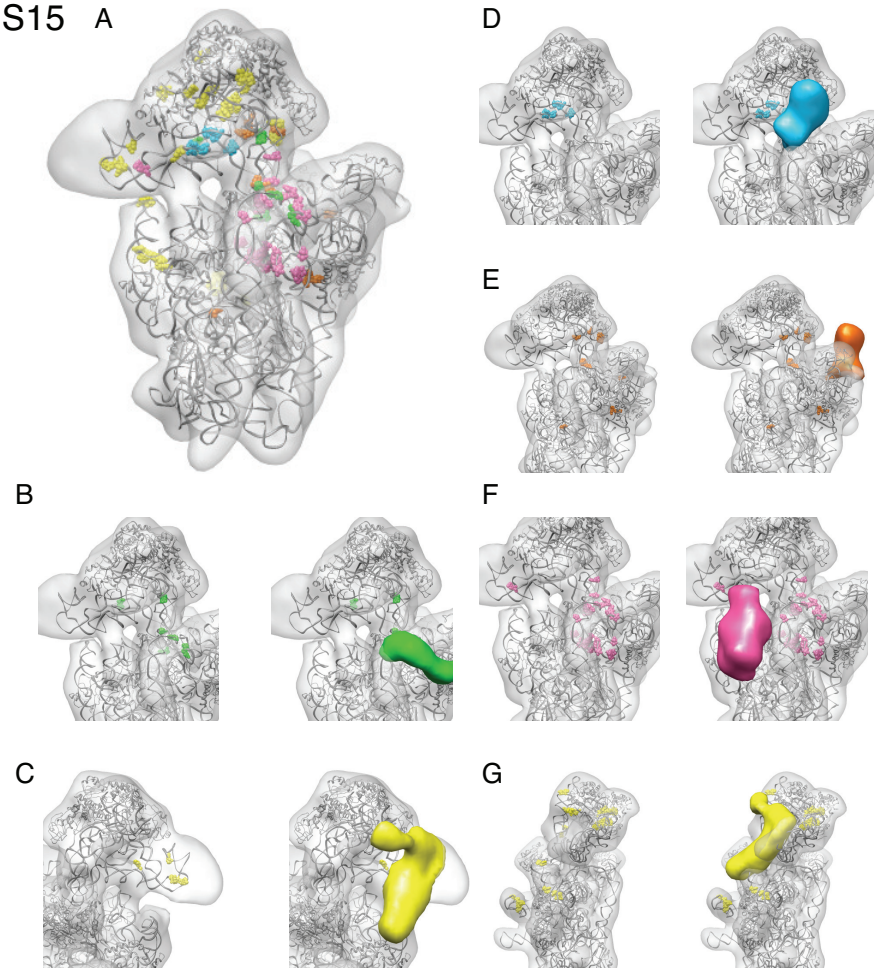

Fig. S15. Comparison of protein placement to previously obtained RNA-protein crosslinks.

A. Sites of crosslinks (Granneman *et al.*, 2010) to specific AFs are shown in space-fill: Dim1(green); Enp1(yellow); Rio2(blue); Nob1(orange;) Tsr1(pink) and Ltv1(yellow). In order to minimize noise, only crosslinks fiitting either one of the following criteria are shown: crosslink was observed at least twice, or at least three crosslinks in a 10 nucleotide window were obtained.

B-G. Comparison of sites for individual crosslinks with the density attributed to the same protein. (B) Dim1 (C) Enp1 (D) Rio2 (E) Nob1 (F) Tsr1 (G) Ltv1.

Fig. S16

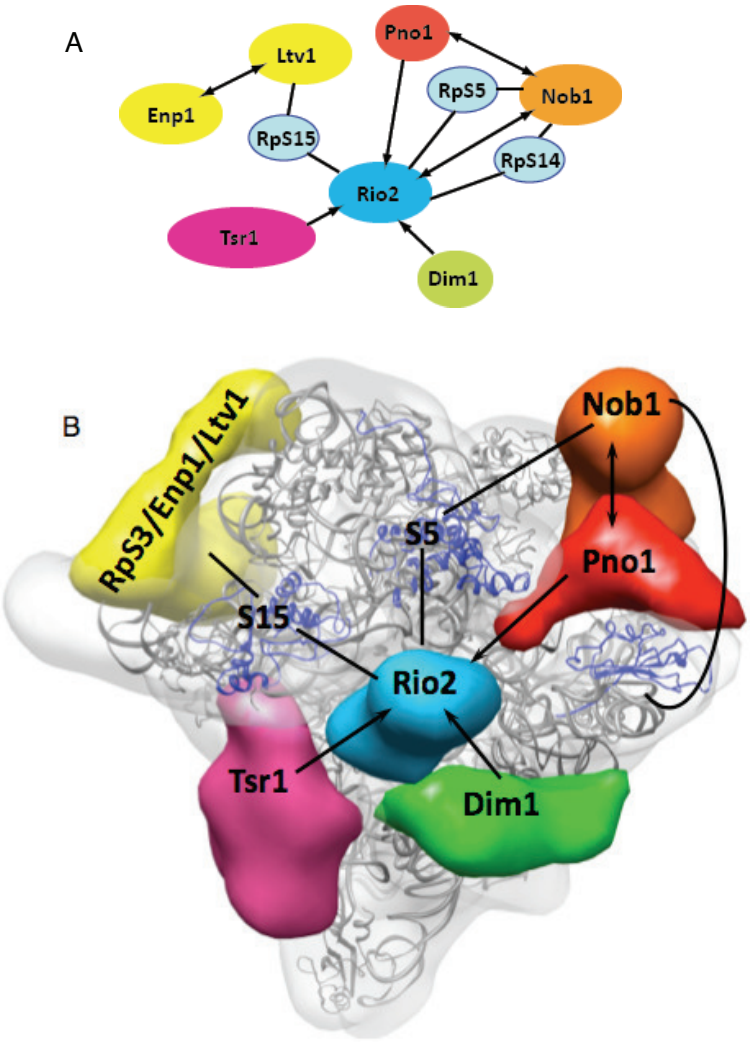

Figure S16. Comparison of cryo-EM AF placement to previously obtained protein-protein interactions.

A. Summary of previously published protein-protein interactions from *in vitro* pulldowns (Campbell & Karbstein, 2011) and yeast 2-hybrid interactions (Loar, 2004; Tone, 2002)

B. Interactions that are consistent with the placement of proteins in the pre-40S map. Ribosomal proteins are shown as blue ribbons.

Fig. S17

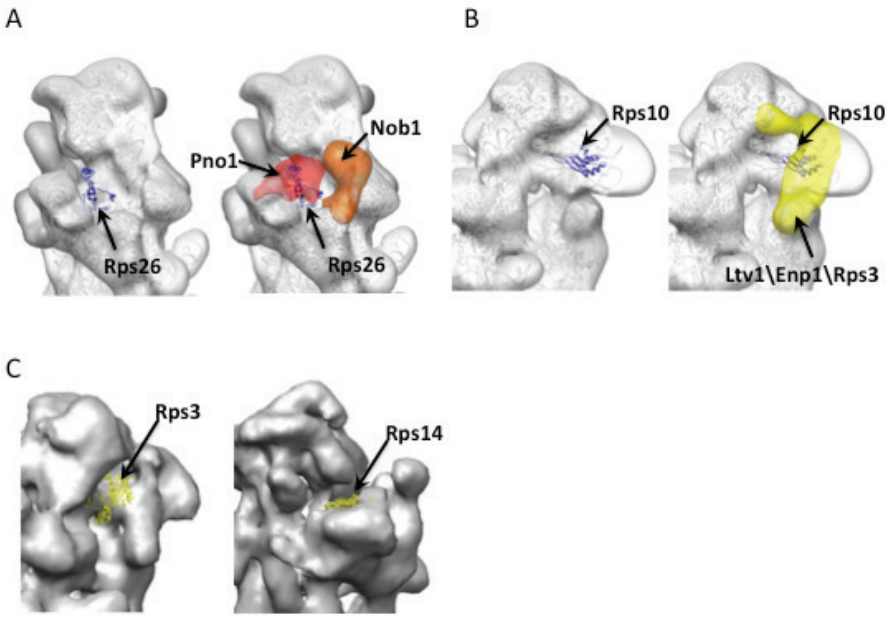

Fig. S17. Rearrangements of Rps in late cytoplasmic 40S particles

A. The binding site for Rps26 (blue ribbon) overlaps with the binding site for Pno1 (red), explaining the absence of Rps26 in the late 40S particles purified herein.
B. The binding site for Rps10 (blue ribbon) overlaps with the binding site for Ltv1/ Enp1/Rps3 (yellow), explaining the absence of Rps10 in the late 40S particles purified herein.
C. Rps3 and Rps14 (yellow ribbons) are not located at their final positions, as their structure/location in the mature 40S is partially outside the electron density of pre-40S.

Ribosomal proteins in this figure are modeled from PDB file 2XZM (Rabl et al., 2011)

Fig. S18

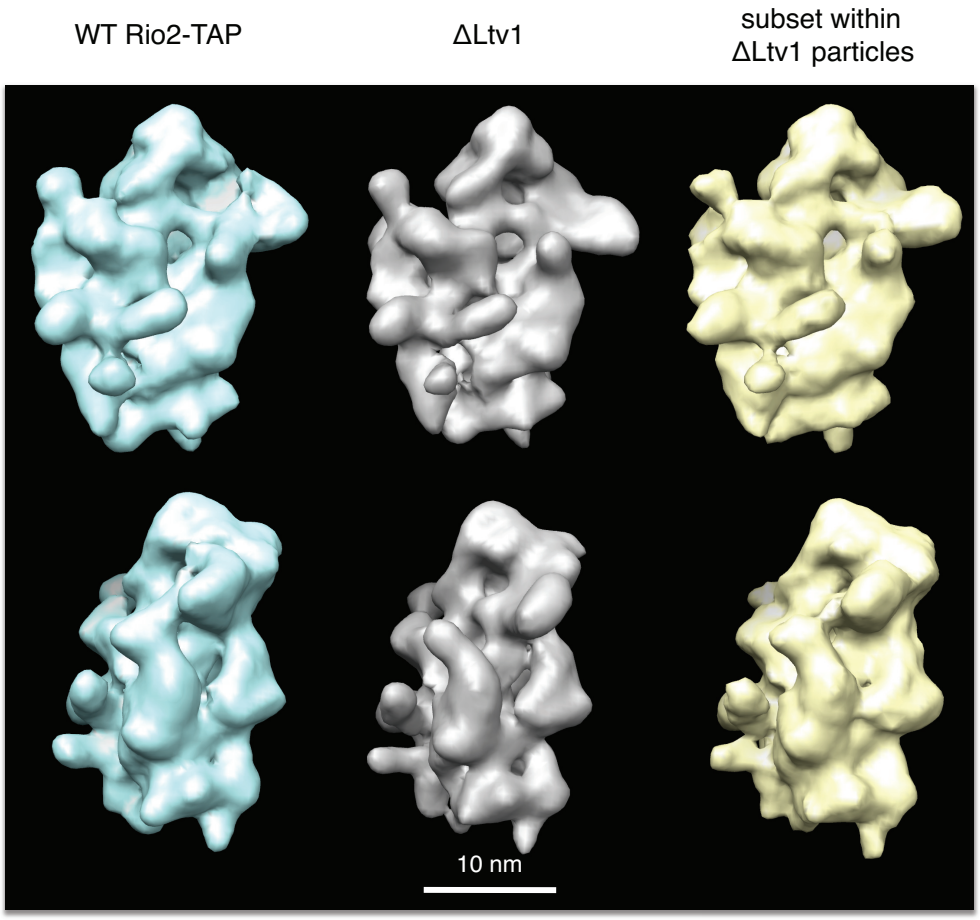

Fig. S18. A subpopulation of ΔLtv1 pre-40S particles contains part of the density bridging helix 16 with the beak (in yellow, right column), similar to WT Rio2-TAP pre-40S (in blue, left column).

Fig. S19

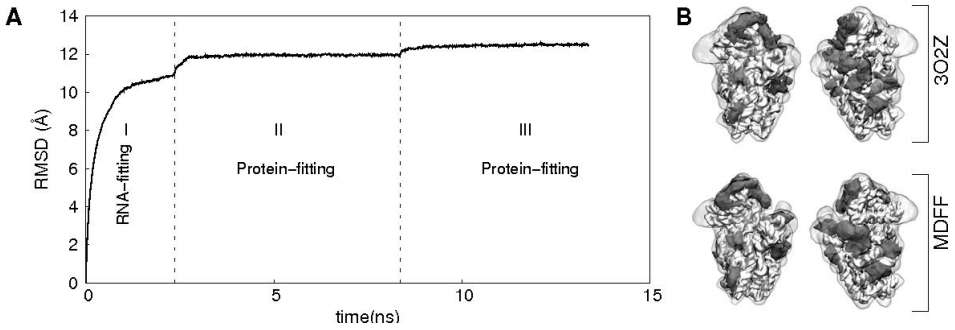

Fig. S19. MDFF results for the wild-type map using the initial structure (PDB code 3O2Z).

A. Root mean square deviation (RMSD) with reference to initial atomic model (PDB ID: 3O2Z) as a function of simulation time (ns). MDFF fitting was carried out in three stages (see text).

B. Pre- and post-MDFF side-view snapshots of initial atomic model (PDB ID: 3O2Z) positioned into the wild-type map. rRNA: silver, Rps: dark gray.

Fig. S20

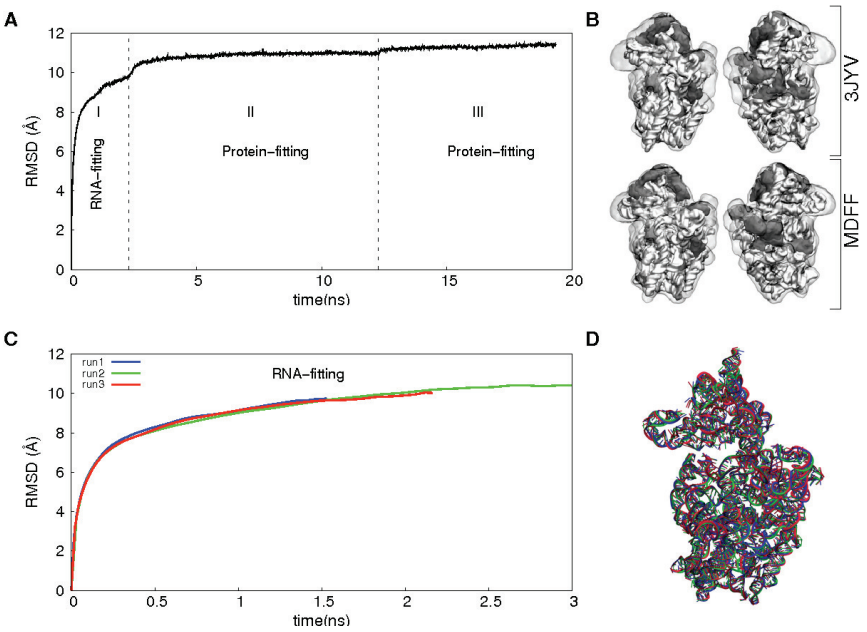

Fig. S20. **Validations in the MDFF protocol with 3JYV fitting into the WT map.**

A. Root mean square deviation (RMSD) with reference to initial atomic model (PDB ID: 3JYV) as a function of simulation time (ns). MDFF was carried out in three stages (see text).

B. Pre- and post-MDFF side-view snapshots of initial atomic model (PDB ID: 3JYV) positioned into the wild-type map. rRNA: silver, Rps: dark gray.

C. RMSD (Å) vs. simulation time (ns) of rRNA in three independent MDFF runs.

D. Overlay of rRNA structures at the end of three independent MDFF runs. RNA backbones are in the same color as RMSD traces in panel C.

Fig. S21

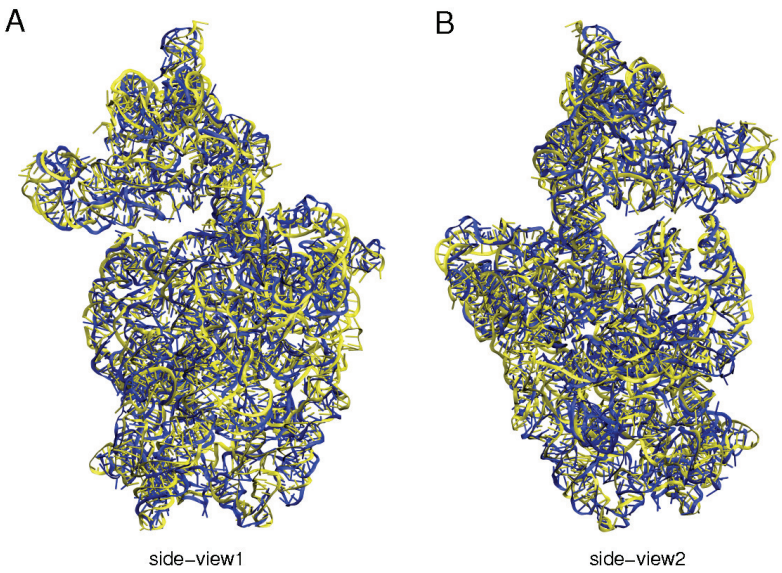

Fig. S21. Comparison of final rRNA fitting from two independent starting structures.

A,**B** Two different views for the overlay of rRNA structures obtained at the end of RNA fitting using MDFF. The end structures were obtained via MDFF from two different starting structures: PDB ID 3JYV (yellow) and PDB ID 3O2Z (blue). We note that the length of RNA varies between the two initial structures at various locations.

Fig. S22

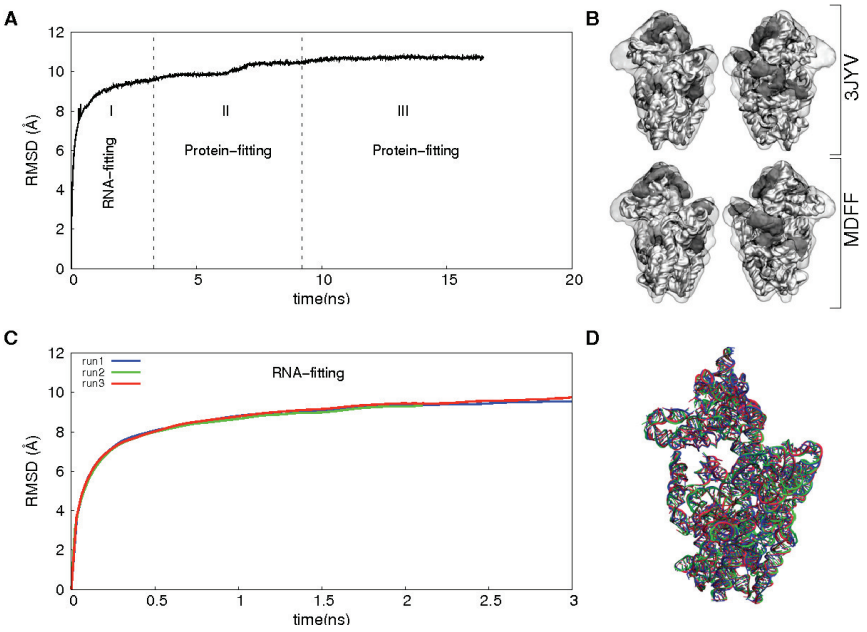

Fig. S22: MDFF results for fitting 3JYV into the Nob1-depleted map.

A. Root mean square deviation (RMSD) with reference to initial atomic model (PDB ID: 3JYV) as a function of simulation time (ns). MDFF was carried out in three stages (see text).

B. Pre- and post-MDFF side-view snapshots of initial atomic model (PDB ID: 3JYV) positioned into the Nob1-depleted map. rRNA: silver, Rps: dark gray.

C. RMSD (Å) vs. simulation time (ns) of rRNA fitting in three independent MDFF runs.

D. Overlay of rRNA structures at the end of three independent MDFF runs. rRNA backbones are in the same color as RMSD traces in panel C.

Fig. S23

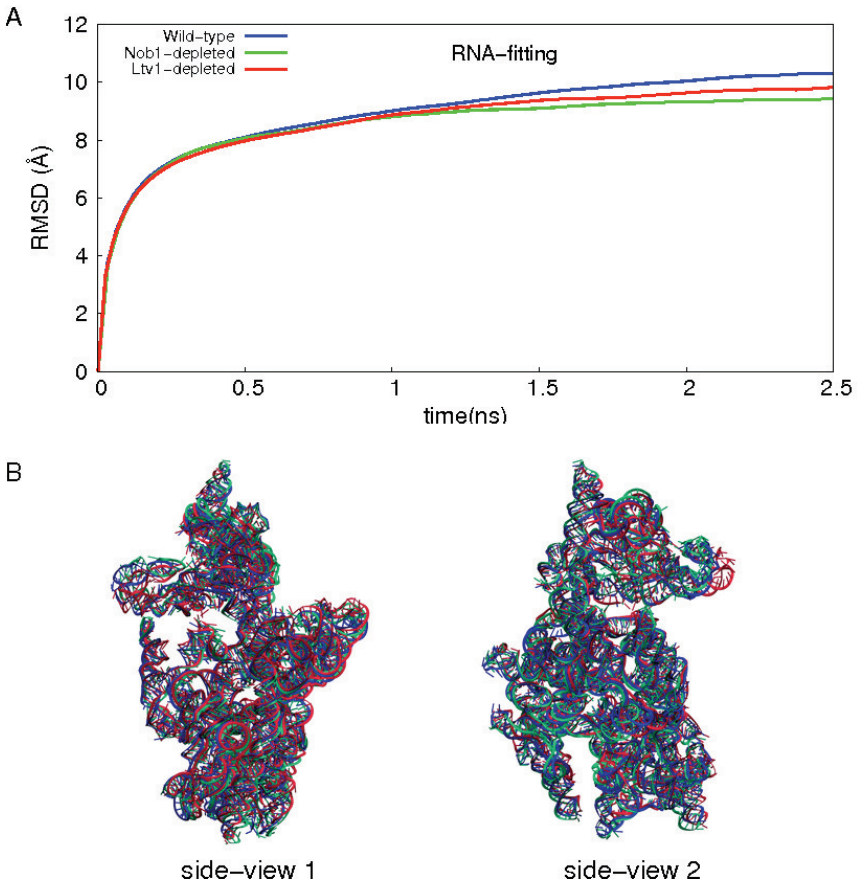

Fig. S23. Comparison of rRNA fitting into three independent cryo-EM maps of pre-40S particle.

A. RMSD (Å) vs. simulation time (ns) for MDFF of rRNA into three independent maps: wild-type, Nob1-depleted, and ΔLtv1. MDFF was carried out independently into three maps with consistent simulation parameters (see text).

B. Two different side-views for the overlay of rRNA structures at the end of MDFF into each map. rRNA backbones are in the same colors as RMSD traces in panel A.

Rps	WT	Ltv1Δ	Gal1::Nob1	Gal1::Rio2	Gal1::Tsr1
0	(19)	(19)	(17)	(52)	(64)
1	(38)	(38)	(46)	(87)	(76)
2	(14)	(14)	(15)	(12)	(49)
3	(37)		(19)	(44)	(117)
4	(26)	(26)	(26)	(36)	(79)
5	(17)	(17)	(27)	(46)	(61)
6	(14)	(14)	(43)	(63)	(53)
7	(29)	(29)	(19)	(55)	(122)
8	(9)	(9)	(4)	(5)	(47)
9	(16)	(16)	(13)	(59)	(81)
10					
11	(11)	(11)	(2)	(29)	(35)
12	(11)	(11)	(19)	(33)	(29)
13	(19)	(19)	(27)	(53)	(58)
14	(18)	(18)	(17)	(55)	(44)
15	(10)	(10)	(16)	(50)	(34)
16	(14)	(14)	(12)	(46)	(62)
17	(14)	(14)	(34)	(60)	(51)
18	(15)	(15)	(22)	(92)	(56)
19	(9)	(9)	(29)	(70)	(46)
20	(7)		(14)	(54)	(41)
21	(4)	(4)	(17)	(11)	(12)
22	(14)	(14)	(17)	(31)	(49)
23	(8)	(8)	(2)	(7)	(19)
24	(18)	(18)	(18)	(34)	(53)
25	(9)	(9)	(13)	(18)	(30)
26				(4)	(3)
27	(12)	(12)	(16)	(13)	(8)
28	(4)	(4)	(13)	(34)	(17)
29	(2)		(9)	(12)	(10)
30	(6)	(6)	(7)	(5)	(12)
31	(3)	(3)	(2)		(9)

Table S1. Mass spectrometry results for ribosomal proteins in pre-40S ribosomes. For each Rps, the number of peptides identified is provided in parentheses.

Rps	WT	Ltv1Δ	Gal1::Nob1	Gal1::Rio2	Gal1::Tsr1
Tsr1	**	**	**	**	*
Ltv1	**		**	**	**
Enp1	**	*	**	**	**
Nob1	**	**	*	*	*
Rio2	**	**	**	*	*
Pno1	**	**	**	**	*
Dim1	**	**	**	*	*
Hrr25	*/-	*/-	*	*	*
Krr1					(14)
Slx9					(8)
Snu13					(3)
Nop56					(16)
Mrt4					(8)
Cka2					(12)
eIF2β					(6)
Yra1				(5)	(7)
Rpt3					(4)
Arp4					(6)
Arp7				(4)	(19)
Arp9				(9)	(18)
Hho1					(3)
Hhf1					(6)
Rtt102					(4)
Pmg1					(6)
Tdh1-3		(40)			(7)
Adt2		(16)			
AtpG		(7)			
AtpJ		(2)			
GlpB	(12)	(2)	(2)		(9)
Rim1					(2)

Table S2. Mass spectrometry results for non-ribosomal proteins in pre-40S ribosomes. Assembly factors bound in stoichiometric amounts are indicated by **; reduced levels are indicated with *. Other assembly factors found by mass spectrometry but not detectable on SDS PAGE gels are listed, with the number of peptides in brackets.

Strain	Description	Genotype	Reference
YKK87	Rio2TAP	BY4741 Rio2TAP::His	Open Biosystems
YKK88	Ltv1TAP	BY4741 Ltv1TAP::His	Open Biosystems
YKK90	Nob1TAP	BY4741 Nob1TAP::His	Open Biosystems
YKK73	Ltv1Δ	BY4741 Ltv1::Kan	Open Biosystems
YKK352	Ltv1Δ/Rio2TAP	BY4741 Ltv1::Kan Rio2TAP::His	This work
YKK347	Enp1HA/Rio2TAP	BY4741 Enp1HA::Kan Rio2TAP::His	This work
	Gal1::Rio2	*MAT***a** *his3Δ leu2Δ met15Δ lys2Δ ura3Δ Rio2::KAN*/pEV80 (*pGAL*::*RIO2-PROTA URA3*)	Vanrobays, 2003
YKK362	Gal1::Rio2/Ltv1TAP	*MAT***a** *his3Δ leu2Δ met15Δ lys2Δ ura3Δ Rio2::KAN Ltv1TAP::His*/pEV80	This work
YKK367	Gal1::Tsr1/Ltv1TAP	BY4741 Gal1Tsr1::Kan Ltv1TAP::His	This work
YKK217	Gal1::Nob1/Rio2TAP	BY4741 Gal1Nob1::Kan	This work

Table S3. Yeast strains used in this study.

rps	PDB	Omitted
Rps0	3O2Z	
Rps1	2XZM	
Rps2	3O2Z	
Rps3		X
Rps4	3O2Z	
Rps5	3IZB	
Rps6		
Rps7		
Rps8		
Rps9	3O2Z	
Rps10		
Rps11	3O2Z	
Rps12		
Rps13	3O2Z	
Rps14	2XZM	
Rps15	3O2Z	
Rps16	3O2Z	
Rps17		X
Rps18	3IZB	
Rps19	3IZB	
Rps20		X
Rps21		
Rps22	3O2Z	
Rps23	3O2Z	
Rps24	3O2Z	
Rps25	3O2Z	
Rps26		
Rps27	3O2Z	
Rps28	3O2Z	
Rps29		X
Rps30		X
Rps31		X

Table S4. Source of PDB coordinates for Rps included in our final MDFF model (those omitted are designated by a X in the far right column).

Map	PDB	Res. (Å)	CC			
			Initial	Step1	Step2	step3
Wild-type	3JYV	18	0.672	0.781	0.786	0.787
Nob1-depl	3JYV	20	0.642	0.764	0.766	0.767
ΔLtv1	3JYV	20	0.645	0.768	-	-
Wild-type	3O2Z	18	0.673	0.795	0.802	0.805

Table S5: Cross-correlation values for final fitting of rRNA and Rps into our 3D maps.

References

1. Lomakin, I.B., et al., Position of eukaryotic initiation factor eIF1 on the 40S ribosomal subunit determined by directed hydroxyl radical probing. Genes Dev, 2003. **17**(22): p. 2786-97.
2. Yu, Y., et al., *Position of eukaryotic translation initiation factor eIF1A on the 40S ribosomal subunit mapped by directed hydroxyl radical probing.* Nucleic Acids Res, 2009. **37**(15): p. 5167-82.
3. Venema, J. and D. Tollervey, *Ribosome synthesis in Saccharomyces cerevisiae.* Annu Rev Genet, 1999. **33**: p. 261-311.
4. Siridechadilok, B., et al., *Structural roles for human translation factor eIF3 in initiation of protein synthesis.* Science, 2005. **310**(5753): p. 1513-5.
5. Passmore, L.A., et al., *The eukaryotic translation initiation factors eIF1 and eIF1A induce an open conformation of the 40S ribosome.* Mol Cell, 2007. **26**(1): p. 41-50.
6. Karbstein, K. and T.P. Begley, *Ribosome, Chemistry of*, in *Wiley Encyclopedia of Chemical Biology*. 2009, John Wiley & Sons, Inc.: Hoboken.
7. Hage, A.E. and D. Tollervey, *A surfeit of factors: why is ribosome assembly so much more complicated in eukaryotes than bacteria?* RNA Biol, 2004. **1**(1): p. 10-5.
8. Connolly, K. and G. Culver, *Deconstructing ribosome construction.* Trends Biochem Sci, 2009. **34**(5): p. 256-63.
9. Beckmann, R., et al., *Architecture of the protein-conducting channel associated with the translating 80S ribosome.* Cell, 2001. **107**(3): p. 361-72.
10. Spahn, C.M., et al., *Structure of the 80S ribosome from Saccharomyces cerevisiae--tRNA-ribosome and subunit-subunit interactions.* Cell, 2001. **107**(3): p. 373-86.
11. Chandramouli, P., et al., *Structure of the mammalian 80S ribosome at 8.7 A resolution.* Structure, 2008. **16**(4): p. 535-48.
12. Woese, C.R., et al., *Secondary structure model for bacterial 16S ribosomal RNA: phylogenetic, enzymatic and chemical evidence.* Nucleic Acids Res, 1980. **8**(10): p. 2275-93.
13. Winker, S. and C.R. Woese, *A definition of the domains Archaea, Bacteria and Eucarya in terms of small subunit ribosomal RNA characteristics.* Syst Appl Microbiol, 1991. **14**(4): p. 305-10.
14. Schnare, M.N., et al., *Comprehensive comparison of structural characteristics in eukaryotic cytoplasmic large subunit (23 S-like) ribosomal RNA.* J Mol Biol, 1996. **256**(4): p. 701-19.
15. Cannone, J.J., et al., *The comparative RNA web (CRW) site: an online database of comparative sequence and structure information for ribosomal, intron, and other RNAs.* BMC Bioinformatics, 2002. **3**: p. 2.

16. Mears, J.A., et al., *Modeling a minimal ribosome based on comparative sequence analysis.* J Mol Biol, 2002. **321**(2): p. 215-34.
17. Fromont-Racine, M., et al., *Ribosome assembly in eukaryotes.* Gene, 2003. **313**: p. 17-42.
18. Dwight, S.S., et al., *Saccharomyces Genome Database (SGD) provides secondary gene annotation using the Gene Ontology (GO).* Nucleic Acids Res, 2002. **30**(1): p. 69-72.
19. Bourne, H.R., D.A. Sanders, and F. McCormick, *The GTPase superfamily: conserved structure and molecular mechanism.* Nature, 1991. **349**(6305): p. 117-27.
20. Leipe, D.D., et al., *Classification and evolution of P-loop GTPases and related ATPases.* J Mol Biol, 2002. **317**(1): p. 41-72.
21. Karbstein, K., *Role of GTPases in ribosome assembly.* Biopolymers, 2007. **87**(1): p. 1-11.
22. Becam, A.M., et al., *Ria1p (Ynl163c), a protein similar to elongation factors 2, is involved in the biogenesis of the 60S subunit of the ribosome in Saccharomyces cerevisiae.* Mol Genet Genomics, 2001. **266**(3): p. 454-62.
23. Gelperin, D., et al., *Bms1p, a novel GTP-binding protein, and the related Tsr1p are required for distinct steps of 40S ribosome biogenesis in yeast.* RNA, 2001. **7**(9): p. 1268-83.
24. Saveanu, C., et al., *Sequential protein association with nascent 60S ribosomal particles.* Mol Cell Biol, 2003. **23**(13): p. 4449-60.
25. Senger, B., et al., *The nucle(ol)ar Tif6p and Efl1p are required for a late cytoplasmic step of ribosome synthesis.* Mol Cell, 2001. **8**(6): p. 1363-73.
26. Wegierski, T., et al., *Bms1p, a G-domain-containing protein, associates with Rcl1p and is required for 18S rRNA biogenesis in yeast.* RNA, 2001. **7**(9): p. 1254-67.
27. Jensen, B.C., et al., *The NOG1 GTP-binding protein is required for biogenesis of the 60 S ribosomal subunit.* J Biol Chem, 2003. **278**(34): p. 32204-11.
28. Kallstrom, G., J. Hedges, and A. Johnson, *The putative GTPases Nog1p and Lsg1p are required for 60S ribosomal subunit biogenesis and are localized to the nucleus and cytoplasm, respectively.* Mol Cell Biol, 2003. **23**(12): p. 4344-55.
29. Hedges, J., M. West, and A.W. Johnson, *Release of the export adapter, Nmd3p, from the 60S ribosomal subunit requires Rpl10p and the cytoplasmic GTPase Lsg1p.* EMBO J, 2005. **24**(3): p. 567-79.
30. Karbstein, K., S. Jonas, and J.A. Doudna, *An essential GTPase promotes assembly of preribosomal RNA processing complexes.* Mol Cell, 2005. **20**(4): p. 633-43.
31. Bassler, J., M. Kallas, and E. Hurt, *The NUG1 GTPase reveals and N-terminal RNA-binding domain that is essential for association with 60 S pre-ribosomal particles.* J Biol Chem, 2006. **281**(34): p. 24737-44.
32. Erzberger, J.P. and J.M. Berger, *Evolutionary relationships and structural mechanisms of AAA+ proteins.* Annu Rev Biophys Biomol Struct, 2006. **35**: p. 93-114.

33. Gadal, O., et al., *A nuclear AAA-type ATPase (Rix7p) is required for biogenesis and nuclear export of 60S ribosomal subunits.* EMBO J, 2001. **20**(14): p. 3695-704.
34. Galani, K., et al., *Rea1, a dynein-related nuclear AAA-ATPase, is involved in late rRNA processing and nuclear export of 60 S subunits.* J Biol Chem, 2004. **279**(53): p. 55411-8.
35. Pertschy, B., et al., *Cytoplasmic recycling of 60S preribosomal factors depends on the AAA protein Drg1.* Mol Cell Biol, 2007. **27**(19): p. 6581-92.
36. Kressler, D., et al., *The AAA ATPase Rix7 powers progression of ribosome biogenesis by stripping Nsa1 from pre-60S particles.* J Cell Biol, 2008. **181**(6): p. 935-44.
37. Nissan, T.A., et al., *A pre-ribosome with a tadpole-like structure functions in ATP-dependent maturation of 60S subunits.* Mol Cell, 2004. **15**(2): p. 295-301.
38. Jankowsky, E. and M.E. Fairman, *RNA helicases--one fold for many functions.* Curr Opin Struct Biol, 2007. **17**(3): p. 316-24.
39. Cordin, O., et al., *The DEAD-box protein family of RNA helicases.* Gene, 2006. **367**: p. 17-37.
40. Tanner, N.K. and P. Linder, *DExD/H box RNA helicases: from generic motors to specific dissociation functions.* Mol Cell, 2001. **8**(2): p. 251-62.
41. Yang, Q., et al., *DEAD-box proteins unwind duplexes by local strand separation.* Mol Cell, 2007. **28**(2): p. 253-63.
42. Chen, Y., et al., *DEAD-box proteins can completely separate an RNA duplex using a single ATP.* Proc Natl Acad Sci U S A, 2008. **105**(51): p. 20203-8.
43. Liu, F., A. Putnam, and E. Jankowsky, *ATP hydrolysis is required for DEAD-box protein recycling but not for duplex unwinding.* Proc Natl Acad Sci U S A, 2008. **105**(51): p. 20209-14.
44. Shibuya, T., et al., *Mutational analysis of human eIF4AIII identifies regions necessary for exon junction complex formation and nonsense-mediated mRNA decay.* RNA, 2006. **12**(3): p. 360-74.
45. Hassett, A., W. Blattler, and J.R. Knowles, *Pyruvate kinase: is the mechanism of phospho transfer associative or dissociative?* Biochemistry, 1982. **21**(25): p. 6335-40.
46. Baird, C.L., et al., *The ATPase reaction cycle of yeast DNA topoisomerase II. Slow rates of ATP resynthesis and P(i) release.* J Biol Chem, 2001. **276**(30): p. 27893-8.
47. Algire, M.A., D. Maag, and J.R. Lorsch, *Pi release from eIF2, not GTP hydrolysis, is the step controlled by start-site selection during eukaryotic translation initiation.* Mol Cell, 2005. **20**(2): p. 251-62.
48. Bleichert, F., et al., *The PINc domain protein Utp24, a putative nuclease, is required for the early cleavage steps in 18S rRNA maturation.* Proc Natl Acad Sci U S A, 2006. **103**(25): p. 9464-9.
49. Song, Y., S. Kim, and J. Kim, *ROK1, a high-copy-number plasmid suppressor of kem1, encodes a putative ATP-dependent RNA helicase in Saccharomyces cerevisiae.* Gene, 1995. **166**(1): p. 151-4.
50. O'Day, C.L., F. Chavanikamannil, and J. Abelson, *18S rRNA processing requires the RNA helicase-like protein Rrp3.* Nucleic Acids Res, 1996. **24**(16): p. 3201-7.

51. Liang, W.Q., J.A. Clark, and M.J. Fournier, *The rRNA-processing function of the yeast U14 small nucleolar RNA can be rescued by a conserved RNA helicase-like protein.* Mol Cell Biol, 1997. **17**(7): p. 4124-32.
52. Venema, J., et al., *Rok1p is a putative RNA helicase required for rRNA processing.* Mol Cell Biol, 1997. **17**(6): p. 3398-407.
53. Colley, A., et al., *Dhr1p, a putative DEAH-box RNA helicase, is associated with the box C+D snoRNP U3.* Mol Cell Biol, 2000. **20**(19): p. 7238-46.
54. Daugeron, M.C., D. Kressler, and P. Linder, *Dbp9p, a putative ATP-dependent RNA helicase involved in 60S-ribosomal-subunit biogenesis, functionally interacts with Dbp6p.* RNA, 2001. **7**(9): p. 1317-34.
55. Granneman, S., et al., *Comprehensive mutational analysis of yeast DEXD/H box RNA helicases required for small ribosomal subunit synthesis.* Mol Cell Biol, 2006. **26**(4): p. 1183-94.
56. Sachs, A.B. and R.W. Davis, *Translation initiation and ribosomal biogenesis: involvement of a putative rRNA helicase and RPL46.* Science, 1990. **247**(4946): p. 1077-9.
57. Ripmaster, T.L., G.P. Vaughn, and J.L. Woolford, Jr., *DRS1 to DRS7, novel genes required for ribosome assembly and function in Saccharomyces cerevisiae.* Mol Cell Biol, 1993. **13**(12): p. 7901-12.
58. de la Cruz, J., et al., *Spb4p, an essential putative RNA helicase, is required for a late step in the assembly of 60S ribosomal subunits in Saccharomyces cerevisiae.* RNA, 1998. **4**(10): p. 1268-81.
59. de la Cruz, J., et al., *Dob1p (Mtr4p) is a putative ATP-dependent RNA helicase required for the 3' end formation of 5.8S rRNA in Saccharomyces cerevisiae.* EMBO J, 1998. **17**(4): p. 1128-40.
60. de la Cruz, J., et al., *The putative RNA helicase Dbp6p functionally interacts with Rpl3p, Nop8p and the novel trans-acting Factor Rsa3p during biogenesis of 60S ribosomal subunits in Saccharomyces cerevisiae.* Genetics, 2004. **166**(4): p. 1687-99.
61. Burger, F., M.C. Daugeron, and P. Linder, *Dbp10p, a putative RNA helicase from Saccharomyces cerevisiae, is required for ribosome biogenesis.* Nucleic Acids Res, 2000. **28**(12): p. 2315-23.
62. Bond, A.T., et al., *Absence of Dbp2p alters both nonsense-mediated mRNA decay and rRNA processing.* Mol Cell Biol, 2001. **21**(21): p. 7366-79.
63. Bernstein, K.A., et al., *Comprehensive mutational analysis of yeast DEXD/H box RNA helicases involved in large ribosomal subunit biogenesis.* Mol Cell Biol, 2006. **26**(4): p. 1195-208.
64. Emery, B., et al., *Has1p, a member of the DEAD-box family, is required for 40S ribosomal subunit biogenesis in Saccharomyces cerevisiae.* Mol Microbiol, 2004. **52**(1): p. 141-58.
65. Lebaron, S., et al., *The splicing ATPase prp43p is a component of multiple preribosomal particles.* Mol Cell Biol, 2005. **25**(21): p. 9269-82.
66. Combs, D.J., et al., *Prp43p is a DEAH-box spliceosome disassembly factor essential for ribosome biogenesis.* Mol Cell Biol, 2006. **26**(2): p. 523-34.
67. Leeds, N.B., et al., *The splicing factor Prp43p, a DEAH box ATPase, functions in ribosome biogenesis.* Mol Cell Biol, 2006. **26**(2): p. 513-22.

68. Liang, X.H. and M.J. Fournier, *The helicase Has1p is required for snoRNA release from pre-rRNA.* Mol Cell Biol, 2006. **26**(20): p. 7437-50.
69. Gavin, A.C., et al., *Functional organization of the yeast proteome by systematic analysis of protein complexes.* Nature, 2002. **415**(6868): p. 141-7.
70. Tollervey, D., *A yeast small nuclear RNA is required for normal processing of pre-ribosomal RNA.* EMBO J, 1987. **6**(13): p. 4169-75.
71. Bally, M., J. Hughes, and G. Cesareni, *SnR30: a new, essential small nuclear RNA from Saccharomyces cerevisiae.* Nucleic Acids Res, 1988. **16**(12): p. 5291-303.
72. Li, H.D., J. Zagorski, and M.J. Fournier, *Depletion of U14 small nuclear RNA (snR128) disrupts production of 18S rRNA in Saccharomyces cerevisiae.* Mol Cell Biol, 1990. **10**(3): p. 1145-52.
73. Morrissey, J.P. and D. Tollervey, *Yeast snR30 is a small nucleolar RNA required for 18S rRNA synthesis.* Mol Cell Biol, 1993. **13**(4): p. 2469-77.
74. Decatur, W.A. and M.J. Fournier, *RNA-guided nucleotide modification of ribosomal and other RNAs.* J Biol Chem, 2003. **278**(2): p. 695-8.
75. Bohnsack, M.T., M. Kos, and D. Tollervey, *Quantitative analysis of snoRNA association with pre-ribosomes and release of snR30 by Rok1 helicase.* EMBO Rep, 2008. **9**(12): p. 1230-6.
76. Kos, M. and D. Tollervey, *The Putative RNA Helicase Dbp4p Is Required for Release of the U14 snoRNA from Preribosomes in Saccharomyces cerevisiae.* Mol Cell, 2005. **20**(1): p. 53-64.
77. Cadwell, C., et al., *The yeast nucleolar protein Cbf5p is involved in rRNA biosynthesis and interacts genetically with the RNA polymerase I transcription factor RRN3.* Mol Cell Biol, 1997. **17**(10): p. 6175-83.
78. Fath, S., et al., *Association of yeast RNA polymerase I with a nucleolar substructure active in rRNA synthesis and processing.* J Cell Biol, 2000. **149**(3): p. 575-90.
79. Krogan, N.J., et al., *High-definition macromolecular composition of yeast RNA-processing complexes.* Mol Cell, 2004. **13**(2): p. 225-39.
80. Krogan, N.J., et al., *Global landscape of protein complexes in the yeast Saccharomyces cerevisiae.* Nature, 2006. **440**(7084): p. 637-43.
81. Collins, S.R., et al., *Toward a comprehensive atlas of the physical interactome of Saccharomyces cerevisiae.* Mol Cell Proteomics, 2007. **6**(3): p. 439-50.
82. Tarassov, K., et al., *An in vivo map of the yeast protein interactome.* Science, 2008. **320**(5882): p. 1465-70.
83. Osheim, Y.N., et al., *Pre-18S ribosomal RNA is structurally compacted into the SSU processome prior to being cleaved from nascent transcripts in Saccharomyces cerevisiae.* Mol Cell, 2004. **16**(6): p. 943-54.
84. Fuller-Pace, F.V., et al., *DbpA: a DEAD box protein specifically activated by 23s rRNA.* EMBO J, 1993. **12**(9): p. 3619-26.
85. Garcia, I. and O.C. Uhlenbeck, *Differential RNA-dependent ATPase activities of four rRNA processing yeast DEAD-box proteins.* Biochemistry, 2008. **47**(47): p. 12562-73.

86. Granneman, S., et al., *The nucleolar protein Esf2 interacts directly with the DExD/H box RNA helicase, Dbp8, to stimulate ATP hydrolysis.* Nucleic Acids Res, 2006. **34**(10): p. 3189-99.
87. Tanaka, N., A. Aronova, and B. Schwer, *Ntr1 activates the Prp43 helicase to trigger release of lariat-intron from the spliceosome.* Genes Dev, 2007. **21**(18): p. 2312-25.
88. Hopfner, K.P. and J.A. Tainer, *Rad50/SMC proteins and ABC transporters: unifying concepts from high-resolution structures.* Curr Opin Struct Biol, 2003. **13**(2): p. 249-55.
89. Higgins, C.F. and K.J. Linton, *The ATP switch model for ABC transporters.* Nat Struct Mol Biol, 2004. **11**(10): p. 918-26.
90. Dong, J., et al., *The essential ATP-binding cassette protein RLI1 functions in translation by promoting preinitiation complex assembly.* J Biol Chem, 2004. **279**(40): p. 42157-68.
91. Kispal, G., et al., *Biogenesis of cytosolic ribosomes requires the essential iron-sulphur protein Rli1p and mitochondria.* EMBO J, 2005. **24**(3): p. 589-98.
92. Yarunin, A., et al., *Functional link between ribosome formation and biogenesis of iron-sulfur proteins.* EMBO J, 2005. **24**(3): p. 580-8.
93. Dong, J., et al., *The novel ATP-binding cassette protein ARB1 is a shuttling factor that stimulates 40S and 60S ribosome biogenesis.* Mol Cell Biol, 2005. **25**(22): p. 9859-73.
94. Andersen, D.S. and S.J. Leevers, *The essential Drosophila ATP-binding cassette domain protein, pixie, binds the 40 S ribosome in an ATP-dependent manner and is required for translation initiation.* J Biol Chem, 2007. **282**(20): p. 14752-60.
95. Valasek, L., et al., *Dual function of eIF3j/Hcr1p in processing 20 S pre-rRNA and translation initiation.* J Biol Chem, 2001. **276**(46): p. 43351-60.
96. Warner, J.R., *The economics of ribosome biosynthesis in yeast.* Trends Biochem Sci, 1999. **24**(11): p. 437-40.
97. Cohen, P., *The regulation of protein function by multisite phosphorylation--a 25 year update.* Trends Biochem Sci, 2000. **25**(12): p. 596-601.
98. Manning, G., et al., *Evolution of protein kinase signaling from yeast to man.* Trends Biochem Sci, 2002. **27**(10): p. 514-20.
99. Ptacek, J., et al., *Global analysis of protein phosphorylation in yeast.* Nature, 2005. **438**(7068): p. 679-84.
100. Ficarro, S.B., et al., *Phosphoproteome analysis by mass spectrometry and its application to Saccharomyces cerevisiae.* Nat Biotechnol, 2002. **20**(3): p. 301-5.
101. Chi, A., et al., *Analysis of phosphorylation sites on proteins from Saccharomyces cerevisiae by electron transfer dissociation (ETD) mass spectrometry.* Proc Natl Acad Sci U S A, 2007. **104**(7): p. 2193-8.
102. LaRonde-LeBlanc, N. and A. Wlodawer, *A family portrait of the RIO kinases.* J Biol Chem, 2005. **280**(45): p. 37297-300.
103. Laronde-Leblanc, N., et al., *Structure and activity of the atypical serine kinase Rio1.* FEBS J, 2005. **272**(14): p. 3698-713.
104. LaRonde-LeBlanc, N. and A. Wlodawer, *Crystal structure of A. fulgidus Rio2 defines a new family of serine protein kinases.* Structure, 2004. **12**(9): p. 1585-94.

105. Schafer, T., et al., *The path from nucleolar 90S to cytoplasmic 40S pre-ribosomes.* EMBO J, 2003. **22**(6): p. 1370-80.
106. Angermayr, M. and W. Bandlow, *RIO1, an extraordinary novel protein kinase.* FEBS Lett, 2002. **524**(1-3): p. 31-6.
107. Geerlings, T.H., et al., *Rio2p, an evolutionarily conserved, low abundant protein kinase essential for processing of 20 S Pre-rRNA in Saccharomyces cerevisiae.* J Biol Chem, 2003. **278**(25): p. 22537-45.
108. Hoekstra, M.F., et al., *HRR25, a putative protein kinase from budding yeast: association with repair of damaged DNA.* Science, 1991. **253**(5023): p. 1031-4.
109. Ho, H.Y., H.H. Lee, and M.Z. Lai, *Overexpression of mitogen-activated protein kinase kinase kinase reversed cAMP inhibition of NF-kappaB in T cells.* Eur J Immunol, 1997. **27**(1): p. 222-6.
110. Kafadar, K.A., et al., *Negative regulation of calcineurin signaling by Hrr25p, a yeast homolog of casein kinase I.* Genes Dev, 2003. **17**(21): p. 2698-708.
111. Petronczki, M., et al., *Monopolar attachment of sister kinetochores at meiosis I requires casein kinase 1.* Cell, 2006. **126**(6): p. 1049-64.
112. Schafer, T., et al., *Hrr25-dependent phosphorylation state regulates organization of the pre-40S subunit.* Nature, 2006. **441**(7093): p. 651-5.
113. Ray, P., et al., *The Saccharomyces cerevisiae 60 S ribosome biogenesis factor Tif6p is regulated by Hrr25p-mediated phosphorylation.* J Biol Chem, 2008. **283**(15): p. 9681-91.
114. Basu, U., et al., *Phosphorylation of mammalian eukaryotic translation initiation factor 6 and its Saccharomyces cerevisiae homologue Tif6p: evidence that phosphorylation of Tif6p regulates its nucleocytoplasmic distribution and is required for yeast cell growth.* Mol Cell Biol, 2003. **23**(17): p. 6187-99.
115. Gallagher, J.E., et al., *RNA polymerase I transcription and pre-rRNA processing are linked by specific SSU processome components.* Genes Dev, 2004. **18**(20): p. 2506-17.
116. Grandi, P., et al., *90S pre-ribosomes include the 35S pre-rRNA, the U3 snoRNP, and 40S subunit processing factors but predominantly lack 60S synthesis factors.* Mol Cell, 2002. **10**(1): p. 105-15.
117. Granneman, S., M.R. Nandineni, and S.J. Baserga, *The putative NTPase Fap7 mediates cytoplasmic 20S pre-rRNA processing through a direct interaction with Rps14.* Mol Cell Biol, 2005. **25**(23): p. 10352-64.
118. Vanrobays, E., et al., *Late cytoplasmic maturation of the small ribosomal subunit requires RIO proteins in Saccharomyces cerevisiae.* Mol Cell Biol, 2003. **23**(6): p. 2083-95.
119. King, T.H., et al., *Ribosome structure and activity are altered in cells lacking snoRNPs that form pseudouridines in the peptidyl transferase center.* Mol Cell, 2003. **11**(2): p. 425-35.
120. Liang, X.H., Q. Liu, and M.J. Fournier, *rRNA modifications in an intersubunit bridge of the ribosome strongly affect both ribosome biogenesis and activity.* Mol Cell, 2007. **28**(6): p. 965-77.
121. Piekna-Przybylska, D., et al., *Ribosome performance is enhanced by a rich cluster of pseudouridines in the A-site finger region of the large subunit.* J Biol Chem, 2008. **283**(38): p. 26026-36.

122. Charette, M. and M.W. Gray, *Pseudouridine in RNA: what, where, how, and why.* IUBMB Life, 2000. **49**(5): p. 341-51.
123. Arnez, J.G. and T.A. Steitz, *Crystal structure of unmodified tRNA(Gln) complexed with glutaminyl-tRNA synthetase and ATP suggests a possible role for pseudo-uridines in stabilization of RNA structure.* Biochemistry, 1994. **33**(24): p. 7560-7.
124. Tollervey, D., et al., *Temperature-sensitive mutations demonstrate roles for yeast fibrillarin in pre-rRNA processing, pre-rRNA methylation, and ribosome assembly.* Cell, 1993. **72**(3): p. 443-57.
125. Liang, X.H., Q. Liu, and M.J. Fournier, *Loss of rRNA modifications in the decoding center of the ribosome impairs translation and strongly delays pre-rRNA processing.* RNA, 2009. **15**(9): p. 1716-28.
126. Lafontaine, D., J. Vandenhaute, and D. Tollervey, *The 18S rRNA dimethylase Dim1p is required for pre-ribosomal RNA processing in yeast.* Genes Dev, 1995. **9**(20): p. 2470-81.
127. Lafontaine, D.L., T. Preiss, and D. Tollervey, *Yeast 18S rRNA dimethylase Dim1p: a quality control mechanism in ribosome synthesis?* Mol Cell Biol, 1998. **18**(4): p. 2360-70.
128. Xu, Z., et al., *A conserved rRNA methyltransferase regulates ribosome biogenesis.* Nat Struct Mol Biol, 2008. **15**(5): p. 534-6.
129. Connolly, K., J.P. Rife, and G. Culver, *Mechanistic insight into the ribosome biogenesis functions of the ancient protein KsgA.* Mol Microbiol, 2008. **70**(5): p. 1062-75.
130. Buchhaupt, M., et al., *Genetic evidence for 18S rRNA binding and an Rps19p assembly function of yeast nucleolar protein Nep1p.* Mol Genet Genomics, 2006. **276**(3): p. 273-84.
131. Draptchinskaia, N., et al., *The gene encoding ribosomal protein S19 is mutated in Diamond-Blackfan anaemia.* Nat Genet, 1999. **21**(2): p. 169-75.
132. Armistead, J., et al., *Mutation of a gene essential for ribosome biogenesis, EMG1, causes Bowen-Conradi syndrome.* Am J Hum Genet, 2009. **84**(6): p. 728-39.
133. Ciechanover, A., *The ubiquitin-mediated proteolytic pathway: mechanisms of action and cellular physiology.* Biol Chem Hoppe Seyler, 1994. **375**(9): p. 565-81.
134. Glickman, M.H. and A. Ciechanover, *The ubiquitin-proteasome proteolytic pathway: destruction for the sake of construction.* Physiol Rev, 2002. **82**(2): p. 373-428.
135. Schwartz, D.C. and M. Hochstrasser, *A superfamily of protein tags: ubiquitin, SUMO and related modifiers.* Trends Biochem Sci, 2003. **28**(6): p. 321-8.
136. Gill, G., *SUMO and ubiquitin in the nucleus: different functions, similar mechanisms?* Genes Dev, 2004. **18**(17): p. 2046-59.
137. Kerscher, O., R. Felberbaum, and M. Hochstrasser, *Modification of proteins by ubiquitin and ubiquitin-like proteins.* Annu Rev Cell Dev Biol, 2006. **22**: p. 159-80.
138. Ulrich, H.D., *The fast-growing business of SUMO chains.* Mol Cell, 2008. **32**(3): p. 301-5.

139. Peng, J., et al., *A proteomics approach to understanding protein ubiquitination.* Nat Biotechnol, 2003. **21**(8): p. 921-6.
140. Panse, V.G., et al., *A proteome-wide approach identifies sumoylated substrate proteins in yeast.* J Biol Chem, 2004. **279**(40): p. 41346-51.
141. Panse, V.G., et al., *Formation and nuclear export of preribosomes are functionally linked to the small-ubiquitin-related modifier pathway.* Traffic, 2006. **7**(10): p. 1311-21.
142. Stavreva, D.A., et al., *Potential roles for ubiquitin and the proteasome during ribosome biogenesis.* Mol Cell Biol, 2006. **26**(13): p. 5131-45.
143. Finley, D., B. Bartel, and A. Varshavsky, *The tails of ubiquitin precursors are ribosomal proteins whose fusion to ubiquitin facilitates ribosome biogenesis.* Nature, 1989. **338**(6214): p. 394-401.
144. Lacombe, T., et al., *Linear ubiquitin fusion to Rps31 and its subsequent cleavage are required for the efficient production and functional integrity of 40S ribosomal subunits.* Mol Microbiol, 2009. **72**(1): p. 69-84.
145. DeLaBarre, B. and A.T. Brunger, *Nucleotide dependent motion and mechanism of action of p97/VCP.* J Mol Biol, 2005. **347**(2): p. 437-52.
146. Pye, V.E., et al., *Going through the motions: the ATPase cycle of p97.* J Struct Biol, 2006. **156**(1): p. 12-28.
147. Shirai, C. and K. Mizuta, *SUMO mediates interaction of Ebp2p, the yeast homolog of Epstein-Barr virus nuclear antigen 1-binding protein 2, with a RING finger protein Ris1p.* Biosci Biotechnol Biochem, 2008. **72**(7): p. 1881-6.
148. Ho, Y., et al., *Systematic identification of protein complexes in Saccharomyces cerevisiae by mass spectrometry.* Nature, 2002. **415**(6868): p. 180-3.
149. Blake, D., et al., *The F-box protein Dia2 overcomes replication impedance to promote genome stability in Saccharomyces cerevisiae.* Genetics, 2006. **174**(4): p. 1709-27.
150. Pan, X., et al., *A DNA integrity network in the yeast Saccharomyces cerevisiae.* Cell, 2006. **124**(5): p. 1069-81.
151. Davierwala, A.P., et al., *The synthetic genetic interaction spectrum of essential genes.* Nat Genet, 2005. **37**(10): p. 1147-52.
152. Fujii, K., et al., *A role for ubiquitin in the clearance of nonfunctional rRNAs.* Genes Dev, 2009. **23**(8): p. 963-74.
153. Dez, C., J. Houseley, and D. Tollervey, *Surveillance of nuclear-restricted pre-ribosomes within a subnucleolar region of Saccharomyces cerevisiae.* EMBO J, 2006. **25**(7): p. 1534-46.
154. Schmid, F.X. and R.L. Baldwin, *Acid catalysis of the formation of the slow-folding species of RNase A: evidence that the reaction is proline isomerization.* Proc Natl Acad Sci U S A, 1978. **75**(10): p. 4764-8.
155. Schmid, F.X., *Protein folding. Prolyl isomerases join the fold.* Curr Biol, 1995. **5**(9): p. 993-4.
156. Sydorskyy, Y., et al., *Nop53p is a novel nucleolar 60S ribosomal subunit biogenesis protein.* Biochem J, 2005. **388**(Pt 3): p. 819-26.
157. Gavin, A.C., et al., *Proteome survey reveals modularity of the yeast cell machinery.* Nature, 2006. **440**(7084): p. 631-6.

158. Oeffinger, M., et al., *Comprehensive analysis of diverse ribonucleoprotein complexes.* Nat Methods, 2007. **4**(11): p. 951-6.
159. Fujiyama-Nakamura, S., et al., *Parvulin (Par14), a peptidyl-prolyl cis-trans isomerase, is a novel rRNA processing factor that evolved in the metazoan lineage.* Mol Cell Proteomics, 2009. **8**(7): p. 1552-65.
160. Traub, P. and M. Nomura, *Structure and function of E. coli ribosomes. V. Reconstitution of functionally active 30S ribosomal particles from RNA and proteins.* Proc Natl Acad Sci U S A, 1968. **59**(3): p. 777-84.
161. Mizushima, S. and M. Nomura, *Assembly mapping of 30S ribosomal proteins from E. coli.* Nature, 1970. **226**(5252): p. 1214.
162. Held, W.A., et al., *Assembly mapping of 30 S ribosomal proteins from Escherichia coli. Further studies.* J Biol Chem, 1974. **249**(10): p. 3103-11.
163. Nierhaus, K.H. and F. Dohme, *Total reconstitution of functionally active 50S ribosomal subunits from Escherichia coli.* Proc Natl Acad Sci U S A, 1974. **71**(12): p. 4713-7.
164. Rohl, R. and K.H. Nierhaus, *Assembly map of the large subunit (50S) of Escherichia coli ribosomes.* Proc Natl Acad Sci U S A, 1982. **79**(3): p. 729-33.
165. Herold, M. and K.H. Nierhaus, *Incorporation of six additional proteins to complete the assembly map of the 50 S subunit from Escherichia coli ribosomes.* J Biol Chem, 1987. **262**(18): p. 8826-33.
166. Green, R. and H.F. Noller, *Reconstitution of functional 50S ribosomes from in vitro transcripts of Bacillus stearothermophilus 23S rRNA.* Biochemistry, 1999. **38**(6): p. 1772-9.
167. Culver, G.M. and H.F. Noller, *In vitro reconstitution of 30S ribosomal subunits using complete set of recombinant proteins.* Methods Enzymol, 2000. **318**: p. 446-60.
168. Maki, J.A., D.J. Schnobrich, and G.M. Culver, *The DnaK chaperone system facilitates 30S ribosomal subunit assembly.* Mol Cell, 2002. **10**(1): p. 129-38.
169. Jiang, M., et al., *Identification of novel Escherichia coli ribosome-associated proteins using isobaric tags and multidimensional protein identification techniques.* J Bacteriol, 2007. **189**(9): p. 3434-44.
170. Dammel, C.S. and H.F. Noller, *A cold-sensitive mutation in 16S rRNA provides evidence for helical switching in ribosome assembly.* Genes Dev, 1993. **7**(4): p. 660-70.
171. Adilakshmi, T., D.L. Bellur, and S.A. Woodson, *Concurrent nucleation of 16S folding and induced fit in 30S ribosome assembly.* Nature, 2008. **455**(7217): p. 1268-72.
172. Ramaswamy, P. and S.A. Woodson, *S16 throws a conformational switch during assembly of 30S 5' domain.* Nat Struct Mol Biol, 2009. **16**(4): p. 438-45.
173. Henras, A.K., et al., *The post-transcriptional steps of eukaryotic ribosome biogenesis.* Cell Mol Life Sci, 2008. **65**(15): p. 2334-59.
174. Wang, Y., et al., *Precision and functional specificity in mRNA decay.* Proc Natl Acad Sci U S A, 2002. **99**(9): p. 5860-5.
175. Hughes, J.M., *Functional base-pairing interaction between highly conserved elements of U3 small nucleolar RNA and the small ribosomal subunit RNA.* J Mol Biol, 1996. **259**(4): p. 645-54.

176. Fayet-Lebaron, E., et al., *18S rRNA processing requires base pairings of snR30 H/ACA snoRNA to eukaryote-specific 18S sequences.* EMBO J, 2009. **28**(9): p. 1260-70.
177. Alkemar, G. and O. Nygard, *Probing the secondary structure of expansion segment ES6 in 18S ribosomal RNA.* Biochemistry, 2006. **45**(26): p. 8067-78.
178. Alkemar, G. and O. Nygard, *Secondary structure of two regions in expansion segments ES3 and ES6 with the potential of forming a tertiary interaction in eukaryotic 40S ribosomal subunits.* RNA, 2004. **10**(3): p. 403-11.
179. Alkemar, G. and O. Nygard, *A possible tertiary rRNA interaction between expansion segments ES3 and ES6 in eukaryotic 40S ribosomal subunits.* RNA, 2003. **9**(1): p. 20-4.
180. Raghunathan, P.L. and C. Guthrie, *RNA unwinding in U4/U6 snRNPs requires ATP hydrolysis and the DEIH-box splicing factor Brr2.* Curr Biol, 1998. **8**(15): p. 847-55.
181. Small, E.C., et al., *The EF-G-like GTPase Snu114p regulates spliceosome dynamics mediated by Brr2p, a DExD/H box ATPase.* Mol Cell, 2006. **23**(3): p. 389-99.
182. Bellare, P., et al., *A role for ubiquitin in the spliceosome assembly pathway.* Nat Struct Mol Biol, 2008. **15**(5): p. 444-51.
183. Tollervey, D., et al., *The small nucleolar RNP protein NOP1 (fibrillarin) is required for pre-rRNA processing in yeast.* EMBO J, 1991. **10**(3): p. 573-83.
184. Venema, J. and D. Tollervey, *RRP5 is required for formation of both 18S and 5.8S rRNA in yeast.* EMBO J, 1996. **15**(20): p. 5701-14.
185. Torchet, C., C. Jacq, and S. Hermann-Le Denmat, *Two mutant forms of the S1/TPR-containing protein Rrp5p affect the 18S rRNA synthesis in Saccharomyces cerevisiae.* RNA, 1998. **4**(12): p. 1636-52.
186. Eppens, N.A., et al., *The roles of Rrp5p in the synthesis of yeast 18S and 5.8S rRNA can be functionally and physically separated.* RNA, 1999. **5**(6): p. 779-93.
187. Jakovljevic, J., et al., *The carboxy-terminal extension of yeast ribosomal protein S14 is necessary for maturation of 43S preribosomes.* Mol Cell, 2004. **14**(3): p. 331-42.
188. Ferreira-Cerca, S., et al., *Roles of eukaryotic ribosomal proteins in maturation and transport of pre-18S rRNA and ribosome function.* Mol Cell, 2005. **20**(2): p. 263-75.
189. Bleichert, F. and S.J. Baserga, *The long unwinding road of RNA helicases.* Mol Cell, 2007. **27**(3): p. 339-52.
190. Dragon, F., et al., *A large nucleolar U3 ribonucleoprotein required for 18S ribosomal RNA biogenesis.* Nature, 2002. **417**(6892): p. 967-70.
191. Hoang, T., et al., *Esf2p, a U3-associated factor required for small-subunit processome assembly and compaction.* Mol Cell Biol, 2005. **25**(13): p. 5523-34.
192. Segerstolpe, A., et al., *Mrd1p binds to pre-rRNA early during transcription independent of U3 snoRNA and is required for compaction of the pre-rRNA into small subunit processomes.* Nucleic Acids Res, 2008. **36**(13): p. 4364-80.
193. Vanrobays, E., et al., *TOR regulates the subcellular distribution of DIM2, a KH domain protein required for cotranscriptional ribosome assembly and pre-40S ribosome export.* RNA, 2008. **14**(10): p. 2061-73.

194. Wilmes, G.M., et al., *A genetic interaction map of RNA-processing factors reveals links between Sem1/Dss1-containing complexes and mRNA export and splicing.* Mol Cell, 2008. **32**(5): p. 735-46.
195. Hopfield, J.J., *Origin of the genetic code: a testable hypothesis based on tRNA structure, sequence, and kinetic proofreading.* Proc Natl Acad Sci U S A, 1978. **75**(9): p. 4334-8.
196. Dez, C., M. Dlakic, and D. Tollervey, *Roles of the HEAT repeat proteins Utp10 and Utp20 in 40S ribosome maturation.* RNA, 2007. **13**(9): p. 1516-27.
197. Wery, M., et al., *The nuclear poly(A) polymerase and Exosome cofactor Trf5 is recruited cotranscriptionally to nucleolar surveillance.* RNA, 2009. **15**(3): p. 406-19.
198. Si, K. and U. Maitra, *The Saccharomyces cerevisiae homologue of mammalian translation initiation factor 6 does not function as a translation initiation factor.* Mol Cell Biol, 1999. **19**(2): p. 1416-26.
199. Menne, T.F., et al., *The Shwachman-Bodian-Diamond syndrome protein mediates translational activation of ribosomes in yeast.* Nat Genet, 2007. **39**(4): p. 486-95.
200. Shammas, C., et al., *Structural and mutational analysis of the SBDS protein family. Insight into the leukemia-associated Shwachman-Diamond Syndrome.* J Biol Chem, 2005. **280**(19): p. 19221-9.
201. Du, Y.C. and B. Stillman, *Yph1p, an ORC-interacting protein: potential links between cell proliferation control, DNA replication, and ribosome biogenesis.* Cell, 2002. **109**(7): p. 835-48.
202. Steiner-Mosonyi, M., et al., *Utp8p is an essential intranuclear component of the nuclear tRNA export machinery of Saccharomyces cerevisiae.* J Biol Chem, 2003. **278**(34): p. 32236-45.
203. Killian, A., et al., *Inactivation of the RRB1-Pescadillo pathway involved in ribosome biogenesis induces chromosomal instability.* Oncogene, 2004. **23**(53): p. 8597-602.
204. Bernstein, K.A., et al., *Ribosome biogenesis is sensed at the Start cell cycle checkpoint.* Mol Biol Cell, 2007. **18**(3): p. 953-64.
205. Rudra, D., et al., *Potential interface between ribosomal protein production and pre-rRNA processing.* Mol Cell Biol, 2007. **27**(13): p. 4815-24.
206. Strub, B.R., et al., *Utp8p is a nucleolar tRNA-binding protein that forms a complex with components of the nuclear tRNA export machinery in Saccharomyces cerevisiae.* Mol Biol Cell, 2007. **18**(10): p. 3845-59.
207. Jwa, M., J.H. Kim, and C.S. Chan, *Regulation of Sli15/INCENP, kinetochore, and Cdc14 phosphatase functions by the ribosome biogenesis protein Utp7.* J Cell Biol, 2008. **182**(6): p. 1099-111.
208. Dez, C. and D. Tollervey, *Ribosome synthesis meets the cell cycle.* Curr Opin Microbiol, 2004. **7**(6): p. 631-7.
209. Granneman, S. and S.J. Baserga, *Crosstalk in gene expression: coupling and co-regulation of rDNA transcription, pre-ribosome assembly and pre-rRNA processing.* Curr Opin Cell Biol, 2005. **17**(3): p. 281-6.
210. Loar, J.W., et al., *Genetic and biochemical interactions among Yar1, Ltv1 and Rps3 define novel links between environmental stress and ribosome biogenesis in Saccharomyces cerevisiae.* Genetics, 2004. **168**(4): p. 1877-89.

211. Juhnke, H., et al., *The essential protein fap7 is involved in the oxidative stress response of Saccharomyces cerevisiae.* Mol Microbiol, 2000. **35**(4): p. 936-48.
212. Gasch, A.P., et al., *Genomic expression programs in the response of yeast cells to environmental changes.* Mol Biol Cell, 2000. **11**(12): p. 4241-57.
213. Ju, Q. and J.R. Warner, *Ribosome synthesis during the growth cycle of Saccharomyces cerevisiae.* Yeast, 1994. **10**(2): p. 151-7.
214. Pleiss, J.A., et al., *Rapid, transcript-specific changes in splicing in response to environmental stress.* Mol Cell, 2007. **27**(6): p. 928-37.
215. Powers, T. and P. Walter, *Regulation of ribosome biogenesis by the rapamycin-sensitive TOR-signaling pathway in Saccharomyces cerevisiae.* Mol Biol Cell, 1999. **10**(4): p. 987-1000.
216. Honma, Y., et al., *TOR regulates late steps of ribosome maturation in the nucleoplasm via Nog1 in response to nutrients.* EMBO J, 2006. **25**(16): p. 3832-42.
217. Bharucha, N., et al., *Analysis of the yeast kinome reveals a network of regulated protein localization during filamentous growth.* Mol Biol Cell, 2008. **19**(7): p. 2708-17.
218. Strittmatter, A.W., et al., *FLO11 mediated filamentous growth of the yeast Saccharomyces cerevisiae depends on the expression of the ribosomal RPS26 genes.* Mol Genet Genomics, 2006. **276**(2): p. 113-25.
219. Valerius, O., et al., *The Saccharomyces homolog of mammalian RACK1, Cpc2/Asc1p, is required for FLO11-dependent adhesive growth and dimorphism.* Mol Cell Proteomics, 2007. **6**(11): p. 1968-79.
220. Jin, R., et al., *Large-scale analysis of yeast filamentous growth by systematic gene disruption and overexpression.* Mol Biol Cell, 2008. **19**(1): p. 284-96.
221. Angermayr, M., et al., *Protein kinase CK2 activates the atypical Rio1p kinase and promotes its cell-cycle phase-dependent degradation in yeast.* FEBS J, 2007. **274**(17): p. 4654-67.
222. Kressler, D., et al., *Fal1p is an essential DEAD-box protein involved in 40S-ribosomal-subunit biogenesis in Saccharomyces cerevisiae.* Mol Cell Biol, 1997. **17**(12): p. 7283-94.
223. Weaver, P.L., C. Sun, and T.H. Chang, *Dbp3p, a putative RNA helicase in Saccharomyces cerevisiae, is required for efficient pre-rRNA processing predominantly at site A3.* Mol Cell Biol, 1997. **17**(3): p. 1354-65.
224. Kressler, D., et al., *Dbp6p is an essential putative ATP-dependent RNA helicase required for 60S-ribosomal-subunit assembly in Saccharomyces cerevisiae.* Mol Cell Biol, 1998. **18**(4): p. 1855-65.
225. Daugeron, M.C. and P. Linder, *Dbp7p, a putative ATP-dependent RNA helicase from Saccharomyces cerevisiae, is required for 60S ribosomal subunit assembly.* RNA, 1998. **4**(5): p. 566-81.
226. Zagulski, M., et al., *Mak5p, which is required for the maintenance of the M1 dsRNA virus, is encoded by the yeast ORF YBR142w and is involved in the biogenesis of the 60S subunit of the ribosome.* Mol Genet Genomics, 2003. **270**(3): p. 216-24.
227. Strunk, B.S. and K. Karbstein, *Powering through ribosome assembly.* RNA, 2009. **15**(12): p. 2083-104.

228. Armache, J.P., et al., *Localization of eukaryote-specific ribosomal proteins in a 5.5-A cryo-EM map of the 80S eukaryotic ribosome.* Proc Natl Acad Sci U S A, 2010. **107**(46): p. 19754-9.
229. Beckmann, R., et al., *Alignment of conduits for the nascent polypeptide chain in the ribosome-Sec61 complex.* Science, 1997. **278**(5346): p. 2123-6.
230. Frank, J., et al., *A model of protein synthesis based on cryo-electron microscopy of the E. coli ribosome.* Nature, 1995. **376**(6539): p. 441-4.
231. Spahn, C.M., et al., *Cryo-EM visualization of a viral internal ribosome entry site bound to human ribosomes: the IRES functions as an RNA-based translation factor.* Cell, 2004. **118**(4): p. 465-75.
232. Taylor, D.J., et al., *Comprehensive molecular structure of the eukaryotic ribosome.* Structure, 2009. **17**(12): p. 1591-604.
233. Ban, N., et al., *The complete atomic structure of the large ribosomal subunit at 2.4 A resolution.* Science, 2000. **289**(5481): p. 905-20.
234. Cate, J.H., et al., *X-ray crystal structures of 70S ribosome functional complexes.* Science, 1999. **285**(5436): p. 2095-104.
235. Harms, J., et al., *High resolution structure of the large ribosomal subunit from a mesophilic eubacterium.* Cell, 2001. **107**(5): p. 679-88.
236. Wimberly, B.T., et al., *Structure of the 30S ribosomal subunit.* Nature, 2000. **407**(6802): p. 327-39.
237. Ben-Shem, A., et al., *Crystal structure of the eukaryotic ribosome.* Science, 2010. **330**(6008): p. 1203-9.
238. Rabl, J., et al., *Crystal structure of the eukaryotic 40S ribosomal subunit in complex with initiation factor 1.* Science, 2011. **331**(6018): p. 730-6.
239. Soudet, J., et al., *Immature small ribosomal subunits can engage in translation initiation in Saccharomyces cerevisiae.* EMBO J, 2010. **29**(1): p. 80-92.
240. Verschoor, A., et al., *Three-dimensional reconstruction of mammalian 40 S ribosomal subunit.* J Mol Biol, 1989. **209**(1): p. 115-26.
241. Trabuco, L.G., et al., *The role of L1 stalk-tRNA interaction in the ribosome elongation cycle.* J Mol Biol, 2010. **402**(4): p. 741-60.
242. Trabuco, L.G., et al., *Applications of the molecular dynamics flexible fitting method.* J Struct Biol, 2011. **173**(3): p. 420-7.
243. Trabuco, L.G., et al., *Flexible fitting of atomic structures into electron microscopy maps using molecular dynamics.* Structure, 2008. **16**(5): p. 673-83.
244. Trabuco, L.G., et al., *Molecular dynamics flexible fitting: a practical guide to combine cryo-electron microscopy and X-ray crystallography.* Methods, 2009. **49**(2): p. 174-80.
245. Campbell, M.G. and K. Karbstein, *Protein-protein interactions within late pre-40S ribosomes.* PLoS One, 2011. **6**(1): p. e16194.
246. Granneman, S., et al., *Cracking pre-40S ribosomal subunit structure by systematic analyses of RNA-protein cross-linking.* EMBO J, 2010. **29**(12): p. 2026-36.
247. Lamanna, A.C. and K. Karbstein, *An RNA conformational switch regulates pre-18S rRNA cleavage.* J Mol Biol, 2011. **405**(1): p. 3-17.
248. Woolls, H.A., A.C. Lamanna, and K. Karbstein, *Roles of Dim2 in ribosome assembly.* J Biol Chem, 2011. **286**(4): p. 2578-86.

249. Vanrobays, E., et al., *Dim2p, a KH-domain protein required for small ribosomal subunit synthesis.* RNA, 2004. **10**(4): p. 645-56.
250. Carron, C., et al., *Analysis of two human pre-ribosomal factors, bystin and hTsr1, highlights differences in evolution of ribosome biogenesis between yeast and mammals.* Nucleic Acids Res, 2011. **39**(1): p. 280-91.
251. Ho, J.H. and A.W. Johnson, *NMD3 encodes an essential cytoplasmic protein required for stable 60S ribosomal subunits in Saccharomyces cerevisiae.* Mol Cell Biol, 1999. **19**(3): p. 2389-99.
252. Sengupta, J., et al., *Characterization of the nuclear export adaptor protein Nmd3 in association with the 60S ribosomal subunit.* J Cell Biol, 2010. **189**(7): p. 1079-86.
253. Ogle, J.M., et al., *Recognition of cognate transfer RNA by the 30S ribosomal subunit.* Science, 2001. **292**(5518): p. 897-902.
254. Sharma, M.R., et al., *Interaction of Era with the 30S ribosomal subunit implications for 30S subunit assembly.* Mol Cell, 2005. **18**(3): p. 319-29.
255. Datta, P.P., et al., *Structural aspects of RbfA action during small ribosomal subunit assembly.* Mol Cell, 2007. **28**(3): p. 434-45.
256. Roy-Chaudhuri, B., N. Kirthi, and G.M. Culver, *Appropriate maturation and folding of 16S rRNA during 30S subunit biogenesis are critical for translational fidelity.* Proc Natl Acad Sci U S A, 2010. **107**(10): p. 4567-72.
257. Ferreira-Cerca, S., et al., *Analysis of the in vivo assembly pathway of eukaryotic 40S ribosomal proteins.* Mol Cell, 2007. **28**(3): p. 446-57.
258. Mulder, A.M., et al., *Visualizing ribosome biogenesis: parallel assembly pathways for the 30S subunit.* Science, 2010. **330**(6004): p. 673-7.
259. Lamanna, A.C. and K. Karbstein, *Nob1 binds the single-stranded cleavage site D at the 3'-end of 18S rRNA with its PIN domain.* Proc Natl Acad Sci U S A, 2009. **106**(34): p. 14259-64.
260. Neueder, A., et al., *A local role for the small ribosomal subunit primary binder rpS5 in final 18S rRNA processing in yeast.* PLoS One, 2010. **5**(4): p. e10194.
261. Desai, P.M. and J.P. Rife, *The adenosine dimethyltransferase KsgA recognizes a specific conformational state of the 30S ribosomal subunit.* Arch Biochem Biophys, 2006. **449**(1-2): p. 57-63.
262. Peterson, A.W., M.L. Pendrak, and D.D. Roberts, *ATP binding to hemoglobin response gene 1 protein is necessary for regulation of the mating type locus in Candida albicans.* J Biol Chem, 2011. **286**(16): p. 13914-24.
263. Santama, N., et al., *Characterization of hCINAP, a novel coilin-interacting protein encoded by a transcript from the transcription factor TAFIID32 locus.* J Biol Chem, 2005. **280**(43): p. 36429-41.
264. Ren, H., et al., *The crystal structure of human adenylate kinase 6: An adenylate kinase localized to the cell nucleus.* Proc Natl Acad Sci U S A, 2005. **102**(2): p. 303-8.
265. Zhang, J., F. Zhang, and X. Zheng, *Depletion of hCINAP by RNA interference causes defects in Cajal body formation, histone transcription, and cell viability.* Cell Mol Life Sci, 2010. **67**(11): p. 1907-18.

266. Pendrak, M.L., S.S. Yan, and D.D. Roberts, *Hemoglobin regulates expression of an activator of mating-type locus alpha genes in Candida albicans.* Eukaryot Cell, 2004. **3**(3): p. 764-75.
267. Ghaemmaghami, S., et al., *Global analysis of protein expression in yeast.* Nature, 2003. **425**(6959): p. 737-41.
268. Tamaki, H., et al., *Glucose-dependent cell size is regulated by a G protein-coupled receptor system in yeast Saccharomyces cerevisiae.* Genes Cells, 2005. **10**(3): p. 193-206.
269. Wilkins, M.R., et al., *Protein identification and analysis tools in the ExPASy server.* Methods Mol Biol, 1999. **112**: p. 531-52.
270. Karbstein, K. and J.A. Doudna, *GTP-dependent formation of a ribonucleoprotein subcomplex required for ribosome biogenesis.* J Mol Biol, 2006. **356**(2): p. 432-43.
271. Johnson, K.A., *Transient-state kinetic analysis of enzyme reaction pathways*, in *The Enzymes: Mechanisms of Catalysis*. 1992, Sigman, D.S. p. 1-61.
272. van Duffelen, M., L.R. Chrin, and C.L. Berger, *Nucleotide dependent intrinsic fluorescence changes of W29 and W36 in smooth muscle myosin.* Biophys J, 2004. **87**(3): p. 1767-75.
273. Leipe, D.D., E.V. Koonin, and L. Aravind, *Evolution and classification of P-loop kinases and related proteins.* J Mol Biol, 2003. **333**(4): p. 781-815.
274. Antunez de Mayolo, P. and J.L. Woolford, Jr., *Interactions of yeast ribosomal protein rpS14 with RNA.* J Mol Biol, 2003. **333**(4): p. 697-709.
275. Strunk, B.S., et al., *Ribosome Assembly Factors Prevent Premature Translation Initiation by 40S Assembly Intermediates.* Science, 2011. **in press**.
276. Vanrobays, E., et al., *Processing of 20S pre-rRNA to 18S ribosomal RNA in yeast requires Rrp10p, an essential non-ribosomal cytoplasmic protein.* EMBO J, 2001. **20**(15): p. 4204-13.
277. Henderson, A. and J.W. Hershey, *Eukaryotic translation initiation factor (eIF) 5A stimulates protein synthesis in Saccharomyces cerevisiae.* Proc Natl Acad Sci U S A, 2011. **108**(16): p. 6415-9.
278. Blaha, G., R.E. Stanley, and T.A. Steitz, *Formation of the first peptide bond: the structure of EF-P bound to the 70S ribosome.* Science, 2009. **325**(5943): p. 966-70.
279. Li, Z., et al., *Rational extension of the ribosome biogenesis pathway using network-guided genetics.* PLoS Biol, 2009. **7**(10): p. e1000213.
280. Longtine, M.S., et al., *Additional modules for versatile and economical PCR-based gene deletion and modification in Saccharomyces cerevisiae.* Yeast, 1998. **14**(10): p. 953-61.
281. Kang, H.A. and J.W. Hershey, *Effect of initiation factor eIF-5A depletion on protein synthesis and proliferation of Saccharomyces cerevisiae.* J Biol Chem, 1994. **269**(6): p. 3934-40.
282. Schwelberger, H.G., H.A. Kang, and J.W. Hershey, *Translation initiation factor eIF-5A expressed from either of two yeast genes or from human cDNA. Functional identity under aerobic and anaerobic conditions.* J Biol Chem, 1993. **268**(19): p. 14018-25.

283. Milkereit, P., et al., *Maturation and intranuclear transport of pre-ribosomes requires Noc proteins.* Cell, 2001. **105**(4): p. 499-509.
284. Valasek, L., et al., *In vivo stabilization of preinitiation complexes by formaldehyde cross-linking.* Methods Enzymol, 2007. **429**: p. 163-83.
285. Puig, O., et al., *The tandem affinity purification (TAP) method: a general procedure of protein complex purification.* Methods, 2001. **24**(3): p. 218-29.
286. Lopez de Heredia, M. and R.P. Jansen, *RNA integrity as a quality indicator during the first steps of RNP purifications : a comparison of yeast lysis methods.* BMC Biochem, 2004. **5**: p. 14.
287. Raue, U., S. Oellerer, and S. Rospert, *Association of protein biogenesis factors at the yeast ribosomal tunnel exit is affected by the translational status and nascent polypeptide sequence.* J Biol Chem, 2007. **282**(11): p. 7809-16.
288. Sonenberg, N. and A.G. Hinnebusch, *Regulation of translation initiation in eukaryotes: mechanisms and biological targets.* Cell, 2009. **136**(4): p. 731-45.
289. Perentesis, J.P., et al., *Saccharomyces cerevisiae elongation factor 2. Genetic cloning, characterization of expression, and G-domain modeling.* J Biol Chem, 1992. **267**(2): p. 1190-7.
290. Pisarev, A.V., et al., *The role of ABCE1 in eukaryotic posttermination ribosomal recycling.* Mol Cell, 2010. **37**(2): p. 196-210.
291. Jao, D.L. and K.Y. Chen, *Tandem affinity purification revealed the hypusine-dependent binding of eukaryotic initiation factor 5A to the translating 80S ribosomal complex.* J Cell Biochem, 2006. **97**(3): p. 583-98.
292. Armache, J.P., et al., *Cryo-EM structure and rRNA model of a translating eukaryotic 80S ribosome at 5.5-A resolution.* Proc Natl Acad Sci U S A, 2010. **107**(46): p. 19748-53.
293. Moritz, M., et al., *Depletion of yeast ribosomal proteins L16 or rp59 disrupts ribosome assembly.* J Cell Biol, 1990. **111**(6 Pt 1): p. 2261-74.
294. Trotter, E.W., et al., *The yeast Tsa1 peroxiredoxin is a ribosome-associated antioxidant.* Biochem J, 2008. **412**(1): p. 73-80.
295. Shenton, D., et al., *Global translational responses to oxidative stress impact upon multiple levels of protein synthesis.* J Biol Chem, 2006. **281**(39): p. 29011-21.
296. Hanawa-Suetsugu, K., et al., *Crystal structure of elongation factor P from Thermus thermophilus HB8.* Proc Natl Acad Sci U S A, 2004. **101**(26): p. 9595-600.
297. Lorsch, J.R. and T.E. Dever, *Molecular view of 43 S complex formation and start site selection in eukaryotic translation initiation.* J Biol Chem, 2010. **285**(28): p. 21203-7.
298. Arava, Y., et al., *Genome-wide analysis of mRNA translation profiles in Saccharomyces cerevisiae.* Proc Natl Acad Sci U S A, 2003. **100**(7): p. 3889-94.
299. Pestova, T.V., I.B. Lomakin, and C.U. Hellen, *Position of the CrPV IRES on the 40S subunit and factor dependence of IRES/80S ribosome assembly.* EMBO Rep, 2004. **5**(9): p. 906-13.
300. Lamphear, B.J., et al., *Mapping of functional domains in eukaryotic protein synthesis initiation factor 4G (eIF4G) with picornaviral proteases. Implications for cap-dependent and cap-independent translational initiation.* J Biol Chem, 1995. **270**(37): p. 21975-83.

301. Bhattacharya, A., et al., *Why Dom34 stimulates growth of cells with defects of 40S ribosomal subunit biosynthesis.* Mol Cell Biol, 2010. **30**(23): p. 5562-71.
302. Jia, M.Z., et al., *Crystal structure of Dim2p: a preribosomal RNA processing factor, from Pyrococcus horikoshii OT3 at 2.30 A.* Proteins, 2007. **69**(2): p. 428-32.
303. Bhaskara, V., et al., *Rad50 adenylate kinase activity regulates DNA tethering by Mre11/Rad50 complexes.* Mol Cell, 2007. **25**(5): p. 647-61.
304. Pertschy, B., et al., *RNA helicase Prp43 and its co-factor Pfa1 promote 20 to 18 S rRNA processing catalyzed by the endonuclease Nob1.* J Biol Chem, 2009. **284**(50): p. 35079-91.
305. LaRonde-LeBlanc, N., et al., *Autophosphorylation of Archaeoglobus fulgidus Rio2 and crystal structures of its nucleotide-metal ion complexes.* FEBS J, 2005. **272**(11): p. 2800-10.
306. Lafontaine, D., et al., *The DIM1 gene responsible for the conserved m6(2)Am6(2)A dimethylation in the 3'-terminal loop of 18 S rRNA is essential in yeast.* J Mol Biol, 1994. **241**(3): p. 492-7.
307. Pulicherla, N., et al., *Structural and functional divergence within the Dim1/KsgA family of rRNA methyltransferases.* J Mol Biol, 2009. **391**(5): p. 884-93.
308. Radermacher, M., et al., *Three-dimensional reconstruction from a single-exposure, random conical tilt series applied to the 50S ribosomal subunit of Escherichia coli.* J Microsc, 1987. **146**(Pt 2): p. 113-36.
309. Seiser, R.M., et al., *Ltv1 is required for efficient nuclear export of the ribosomal small subunit in Saccharomyces cerevisiae.* Genetics, 2006. **174**(2): p. 679-91.
310. Brink, J., et al., *Experimental verification of conformational variation of human fatty acid synthase as predicted by normal mode analysis.* Structure, 2004. **12**(2): p. 185-91.
311. Menetret, J.F., et al., *Architecture of the ribosome-channel complex derived from native membranes.* J Mol Biol, 2005. **348**(2): p. 445-57.
312. Ohi, M., et al., *Negative Staining and Image Classification - Powerful Tools in Modern Electron Microscopy.* Biol Proced Online, 2004. **6**: p. 23-34.
313. Ludtke, S.J., P.R. Baldwin, and W. Chiu, *EMAN: semiautomated software for high-resolution single-particle reconstructions.* J Struct Biol, 1999. **128**(1): p. 82-97.
314. Frank, J., et al., *SPIDER and WEB: processing and visualization of images in 3D electron microscopy and related fields.* J Struct Biol, 1996. **116**(1): p. 190-9.
315. Grigorieff, N., *FREALIGN: high-resolution refinement of single particle structures.* J Struct Biol, 2007. **157**(1): p. 117-25.
316. Taylor, D.J., et al., *Structures of modified eEF2 80S ribosome complexes reveal the role of GTP hydrolysis in translocation.* EMBO J, 2007. **26**(9): p. 2421-31.
317. Penczek, P.A., J. Frank, and C.M. Spahn, *A method of focused classification, based on the bootstrap 3D variance analysis, and its application to EF-G-dependent translocation.* J Struct Biol, 2006. **154**(2): p. 184-94.
318. Milligan, R.A. and P.N. Unwin, *Location of exit channel for nascent protein in 80S ribosome.* Nature, 1986. **319**(6055): p. 693-5.
319. Humphrey, W., A. Dalke, and K. Schulten, *VMD: visual molecular dynamics.* J Mol Graph, 1996. **14**(1): p. 33-8, 27-8.

320. Nilsson, J., et al., *Comparison of fungal 80 S ribosomes by cryo-EM reveals diversity in structure and conformation of rRNA expansion segments.* J Mol Biol, 2007. **369**(2): p. 429-38.
321. Thompson, J.D., D.G. Higgins, and T.J. Gibson, *CLUSTAL W: improving the sensitivity of progressive multiple sequence alignment through sequence weighting, position-specific gap penalties and weight matrix choice.* Nucleic Acids Res, 1994. **22**(22): p. 4673-80.
322. Norberto de Souza, O. and R.L. Ornstein, *Molecular dynamics simulations of a protein-protein dimer: particle-mesh Ewald electrostatic model yields far superior results to standard cutoff model.* J Biomol Struct Dyn, 1999. **16**(6): p. 1205-18.
323. Phillips, J.C., et al., *Scalable molecular dynamics with NAMD.* J Comput Chem, 2005. **26**(16): p. 1781-802.
324. Mackerell, A.D., Jr., M. Feig, and C.L. Brooks, 3rd, *Extending the treatment of backbone energetics in protein force fields: limitations of gas-phase quantum mechanics in reproducing protein conformational distributions in molecular dynamics simulations.* J Comput Chem, 2004. **25**(11): p. 1400-15.
325. Wriggers, W., *Using Situs for the integration of multi-resolution structures.* Biophys Rev, 2010. **2**(1): p. 21-27.